The Dissertation Committee for Bradley Tyler Gooch Certifies that this is the approved version of the following dissertation:

The Effects of Sedimentary Basins on the Dynamics of the East Antarctic Ice Sheet from Enhanced Groundwater and Geothermal Heat Flow

Committee:

Donald D. Blankenship, Supervisor

Ian W. Dalziel

Omar Ghattas

Marc A. Hesse

Duncan A. Young

The Effects of Sedimentary Basins on the Dynamics of the East Antarctic Ice Sheet from Enhanced Groundwater and Geothermal Heat Flow

by

Bradley Tyler Gooch, B.S.; M.S.

Dissertation

Presented to the Faculty of the Graduate School of

The University of Texas at Austin

in Partial Fulfillment

of the Requirements

for the Degree of

Doctor of Philosophy

The University of Texas at Austin

May 2016

The Effects of Sedimentary Basins on the Dynamics of the East Antarctic Ice Sheet from Enhanced Groundwater and Geothermal Heat Flow

Bradley Tyler Gooch, Ph.D.

The University of Texas at Austin, 2016

Supervisor: Donald D. Blankenship

It is well known that ice sheets heavily influence groundwater systems, however, the impact of groundwater on ice sheet dynamics is not. This poorly understood aspect of ice-sheet hydrology is relevant to the subglacial hydrology of ice sheets lacking surface or englacial meltwater such as the East Antarctic Ice Sheet (EAIS). How groundwater systems redistribute geothermal heat at the base of an ice sheet is also largely unknown. Geothermal heat and subglacial hydrology are important basal processes controlling ice flow. Large sedimentary basins underlie the EAIS, which likely play host to many groundwater systems. I hypothesized that groundwater systems in these sedimentary basins may be the main water transport mechanism over water sheets (or films) at large scales in the interior of the ice sheet where basal melt rates are very low. I also hypothesized that these groundwater systems are likely important to the basal processes (specifically heat flux) and dynamics of the EAIS (particularly in rheological and sliding behavior). To test these, I created various one- and two-dimensional numerical models incorporating relevant datasets and conservative assumptions about the subsurface. The models ranged from simple groundwater and thermal simulations to a complex

subsurface fluid and thermal model coupled to a fully dynamic ice sheet simulator. The models suggest that groundwater most likely has measurable effects on the dynamics of ice sheets like the EAIS. I have shown that probable groundwater systems underneath the interior of the EAIS can likely transport most of the meltwater produced and that groundwater can strongly affect the heat flux (positively, as well as, negatively) at the ice base under kilometers of relatively slow-moving ice. I have also not only shown that groundwater systems under the EAIS are strongly controlled by the ice sheet's dynamics but that groundwater systems have a feedback to the ice dynamics, mostly through enhanced basal sliding and changes to the ice rheology. These results provide the justification to include groundwater in future simulations of the EAIS as well as a call to collect more data to better delineate its subsurface sedimentary basins – a critical input for groundwater and heat transport modeling.

Table of Contents

List of Tables

List of Figures

Figure 3.8. Map of the reconstructed assemblage of the East Antarctic (EANT) and Australian (AUS) plates at 160 Ma with present day, surface radiogenic heat production values (calculated mainly from *Champion et al*. [2007] and *Carson and Pittard* [2012]). The relative global tectonic plate (plates in light gray) assemblage at 160 Ma and the extent of the study area are shown in the inset map. The grouping extents used for the heat production statistics are in each of the lettered boxes. The averages for the heat production groupings are 1.08 (standard deviation 1.53), 4.27 (std. 28.75), and 1.43 (std. 2.59) $\mu W/m^3$ for boxes A, B, and C, respectively. The geophysically derived fault and tectonic interpretations from *Aitken et al*. [2014] are shown with green lines. The Wilkes Subglacial Basin (WSB) covers much of the area at or below sea level from the coast towards the South Pole. The Aurora Subglacial Basin (ASB) extends in a similar manner to the WSB but from a different direction; it also terminates near the WSB's terminus. Probable groundwater impact areas (see Section 3.3.3) are included as red-hatched zones. Areas where the present-day bed elevation from *Fretwell et al*. [2013] is at or below mean sea level are colored blue and those above are in dark gray. Locations where geophysical data availability is limited or non-existent and are of added hydrogeological and geochemical interest in line with this study for future aerogeophysical surveying are designated with question marks (?). The present-day East Antarctic Ice Sheet (EAIS) grounding line from *Bohlander and Scambos* [2007] is included in brown. Present-day coastlines [*Wessel and Smith*, 1996; v2.3.3] on other plates are shown as blue lines. 92

Figure S4.17. Basal water sheet groundwater sources (and sinks, if negative) along the model flowline shown in Figure 4.1 for the simulation including sliding. For fluxes ranging many orders of magnitude above and below zero, the positive (POS) and negative (NEG) components are shown separately. Also, where the values are split into the two components, an average is displayed for all values in order to define the overall sign and magnitude of the flux. The mean for the high groundwater ($k_0 = 10^{-11}$ m^2) and low groundwater ($k_0 = 10^{-18}$ m^2) are 346.83 and 3.46×10^{-5} mm/yr, respectively. As the groundwater properties are the same in the simulation without sliding (not shown), their mean values are the same. Figure 4.9 shows these groundwater volume flux trends along with the other water sheet sources. 182

Figure S4.20. Various model results from the low groundwater sliding calibration ($cf = 2\times10^{12}$ for $k0 = 10^{-18}$ m^2). (a) Represents the lateral boundary temperatures for both simulations (i.e. high/low groundwater). (b) Computed temperatures for the results from the low groundwater scenario. Note that the pressure melting temperature ranges from 0° to about -4° Celsius (see Figure S4.2). (c) Total vertical heat flux (in mW/m^2) comparisons at the ice/bed interface and Moho along the model flowline shown in Figure 4.1. Both simulations produced the same heat flux at the Moho. Note that both the high and low groundwater results have been split into positive (POS) and negative (NEG) components for proper comparison. A mean of both heat flux results for each of the parameterizations of groundwater is shown as a solid horizontal bar. The means for the high and low groundwater parameterizations with slip are 2,995.1 and 94.381 mW/m^2, respectively. (d) Vertical conductive component of the heat flux (in mW/m^2). The means for the high and low groundwater parameterizations are 110.12 and 63.889 mW/m^2, respectively. Note that the three most commonly used, recent vertical geothermal heat flux datasets for East Antarctica [*Shapiro and Ritzroller*, 2004; *Fox Maule et al*., 2005; and *An et al*., 2015b], sampled along the model flowline, have been plotted for comparison, as in Figure 4.8..... 187

Figure S4.22. Map of the Totten Glacier and surrounding ice sheet catchment emptying along the Sabrina Coast in East Antarctica with the model flowline (X to X'; 1,363 km in total length with 100 km segments noted) discussed in this article. Important places or those discussed in this article are highlighted; ASB – Aurora Subglacial Basin, DC – Dome C, HA – Highland A, HB – Highland B, LD – Law Dome, RB – Ridge B, SSB – Sabrina Subglacial Basin, and T – Totten Glacier. The red outline represents the larger ice catchment boundaries [*Zwally et al.,* 2012] and, where at the coast, represents overlap with the grounding line [*Bindschadler et al.,* 2011]; the precise catchment for Totten Glacier was measured and is displayed as a function of flowline coordinate in Figure S4.1. Surface ice flow speeds and direction are from the MEaSUREs dataset [*Rignot et al.,* 2011]. The subglacial water flowpaths and the bed elevation are based on the Bedmap2 dataset [*Fretwell et al.,* 2013]. All latitude and longitude graticules in the inset and main figure are in 10° increments with the Antarctic Circle shown as a dashed line. The subglacial lake inventory references are: B09 – *Blankenship et al.* [2009], S09 – *Smith et al.* [2009], and W12 – *Wright and Siegert* [2012]. A version of this map with the background indicating bed elevation instead of measured ice surface speed is given in Figure 4.1. 191

Chapter 1: Introduction

1.1 Background Information and Observations of Groundwater and Subglacial Hydrology

Glacial ice moves via two component mechanisms: by internally deforming and by sliding at its base. Observing the surface velocity of ice is a relatively straightforward task as there have been great technological improvements in measuring its speed remotely at a precise level. Understanding the relative contribution of each of the above components (i.e. creep and sliding) and the parameters that affect them are not well understood despite being actively studied for many decades. A poorly understood process affecting both of these components is the amount of heat flowing at the base of the ice. This heat originates through either the frictional heating from the basal shear of the ice or from geothermal heat at the ice base. Basal heat flux underneath the ice affects the ice thermal structure, which alters how the ice flows. This is because the temperature profile with depth of the ice dictates how it will flow by internal deformation [*Glen*, 1955; *Mellor and Testa*, 1969], which also generates heat within the ice.

Accessing the base of any glacier or ice sheet to record basal heat flux is challenging and cost-prohibitive so direct measurements are very sparse for even well-studied glaciers and even less so for ice sheets. Another poorly understood process that greatly affects the sliding component of movement is the amount of water at the bottom of the ice. This water originates from melting basal ice, ice surface water draining to the base, or groundwater influx through the porous media below the ice. The water content underneath the ice has been shown to greatly affect the sliding velocity of ice [e.g. *Alley*, 1989; *Stearns et al.*, 2008; *Schoof*, 2010]. This water essentially acts as a basal lubricant (increased sliding) underneath the ice or indirectly as water filling a porous sediment layer beneath the ice altering sliding or shearing behavior [*Blankenship et al.*, 1986; *Alley et al.* 1986; *Clarke*, 1987; *Tulaczyk et al.*, 2000]. A commonality between these two

parameters is that they are tightly coupled. The basal heat flux and water at the base of the ice greatly affect each other. Subglacial water can advect heat at the base of the ice possibly leading to basal heat anomalies [*Clarke et al.*, 1984; *Echelmeyer*, 1987]. The water carrying the extra heat can also increase basal melting, effectively creating excess water, leading to the possibility of higher water pressure, water volume reorganization, and glacial sliding [*Blankenship et al.*, 1993; *Tulacyzk et al.*, 2000; *Fahnestock et al.*, 2001].

Studying these specific, poorly constrained processes should improve understanding in how critical subglacial dynamics are in assessing the movements of ice. Being able to better predict the future behavior of glaciers and ice sheets as they relate to sea level and climate change is one of the key scientific objectives of societally important research according to various funding agencies, inter-governmental panels, and scientific organizations. Predicting this kind of behavior is also critical for the subsurface integrity planning for the sequestration of carbon dioxide or for waste isolation sites at high-latitudes that could become glaciated again [e.g. *Person et al.*, 2012]. Finally, it is important in a very practical way to glaciologists looking to drill down to a "dry bed" to obtain old ice cores in order to not contaminate isolated subglacial environments sustained by a "wet" one.

A poorly understood aspect of ice sheet hydrology is the role that groundwater transport contributes to a subglacial water system of an ice sheet lacking surface or englacial meltwater such as the East Antarctic Ice Sheet (Figures 1.1, 1.2). Generally, the East Antarctic Ice Sheet is considered to have been relatively stable over long periods since its formation approximately 34 Ma but recent evidence [e.g. *Gallagher et al.*, 2013; *Young et al.*, 2011] points to potential instabilities during its existence. These potential instabilities may depend heavily on the dynamics of the subglacial water system [*Schoof*, 2010; see Figure 1.3], an active field of research in glaciology. Even though *Alley* [1989] set the paradigm for most modern numerical glacio-hydrological models by influentially

stating the importance of groundwater transport to be minimal, he only was doing so because the system he and most of those that followed looked at was in an area of faster sliding ice (i.e. where subglacial water pressure is high: mountain glaciers and ice streams [e.g. *Weertman*, 1966, 1972; *Lliboutry*, 1968; *Röthlisberger*, 1972; *Shreve*, 1972; *Nye*, 1976; *Walder*, 1986; *Creyts and Schoof*, 2009; *Hewitt*, 2011; *Kingslake and N*g, 2013; *Werder et al.*, 2013; *Flowers*, 2015]). Because few in the subglacial research community are concerned with regions of ice sheets where sliding speeds are so low or non-existent (i.e. where subglacial water pressure is low [e.g. *Rémy et al.*, 2003; *Wingham et al.*, 2006; *Carter et al.*, 2009a; *Livingstone et al.*, 2013; *Wright et al.*, 2012, 2014]), it makes sense that groundwater transport is usually not a concern for numerical models of subglacial hydrology. However, because there are vast areas in East Antarctica where sliding speed at the base is near or at zero and meltwater (generally <10 mm/yr; Figure 1.4) is assumed to only exist at the base of the ice sheet, this presents an opportunity for new hypotheses to be tested. It is also important to note that it has been documented that subglacial groundwater has been attributed to the anomalous heat input into the ice without necessarily coming in contact with it [*Clarke et al.*, 1984; *Echelmeyer*, 1987] which has broad implications that have not been fully explored by the glaciological community.

Nearly all work dealing with the interaction of ice sheets and hydrogeologic systems has been to infer or estimate what effect ice sheets have on groundwater flow but almost none that do the reverse. Over the past few decades, there have been a steady number of studies done on the effect of continental ice sheets on the groundwater flowing underneath them [*Boulton et al.*, 1993, 1995; *Piotrowski*, 1997; *Breemer et al.*, 2002; *Person et al.*, 2007; *Lemieux et al.*, 2008]. Most have simply modeled the presence of the ice sheet by adding pressure to the water equal to some great fraction of the total force of the ice above [e.g. *Person et al.*, 2003; *Sykes et al.*, 2011] or as a constant water flux boundary condition [e.g. *Boulton et al.*, 1995; *Van Weert et al.*, 1997]. Still, others have constructed more elaborate and complex models that incorporate the transport of heat for

tracking transient permafrost features [e.g. *Bense and Person*, 2008] and/or isostatic effects on the aquifer to compensate for a dynamic ice mass above [*Neuzil*, 2012]. Some have even attempted to implicitly couple ice sheet model outputs as updated boundary conditions to their groundwater models [*Lemieux et al.*, 2008]. Most of these studies conclude in a similar manner revealing that the regional flow directions are largely reversed and magnitudes slowed considerably after becoming deglaciated, i.e. losing the added pressure. All of these studies benefited from the amount of subsurface geologic characterization for their respective locations due to a relative abundance of drilling information but lacked the detailed information of the precise ice sheet geometry in the past whereas my research faces the opposite reality. *Flowers et al.* (2005) represents the only known example to me of a true attempt at simultaneously coupling ice sheet dynamics with a basal hydrologic system that incorporates interface water flow to groundwater flow. While the model treats the change of ice as a three-dimensional problem, it handles both of the basal water systems as vertically averaged ones that effectively reduce them from three to two dimensions. The model also does not explicitly transport heat in the subsurface. The groundwater system in the model is implied to being an important drainage mechanism under at least part of the Vatnajokull ice cap in Iceland but not clearly as a mechanism that directly or indirectly affects ice behavior.

There is, however, little known about the geologic subsurface of East Antarctica. Numerous geologic configurations of East Antarctica have been proposed despite the sparse direct sampling of the surface geology due to high costs and efforts in ice drilling. Most of the proposed ideas for the subglacial geology of East Antarctica come from interpretations of geophysical data [e.g. *Ferraccioli et al.*, 2009; *Goodge and Finn*, 2010; *Aitken et al.*, 2014], tectonic reconstructions with given knowledge from formerly contiguous landmasses [e.g. *Dalziel*, 1991; *Goodge et al.*, 2010; *Boger*, 2011], geologic analyses of sparse mountain outcrops [*Goodge and Finn,* 2010], and from offshore submarine fan deposits sampled by research vessels [*Goodge and Fanning*, 2010;

Veevers and Saeed, 2011]. The geologic history of the area is long and complex as it spans as far back as Paleoproterozoic to Archean age cratonic rocks, mostly in the center known as the Mawson Craton [*Aitken et al.*, 2014; *Boger*, 2011], to sedimentary basins (surrounding or laying inside the craton) disturbed by glacial advance and retreat since the Oligocene [e.g. *Young et al.*, 2011; *Frederick*, 2015]. Most tectonic hypotheses of defining the geology of East Antarctica stem from plate tectonic reconstructions. The geology in the area of the Great Australian Bight is considered to be most directly analogous due to its proximal connection to Wilkes Land before the late Mesozoic and seemingly traceable fault line structure across the rift margin of the Southern Ocean [*Gibson et al.*, 2013]. Based on existing work on this topic, locations of the basic delineation between probable crystalline and sedimentary structure, along with fault zone locations, are possible on a regional-to-basin scale. The addition of subglacial bed roughness data from ice penetrating radar is an important tool to assist with the interpretation as "smoother" beds likely represent different eroded geology than "rougher" ones [*Shepard et al.*, 2001; *Siegert et al.*, 2005; *Li et al.*, 2010]. With this information, it is also possible to roughly estimate the general hydraulic properties (i.e. very impermeable vs. likely permeable) of the subsurface of East Antarctica.

1.2 RESEARCH QUESTION – DOES GROUNDWATER TRANSPORT HAVE A SIGNIFICANT EFFECT ON THE DYNAMICS OF AN ICE SHEET, SPECIFICALLY THE EAST ANTARCTIC ICE SHEET?

My research sought to answer how significant groundwater is to the dynamics of ice sheets, specifically, the East Antarctic Ice Sheet. In particular, my research focuses on the dynamics of the deep interior ice over the large subglacial basins of the East Antarctic Ice Sheet (Figure 1.2), the largest and likely longest-lived ice body currently resident on the Earth. My work also looks into the relative contribution of groundwater to the ice sheet dynamics near the grounding line. The amount of water in the East Antarctic Ice Sheet is equivalent to about 60 meters of sea level rise [*Williams and Hall*, 1993] and the amount in the particular submarine basins of interest (Aurora and Wilkes

Subglacial Basins; Figure 1.2) are at about 15 meters of sea level [*Fox*, 2010]. The average annual ice surface temperatures are some of the coldest recorded and sees very little surface melt on top of its average 2-4 km thick ice, meaning that the subglacial bed is largely disconnected and insulated from the surface. The elevations in some of the subglacial basins represent the lowest bed surface elevations in Antarctica. Adding to an already poorly constrained geothermal heat flux, radiogenic heat-producing rock bodies exist across the passive margin from East Antarctica in the South Australian Heat Flow Anomaly which are among the highest heat producing granites in the world [*McLaren et al.*, 2003; *Carson et al.*, 2013]. Highly heterogeneous crustal heat fluxes at the likely scales also observed in Australia are currently not incorporated into numerical ice sheet models.

As I previously mentioned, very little research has shown the effect that groundwater flow has on a continental ice sheet. Most studies have focused on the effect past ice sheets could have had on groundwater systems in areas of well-studied aquifers that are no longer glaciated [see the thorough review from *Person et al.*, 2012] and none that deal with a currently ice-covered continent such as East Antarctica. There is a possibility that groundwater could contribute heavily to the subglacial water system and to the overlying ice sheet's dynamics, including a major driver of subsurface heat transfer. For my research, I sought to explore how significant this process is in the dynamics of ice sheets, specifically, the East Antarctic Ice Sheet. My main research interest and its importance to society is the relevance of groundwater in potential ice instabilities, which depend heavily on the dynamics of the subglacial water system, in the East Antarctic Ice Sheet that will likely contribute to sea-level rise.

1.3 General Hypothesis – Groundwater Affects East Antarctic Ice Dynamics via Adjustment of the Subglacial Hydrologic System and Heat Flux at the Ice Base

For my research question, I hypothesized that groundwater transport has the potential to carry and redistribute meltwater from the base of the ice, as well as, affect the melt rates of the interior of the East Antarctic Ice Sheet which should lead to measurable changes in the sliding and deformation speed of the ice sheet. In subglacial hydrological models (Figure 1.3), adding a groundwater flow domain would allow for the storage of water that would otherwise only be modeled inside a thin porous sheet or in a channelized manner at the base of the ice, typical of the current approach in the literature [e.g. *Walder and Fowler*, 1994; *Creyts and Schoof*, 2009; *Le Brocq et al.*, 2009; *Hewitt*, 2011; *Goeller et al.*, 2012; *Schoof et al.*, 2012; *Werder et al.*, 2013]. This added domain should allow basin-scale water volumes that are rarely factored into the modeled hydrologic budgets of ice sheet meltwater. That addition should have a substantial effect on the way subglacial drainage works in the interior of the East Antarctic Ice Sheet because water can drain into the subsurface instead of having to be routed entirely along a thin interface. The flow of water could essentially work around sections of the bed that are frozen and are not a path for subglacial water flow. The potential input of water back into the basal hydrologic system would likely be orders of magnitude higher than the current estimated basal melt rates for the deep interior of the East Antarctic Ice Sheet and would affect the basal sliding velocity of the ice. This subsurface transport mechanism would also alter the flow of geothermal heat to the base of the ice by advecting heat through permeable zones underneath the ice in porous rock or sediment. The alteration of the geotherm would result in the redistribution and warming (or cooling) of water that could come into contact with the base of the ice in a more heterogeneous nature than if the subsurface flow mechanism was ignored entirely, which could lead to more heterogeneous basal melt rates. This would then affect the dynamics of the overlying ice sheet by effectively taking away mass from or adding more mass to the ice sheet and altering the thermal profile of the ice.

All of the above subsurface processes could also heavily change the rheology of unconsolidated sediments lying directly beneath the ice, such as a till deposit, which are temperature dependent thus altering the deformation rate of the sediments with the ice above it. *Alley* [1989] and others [e.g. *Alley et al.*, 1989; *Blankenship et al.*, 2001; *Bougamont and Tulacyzk*, 2003] have shown that the dynamics of till layers can directly affect the dynamics of the ice above, specifically through sliding or shear velocity modulation. This is another way in which the addition of subsurface flow modeling to a general basal hydrology model could indirectly demonstrate the neglected factors' importance in causing a change in ice dynamics.

1.4 General Approach to Test Groundwater Hypothesis and Scope of Chapters

To test the general hypothesis of groundwater's significance on the dynamics of the East Antarctic Ice Sheet, I created numerical models of varying levels of complexity based on the most current geological and geophysical datasets and using very conservative assumptions for the hydraulic properties. To create these numerical models, I solely used COMSOL (COMSOL, Inc.), which is commercial numerical modeling software for solving multiphysics differential equations using the finite element method. COMSOL also has highly polished figure and graphics plotting functionality, which I used to produce many of the modeling results presented in the following chapters. I also used Geographic Information System software, both ArcGIS (ESRI, Inc.) and QGIS, for the analysis of geographic data. Finally, I used EXCEL (Microsoft Corporation) and MATLAB (The MathWorks, Inc.) to analyze data, plot theoretical values, pre-/post-process data, and produce figures that required a higher level of customization than COMSOL could accommodate. I will briefly discuss the following chapters, each of which is a stand-alone article submitted to a peer-reviewed journal, that I was the lead author on and wrote myself. My co-authors did however help with various technical issues and reviews of the final manuscripts. Each of these chapters is in line with the over-arching goal of testing my general hypothesis (Section 1.3).

In my first approach highlighted in Chapter 2 [submitted as Gooch et al. (in review) *The Cryosphere Discussions*], I compared the water volume fluxes of groundwater, given a large span of hydraulic properties possible for the central East Antarctic interior geology (see Table 1.1), to basal ice melt rates. I also compared the transmissivities of hypothetical groundwater systems to water sheet systems. From those, I made the observation that groundwater systems have the ability to handle most or all of the basal meltwater produced in the interior of the East Antarctic Ice Sheet, specifically near Dome C (Figure 1.1). Given that theoretical foundation, I produced a novel groundwater model combining steady groundwater flow and a basal water sheet system. I then was able to compare the results of various parameterizations to observe how the water sheet responded to different groundwater forcings. I also compared the actual transmissivities of the groundwater and water sheet systems. Additionally, I looked at how the water sheet patterns compared to basal radar reflections, which are heavily dependent on the presence of subglacial water.

I then chose to look at how groundwater systems interact with other geologic processes, specifically geomechanics (i.e. hydromechanical effects) and geothermal heat flow (i.e. heat advection via porewater), which is documented in Chapter 3 [published as Gooch et al. (2016) in *Geochemistry, Geophysics, Geosystems*]. I created very simple, diagnostic one-dimensional numerical models of vertical heat flux for a column consisting of the lithosphere and a two-phase cryosphere (i.e. water and ice, dependent on temperature) where I applied various groundwater flux forcings to observe how the basal heat flux would be altered. Then I modeled a subset of the domain, the sedimentary basin, for its transient behavior due to an evolving ice column (modeled as a hydraulic forcing function at the ice/bed interface) to observe how the subsurface would hydromechanically respond to changing ice thickness. Finally, I integrated various geochemical and geophysical datasets, along with previously published tectonic interpretations, from East Antarctica and Australia to roughly map where groundwater

processes would have the most likely impact on ice dynamics (similar to the modeled processes) and visualize the heterogeneity in the radiogenic heat production of the East Antarctic crust.

In Chapter 4 [to be submitted as Gooch et al. (in preparation) *Journal of Geophysical Research*], I demonstrate how I combined what I learned from the previous chapter's results to produce a dynamic, two-dimensional ice sheet model (steady flowline) with subglacial hydrology coupled to hypothetical groundwater systems. The ice sheet model is a fully thermomechanical, Stokes flow representation of the ice sheet flowline attached to the lithospheric section (including estimated sedimentary basins) down to the top of the asthenosphere (i.e. known temperature boundary). The flowline selected is a subglacial water flowpath that parallels surface ice sheet motion from the ice divide through the Totten Glacier Catchment to the grounding line under Totten Glacier (Figure 1.1). These groundwater systems, which were parameterized as a high and extremely low level of permeability (i.e. groundwater flux), acted as a forcing function on the ice sheet dynamics. The model also contains a sliding function based on the subglacial water system, which I turned on and off to observe what impact groundwater had on the sliding function as well as the ice sheet dynamics.

1.5 FIGURES AND TABLES

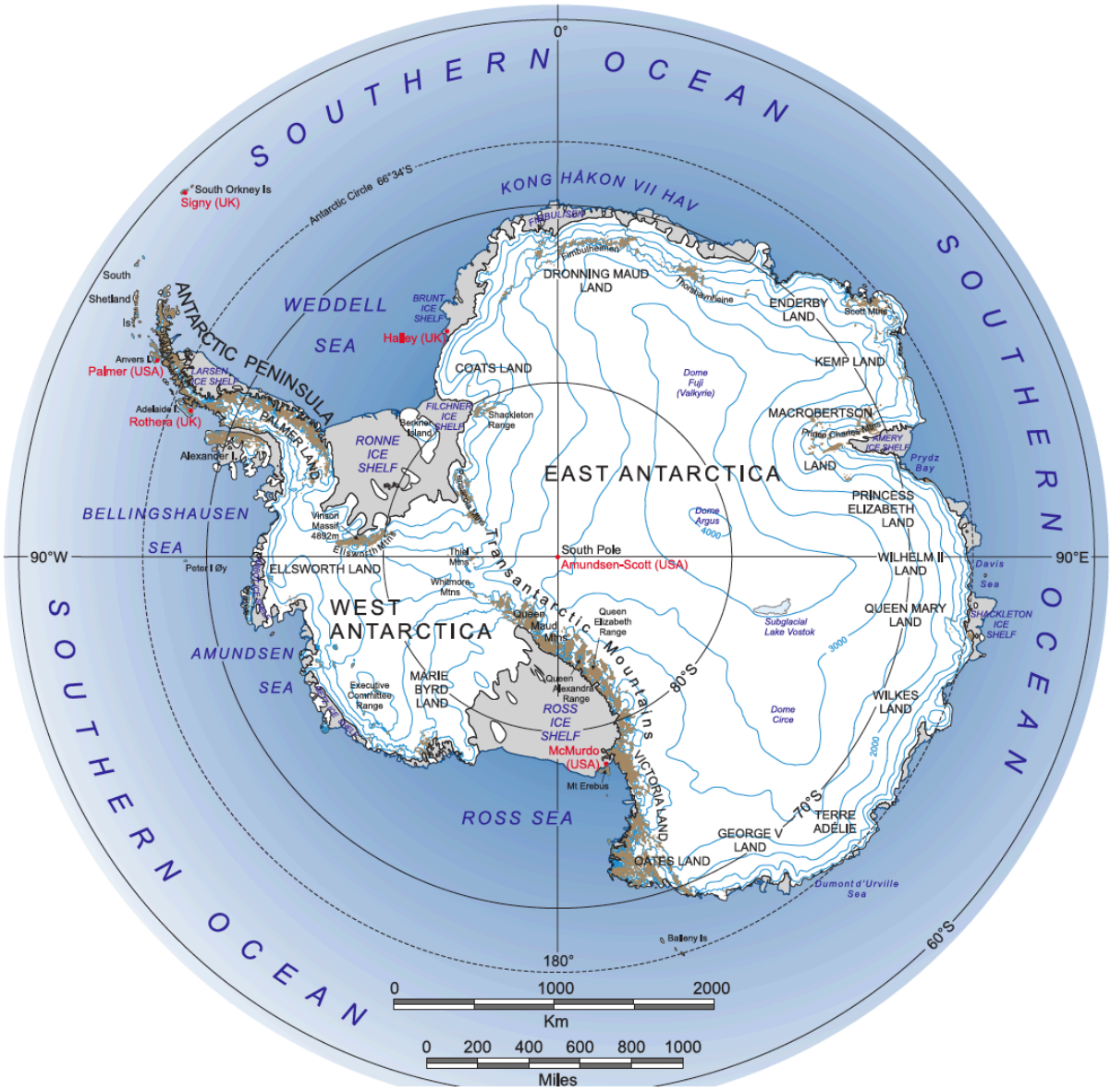

Figure 1.1. Geographic map of Antarctica with the West and East Antarctic Ice Sheets shown [*British Antarctic Survey*, 2007]. The brown shaded areas are those containing exposed rock and the gray shaded areas are ice shelves. The main areas of interest in East Antarctica lie from Oates Land to Wilkes Land and into the interior past Dome C (Circe or Concordia). The ice shelf near Wilkes Land is the Totten Glacier Ice Shelf.

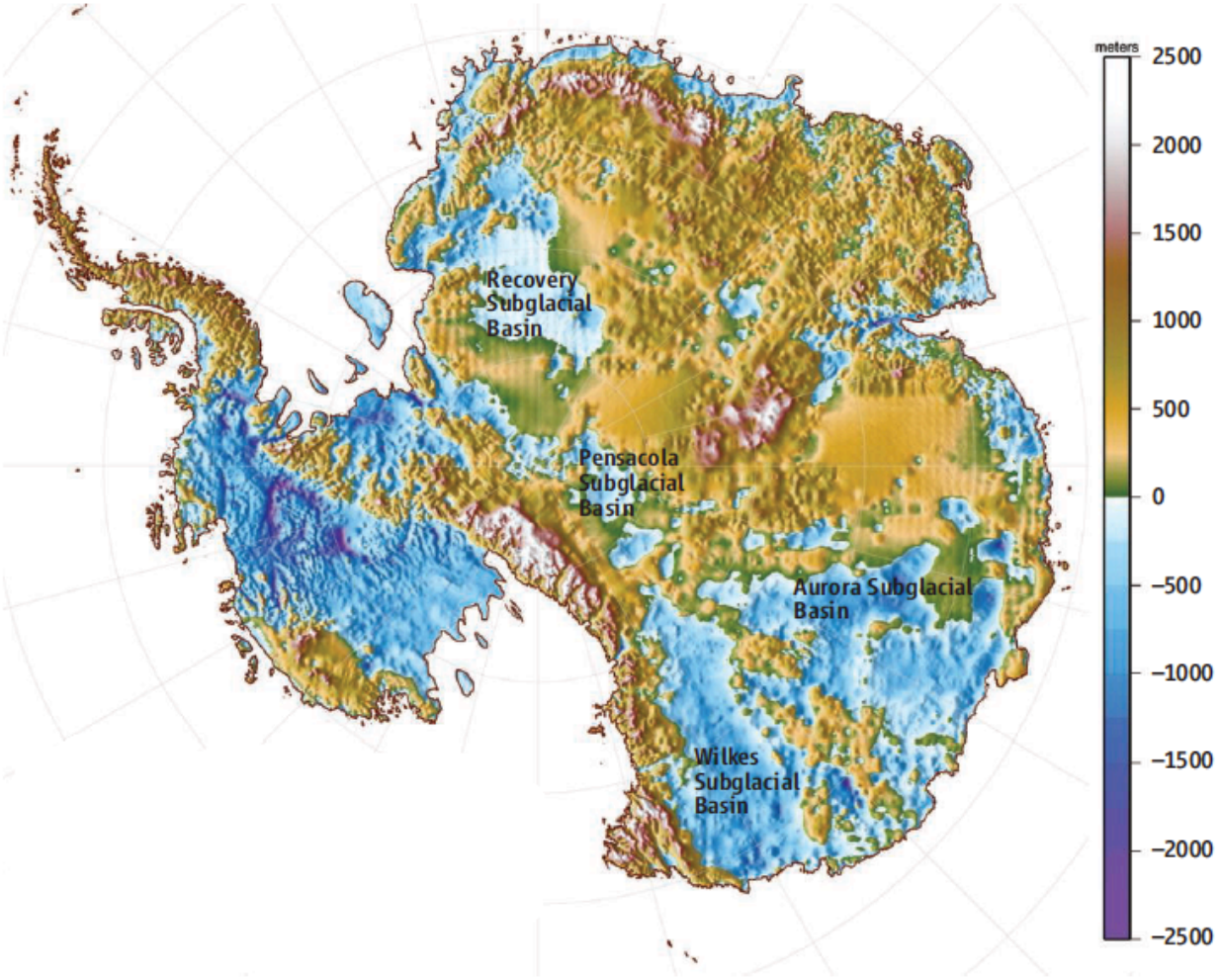

Figure 1.2. Estimated bed elevation map of Antarctica with the various subglacial basins listed, such as the Wilkes and Aurora, which are mentioned in the text [*Fox*, 2010]. Elevation is in meters above present sea level.

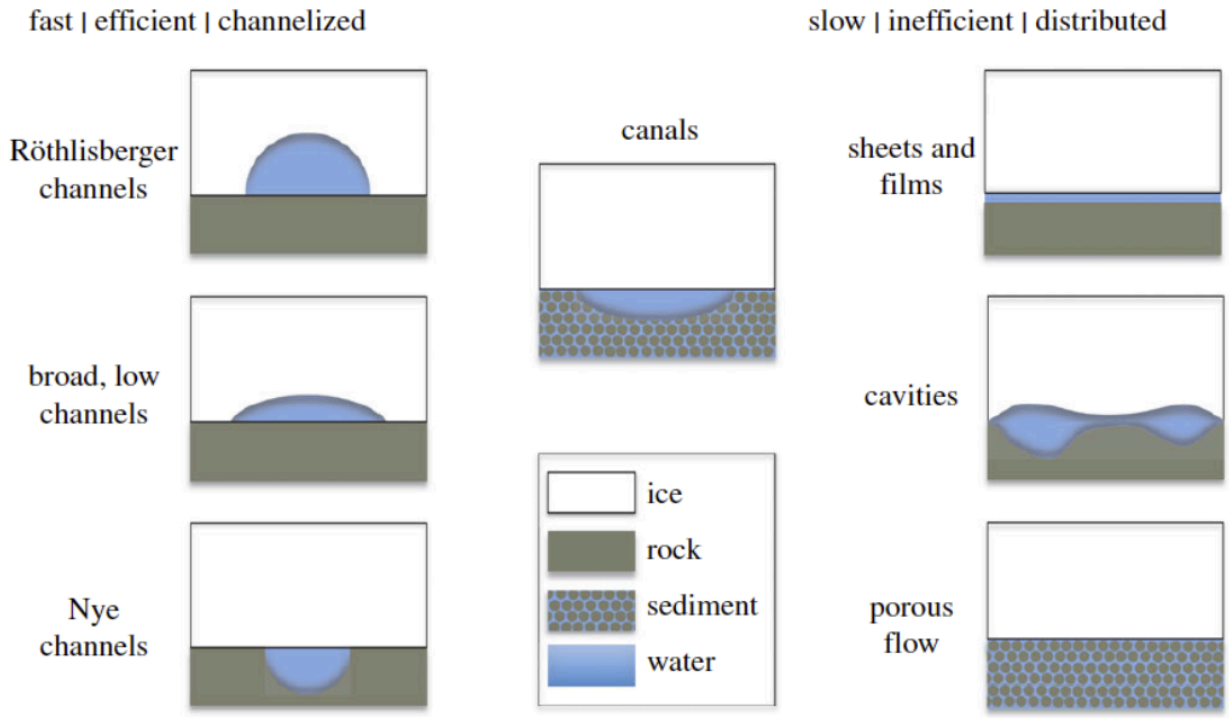

Figure 1.3. Various cross-sectional models of subglacial hydrological flow systems from *Flowers* [2015].

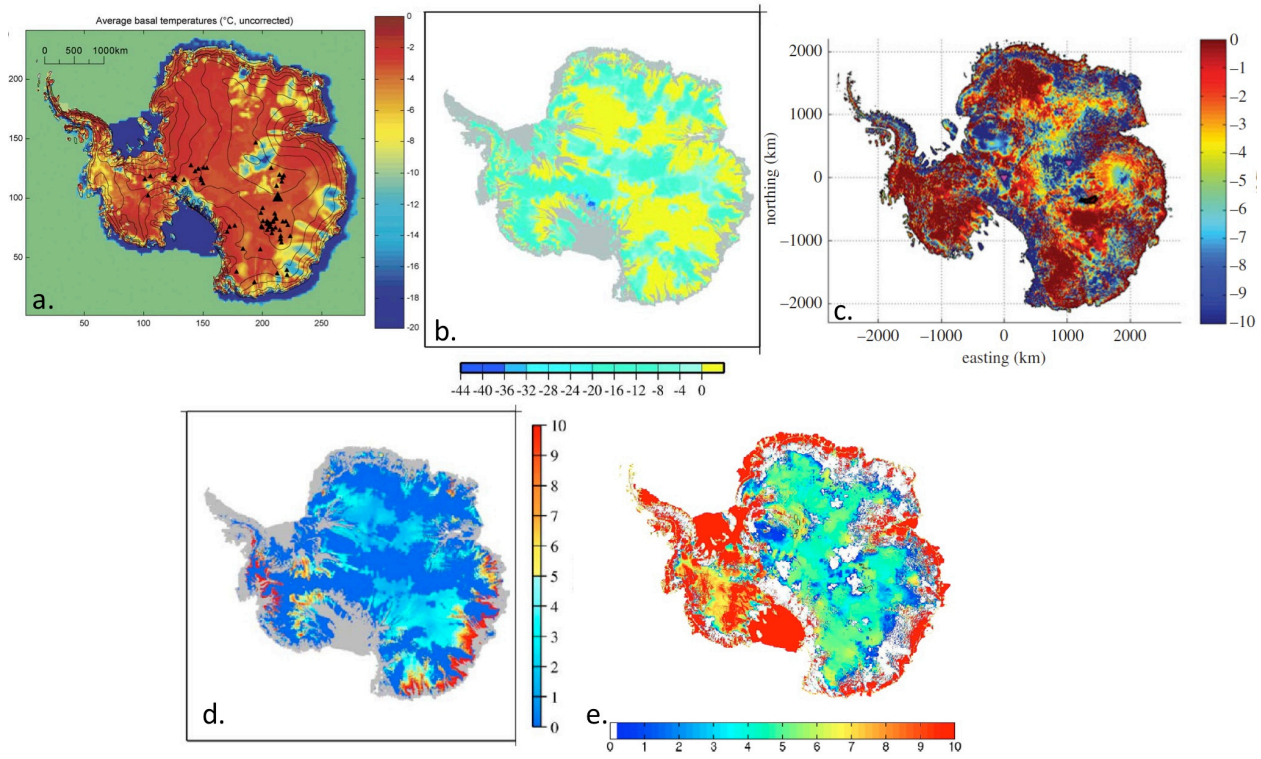

Figure 1.4. (a) Modeled basal temperature of Antarctica (in °C), not corrected for pressure [*Siegert et al.*, 2005]. (b) Modeled basal temperature (in °C), corrected for pressure [*Llubes et al.*, 2006] (c) Modeled basal temperature (in °C), corrected for pressure [*Pattyn et al.*, 2015]. (d) Modeled basal melt rates in mm/yr of water [*Llubes et al.*, 2006]. (e) Modeled basal melt rates in mm/yr of water (truncated at 10 mm/yr) [*Pattyn*, 2010].

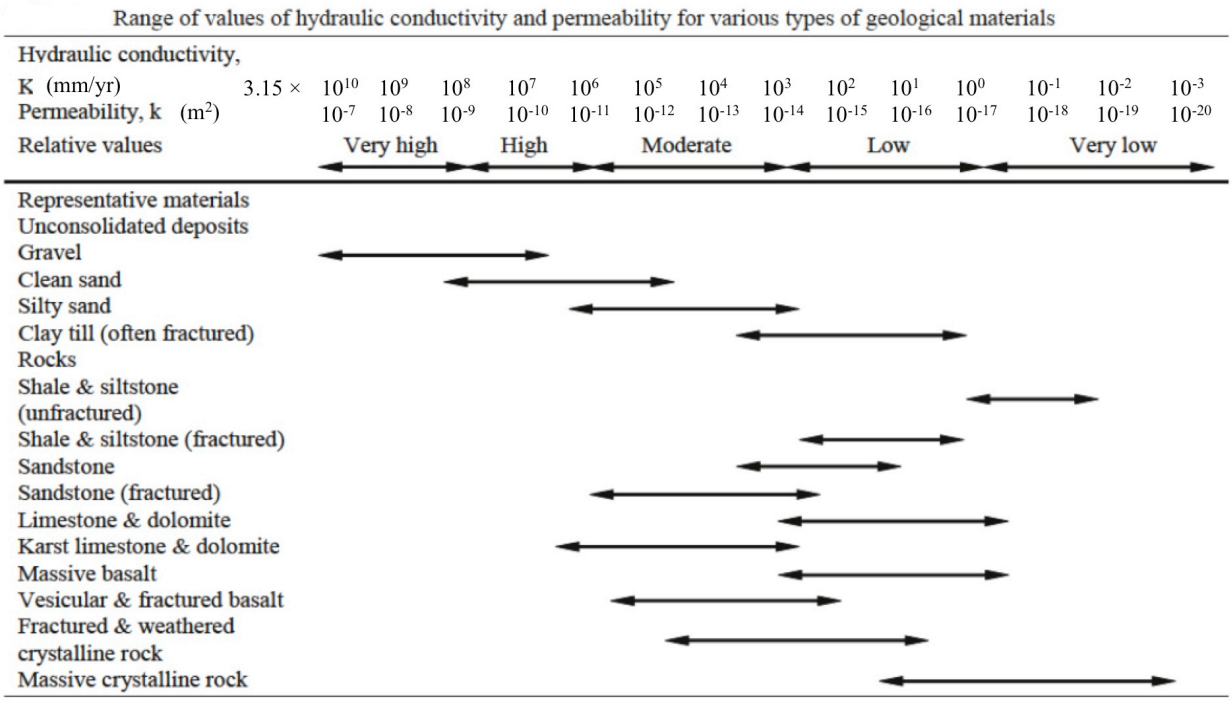

Table 1.1. Hydraulic properties for a range of geologic materials. Modified from *Singhal and Gupta* [Table 8.2; 2010] on the basis that 1 darcy ≈ 10^{-12} m^2 and 1 m/s ≈ 3.15×10^{10} mm/year.

1.6 REFERENCES

Aitken, A. R. A., D. A. Young, F. Ferraccioli, P. G. Betts, J. S. Greenbaum, T. G. Richter, J. L. Roberts, D. D. Blankenship, and M. J. Siegert (2014), The subglacial geology of Wilkes Land, East Antarctica, Geophys. Res. Lett., 41, 2390–2400.

Alley, R. B., D. D. Blankenship, C. R. Bentley, and S. T. Rooney (1986), Deformation of Till beneath Ice Stream-B, West-Antarctica, Nature, 322(6074): 57-59.

Alley, R. B. (1989), Water-pressure coupling of sliding and bed deformation: I. Water system, J. Glaciol., 35(119), 108–118.

Bense, V. F., and M. A. Person (2008), Transient hydrodynamics within intercratonic sedimentary basins during glacial cycles, J. Geophys. Res., 113(F4), F04005, doi:10.1029/2007JF000969.

Blankenship, D. D., C. R. Bentley, S. T. Rooney and R. B. Alley (1986), Seismic Measurements Reveal a Saturated Porous Layer beneath an Active Antarctic Ice Stream, Nature 322(6074): 54- 57.

Blankenship, D. D., et al. (1993), Active volcanism beneath the West Antarctic ice sheet and implications for ice-sheet stability. Nature 361, 526–529.

Boger, S. D. (2011), Antarctica—Before and after Gondwana, Precam. Res., 19, 335–371, doi: 10.1016/j.gr.2010.09.003.

Boulton, G. S., T. Slot, K. Blessing, P. Glasbergen, T. Leijnse, and K. van Gijssel (1993), Deep circulation of groundwater in overpressured subglacial aquifers and it's geological consequences, Quat. Sci. Rev., 12, 739–745.

Boulton, G. S., P. B. Caban, and K. van Gijssel (1995), Groundwater flow beneath ice sheets: Part I—Large scale patterns, Quat. Sci. Rev., 14, 545–562.

British Antarctic Survey: Antarctica Overview Map, (2007), http://lima.usgs.gov/documents/LIMA_overview_map.pdf, accessed: 2016-03-19.

Breemer, C. H., P. U. Clark, and R. Haggerty (2002), Modeling the subglacial hydrology of the late Pleistocene Lake Michigan lobe, Laurentide Ice Sheet, Geol. Soc. Am. Bull., 114(6), 665–674.

Carson, C. J., S. McLaren, J. L. Roberts, S. D. Boger, and D. D. Blankenship (2013), Hot rocks in a cold place: high sub-glacial heat flow in East Antarctica, J. Geol. Soc. London., 171(1), 9–12.

Carter, S. P., D. D. Blankenship, D. A. Young, and J. W. Holt (2009), Using radar-sounding data to identify the distribution and sources of subglacial water: Application to Dome C, East Antarctica, J. Glaciol., 55(194), 1025–1040, doi:10.3189/002214309790794931.

Clarke, G. K. C., S. G. Collins, and D. E. Thompson (1984), Flow, thermal structure, and subglacial conditions of a surge-type glacier, Can. J. Earth Sci., 21, 232–240.

Clarke, G. K. C. (1987), Subglacial till: A physical framework for its properties and processes, J. Geophys. Res., 92, 9023–9037.

Creyts, T. T., and C. G. Schoof (2009), Drainage through subglacial water sheets, J. Geophys. Res., 114, F04008, doi:10.1029/2008JF001215.

Dalziel, I. W. D. (1991), Pacific margins of Laurentia and East Antarctica-Australia as a conjugate rift pair: Evidence and implications for an Eocambrian supercontinent, Geology, 19, 598–601.

Echelmeyer, K. (1987), Anomalous heat flow and temperatures associated with subglacial water flow, The Physical Basis of Ice Sheet Modelling (Proceedings of the Vancouver Symposium, August 1987). IAHS Publ. no. 170.

Fahnstock, M., W. Abdalati, I. Joughin, J. Brozena, and P. Gogineni (2001), High geothermal heat flow, basal melt and the origin of rapid ice flow in central Greenland, Science, 294, 2338–2342.

Ferraccioli, F., E. Armadillo, T. Jordan, E. Bozzo, and H. Corr (2009), Aeromagnetic exploration over the East Antarctic Ice Sheet: A new view of the Wilkes Subglacial Basin, Tectonophysics, 478(1-2), 62–77.

Flowers, G. E., S. J. Marshall, H. Björnsson, and G. K. C. Clarke (2005), Sensitivity of Vatnajökull ice cap hydrology and dynamics to climate warming over the next 2 centuries, J. Geophys. Res. Earth Surf., 110(F2), F02011.

Flowers, G. E. (2015), Modelling water flow under glaciers and ice sheets, Proc. A, (471).

Fox, D. (2010), Could East Antarctica be headed for big melt?, Science, 328(June), 1630–1631.

Frederick, B. C. (2015), Submarine Sedimentary Basin Analyses for the Aurora and Wilkes Subglacial Basins and the Sabrina Coast Continental Shelf, East Antarctica, Ph.D. dissertation, Univ. of Texas, Austin, Texas, USA.

Fretwell, P., et al. (2013), Bedmap2: Improved ice bed, surface and thickness datasets for Antarctica, The Cryosphere, 7, 375–393, doi:10.5194/tc-7-375-2013.

Gallagher, S. J., G. Villa, R. N. Drysdale, B. S. Wade, H. Scher, Q. Li, M. W. Wallace, and G. R. Holdgate (2013), A near-field sea level record of East Antarctic Ice Sheet instability from 32 to 27 Myr, Paleoceanography, 28, doi: 10.1029/2012PA002326

Gibson, G.M., J.M. Totterdell, L.T. White, C.M. Mitchell, A.R. Stacey, M.P. Morse, and A. Whitaker (2013), Pre-existing basement structure and its influence on continental

rifting and fracture zone development along Australia's southern rifted margin, J. Geol. Soc., 170, 365–377.

Glen, J.W., (1955), The creep of polycrystalline ice, Proc. Roy. Soc. Lond. A228 (1175), 519–538.

Goeller, S., M. Thoma, K. Grosfeld, and H. Miller (2012), A balanced water layer concept for subglacial hydrology in large scale ice sheet models, The Cryosphere, 6(6), 5225–5253, doi:10.5194/tcd-6-5225-2012.

Gooch, B. T., D. A. Young, and D. D. Blankenship (2016), Potential groundwater and heterogeneous heat source contributions to ice sheet dynamics in critical submarine basins of East Antarctica, Geochem. Geophys. Geosyst., 17, doi:10.1002/2015GC006117.

Gooch, B.T., S. P. Carter, O. Ghattas, D. A. Young, and D. D. Blankenship (in review), Groundwater dominance in the subglacial hydrology of ice sheet interiors: example at Dome C, East Antarctica, The Cryosphere Discuss.

Gooch, B.T., M. Rückamp, D. A. Young, and D. D. Blankenship (in preparation), Groundwater impact on the Totten Glacier Catchment basal water system: Results of a thermomechnical ice sheet model, J. Geophy. Res. Earth Surf.

Goodge, J. W., and C. M. Fanning (2010), Composition and age of the East Antarctic Shield in eastern Wilkes Land determined by proxy from Oligocene-Pleistocene glaciomarine sediment and Beacon Supergroup sandstones, Antarctica, Geological Society of America Bulletin, 122(7-8), 1135–1159, doi:10.1130/B30079.1.

Goodge, J. W., C. M. Fanning, D. M. Brecke, K. J. Licht, and E. F. Palmer (2010), Continuation of the Laurentian Grenville Province across the Ross Sea Margin of East Antarctica, The Journal of Geology, 118(6), 601–619, doi:10.1086/656385.

Goodge, J. W., and C. A. Finn (2010), Glimpses of East Antarctica: Aeromagnetic and satellite magnetic view from the central Transantarctic Mountains of East Antarctica, Journal of Geophysical Research, 115(B9), B09103, doi:10.1029/2009JB006890

Hewitt, I. (2011), Modelling distributed and channelized subglacial drainage: The spacing of channels, J. Glaciol., 57(202), 302–314, doi:10.3189/002214311796405951.

Kingslake J, and F. Ng (2013), Modelling the coupling of flood discharge with glacier flow during jökulhlaups, Ann. Glaciol. 54, 25–31, doi:10.3189/2013AoG63A331.

Le Brocq, A., A. Payne, M. Siegert, and R. Alley (2009), A subglacial water-flow model for West Antarctica, J. Glaciol., 55(193), 879–888.

Lemieux, J. M., E. A. Sudicky, W. R. Peltier, and L. Tarasov (2008), Dynamics of groundwater recharge and seepage over the Canadian landscape during the Wisconsinian glaciation, J. Geophys. Res. Earth Surf., 113(F1), F01011.

Li, X., B. Sun, M. J. Siegert, R. G. Bingham, X. Tang, D. Zhang, X. Cui, and X. Zhang (2010), Characterisation of subglacial landscapes by a two-parameter roughness index, J. Glaciol., 56, 831–836, doi:10.3189/ 002214310794457326.

Livingstone, S. J., C. D. Clark, J. Woodward, and J. Kingslake (2013), Potential subglacial lake locations and meltwater drainage pathways beneath the Antarctic and Greenland ice sheets, The Cryosphere, 7(6), 1721–1740, doi:10.5194/tc-7-1721-2013.

Lliboutry, L. (1968), General theory of subglacial cavitation and sliding of temperate glaciers. J. Glaciol., 7(49), 21-58.

Llubes, M., C. Lanseau, and F. Remy (2006), Relations between basal condition, subglacial hydrological networks and geothermal flux in Antarctica, Earth Planet. Sci. Lett., 241(3-4), 655–662, doi:10.1016/j.epsl.2005.10.040.

McLaren, S., M. Sandiford, M. Hand, N. Neumann, L. Wyborn, and I. Bastrakova (2003), The hot southern continent; heat flow and heat production in Australian Proterozoic terranes, Spec. Pap. - Geol. Soc. Am., 372, 157–167.

Mellor, M. and R. Testa (1969). Effect of temperature on the creep of ice. Journal of Glaciology, 8:131–145.

Neuzil, C. E. (2012), Hydromechanical effects of continental glaciation on groundwater systems, Geofluids, 12(1), 22-37.

Nye, J. F. (1976) Water flow in glaciers: Jökulhlaups, tunnels and veins, J. Glaciol., 17, 181–207.

Pattyn, F. (2010), Antarctic subglacial conditions inferred from a hybrid ice sheet/ice stream model, Earth Planet. Sci. Lett., 295(3-4), 451–461, doi:10.1016/j.epsl.2010.04.025.

Pattyn, F., S. Carter, and M. Thoma (2015), Advances in modelling subglacial lakes and their interaction with the Antarctic ice sheet, Phil. Trans. R. Soc.

Person, M., B. Dugan, J. B. Swenson, L. Urbano, C. Stott, J. Taylor, M. Willett (2003) Pleistocene hydrogeology of the Atlantic continental shelf, New England. Geo. Soc. of America Bulletin, 115, 1324–43.

Person, M., J. McIntosh, V. Bense, and V. H. Remenda (2007), Pleistocene hydrology of North America: The role of ice sheets in reorganizing groundwater flow systems, Rev. Geophys., 45(3), RG3007.

Person, M., V. Bense, D. Cohen, and A. Banerjee (2012), Models of ice-sheet hydrogeologic interactions: A review, Geofluids, 12(1), 58–78.

Piotrowski, J. (1997), Subglacial hydrology in north-western Germany during the last glaciations: Groundwater flow, tunnel valleys and hydrological cycles, Quat. Sci. Rev., 16, 169–185.

Rémy, F., T. Laurent, B. Legresy, A. Forieri, C. Bianchi, and I. E. Tabacco (2003), Lakes and subglacial hydrological networks around Dome C, East Antarctica, Ann. Glaciol., 37, 252–256.

Röthlisberger, H. (1972), Water pressure in intra- and subglacial channels, J. Glaciol., 11(62), 177–203.

Schoof, C. (2010), Ice-sheet acceleration driven by melt supply variability, Nature, 468(7325), 803–806, doi:10.1038/nature09618.

Schoof, C., I. J. Hewitt, and M. A. Werder (2012), Flotation and free surface flow in a model for subglacial drainage. Part 1. Distributed drainage, Journal of Fluid Mechanics, 702, 126–156, doi:10.1017/jfm.2012.165.

Shepard, M. K., B. A. Campbell, M. H. Bulmer, T. G. Farr, L. R. Gaddis, and J. J. Plaut (2001), The roughness of natural terrain: A planetary and remote sensing perspective, J. Geophys. Res., 106, 32,777–32,795.

Shreve, R. L. (1972), Movement of water in glaciers, J. Glaciol., 11(62), 205–214.

Siegert, M. J., J. P. Taylor, and J. Antony (2005), Spectral roughness of subglacial topography and implications for former ice-sheet dynamics in East Antarctica, Global Planet. Change, 45, 249–263.

Singhal, B. B. S., and R. P. Gupta (2010), Applied hydrogeology of fractured rocks (Vol. 430). New York: Springer.

Stearns, L., B. Smith, and G. Hamilton (2008), Increased flow speed on a large East Antarctic outlet glacier caused by subglacial floods, Nat. Geosci., 1(12), 827–831, doi:10.1038/ngeo356.

Sykes J, S. Normani, and Y. Yin (2011), OPG's deep geologic repository for low and intermediate level nuclear waste, NWMO DGR-TR- 2011-16, 256 P.

Tulaczyk, S., W. B. Kamb, and H. F. Engelhardt (2000), Basal mechanics of ice stream B, West Antarctica 2. Undrained plastic bed model, J. Geophys. Res, 105, 483–494.

van Weert, F. H. A., K. van Gijssel, A. Leijnse, and G. S. Boulton (1997), The effects of Pleistocene glaciations on the geohydrological system of northwest Europe, J. Hydrol., 195(1–4), 137–159.

Veevers, J. J., and A. Saeed (2011), Age and composition of Antarctic bedrock reflected by detrital zircons, erratics, and recycled microfossils in the Prydz Bay-Wilkes Land-

Ross Sea-Marie Byrd Land sector (70°–240°E), Gondwana Res., doi: 10.1016/j.gr.2011.03.007.

Walder, J. (1986), Hydraulics of subglacial cavities, J. Glaciol., 32(112), 439–445.

Walder, J. S., and A. Fowler (1994), Channelized subglacial drainage over a deformable bed, J. Glaciol., 40(134), 3–15.

Weertman, J. (1966), Effect of a basal water layer on the dimensions of ice sheets, J. Glaciol., 6(44), 191–207.

Weertman, J. (1972), General theory of water flow at the base of a glacier or ice sheet, Rev. Geophys., 10(1), 287–333, doi:10.1029/RG010i001p00287.

Werder, M. A., I. J. Hewitt, C. G. Schoof, and G. E. Flowers (2013), Modeling channelized and distributed subglacial drainage in two dimensions, J. Geophys. Res. Earth Surf., 118, 2140–2158, doi:10.1002/jgrf.20146.

Williams, R.S., and D. K. Hall (1993), Glaciers, in Atlas of Satellite Observations Related to Global Change, R. J. Gurney, J.L. Foster and C. L. Parkinson, Cambridge University Press, London, 401-422.

Wingham, D. J., M. J. Siegert, A. Shepherd, and A. S. Muir (2006), Rapid discharge connects Antarctic subglacial lakes, Nature, 440, 1033–1036, doi:10.1038/nature04660.

Wright, A. P., et al. (2012), Evidence of a hydrological connection between the ice divide and ice sheet margin in the Aurora Subglacial Basin, East Antarctica, J. Geophys. Res., 117, F01033, doi:10.1029/2011JF002066.

Wright, A. P., D. A. Young, J. L. Bamber, J. A. Dowdeswell, A. J. Payne, D. D. Blankenship, and M. J. Siegert (2014), Subglacial hydrological connectivity within the Byrd Glacier catchment, East Antarctica, J. Glaciol., 60(220), 345–352, doi:10.3189/2014JoG13J014.

Young, D. A., et al. (2011), A dynamic early East Antarctic Ice Sheet suggested by ice-covered fjord landscapes, Nature, 474(7349), 72–75.

Chapter 2: Possible groundwater dominance in the subglacial hydrology of ice sheet interiors: example at Dome C, East Antarctica[1]

Abstract

We hypothesize that groundwater systems may be the main water transport mechanism over (distributed, inefficient) water sheets at large scales in the interiors of ice sheets where melt rates are very low. We compare melt rate magnitudes to potential groundwater volume fluxes and also calculate the theoretical transmissivity ranges of subglacial water sheet and groundwater flow systems. Theoretical groundwater systems are on par with or more transmissive than water sheets for the upper half of the permeability spectrum. In addition, we develop a 2D flow path model that connects subglacial lakes near Dome C, East Antarctica. This model integrates subglacial water sheet flux and hypothetical groundwater flow forcing, better bridging two historically disparate modeling frameworks – subglacial hydrology and ice sheet hydrogeology. Our model results suggest that the water sheet thickness can be highly dependent on groundwater flux and that the water sheet transmissivity is within the total range of the modeled groundwater system transmissivity. We infer from these results that subglacial lake stability and basal radar reflections underneath the interior of East Antarctica may possibly be affected by groundwater flow.

2.1 Observations and Background Information

While much study has been given to the ways in which basal meltwater transports under faster flowing ice bodies (i.e. mountain glaciers and ice streams) (e.g. *Weertman* [1966] or *Shreve* [1972]; for review, see *Flowers* [2015]), relatively much less has been done to show how meltwater transports under the interiors of continental ice sheets like the East Antarctic Ice Sheet [e.g. *Carter et al.*, 2009a; *Wright et al.*, 2012, 2014].

[1] A version of this chapter was submitted as Gooch, B.T., S.P. Carter, O. Ghattas, D.A. Young, and D.D. Blankenship (in review), Possible groundwater dominance in the subglacial hydrology of ice sheet interiors: example at Dome C, East Antarctica, *The Cryosphere Discussions*.

Subglacial melt rates under the vast majority of the interiors of these kinds of ice sheets are estimated to be very low compared to the higher melting zones underneath ice streams (<10 mm/yr [*Pattyn*, 2010]). Some [e.g. *Creyts nad Schoof*, 2009] have modeled the transport of subglacial meltwater via water sheets sitting at the ice/bed interface while others [e.g. *Boulton and Jones*, 1979] have used groundwater flow through the porous sediment or bedrock. While porous groundwater flow is not capable of transporting the bulk of the meltwater underneath ice streams and outlet glaciers [*Alley*, 1989], those areas are a small fraction of the total area underneath the interiors of ice sheets like that present in East Antarctica. Groundwater systems could still be important in considering the flow of meltwater for much of the ice sheet interior and useful to consider in future continental ice sheet models. Ice sheets have been shown to affect regional-to-continental scale groundwater flow systems, which is a closely related field of active research [e.g. *Boulton et al.*, 1995; *Piotrowski*, 1997; *Person et al.*, 2007a; *Lemieux et al.*, 2008].

The presence of large and small subglacial lakes underneath the East Antarctic Ice Sheet (and West Antarctic) is now well established [*Wright and Siegert*, 2014]. Originally, subglacial lakes were thought of as long-lasting stable environments whose behavior impacted only the overlying ice and received their water entirely from local sources [*Tikku et al.*, 2005]. More recently, it has been shown that not only are subglacial lakes capable of releasing many cubic kilometers of water in a period of about a year [*Fricker et al.*, 2007], but that these periodic releases can significantly impact the flow of ice downstream [*Stearns et al.*, 2008]. Lake activity has been modeled as driven by thermodynamic and deformation processes concentrated at the ice/bed interface [*Carter et al.*, 2009b, 2015] – processes that will be less important in a groundwater-driven system. The observed filling rates for many of the lakes now known to underlie most of the fast-flowing ice streams appear to require meltwater input from the entire subglacial hydraulic catchment [*Carter et al.*, 2011], meaning that hydraulic processes in the uppermost part of the hydraulic catchment influence the quantity, chemistry, and biology

of water much further downstream. Consequently, a complete understanding of the subglacial hydraulic system begins with an examination of its headwaters.

Although much attention has recently focused on "active lakes" in fast flowing ice streams and outlet glaciers, the first lakes discovered in Antarctica were found close to the ice divides (i.e. slower ice) using radio-echo sounding (RES; also known as ice-penetrating radar). The criterion used to identify lakes with RES ("radar lakes") is a hydraulically flat, bright reflection of consistent reflectivity that is brighter than its surroundings [*Carter et al.*, 2007]. When this same criterion is applied to RES data from "active lakes" (with the exception of Subglacial Lake Mercer [*Carter et al.*, 2007; *Fricker et al.*, 2007]) it often fails at least one if not multiple tests for detecting "radar lakes" such as hydraulic flatness, specularity, and brightness relative to its surroundings [e.g. *Christianson et al.*, 2012; *Siegert et al.*, 2014; *Wright et al.*, 2014]. Conversely, satellite and GPS data collected over most "radar lakes" (with the exception of the Adventure Trench lakes of *Wingham et al.* [2006]) show no detectable change. Towards understanding these observations, Carter et al. [2015] investigated drainage mechanisms necessary to sustain "active lakes" and argued that they would likely exist in areas that befoul traditional radar detection methods due to the lakes being surrounded by saturated sediments that impair the radar reflection contrast. In this work we explore drainage mechanisms for "radar lakes" that may explain why they do not typically exhibit detectable vertical surface motion.

2.2 HYPOTHESES

We hypothesize that groundwater systems may have a significant role in the subglacial hydrological systems proximal to ice divides (and perhaps much of the areas with low melt rates) underneath continental ice sheets such as the East Antarctic Ice Sheet. This is due to the low production of meltwater, usually <10 mm/yr, underneath areas of very low basal shear stress (i.e. low frictional heating from slow moving ice).

These behaviors are demonstrated in Figure 2.1a where we compare a range of melt rates at the base of a hypothetical ice sheet that is similar to basal conditions in the interior of East Antarctica close to an ice divide (see Figure S2.4 for the specific area used) to the volume flux of groundwater (see *Stauffer* [2006] for definition) across the majority of hydrogeologic values (see Table 8.2 of *Singhal and Gupta* [2010]), given interior East Antarctic pressure potentials. The groundwater volume flux, q [mm/yr], is equal to $-k\nabla P/\mu$ where k is the permeability [m^2] of the porous medium, μ is the dynamic viscosity of the water (8.94×10^{-4} Pa s), and ∇P is the gradient of the pore water pressure [Pa/m]. Figure 2.1a shows that groundwater volume flux values are on par with melt rate magnitudes (1-100 mm/yr) at high-to-moderate permeability for low-pressure gradients and from moderate-to-low permeability at higher-pressure gradients. This means that for roughly half of the hydrogeologic permeability spectrum meltwater can be transported as groundwater.

This hypothesis is further supported by calculations of the transmissivity of groundwater systems compared to a subglacial water sheet (or films; a lá *Weertman* [1966]), which is still the *de facto* model for continental scale subglacial water transport [*Le Brocq et al.*, 2009]. Transmissivity is a measure of a water system to carry water laterally and equal to the product of the conductivity of the water system and the thickness of that system. Figure 2.1b shows the transmissivity of the conductivity end members of the groundwater and water sheet systems (see Appendix A for the specific mathematical details). These comparisons also demonstrate that more water can be transmitted via groundwater than via water sheet systems for roughly half of the hydrogeologic permeability spectrum.

We also hypothesize that given the potential in subglacial water transport via groundwater that subglacial lakes may be fairly stable through the ability of the bed substrate to diffuse excess water away without giving an ice surface expression. This effect could explain why so many of the "radar lakes" in the interior of East Antarctica

are not observable from ice surface elevation changes (cf. "active lakes"). Finally, we hypothesize that the ice sheet corrected basal radar return signal known as the basal reflection coefficient, assuming to be dominantly a function of the water content as the base of the ice sheet [*Peters et al.*, 2007], could be directly resultant from the hydrogeologic properties of the bed. This would mean that a groundwater system present at the ice sheet bed could alter the signal of the radar return by modulating the basal water sheet thickness. We leave this third hypothesis untested here as it is out of the scope of this work.

2.3 NUMERICAL MODELING METHODS

To further test these hypotheses we developed a novel 1D subglacial interface water sheet model (applicable here due to the large length scale) coupled to a 2D groundwater model applied to the study area of Dome C in East Antarctica (see Figure 2.2). The objective of our model was to utilize groundwater volume flux at the ice/bed interface to determine water sheet thickness and then use the modeled groundwater aquifer transmissivity as a point of comparison to the water sheet's transmissivity. We chose Dome C (see Figure 2.2) for the model study area as it has been examined extensively for various reasons, including hydrological studies [e.g. *Forieri et al.,* 2004; *Tikku et al.*, 2005; *Parrenin et al.*, 2007; *Carter et al.*, 2009b]. Dome C is also located in an area of high "radar lake" density and paucity of "active lakes" [*Wright et al.*, 2014], which was advantageous for hypothesis testing. A critical input for the numerical model was the availability of lower-error melt rates in the study area [*Carter et al.,* 2009b]. The vast majority of the area is estimated to be at pressure-melting temperature at the ice base so all the work we present here at the ice base and in the subsurface assumes that water is in a liquid state and that thermodynamic modeling is not required [*Siegert et al.*, 2007; *Pattyn*, 2010]. The presence of subglacial lakes also validates this assumption. The numerics of the coupled model are purposefully simplistic and applicable to areas similar to Dome C (mainly the interiors of continental ice sheets). The key characteristics of our

model's applicability are areas: larger than that of mountain glacier terrains, having low ice surface slopes, and low melt rates from very slow basal ice velocity. Dome C exhibits all of the above and is an ideal location for the model development. We determined the flow line along which the model was developed (see Figure 2.2) by a method used by *Carter et al.* [2009a].

As previously mentioned, our simplistic model was designed to understand how the water sheet thickness and a hypothetical groundwater system might interact and correlate to subglacial lake stability under the East Antarctic Ice Sheet. The groundwater portion of the model utilizes a steady, fully saturated Darcy flow approach. This is applicable as any available meltwater would drain into a dry subsurface before going into the water sheet until the porous media was fully saturated which should be the case since it has probably existed in this configuration for tens of millions of years [e.g. *Huybrechts*, 1993; *Siegert et al.*, 2005; *Young et al.*, 2011]. Since we do not have actual data about the subsurface hydraulic system, we simply adjust various permeability assumptions covering a wide range of geologic possibilities for the area. We also leave the top boundary as a constant head boundary to simply produce groundwater fluxes as an applied forcing to the water sheet (we provide further description of this later).

The 2D governing equation for steady state, fully saturated groundwater flow is

$$-\nabla \cdot \left(\frac{k}{\mu}\nabla P + \rho_w g \nabla z_b\right) = 0 \tag{2.1}$$

where P is the pore water pressure to be solved, $\nabla \cdot$ is the divergence (used here in two dimensions as $\partial/\partial x + \partial/\partial z$), k is the matrix permeability, μ is the viscosity of the water, z_b is the bed elevation, and ∇ is the gradient (also used here in two dimensions as $\partial/\partial x\, \boldsymbol{i} + \partial/\partial z\, \boldsymbol{k}$, where $\boldsymbol{i}$ and $\boldsymbol{k}$ are unit vectors). Note that the term inside the parentheses is the 2D groundwater volume flux (i.e. $q = -\frac{k}{\mu}\nabla P + \rho_w g \nabla z_b$, which is

similar to the previous form used for 1D flow where $q = -\frac{k}{\mu}\nabla P$) at any given location in the model domain. The matrix permeability, k, is evaluated using an exponential decay function (á la *Athy* [1930] and *Sclater and Christie* [1980]): $k = k_0 e^{-A(z_b - z)}$. Here, k_0 is the permeability at the top of the groundwater aquifer (i.e. bed elevation) which is allowed to vary in the model through a wide hydrogeologic range, A is a decay parameter, and z is the elevation so that $z_b - z$ is the depth in the aquifer from the bed. The bottom of the aquifer is set at 1,500 m below sea level arbitrarily to allow a depth that enables regional groundwater flow [*Jiang et al*., 2009] and is less than the geophysically estimated thickness of the sedimentary basin fill for this area (~1-3 km; *Frederick* [2015]), which we chose in order to keep our argument more conservative (i.e. keeping the aquifer thickness minimized for transmissivity calculation). We also note that, for depths past a few hundred meters, the depth of the aquifer bed does not really impact the value of the groundwater volume flux at the ice/bed interface. The value of the decay exponent (A) is 5×10^{-3} m^{-1} as used in *Jiang et al*. [2009] in order to allow for a balance between regional and local groundwater flow systems; we also use this value as it is a more aggressive decay constant which allows us to make our argument more conservative. As our sole model parameterization, we vary the sediment surface permeability of the bed, k_0, from a high value of 10^{-10} m^2 (referred to subsequently as $high\ k_0$) to 10^{-18} m^2 ($low\ k_0$) with a medium value of 10^{-14} m^2 ($med\ k_0$) in order to test a wide range of geologic possibilities for Dome C (see Figure S2.2 for a graphical view) and utilize groundwater flux as a sort of forcing function to the water sheet system above. Subglacial lakes were modeled as extensions of the groundwater domain by assigning the subglacial lakes an isotropic, homogeneous value of k_0 to obtain physically reasonable values of groundwater volume flux along the lake boundaries. The top and left boundaries are constant head boundaries (sits atop the lakes where they are present) and the bottom and right are no flow boundaries (i.e. water does not flow to the right of A or past the bottom boundary; see Figure 2.2c).

The governing equation for the water sheet was modeled similar to that of an expandable fracture where the laminar flow is directed between two parallel plates. The glaciological community (specifically, *Weertman* [1966]) adapted this equation to describe the flow of water at the interface of an ice sheet by solving for sheet thickness (akin to fracture aperture), d, instead of pore pressure. The resulting 1D governing equation of the water sheet is

$$-\nabla_x \cdot \left(\frac{d^3}{12\mu}\nabla_x P_{ws}\right) = \dot{b} + G \tag{2.2}$$

where d is the water sheet thickness to be solved for, P_{ws} is the given water sheet pressure, $\nabla_x \cdot$ is the one-dimensional divergence (i.e. d/dx), μ is the viscosity of the water, ∇_x is the one-dimensional gradient (i.e. d/dx), $\dot{b}$ is the melt rate from the base of the ice (a given source term from a another model's output; see Appendix B), and G is another source term to the water sheet that equals the modeled groundwater volume flux normal to the ice/bed interface ($G = q \cdot \boldsymbol{n}$), which is along the constant head boundary of the 2D groundwater model domain. Note that it is through the source term G that we couple the output of the groundwater volume flux to the water sheet system. Plots of G and $\dot{b}$ are shown in Figure S2.3. The water sheet pressure is equal to the overlying ice sheet pressure, which is a fair assumption for this setting [*Le Brocq et al.*, 2009]. Therefore, the given water sheet pressure is calculated as $P_{ws} = \rho_i g(s - i) + \rho_w g(i - z_b) + \rho_w g z_b$, where ρ_i is the density of ice, ρ_w is the water density, g is the acceleration due to gravity, s is the elevation of the ice sheet surface, i is the elevation of the base of the ice, and z_b is the elevation of the bed. The term in the middle allows for the pressure contribution of subglacial lakes such that where subglacial lakes exist $i \neq z_b$ otherwise $i = z_b$. The pressure for the constant head boundary in Equation 2.1 uses this same formulation with the exception of the term accounting for the lake as that boundary lies above the lakes. The segments of the water sheet underlying the subglacial lakes are set to zero as to only model around them and set a required boundary condition. The value

of the water viscosity (μ) is 8.94x10^{-4} Pa s and the ice (ρ_i) and water (ρ_w) densities are 920 and 1,000 kg/m^3, respectively. More specifics about the model and its implementation into COMSOL Multiphysics (COMSOL, Inc.), an automated partial differential equations solver utilizing the finite element method, can be found in Appendix B.

2.4 RESULTS

The modeled results consist primarily of the water sheet thickness and the subsurface pore pressure (or hydraulic head) that are used to calculate water flux in both the aquifer and water sheet. Transmissivities can also be calculated using these results. The modeled water sheet thicknesses and resulting groundwater and water sheet transmissivities are plotted in Figures 2.3a and 2.3b, respectively. The results of the groundwater simulation are shown in Figure 2.4. There are four different model results based on the input parameterizations of groundwater flux in addition to the given melt rate (i.e. $high\ k_0$, $med\ k_0$, $med\ k_0$, and $melt\ only$). The modeled water sheet thicknesses (Figure 2.3a) fall into two distinct groups with all but one parameterization ($high\ k_0$) essentially plotting the same as the $melt\ only$ result with minor deviations, if any. The parameterizations that follow the $melt\ only$ profile start at zero where subglacial lakes exist and gradually grow to a maximum before the next lake and repeat this process a few times. The maximum sheet thickness of these is about 2.5 mm. The $high\ k_0$ results are much different than the others. They fluctuate much more steeply than the others and reach larger thicknesses at their maximum (~4-4.5 mm).

The calculated transmissivities of the modeled water sheet thicknesses compared to the groundwater systems can be seen in Figure 2.3b. We calculated the transmissivities (T) for the model results a few different ways. For the groundwater values, we calculated the mean hydraulic conductivity (K) of the varied groundwater models by taking the average function value integral of the depth-dependent formulation

for permeability, k (see Numerical Modeling Methods for the depth-dependent function). For the saturated thickness, b, of the groundwater subdomain we used the depth of aquifer along the profile. The product of these two values gave the 100% transmissivity value. The 10% value simply takes 10% of the 100% transmissivity value for an added level of conservative estimation. The transmissivities for the modeled water sheet simply use the product of the average water velocity and the water sheet thickness. Our choice of the depth-averaged water velocity (see Appendix A for specific formulation) instead of hydraulic conductivity was to again allow for potentially higher values of transmissivity to more conservatively compare to those of the groundwater system. The water sheet transmissivities for all parameterizations cover many orders of magnitude of transmissivity (~5 by grouping or ~6 total) and extend above and below the $med\ k_0$ groundwater values at both the full (100%) and fractional (10%) aquifer thickness values. Only the $high\ k_0$ sheet parameterization reaches the highest fractional aquifer thickness transmissivity. Overall, the range of groundwater transmissivities envelops those of the water sheet system.

The results from the 2D groundwater model domain are shown in Figure 2.4 which specifically depicts the $high\ k_0$ model case. This figure is representative of the other models as it plots the horizontal pressure gradient, streamlines, and the relative magnitude and direction vectors of the groundwater volume flux that do not change with model parameterization. While the dominant driving force in groundwater flow is the ice sheet surface slope, localized bedrock effects can exert change in flow magnitude and even localized reversal in flow direction. Places where the horizontal pressure gradient is positive (to the left) low to negative (to the right) correlate well to locations of increased water sheet depth in the $high\ k_0$ model case (see Figure 2.3a) while locations where flow is strongly positive (or there are lakes) correlate to absences of a modeled water sheet.

2.5 DISCUSSION

The numerical modeling results suggest that the addition of a groundwater flow system to a water sheet model of subglacial hydrology is critical for hydrological modeling under the interiors of continental ice sheets where melt rates are low (<10 mm/yr). This result specifically applies to continental ice sheet interiors containing bedrock surfaces whose surface permeability is within roughly the upper half of the permeability spectrum (>10^{14} m^2 ($med\ k_0$); see Table 8.2, *Singhal and Gupta* [2010]). This is supported by the similarity in output water sheet thickness for most of the model parameterizations where all are largely the same as the $melt\ only$ run except for the highest surface permeability parameterization ($high\ k_0$; see Figure 2.3). The deviation from the $melt\ only$ thickness trend starts at the $med\ k_0$ parameterization, which occurs because the $med\ k_0$ groundwater volume fluxes are on par with the melt rate (see Figure S2.3). According to our model results, places where the surface and bed slopes are in unison are unfavorable for water sheet development, given the permeability is higher than the $med\ k_0$ parameterization (cf. Figures 2.3a and 2.4). This is logical as the localized zones of low or reversed groundwater flow (compared to the regional flow direction to the left) would cause the water sheet to thicken to accommodate the regional gradient of water flow at the ice/bed interface. We believe this to be significant as roughly half of the hydraulic materials (i.e. geology) possibly extant in the bed could have a dominant control over the development of the basal water sheet system.

The groundwater modeling results (Figure 2.4) show that there are many groundwater flow cells (with nested cells within them as well) throughout the model domain along the hydraulic flow path. While the flow is essentially horizontal there is some deviation from horizontal (i.e. slightly toward the vertical) in some locations. From our limited two-dimensional groundwater domain, we see that the continuous groundwater transport across the entire domain is not probable as the directional (i.e. sign) changes in horizontal pressure gradient act as divides for subsurface fluid flow. A prominent example of one of these divides is at about 115 km (see Figure 2.4); this

essentially cuts the upstream lakes off from the downstream one. However, given that water flow along the flow paths of the water sheet system strictly follows the smoothed gradient of the ice sheet surface slope in this scenario, it could be argued that groundwater could connect subglacial lakes by a combination of subsurface and subglacial water flow. This may be how the system works in reality where more transmissive groundwater systems transport large amounts of water (relatively slowly) over time and discharge water into the water sheet (where pressure gradients dictate they exist) which then carry water back into downstream groundwater systems, thus forming a larger-scale subglacial water transport system. However, out-of-plane groundwater transport (i.e. a 3D subsurface domain) might also connect the subglacial lakes without direct need for the water sheet system.

Comparing the transmissivities of the modeled water sheet and groundwater systems, we find that roughly half of the hydraulic materials possible for the substrate lining the ice base could transport roughly the same amount or more water than the water sheets (Figure 2.3b). Even when we reduce the amount of groundwater aquifer thickness by an order of magnitude, which would be analogous to decreasing the aquifer thickness to one-tenth its modeled thickness, roughly the same trend with half of the hydrogeologic spectrum being on par or dominating the water sheet transmissivity is observed. In fact, it is only through the greatest modulation of groundwater flux that the water sheet is able to obtain its greatest modeled thickness, and thus, transmissivity for this modeling scenario.

Our results also suggest that subglacial lake stability in lower melt areas could be due to groundwater, where it is the dominant transfer mechanism. This would explain a paucity of ice surface topographic expressions of lake dynamics (rapid filling and expulsion). Finally, we note that the nature of basal radar reflection coefficients, which are heavily influenced by the presence of water at the bed, might have a great deal of influence from groundwater flux at the bed. We note this as the pattern of basal refection

strength (Figure 2.2b) along the flow path does not trend the same as the water sheet (i.e. smoothly increasing) under low groundwater forcing but might with the higher forcing (i.e. correlation between $high\ k_0$ water sheet thickness and radar return coefficient peaks). However, there are many more complexities that influence the radar return signals at the ice/bed interface and we acknowledge that this will need further rigorous testing to better understand. Future efforts should eventually extend this model to a three-dimensional framework (i.e. 2D water sheet; 3D groundwater) that couples ice dynamics and heat transport for permafrost development and melt-rate calculations. This methodology for a coupled water sheet and groundwater system in ice sheet interiors, in combination with recent advances in ice-penetrating radar [*Schroeder et al.*, 2014], may eventually assist in the ability to characterize sub-ice hydraulic (possibly even geologic) properties with careful treatment.

2.6 CONCLUSION

Our numerical model presented here demonstrates a basic method for coupling water sheet transport to two-dimensional groundwater model output forcing, which is our initial attempt to connect two segmented communities trying to solve very closely related problems [cf. *Flowers*, 2015; *Person et al.*, 2012]. Our current approach is especially well suited for ice sheets that are at thick enough to support a pressure-melting temperature at their base with minimal basal ice velocities (i.e. low frictional melt component). For ice sheets that do not meet these criteria, other approaches such as groundwater/channel coupling [*Boulton et al.*, 2007] may be more appropriate or the groundwater system may be negated altogether [e.g. *Kyrke-Smith et al.*, 2014] if the flux magnitudes are small enough when compared to a very efficient basal water system. Our model, as a two-dimensional model, may suffer due to a lack in accommodation of three-dimensional effects and interpolation biases in the topography. It is also possible that large heterogeneities in the hydrogeologic properties of the subsurface could cause deviations from the model. One example of this is karstic limestone (high, heterogeneous

conductivity), which has been proposed for the area [*Forieri et al.*, 2004], further supporting our hypothesis of a groundwater-dominant hydrologic system. However, our results do demonstrate that further advancement of subglacial groundwater transport mechanisms needs to take place (given the availability of greater subglacial geophysical and geologic information, another important task for current Antarctic research) and be incorporated into the subglacial hydrologic components of ice sheet models.

2.7 FIGURES

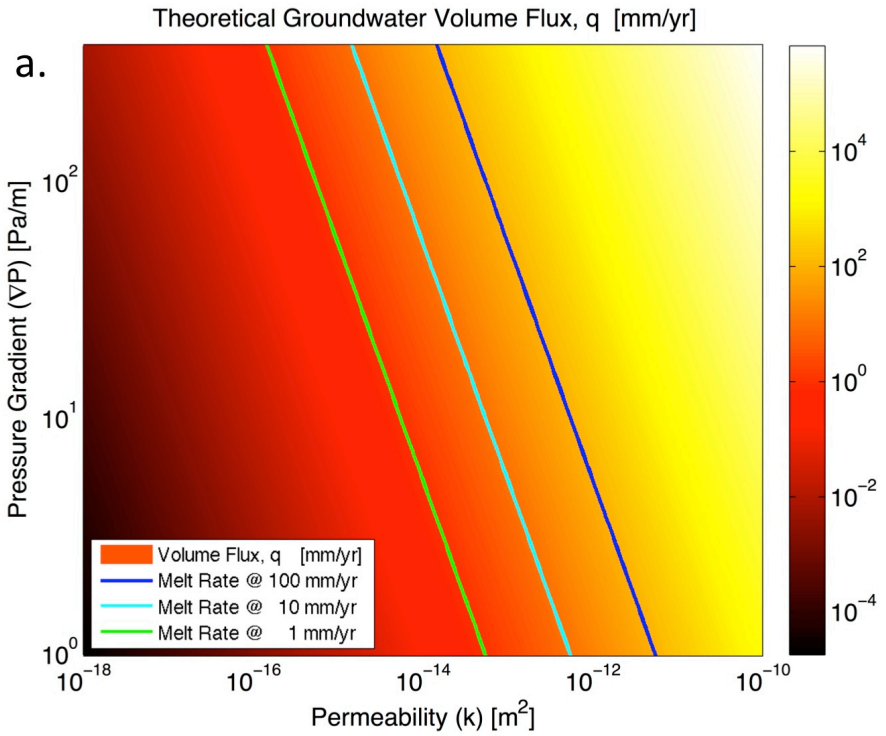
Theoretical Groundwater Volume Flux, q [mm/yr]
a.
Pressure Gradient (∇P) [Pa/m]
Permeability (k) [m2]
Volume Flux, q [mm/yr]
Melt Rate @ 100 mm/yr
Melt Rate @ 10 mm/yr
Melt Rate @ 1 mm/yr

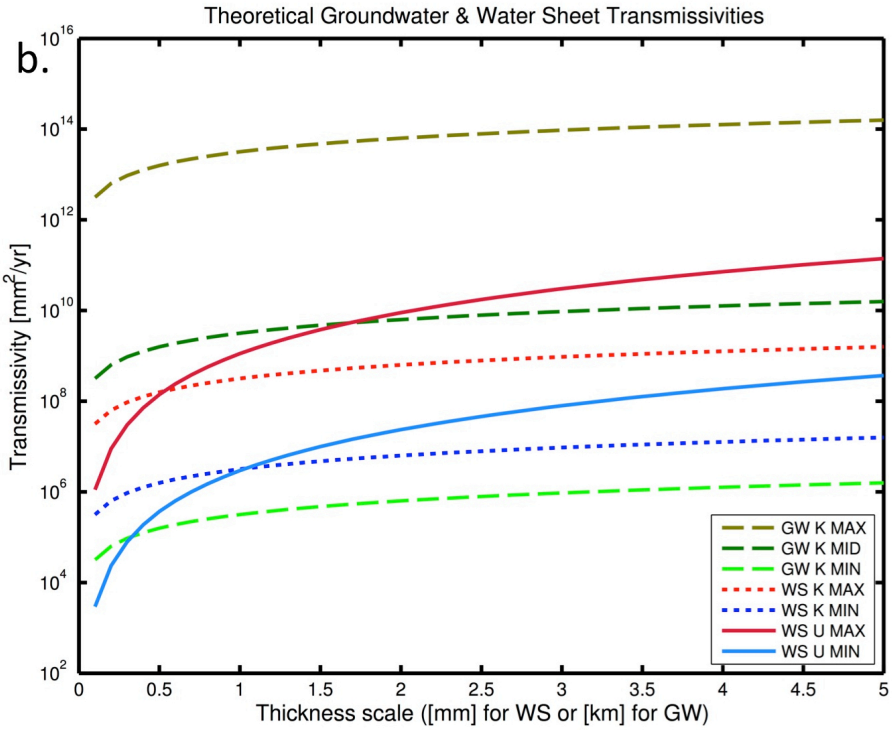
Theoretical Groundwater & Water Sheet Transmissivities
b.
Transmissivity [mm2/yr]
Thickness scale ([mm] for WS or [km] for GW)
GW K MAX
GW K MID
GW K MIN
WS K MAX
WS K MIN
WS U MAX
WS U MIN

Figure 2.1. (a) Plot of theoretical groundwater volume flux, q, over a wide range of permeabilities, k, (from "Very Low" (left) to "High" (right); see Table 8.2, *Singhal and Gupta* [2010]) and a typical range of pressure gradients (∇P) for interior East Antarctica (see Figure S2.4 for the specific area). The range of pressure gradients extend from 1 to ~380 (10^0-$10^{2.58}$) Pa/m. Basal ice sheet melt rates of 1, 10, and 100 mm/yr have been plotted for comparison. The range of permeability may be converted to hydraulic conductivity, K, giving a range of 10^{-11} (left) to 10^{-3} (right) m/s. (b) Plot of theoretical groundwater (GW) and basal water sheet (WS) minimum (MIN) and maximum (MAX) transmissivities given various hydraulic conductivities (K) or average water velocities (U). See Appendix A for specifics on the calculations of individual transmissivities for each plotted line.

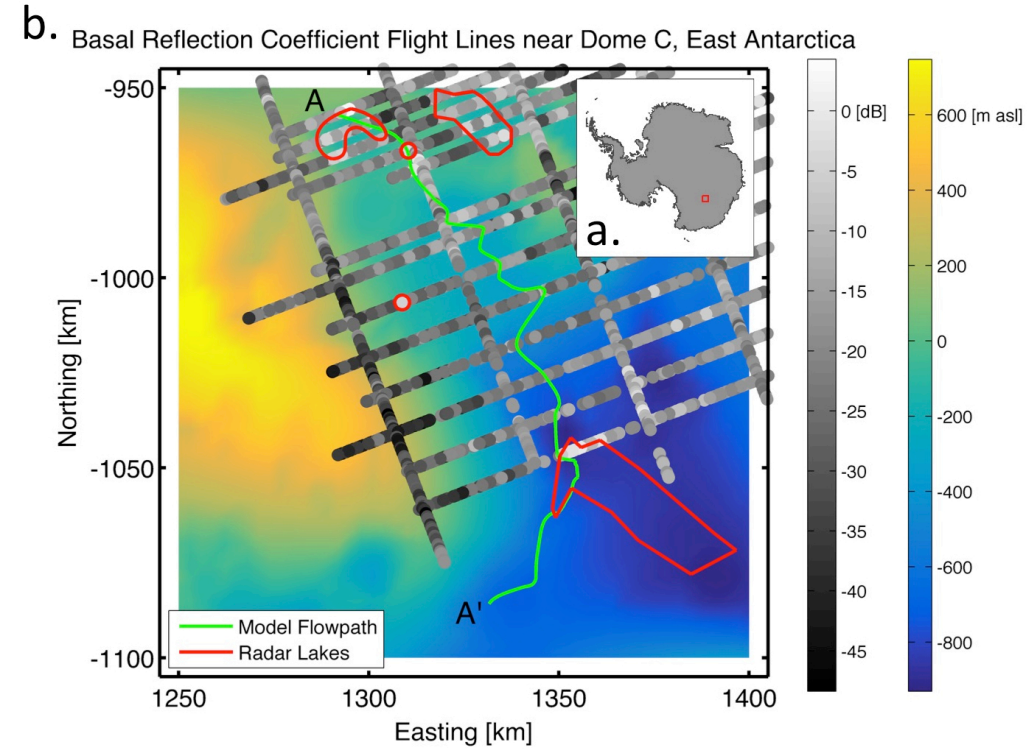
b.
Basal Reflection Coefficient Flight Lines near Dome C, East Antarctica
A
A'
a.
Model Flowpath
Radar Lakes
Northing [km]
Easting [km]
-950
-1000
-1050
-1100
1250
1300
1350
1400
0 [dB]
-5
-10
-15
-20
-25
-30
-35
-40
-45
600 [m asl]
400
200
0
-200
-400
-600
-800

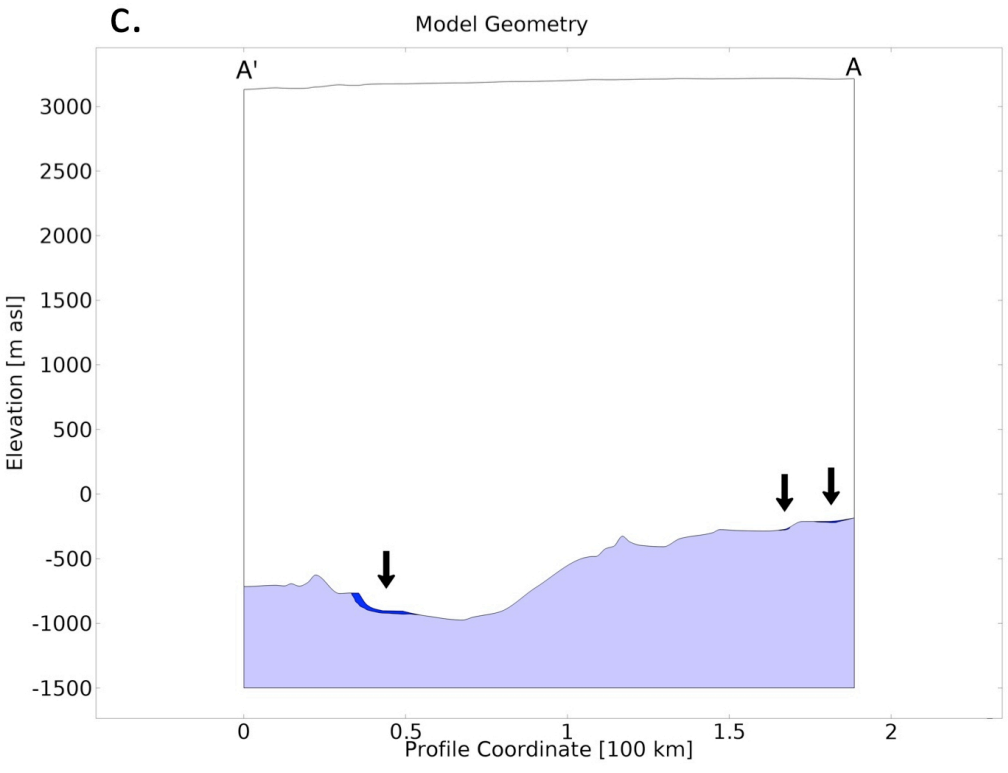
c.
Model Geometry
A'
A
Elevation [m asl]
3000
2500
2000
1500
1000
500
0
-500
-1000
-1500
0
0.5
1
1.5
2
Profile Coordinate [100 km]

Figure 2.2. (a) Location of the study area used in the model. The red box denotes area in interior East Antarctica for (b). (b) Ice/bed interface elevation [*Fretwell et al*., 2013] and radar basal reflection coefficient shown as flight line data points (in dB; [*Carter et al*., 2009b]) in the study area along with the model line and subglacial lake locations. In order from A-A' (downstream) along the model line, the subglacial lakes plotted in red are Horseshoe, WLK 17, and Vincennes. Note that the lakes coincide with brighter (i.e. higher dB) reflections. (c) Model geometry used for the coupled 2D groundwater and 1D sub-ice water sheet model. Light blue denotes the groundwater subdomain and the dark blue denotes the subglacial lakes (marked by arrows). The white above represents the ice sheet subdomain, which is not explicitly modeled here but shown for context. Note the high level of vertical exaggeration (~40x). All elevations are in meters above current sea level.

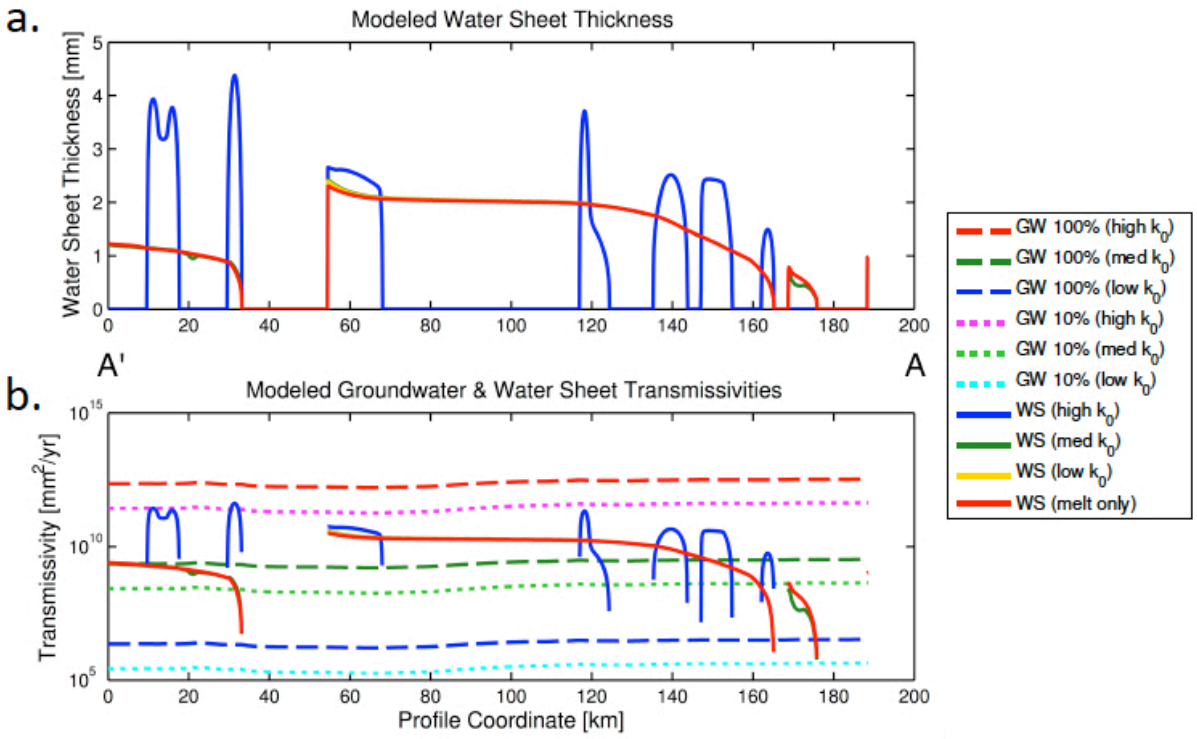

Figure 2.3. (a) Plot of the modeled water sheet thickness for varying source (G) parameterizations. Most of the parameterizations have similar results with the outlier being the model with the source parameterization utilizing the highest bed surface permeability coupled to the melt input (melt+gw ($high\ k_0$)). Note that all results are at zero where subglacial lakes exist due to the Dirichlet boundary condition. The three subglacial lakes along the profile are at coordinates 33.2-54.4, 165.2-168.7, and 176.2-188.3 kilometers. (b) Plot of the calculated transmissivities of the modeled water sheet (WS) thicknesses and the groundwater (GW) aquifer thickness. The groundwater aquifer thickness is calculated at full thickness (100%) as well as 10% in order to calculate low-end values for comparison. See Results for a detailed explanation of the hydraulic conductivities (K) used in the transmissivity (T) calculation for each plotted line. Note: the location of the profile A-A' is shown in Figure 2.2b.

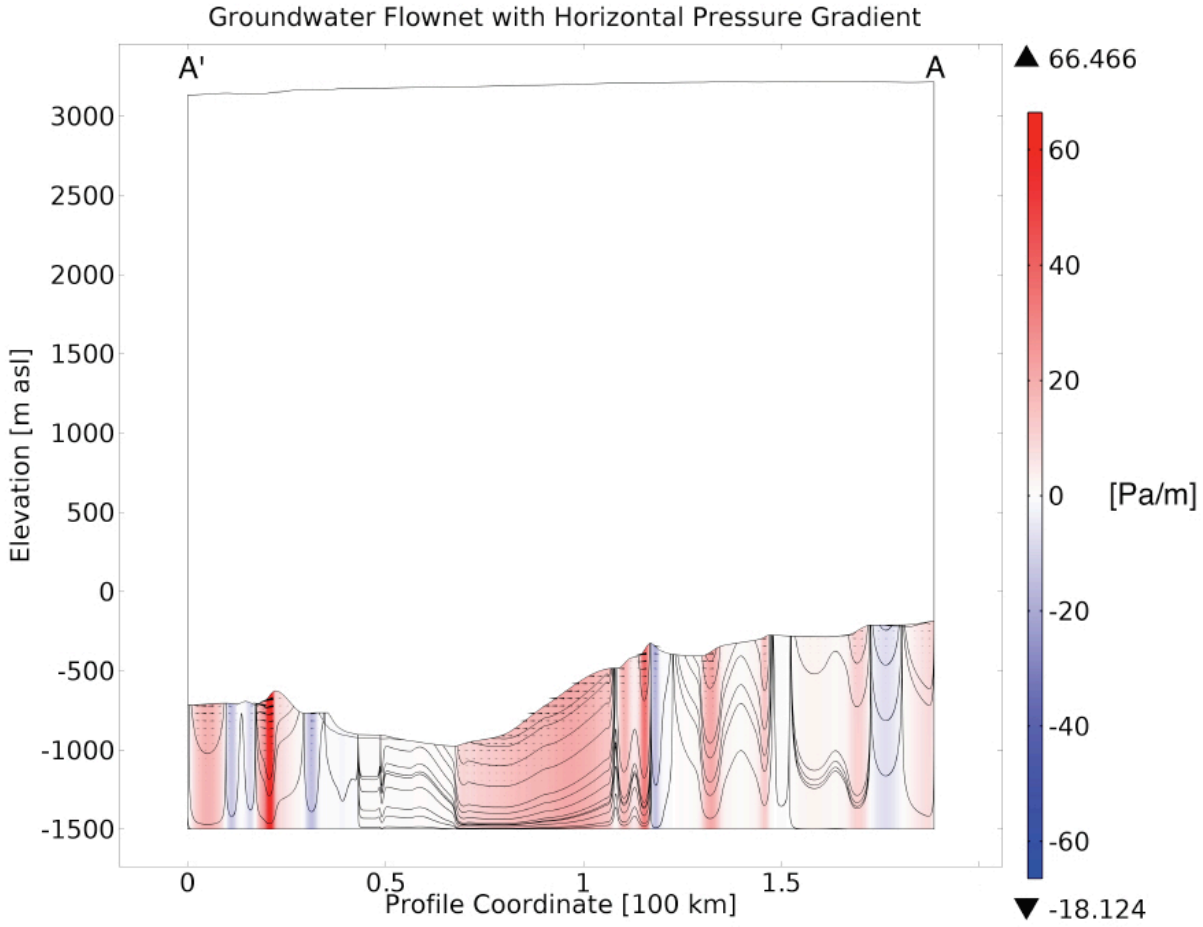

Figure 2.4. Plot of the modeled subsurface horizontal pressure gradient and the groundwater flownet streamlines (melt+gw ($high\ k_0$) model case). Relative magnitude vector arrows are included to demonstrate the flow directions. The three subglacial lakes along the profile are at coordinates 33.2-54.4, 165.2-168.7, and 176.2-188.3 kilometers. Negative pressure gradients (blue) cause water to flow to the right while positive pressure gradients (red) cause flow to the left (i.e. with the downstream subglacial water flow). Note: the location of the profile A-A' is shown in Figure 2.2b. Also note the high level of vertical exaggeration (~40x) and that the horizontal flow vector is shown, as it is the dominant flow vector over the vertical (not shown).

2.8 APPENDICES

2.8.1 Appendix A

Figure 2.1a shows the ranges of groundwater volume flux, q, for a very wide range of permeabilities (k) and a range of water pressure gradients (∇P) present in EA. The range of pressure gradients were selected using the area shown in Figure S2.4, which yielded a range of 1 to ~380 (10^0-$10^{2.58}$) Pa/meter. The range of permeabilities we used was derived from Table 8.2 in *Singhal and Gupta* [2010]; note that the "Very high" data were excluded in order to have a more conservative comparison. We calculated the groundwater transmissivities (T) in Figure 2.1b by using the maximum and minimum permeabilities used in Figure 2.1a and converted them to a hydraulic conductivity (K) maximum and minimum of 10^{-3} and 10^{-11} m/s, respectively. We also calculated a medium value using 10^{-7} m/second. These hydraulic conductivities were multiplied by a saturated thickness (b) to complete the transmissivity calculation (i.e. $T = Kb$). To calculate the transmissivities of water sheets we chose two approaches. The standard approach simply used published [*Flowers and Clarke*, 2002] maximum and minimum hydraulic conductivities of 10^{-2} and 10^{-4} m/s, respectively. Another method was to calculate the depth-averaged velocity of the water sheet ($d^2\nabla P/12\mu$; laminar flow between parallel plates [*Weertman*, 1966]) and use this instead of the hydraulic conductivities from before. We calculated a maximum and minimum depth-averaged water velocity in the sheet by using the maximum and minimum pressure gradients used in Figure 2.1a's calculations. This calculation provided us with a wider range of water sheet transmissivities in order to more conservatively compare with groundwater transport.

2.8.2 Appendix B

We calculated the basal melt rates from a combined vertical strain inversion and temperature model that used age-dated internal ice layers in RES data to calculate a vertical velocity and paleo-ice accumulation rate. The model then incorporated

paleotemperatures from the Dome C Ice Core [*Parrenin et al.*, 2007] and geothermal flux values from the seismic tomography work of *Shapiro and Ritzwoller* [2004] to obtain a vertical temperature distribution for the ice and for this study a basal melt rate. A fuller description of this method appears in *Carter et al.* [2009b]. We obtained flow paths by first plotting a contour map of the hydropotential and then tracing continuous local minima using the law of V's first practiced by *Dupain-Triel* [1791]. At the intersections between this proto-flow path and the tracks of the available RES data we then found the nearest local minima in the hydropotential along the flow path. Our hydropotential was based on RES ice surface elevations and ice thickness and also utilized Bedmap2 [*Fretwell et al.*, 2013] where such RES data are sparse.

We used COMSOL Multiphysics (v.4.3b; COMSOL, Inc.) to create the coupled model presented in Numerical Modeling Methods. The model uses Equation 2.1 (as a preprogramed 2D module in COMSOL) with a modified version of Equation 2.2 for stability reasons (as a custom 1D PDE into COMSOL). The coupling of the two models comes in as the groundwater volume flux (G) normal to the bed surface (as an edge in 2D). We see this approach as novel as few efforts have incorporated groundwater with a subglacial hydrological model and none to our knowledge have simultaneously solved for the water sheet thickness (d), which is critical for comparing where each system may dominate over the other.

Our 2D groundwater system was easily modeled via COMSOL as it is preconfigured to handle Darcian groundwater flow models in one to three dimensions. Modeling the lakes required treating them in the same domain as the groundwater system versus the approach used by others [*Singha and Loheide*, 2011] where lakes are given unreasonably high permeabilities, which would skew the true groundwater flux values at the lake/bed interface. The choice of a fully saturated model and constant head boundary along the top resulted from our desire to keep the pressure equal to the overburden pressure at the ice/bed interface and also be able to observe how the groundwater volume

flux varies over that distance. If we had instead applied the melt rate as the boundary condition the flux would be equal to the melt rate (all positive into the aquifer), which would be unrealistic. While our choice is not fully realistic either, it does provide a better idea of how the two hydrological systems might interact. Another assumption was the neglect of a coupling back to the pressure function in the groundwater head from the modeled water sheet. This is because the water sheet depth, d, is smaller than the elevation change in the topography by many orders of magnitude (~5). Adding in this update to the solver would have caused unnecessary computation with little-to-no effect on the groundwater solution.

The 1D water sheet model required substantial more effort to accomplish a realistic modeling result. In order to provide a stable solution, a slight modification during the numerical implementation of Equation 2.2 had to occur. Applying the divergence to the inner terms of the LHS of Equation 2.2 yields the expanded form

$$-\nabla_x \cdot \left(\frac{d^3}{12\mu}\nabla_x P_{ws}\right) = -\frac{3d^2}{12\mu}\cdot \nabla_x P_{ws}\cdot \nabla_x d - \frac{d^3}{12\mu}\cdot {\nabla_x}^2 P_{ws} \tag{2.3}$$

which is the first step to solve for the unknown d instead of P_{ws} which is known here. Taking the RHS of Equation 2.2 and substituting into the LHS of Equation 2.3 gives

$$\dot{b} + G = -\frac{3d^2}{12\mu}\cdot \nabla_x P_{ws}\cdot \nabla_x d - \frac{d^3}{12\mu}\cdot {\nabla_x}^2 P_{ws} \tag{2.4}$$

which is the correct form of a steady nonlinear convection absorption equation in d. However, standard numerical methods for this equation are not stable. As with previous finite difference approaches to numerical stability (e.g. upwinding), we have also incorporated stability for finite elements known as artificial, or streamline, diffusion [*Hauke and Hughes*, 1994] by adding a very small diffusive term to the RHS giving

$$\dot{b} + G = -\frac{3d^2}{12\mu} \cdot \nabla_x P_{ws} \cdot \nabla_x d - \frac{d^3}{12\mu} \cdot \nabla_x{}^2 P_{ws} - \nabla_x \cdot \left(\frac{|\nabla_x P_{ws}|}{12\mu} \cdot \frac{3d^2}{2} \cdot \mathrm{h} \cdot \nabla_x d \right) \tag{2.5}$$

where h is the element size and $|\nabla_x P_{ws}|$ is the absolute first pressure derivative with respect to x. Rearranging and simplifying Equation 2.5 yielded the more compact form of

$$\dot{b} + G = -\nabla_x \cdot \left(\frac{|\nabla_x P_{ws}| \, d^2 h}{8\mu} \nabla_x d \right) - \frac{3d^2 \nabla_x P_{ws}}{12\mu} \cdot \nabla_x d - \frac{d^2 \nabla_x{}^2 P_{ws}}{12\mu} d \tag{2.6}$$

which is in the more familiar form of a steady convection diffusion equation with an absorption term and source

$$f = -\nabla_x \cdot (\mathrm{c} \nabla_x u) - \beta \cdot \nabla_x u + au \tag{2.7}$$

where f is the source, u is the dependent variable, and the rest are coefficients. The diffusive term is characterized by the coefficient c, the convective component is characterized by the β coefficient, and the absorptive term is characterized by the coefficient a. Note that these coefficients depend on the unknown d, and therefore Equation 2.6 is a nonlinear convection diffusion equation. This form is in a format easily solved with COMSOL (as it is preprogrammed to handle this form for both linear and nonlinear equations) given one final step. The last step in solving Equations 2.1 and 2.6 (originally Equation 2.2) simultaneously is to provide a stable input pressure function into Equation 2.6. The key to this is similar to other glaciological works [*Le Brocq et al.*, 2006] where the pressure function must have its local minima removed. This step was done by hand in a spreadsheet with a graphic that depicted instantaneous changes made to the profile. The "filled" function also required smoothing to provide continuous derivatives in the pressure function. Figure S2.1 provides a comparison of this workflow's output in a graphical format.

The model specifics varied according to the specific physics solved in the model domain. The two-dimensional part of the domain (i.e. groundwater physics) contained 93,331 triangular finite elements and the one-dimensional part (i.e. water sheet physics) contained 3,815 edge elements yielding a total for the coupled model at 97,146 elements. The element size for the bulk of the entire model domain is 100 m with the groundwater subdomain having an element size range of 17 - 132 m and the water sheet subdomain having edge element sizes ranging 2 - 101 meters. When run separately on a modern laptop (c. 2010), COMSOL calculates the solution to solely the groundwater equation in ~12 s and the water sheet alone in ~16 s but when coupled, solution times range from ~1 min to over 20 min depending on the parameterization of k_0.

2.9 REFERENCES

Alley, R. B. (1989), Water-pressure coupling of sliding and bed deformation, I, Water system, J. Glaciol., 35, 108–118.

Athy, L. F. (1930), Density, porosity, and compaction of sedimentary rocks, AAPG Bull., 14, 1– 23.

Boulton, G. S., and A. S. Jones (1979), Stability of temperate ice sheets resting on beds of deformable sediment, J. Glaciol., 24, 29–43.

Boulton, G. S., P. E. Caban, and K. Van Gijssel (1995), Groundwater flow beneath ice sheets: part 1—Large scale patterns, Quat. Sci. Rev., 14, 545–562.

Boulton GS, R. Lunn, P. Vidstrand, and S. Zatsepin (2007), Subglacial drainage by groundwater–channel coupling, and the origin of esker systems: Part 2 – theory and simulation of a modern system, Quat. Sci. Rev., 26, 1091–1105.

Carter, S. P., D. D. Blankenship, M. E. Peters, D. A. Young, J. W. Holt, and D. L. Morse (2007), Radar-based subglacial lake classification in Antarctica, Geochem. Geophys. Geosyst., 8, Q03016, doi:10.1029/2006GC001408.

Carter, S. P., D. D. Blankenship, D. A. Young, M. E. Peters, J. W. Holt, and M. J. Siegert (2009a), Dynamic distributed drainage implied by the flow evolution of the 1996–1998 Adventure Trench subglacial lake discharge, Earth Planet. Sci. Lett., 283(1–4), 24–37, doi:10.1016/j.epsl.2009.03.019.

Carter, S. P., D. D. Blankenship, D. A. Young, and J. W. Holt (2009b), Using radar-sounding data to identify the distribution and sources of subglacial water: Application to Dome C, East Antarctica, J. Glaciol., 55(194), 1025–1040, doi:10.3189/002214309790794931.

Carter, S. P., H. A. Fricker, D. D. Blankenship, J. V. Johnson, W. H. Lipscomb, S. F. Price, and D. A. Young (2011), Modeling 5 years of subglacial lake activity in the MacAyeal Ice Stream (Antarctica) catchment through assimilation of ICESat laser altimetry, J. Glaciol., 57(206), 1098–1112.

Carter, S. P., H. A. Fricker, and M. R. Siegfried (2015), Active lakes in Antarctica survive on a sedimentary substrate – Part 1: Theory, The Cryosphere Discuss., 9, 2053-2099, doi:10.5194/tcd-9-2053-2015.

Christianson, K., R. W. Jacobel, H. J. Horgan, S. Anandakrishnan, and R. B. Alley (2012), Subglacial Lake Whillans—Ice-penetrating radar and GPS observations of a shallow active reservoir beneath a West Antarctic ice stream, Earth Planet. Sci. Lett., 331-332, 237–245, doi:10.1016/j.epsl.2012.03.013.

Creyts, T. T., and C. G. Schoof (2009), Drainage through subglacial water sheets, J. Geophys. Res., 114, F04008, doi:10.1029/2008JF001215.

Dupain-Triel, J. L. (1791), La France considérée dans les différentes hauteurs de ses plaines: ouvrage spécialement destiné al'instruction de la jeunesse, (BN, Cartes et Plans, map No. Ge. D.15126) Hérault, Paris.

Flowers, G. E., and G. K. C. Clarke (2002), A multicomponent coupled model of glacier hydrology: 1. Theory and synthetic examples, J. Geophys. Res., 107(B11), 2287, doi:10.1029/2001JB001122.

Flowers, G. E. (2015), Modelling water flow under glaciers and ice sheets, Proc. A, (471).

Forieri, A., L. Zuccoli, A. Bini, A. Zirizzotti, F. Remy, and I. E. Tabacco (2004), New bedrock map of Dome C, Antarctica, and morphostructural interpretation of the area, Ann. Glaciol., 39(1), 321-325.

Frederick, B. C. (2015), Submarine Sedimentary Basin Analyses for the Aurora and Wilkes Subglacial Basins and the Sabrina Coast Continental Shelf, East Antarctica, Ph.D. dissertation, Univ. of Texas, Austin, Texas, USA.

Fretwell, P., et al. (2013), Bedmap2: Improved ice bed, surface and thickness datasets for Antarctica, The Cryosphere, 7, 375–393, doi:10.5194/tc-7-375-2013.

Fricker, H. A., et al. (2007), An active subglacial water system in West Antarctica mapped from space, Science, 315(5818), 1544–1548, doi:10.1126/science.1136897.

Hauke, G., and T. J. R. Hughes (1994), A unified approach to compressible and incompressible flows, Computer Methods in Applied Mechanics and Engineering, 113(3), 389-395.

Huybrechts, P. (1993), Glaciological modelling of the late cenozoic East Antarctic Ice Sheet: Stability or dynamism?, Geogr. Ann., 75A(4), 221–238.

Jiang, X.-W., L. Wan, X.-S. Wang, S. Ge, and J. Liu (2009), Effect of exponential decay in hydraulic conductivity with depth on regional groundwater flow, Geophys. Res. Lett., 36, L24402, doi:10.1029/2009GL041251.

Kyrke-Smith, T. M., R. F. Katz, and A. C. Fowler (2014), Subglacial hydrology and the formation of ice streams, Proc. Phys. Soc. London, Sect. A, 470, 20,130,494, doi:10.1098/rspa.2013.0494.

Le Brocq, A. M., A. J. Payne, and M. J. Siegert (2006), West Antarctic balance calculations: Impact of flux-routing algorithm, smoothing and topography, Comput. Geosci., 32(10), 1780–1795.

Le Brocq, A., A. Payne, M. Siegert, and R. Alley (2009), A subglacial water-flow model for West Antarctica, J. Glaciol., 55(193), 879–888.

Lemieux, J.-M., E. Sudicky, W. Peltier, and L. Tarasov (2008), Dynamics of groundwater recharge and seepage over the Canadian landscape during the Wisconsinian glaciation, J. Geophys. Res., 113, F01011, doi:10.1029/2007JF000838.

Parrenin, F., et al. (2007), The EDC3 chronology for the EPICA dome C ice core, Clim. Past, 3(3), 485–497.

Pattyn, F. (2010), Antarctic subglacial conditions inferred from a hybrid ice sheet/ice stream model, Earth Planet. Sci. Lett., 295(3-4), 451–461, doi:10.1016/j.epsl.2010.04.025.

Person, M., J. McIntosh, V. Bense, and V. Remenda (2007), Pleistocene hydrology of North America: The role of ice sheets in reorganizing groundwater systems, Rev. Geophys., 45, RG3007, doi:10.1029/2006RG000206.

Person, M., V. Bense, D. Cohen, and A. Banerjee (2012), Models of ice-sheet hydrogeologic interactions: A review, Geofluids, 12, 58–78.

Peters, M. E., D. D. Blankenship, S. P. Carter, S. D. Kempf, D. A. Young, and J. W. Holt (2007), Along-track focusing of airborne radar sounding data from West Antarctica for improving basal reflection analysis and layer detection, IEEE Trans. Geosci. Remote Sens., 45(9), 2725–2736, doi:10.1109/TGRS.2007.897416.

Piotrowski, J. (1997), Subglacial hydrology in north-western Germany during the last glaciations: Groundwater flow, tunnel valleys and hydrological cycles, Quat. Sci. Rev., 16, 169–185.

Schroeder, D. M., D. D. Blankenship, D. A. Young, A. E. Witus, and J. B. Anderson (2014), Airborne radar sounding evidence for deformable sediments and outcropping bedrock beneath Thwaites Glacier, West Antarctica, Geophys. Res. Lett., 41, 7200–7208, doi:10.1002/2014GL061645.

Sclater, J. G., and P. Christie (1980), Continental stretching: An explanation of the post-mid-cretaceous subsidence of the central North Sea basin, J. Geophys. Res. Solid Earth, 85(B7), 3711-3739.

Shapiro, N. M., and M. H. Ritzwoller (2004), Inferring surface heat flux distributions guided by a global seismic model: Particular application to Antarctica, Earth Planet. Sci. Lett., 223, 213–224.

Shreve, R. L. (1972), Movement of water in glaciers, J. Glaciol., 11(62), 205–214.

Siegert, M. J., J. P. Taylor, and J. Antony (2005), Spectral roughness of subglacial topography and implications for former ice-sheet dynamics in East Antarctica, Global Planet. Change, 45, 249–263.

Siegert, M. J., A. Le Brocq, and A. J. Payne (2007), Hydrological connections between Antarctic subglacial lakes and the flow of water beneath the East Antarctic Ice Sheet, in Glacial Sedimentary Processes and Products, Spec. Publ., vol 39, edited by M. J. Hambrey et al., pp. 3–10, Int. Assoc. of Sedimentol., Malden, Mass.

Siegert, M. J., N. Ross, H. Corr, B. Smith, T. Jordan, R. G. Bingham, F. Ferraccioli, D. M. Rippin, and A. Le Brocq (2014), Boundary conditions of an active West Antarctic subglacial lake: implications for storage of water beneath the ice sheet, The Cryosphere, 8 (1), 15–24, doi:10.5194/tc-8-15-2014.

Singha, K., and S. P. Loheide II (2011), Linking physical and numerical modelling in hydrogeology using sand tank experiments and COMSOL Multiphysics, Int. J. Sci. Educ., 33(4), 547–571.

Singhal, B. B. S., and R. P. Gupta (2010), Applied Hydrogeology of Fractured Rocks, Kluwer Acad., Dordrecht, The Netherlands.

Stauffer, P. H. (2006), Flux flummoxed: A proposal for consistent usage, Ground water, 44(2), 125-128.

Stearns, L., B. Smith, and G. Hamilton (2008), Increased flow speed on a large East Antarctic outlet glacier caused by subglacial floods, Nat. Geosci., 1(12), 827–831, doi:10.1038/ngeo356.

Tikku, A. A., et al. (2005), Influx of meltwater to subglacial Lake Concordia, East Antarctica, J. Glaciol., 51(172), 96–104.

Weertman, J. (1966), Effect of a basal water layer on the dimensions of ice sheets, J. Glaciol., 6(44), 191–207.

Wingham, D. J., M. J. Siegert, A. Shepherd, and A. S. Muir (2006), Rapid discharge connects Antarctic subglacial lakes, Nature, 440, 1033–1036, doi:10.1038/nature04660.

Wright, A., and M. Siegert (2012), A fourth inventory of Antarctic subglacial lakes Antarctic, Science, 24(06), 659–664, doi:10.1017/S095410201200048X.

Wright, A. P., et al. (2012), Evidence of a hydrological connection between the ice divide and ice sheet margin in the Aurora Subglacial Basin, East Antarctica, J. Geophys. Res., 117, F01033, doi:10.1029/2011JF002066.

Wright, A. P., D. A. Young, J. L. Bamber, J. A. Dowdeswell, A. J. Payne, D. D. Blankenship, and M. J. Siegert (2014), Subglacial hydrological connectivity within the Byrd Glacier catchment, East Antarctica, J. Glaciol., 60(220), 345–352, doi:10.3189/2014JoG13J014.

Young, D. A., et al. (2011), A dynamic early East Antarctic Ice Sheet suggested by ice-covered fjord landscapes, Nature, 474(7349), 72–75.

2.10 SUPPLEMENTARY FIGURES

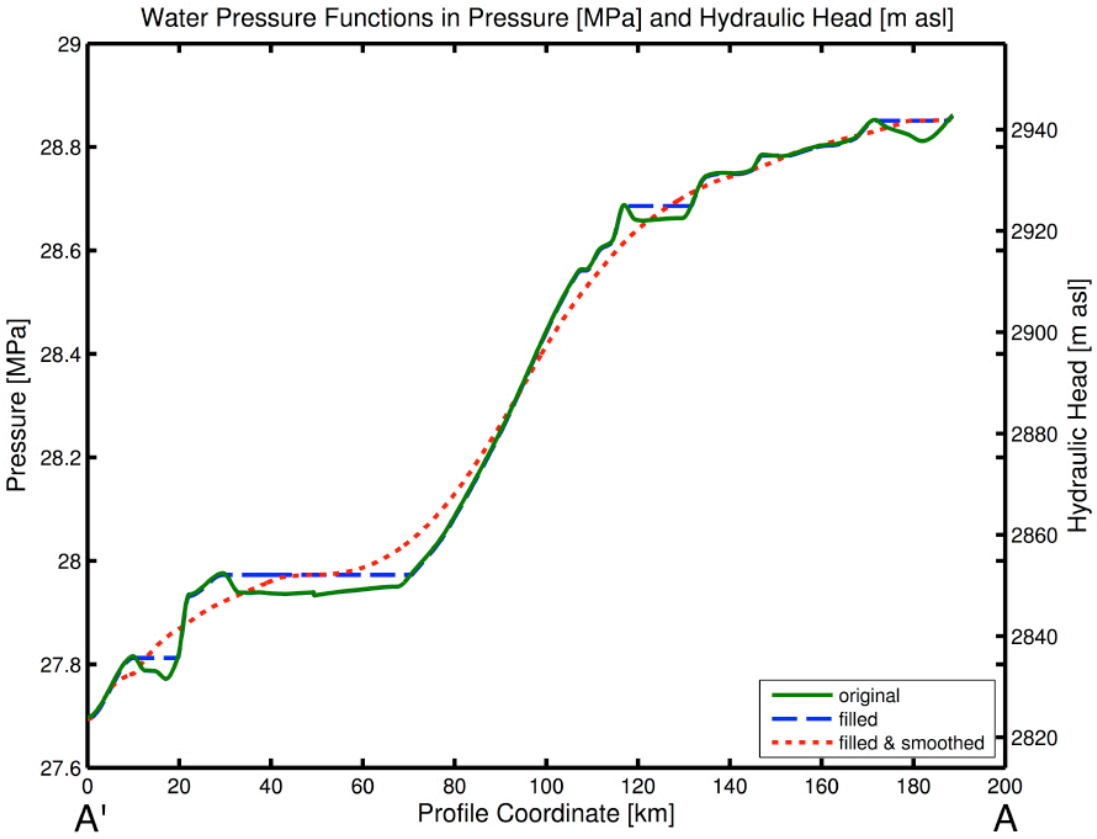

Figure S2.1. Plot of the water pressure at the subglacial bed (P_{ws}). Pressure is defined as absolute pressure (MPa) and as hydraulic head (m asl). The original pressure function (solid green line) was filled (dashed blue line) and smoothed (dotted red line) in order to allow a smooth, solvable solution to the 1D water sheet equation (2.2). Note: the location of the profile A-A' is shown in Figure 2.2b.

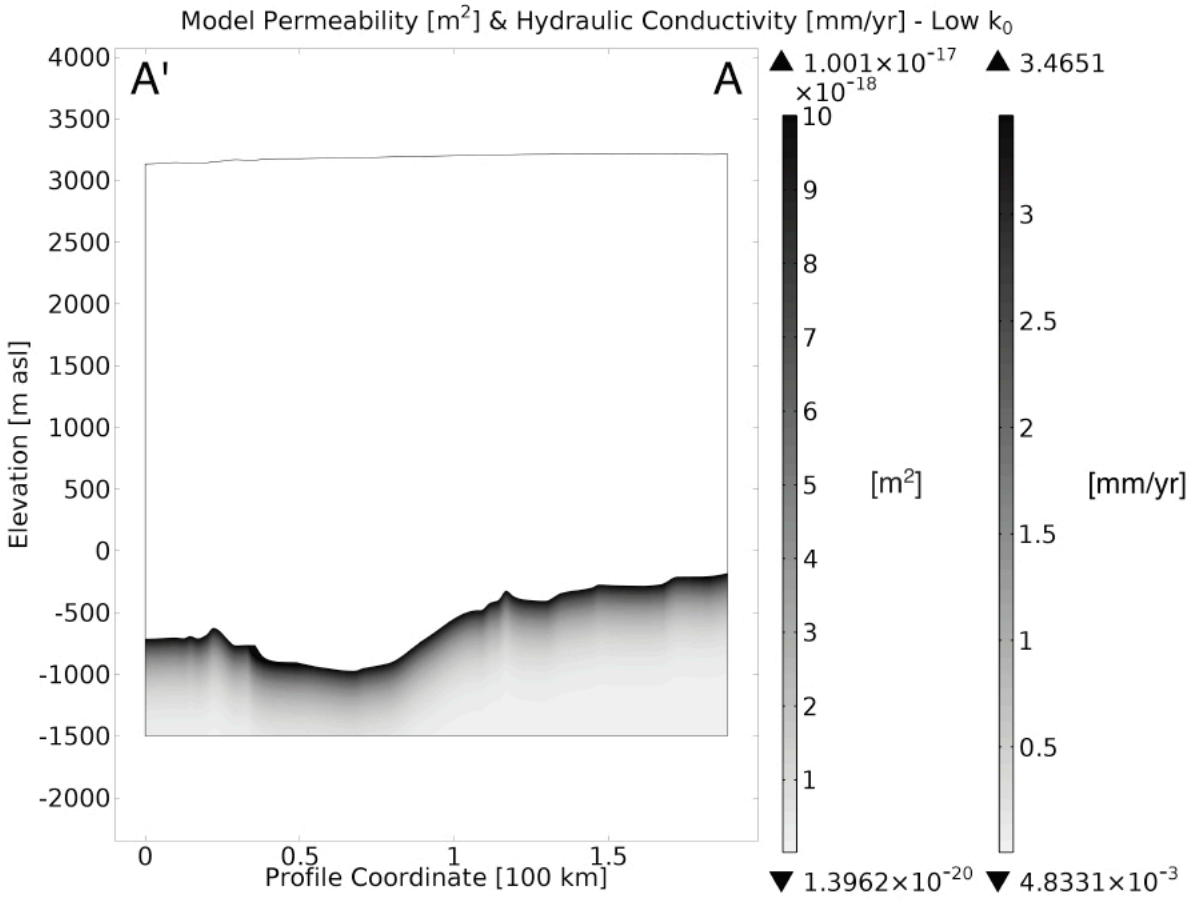

Figure S2.2. Plot of the permeability and equivalent hydraulic conductivity used in the groundwater subdomain for the lowest k_0 parameterization. As all the parameterizations follow the same exponential law of decreasing permeability with depth, the medium and highest parameterizations are simply 10^3 and 10^6 times the low k_0 (or K_0), respectively. Note that the subglacial lakes are given an isotropic, homogeneous value of k_0. Also note that the location of the profile A-A' is shown in Figure 2.2b.

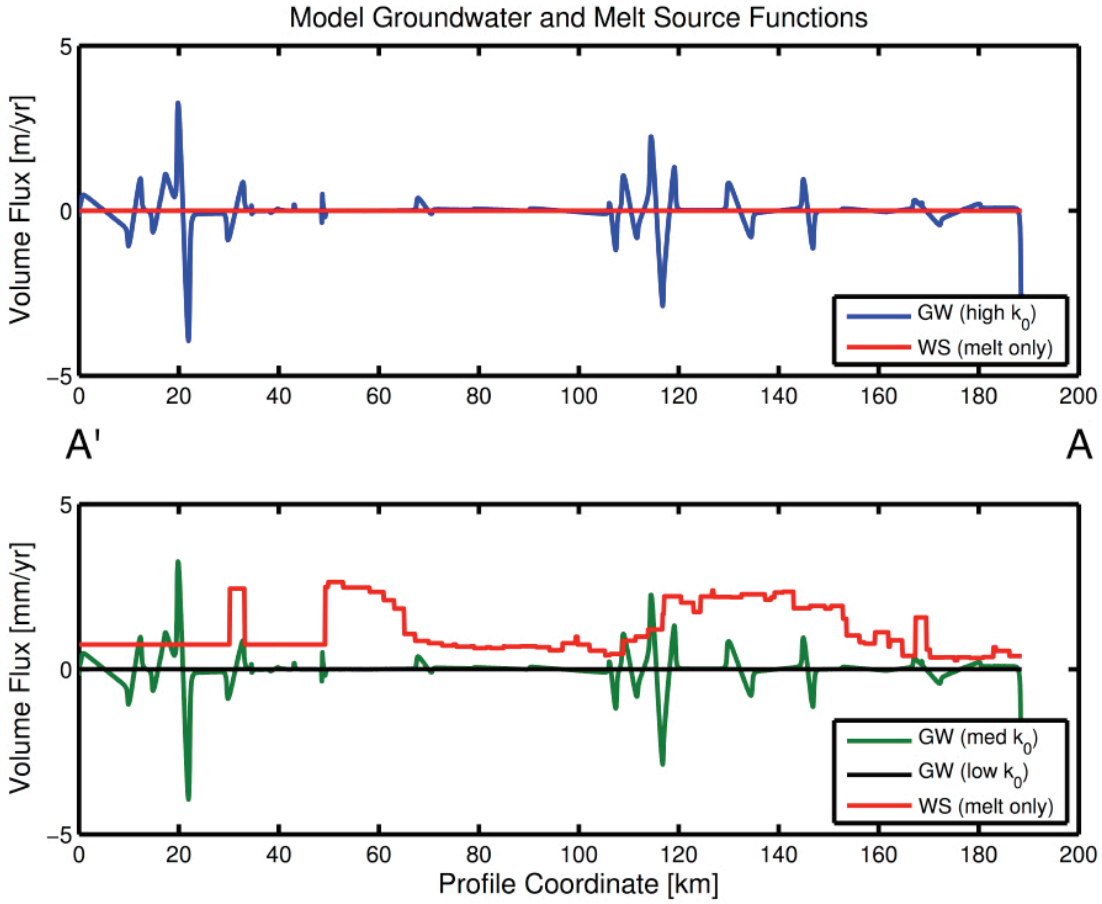

Figure S2.3. Plot of the groundwater (GW) and basal ice melt rate (WS [*Carter et al.*, 2009b]) sources used to calculate the source term (G and b, respectively) parameterizations. The location of the profile A-A' is shown in Figure 2.2b. The scale of the top plot is three orders of magnitude greater than the bottom (i.e. m/yr vs. mm/yr). Note that the various groundwater volume fluxes, q, have identical trends but are three (or six if low vs. high) orders of magnitude apart from each other. It is important to also note that the groundwater values are derived from the model and the melt rates are given *a priori*.

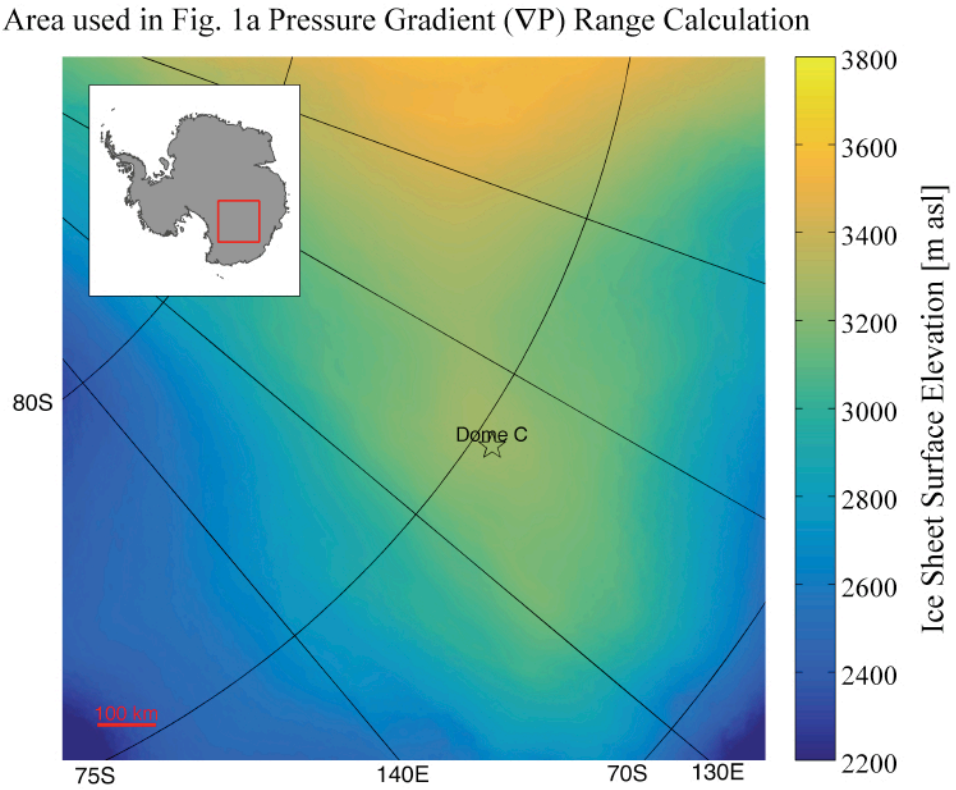

Figure S2.4. Plot of the area used to calculate the range of pressure gradients (∇P) used in Figure 2.1a. The surface elevation of the ice sheet uses the Bedmap2 dataset [*Fretwell et al.*, 2013] and shows the location of Dome C.

2.11 SUPPLEMENTARY REFERENCES

Carter, S. P., D. D. Blankenship, D. A. Young, and J. W. Holt (2009b), Using radar-sounding data to identify the distribution and sources of subglacial water: Application to Dome C, East Antarctica, J. Glaciol., 55(194), 1025–1040, doi:10.3189/002214309790794931.

Fretwell, P., et al. (2013), Bedmap2: Improved ice bed, surface and thickness datasets for Antarctica, The Cryosphere, 7, 375–393, doi:10.5194/tc-7-375-2013.

Chapter 3: Potential Groundwater and Heterogeneous Heat Source Contributions to Ice Sheet Dynamics in Critical Submarine Basins of East Antarctica[2]

Abstract

We present the results of two numerical models describing contributions of groundwater and heterogeneous heat sources to ice dynamics directly relevant to basal processes in East Antarctica. A two-phase, one-dimensional hydrothermal model demonstrates the importance of groundwater flow in vertical heat flux advection near the ice/bed interface. Typical, conservative vertical components of groundwater volume fluxes (from either topographical gradients or vertically channeled flow) on the order of ±1-10 mm/yr can alter vertical heat flux by ±50-500 mW/m^2 given parameters typical for the interior of East Antarctica. This heat flux has the potential to produce considerable volumes of meltwater depending on basin geometry and geothermal heat production. A one-dimensional hydromechanical model demonstrates that groundwater is mainly recharged into saturated, partially poroelastic (i.e. vertical stress only; not coupled to a deformation equation) sedimentary aquifers during ice advance. During ice retreat, groundwater discharges into the ice/bed interface, which may contribute to water budgets on the order of 0.1-1 mm/yr. We also present an estimated map of potentially heterogeneous heat flow provinces using radiogenic heat production data from East Antarctica and southern Australia, calculated sedimentary basin depths, and radar-derived bed roughness. These are overlaid together to delineate the areas of greatest potential effect from these modeled processes on the ice sheet dynamics of the East Antarctic Ice Sheet.

---

[2] A version of this chapter was published as Gooch, B. T., D. A. Young, and D. D. Blankenship (2016), Potential groundwater and heterogeneous heat source contributions to ice sheet dynamics in critical submarine basins of East Antarctica, *Geochemistry, Geophysics, Geosystems*, 17, doi:10.1002/2015GC006117.

3.1 OBSERVATIONS

Recent studies [e.g., *Mackintosh et al.,* 2011*; Fretwell et al.* 2013*; Mengel and Levermann* 2014*; Pollard et al.,* 2015] have shown the potential instability of the East Antarctic Ice Sheet (see Figure 3.1 for location) in basins lying well below sea level to represent significant contributions to sea level rise (roughly 20 m). Attempting to model this ice sheet accurately for various purposes (e.g. targeting old ice core sites or simulating future ice sheet behavior) has been a field of active research for some time [*Huybrechts and Oerlemans,* 1988*; Wilch and Hughes,* 2000*; Pattyn,* 2008*; Van Liefferinge and Pattyn,* 2013*; Sun et al.,* 2014*; Pollard et al.,* 2015]. The specifics of ice sheet dynamics depend on many factors including, but not limited to, solar radiation, precipitation, climate, ocean influences, and bed topography and geology. While surface measurements are easier to obtain compared to the subsurface measurements, the subsurface factors are of great importance to the overall ice sheet's stability [e.g., *Blankenship et al*., 1986, 1993, 2001; *Lowe and Anderson*, 2003; *Hughes et al.*, 2011; *Thoma et al.*, 2012; *Schroeder et al.*, 2014]. While a few continental ice sheet models incorporate limited subglacial data and estimations of bed geometry, homogeneous geothermal heat flux, and interfacial water systems (e.g., PISM, *Winkelmann et al.* [2011]), others elements such as groundwater flow, sediment erosion, heterogeneous geothermal heat flux, and poroelastic sediments are rarely incorporated [e.g. *Flowers et al.*, 2005; *Pattyn*, 2010]. These processes are most likely critical additions needed in ice sheet modeling. This research seeks to investigate the nature of some of these subglacial processes on the East Antarctic Ice Sheet, in particular, groundwater flow and heterogeneous geothermal heat flux (see Figure 3.1 for the specific area of focus).

3.1.1 Observations – Geothermal Heat Flux

Geothermal heat flux in East Antarctica has been estimated using various approaches. One approach utilizes global surface wave tomography to extrapolate known surface heat flux measured globally to Antarctica (i.e. *Shapiro and Ritzwoller*, 2004). Another approach [*Fox Maule et al*., 2005] utilizes satellite magnetic data to map the

depth to the base of the magnetic crust (i.e. Curie depth or isotherm) in East Antarctica and then model the heat flux from the Curie isotherm to the surface using a very simplified bulk geologic heat transfer model. Yet another approach takes geologic data from Australia and East Antarctica to speculate the heat flux values that may exist using tectonic plate reconstruction [e.g. *Pollard et al*., 2005]. *Pattyn* [2010] combined all of those approaches and known subglacial lake distributions to produce a geothermal heat flux map. While none of these approaches has yielded a high-enough resolution estimate of the thermal structure of East Antarctica for adequate ice sheet simulation, they represent the de facto choice for ice sheet modelers until further geologic data is obtained (i.e. thermal properties of the crust such as thermal conductivity and radiogenic heat production).

3.1.2 Observations – Groundwater

The flow of groundwater beneath ice sheets has historically been of interest to glaciologists (see *Piotrowski* [2006] for review). The importance of groundwater in affecting ice dynamics has been diminished by the glaciological community as an important physical process due to its lack of water transmissivity when compared to the flow of water at the base of the ice [*Alley*, 1989]. Despite this, many studies have still cited it as a potential cause for concern when modeling cryospheric systems [*Clarke et al*., 1984; *Echelmeyer*, 1987; *Waddington*, 1987; *Cutler et al*., 2000; *Flowers et al*., 2005; *Boulton*, 2010; *Christofferson et al*., 2014]. However, there has been a considerable amount of effort to understand how past glaciers and ice sheets affect regional groundwater systems (see *Person* [2012] for review). Many studies have come to the conclusion that ice sheets have reorganized groundwater flow systems and even reversed flow directions [e.g. *Grasby et al*., 2000; *Person et al*., 2007; *Piotrowski et al*., 2009; *McIntosh et al*., 2011]. Due to the difference in the relax times of the sediments in the upper crust, many groundwater systems previously burdened by ice sheets no longer

present still exhibit subsurface pore pressures higher than expected [e.g. *Siegel et al*., 2014], known as fossil, or anomalous, pore pressure.

3.2 HYPOTHESIS – GROUNDWATER FLUX IMPACT ON EAST ANTARCTIC ICE SHEET DYNAMICS

Given that it is well known that ice sheets can affect groundwater systems [e.g. *Grasby and Chen*, 2005; *Bense and Person*, 2008; *Neuzil*, 2015] it is only natural to ask if the reverse is true. Our research here seeks to start answering that question with particular attention to the East Antarctic Ice Sheet. While not being able to fully carry the entirety of basal ice meltwater [*Alley*, 1989], we hypothesize that groundwater may still be important when coupled to other physical processes connected to ice dynamics such as altering geothermal heat flux or interacting with the water system at the base of the East Antarctic Ice Sheet. For example, *Clarke et al*. [1984] pointed to groundwater flow as a leading cause for elevated heat flux at the base of Trapridge Glacier in Canada; *Echelmeyer* [1987] and *Waddington* [1987] also discussed this topic in greater detail. *Christofferson et al*. [2014] discussed the possibility that groundwater in the till underneath ice streams along the Siple Coast of West Antarctica could be the cause for excess basal water. *Lemieux et al*. [2008a] modeled the groundwater system under the former Canadian Laurentide and found that a great deal of groundwater could be discharged as a result of dwindling ice sheet volumes.

The East Antarctic Ice Sheet (see Figure 3.1) is a present-day, continental ice sheet that provides an example for study in attempting to answer our hypothesis. While much study has been dedicated to groundwater research in previously glaciated terrains (such as the former Fennoscandian and Laurentide ice sheets), extending this work to a current, continental ice sheet (i.e. East Antarctic Ice Sheet) will provide critical constraints to the impact of groundwater hydrology on basal ice dynamics from subglacial hydrological and geothermal heat flux alteration. The biggest drawback with the East Antarctic example has been the paucity of subsurface data (e.g. hydrogeological

or thermal properties) but developments in airborne and satellite remote sensing are improving this situation. Another benefit of the choice of the East Antarctic Ice Sheet for study is that these and other results to follow will help inform ice sheet modelers of previously neglected subglacial processes that may be important for simulations crucial to society's interest in future sea-level rise prediction and siting of future ice core drilling (frozen ice at the bed is desirable). Current numerical ice sheet models specific to East Antarctic Ice Sheet dynamics do not take into account elevated, heterogeneous geothermal flux at or the presence of groundwater below the ice/bed interface in the sedimentary basins that underlie much of the ice sheet which are below sea level. This is due to the sparse amount of subsurface data below the thick ice sheet but our research will attempt a first pass estimate at the importance of the aforementioned subglacial factors specific to the East Antarctic Ice Sheet.

Our research presented here is divided into three parts. The first two parts are numerical models meant to test the importance of two different basal processes relevant to ice sheet dynamics that are linked to groundwater flow in the subsurface, in particular, those occurring with deep sedimentary basins. The final part represents our analysis of geophysical data to define potential locations of deep sedimentary basins and geochemical data to estimate the range of heterogeneity in radiogenic heat production of the upper East Antarctic crust. Delineating these two basal elements yields areas where our numerically modeled subglacial processes would likely be a significant contributing factor in affecting ice sheet dynamics in East Antarctica. We will demonstrate in this research that understanding these two elements is crucial to better predicting future ice sheet behavior in a rapidly changing climate.

3.3 Experimental Design and Methods

We designed two deterministic numerical models using COMSOL Multiphysics (COMSOL, Inc.), an automated partial differential equations solver utilizing finite

elements, to test different physical aspects of the hypothesis (Figures 3.2-3.3 and Sections 3.3.1-3.3.2 describe and illustrate these models in detail). One is a model to test the effect of groundwater on the thermal structure of the simulated crust and ice sheet in East Antarctica (see Figure 3.2 and Section 3.3.1). The other model tests the relation of ice sheet evolution and groundwater dynamics (see Figure 3.3 and Section 3.3.2). Finally, thermal data from various sources for East Antarctica and Australia (formerly connected along a shared tectonic plate margin) were compiled in context along with geophysical data to delineate areas where the models' results suggest they may be important in present day East Antarctica. All of the parameters we used in the two different numerical models along with their usage references are listed in Table 3.1. We chose parameters to most conservatively estimate the physical effects at the ice/bed interface whenever possible and are most applicable, but not limited, to the area highlighted in Figure 3.1.

3.3.1 Experimental Design and Methods – Hydrothermal Model

To test the physical effect of groundwater on East Antarctic Ice Sheet thermal structure, we constructed a steady state, one-dimensional numerical heat transfer model (see Figure 3.2 for details). The three sections in the model (from deepest to shallowest) are the crystalline basement rock, the sedimentary basin, and finally the ice sheet. The model incorporates conductive heat transfer throughout the domain and couples advective heat transfer in the fully saturated porous media (i.e. sedimentary basin) and ice column. It also allows for the phase change of ice and water in the ice column. The model is one-dimensional for simplicity in order to demonstrate the most straightforward ice physics relationship and to cut down on computational expense. We chose a steady-state model to evaluate the magnitude of change in heat vertical heat flux (from groundwater advection and increased heat production) and solved for the basal ice temperatures possible for an example likely to exist in the focus area (likely in a pseudo steady state at present; see Figure 3.1). We varied the prescribed groundwater volume fluxes [*Stauffer*, 2006] in both magnitude (decreasing permeability with depth) and direction (i.e.

exfiltration or infiltration). Vertical ice flow (downward advection from surface accumulation at ice divides) is kept constant for all model simulations. The ice sheet column is modeled as one being proximal to an ice sheet divide (i.e. lateral ice advection neglected; generally the thickest part of an ice sheet) in order to more clearly elucidate the effects of groundwater-advected heat flux on the ice sheet thermal state. The governing equations (described below) we used vary along the column depending on the model section component (i.e. where heat is advected or transferred via diffusion only) but are all coupled seamlessly by COMSOL Multiphysics.

The majority of the model domain length extends from the Curie isotherm (~580°C [e.g. *Fox Maule et al*., 2005]), the depth to the base of the magnetic crust, (33 km below the ice/bed interface) to the top of the crystalline basement rock (3 km below the ice/bed interface) that forms the bottom section. These depths, as well as, those in the next section are derived from recent geophysical analyses of East Antarctica [*Aitken et al*., 2014; *Frederick*, 2015] as well as drawing on earlier work [*Drewry*, 1976; *Shapiro and Ritzwoller*, 2004; *Studinger et al*., 2004; *Fox Maule et al*., 2005; *Ferraccioli et al*., 2009; *Jordan et al*., 2013]. We chose to rely on a Dirichlet boundary condition (i.e. temperature) at the bottom of the model domain instead of Neumann boundary condition (i.e. heat flux) as a generally known temperature (~580°C) exists at a specific estimated depth for the model focus area and is also the general approach taken for these types of estimates [e.g. *Fox Maule et al*., 2005; *Petrunin et al*., 2013]. The governing equation in this bottom section is a steady-state heat diffusion equation

$$0 = \nabla \cdot (\kappa_b \nabla T) + Q_b \tag{3.1}$$

where $\nabla \cdot$ is the divergence (used here in one dimension as d/dz), κ_b is the thermal conductivity of the basement rock, ∇ is the gradient (also used here in one dimension as d/dz), T is the temperature to be solved, and Q_b is a source term for the added radiogenic heat production due to the decay of naturally occurring radioactive elements in the rock.

The radiogenic heat production, Q_b, is evaluated as $Q_b = Q_0 e^{-d/D}$ [Lachenbruch, 1970], where Q_0 is the heat production at the top of the basement rock which is varied between two values, d is the depth, and D is a characteristic length scale typical for this kind of setting [*Jaupart*, 1986; *Waples*, 2001]. The two crustal values of basement surface heat production were selected as a representation of a lower (0.5 μW/m^3) and higher (5 μW/m^3) value typical of global continental crust and Australian crust, respectively [*Sandiford and McLaren*, 2002; *McLaren et al*., 2003]. The reason for the higher number is that the Australian crust across the extensional margin from East Antarctica has a largely elevated average heat production and is considered analogous for interpreting the possibility of East Antarctic crust along with its limited thermal data [*Carson et al*., 2013].

The middle section of the column (3 to 0 km below the ice/bed interface) is a porous medium containing sedimentary rock and water that represents a typical sedimentary basin above the basement rock (for the area indicated in Figure 3.1) and draws from earlier work for its estimated depth [*Studinger et al*., 2004; *Ferraccioli et al*., 2009; *Jordan et al*., 2013; *Aitken et al*., 2014; *Frederick*, 2015]. The governing equation used is the steady-state heat advection-diffusion equation

$$\rho_w C_{p,w} u_w \cdot \nabla T = \nabla \cdot \left(\kappa_{eq} \nabla T\right) + Q_s \tag{3.2}$$

where ρ_w is the density of the water in the pore space, $C_{p,w}$ is the specific heat capacity of the water, u_w is the groundwater volume flux [*Stauffer*, 2006], κ_{eq} is the equivalent thermal conductivity of the porous medium and fluid mixture, and Q_s is the bulk radiogenic heat production of that mixture (only the sediment is radiogenic though). The left hand side of the equation is the convective component and the first term of the right hand side (RHS) is the diffusive component. The volume flux of the water, u_w, is prescribed as $u_w = V_0 e^{-Ad}$, where V_0 is the groundwater volume flux at the top of the

sediment column varied in the model from -10 to 10 mm/yr (conservatively low for the vertical component of typical groundwater volume flux magnitudes from topographically driven flow), A is a decay parameter typical for this kind of setting [*Jiang et al*., 2009], and d is the depth. The exponential decay in volume flux magnitude correlates with an exponential decrease in sediment porosity (and permeability) with depth (á la *Athy* [1930], *Sclater and Christie* [1980], and *McKenna and Sharp* [1998]). As we do not treat permafrost formation in this model (to give proper treatment for this would require extensive computational expense), we did not allow the prescribed volume of water to be temperature dependent (i.e. approaching zero as the pressure-melting temperature is reached). The approach is reasonable as studies suggest much of the area under the ice sheet shown in Figure 3.1 is at the pressure melting temperature [e.g. *Siegert and Dowdeswell*, 1996; *Pattyn,* 2010*; Van Liefferinge and Pattyn,* 2013] and is validated here given that only one of the ten simulations produced a basal temperature below the pressure melting temperature. The equivalent thermal conductivity of the porous medium, κ_{eq}, is evaluated as $\kappa_{eq} = \phi\kappa_w + (1-\phi)\kappa_s$, where κ_w is the thermal conductivity of water, κ_s is a typical sedimentary rock thermal conductivity [*Beardsmore and Cull*, 2001], and ϕ is the porosity. The porosity, ϕ, is evaluated as $\phi = \phi_0 e^{-bd}$ [*Athy*, 1930], where ϕ_0 is the surface porosity of a typical crustal value [*Gleeson et al*., 2011; *Gleeson et al*., 2014], b is a porosity decay term appropriate for this kind of setting [*Sclater and Christie*, 1980; *Jiang et al*., 2010], and d is the depth.

The top section (0 to 3 km above the ice/bed interface) of the model represents a simulated column of ice proximal to an ice sheet divide (see Figure 3.1 for general area of applicability). The governing equation used is a steady-state heat advection-diffusion equation similar to above but lacks a source term and allows for the phase change of ice and water

$$\rho C_p u_i \cdot \nabla T = \nabla \cdot (\kappa \nabla T) \tag{3.3}$$

where ρ is the density of the fluid (ice or water; temperature dependent), C_p is the specific heat capacity of the fluid, u_i is the vertical advection of the ice, and κ is the thermal conductivity of the fluid. The vertical advection of ice, u_i, is defined as a depth dependent function $u_i = u_{i,0}\left(1 - \frac{H-z}{H}\right)^m$ [*Price et al*., 2002] where $u_{i,0}$ is equal to the average surface accumulation rate (negative value here as it is directly downward) of ice typical for interior East Antarctica [*Mosley-Thompson et al*., 1999; *Price et al*., 2002], H is the total thickness of the ice sheet, m is an accumulation parameter typical for interior East Antarctica [*Price et al*., 2002], and z is the elevation from the ice sheet base. The pressure melting temperature for the ice is evaluated as $T_m = 0°\text{C} - \frac{H}{1149\,[m]}$ [*Siegert and Dowdeswell*, 1996] which equates to -2.61°C for this model. The density of the fluid, ρ, is evaluated as $\rho = \frac{\theta\rho_i C_{p,i} + (1-\theta)\rho_w C_{p,w}}{\theta C_{p,i} + (1-\theta)C_{p,w}}$ where θ is the fraction of ice, ρ_i is the density of ice, ρ_w is the density of water, $C_{p,i}$ is the specific heat capacity of ice, and $C_{p,w}$ is the specific heat capacity of water. The specific heat capacity, C_p, of the material is evaluated as $C_p = \theta C_{p,i} + (1-\theta)C_{p,w} + L\frac{d\,(1-\theta)}{dT}$ where L is the latent heat from ice melting to water. Note that the latent heat term is not time-dependent and is critical for calculating the steady phase boundary between water and ice in this section of the model domain (initially all ice in the model setup). The thermal conductivity, κ, is evaluated as $\kappa = \theta\kappa_i + (1-\theta)\kappa_w$, where κ_i is the thermal conductivity of ice and κ_w is the thermal conductivity of water. These formulations are based on the module for heat transfer accounting for phase change in COMSOL Multiphysics (v4.3b).

The governing equations (Equations 3.1-3.3) were solved using COMSOL Multiphysics with a mesh size of 1 meter giving 36,000 domain elements. Dirichlet boundary conditions we used in the model are temperature conditions at the top and bottom. A temperature at the bottom, T_b, of 580°C represents the Curie isotherm and the top, T_i, with -50°C for the ice sheet surface. We selected the temperature at the Curie isotherm based on common usage for this depth [*Fox Maule et al*. 2005; *Rajaram et al*.

2009] while the ice sheet surface temperature is an annual average for present day, interior East Antarctica [*Comiso* 2000; *Price et al*. 2002]. Due to COMSOL's solving efficiency, current notebook computer performance, and the problem's single dimension in steady state, the solution time was within minutes.

3.3.2 Experimental Design and Methods – Hydromechanical Model

To test the effect of potential East Antarctic Ice Sheet evolution on the groundwater volume flux at the ice/bed interface, we created a transient one-dimensional, numerical groundwater model (see Figure 3.3 for details). The model was largely based on the same approach used by *Lemieux et al*. [2008b] to validate a three-dimensional continental groundwater model forced by ice sheet model output. The domain of the model is a sedimentary basin with fully saturated (i.e. Darcy flow) pore space similar to the basin in the previous model. The ice sheet was evolved through a partial mock glacial cycle that is simulated by growing (advance) and shrinking (retreat) a water equivalent ice column over the top of the 3 km sediment column. While the specific timing used here is arbitrary and the same as used by *Lemieux et al*. [2008b], the rate of change is similar to that of rapidly declining ice elsewhere in Antarctica [*Christoffersen et al*., 2014]. While this model could have been coupled to the hydrothermal model described in the previous section, the goal with this model was to deterministically simulate solely the transient pressure effects of an ice sheet on a groundwater system given similar geometry and parameters typical of the area of focus in East Antarctica shown in Figure 3.1. Again, Table 3.1 contains all of the parameter information we used in the model simulation along with references for usage precedence. This model is governed by a form of the transient groundwater flow equation that is partially coupled to the ice sheet stress (i.e. vertical only; see *Ingebritsen et al*. [2006])

$$\rho_w S \frac{\partial P}{\partial t} - \nabla \cdot \rho_w \left(\frac{k}{\mu} \nabla P \right) = \rho_w S \zeta \frac{\partial \sigma_{zz}}{\partial t} \tag{3.4}$$

where ρ_w is the density of water (representing a density equivalent of ice; see Figure 3.3), S is the uniaxial specific storage, P is the pore water pressure to be solved, $\nabla \cdot$ is the divergence (used here in one dimension as d/dz), k is the matrix permeability, μ is the viscosity of the water, ∇ is the gradient (also used here in one dimension as d/dz), ζ is the one-dimensional loading efficiency, and σ_{zz} is the vertical stress from the ice sheet. The right hand side of the equation is an *a priori* source term that represents the addition of pore pressure from the ice sheet (see *Neuzil et al*. [2012]). The loading efficiency is set at 0.2 and the specific storage at 1.02×10^{-10} Pa^{-1}, which are consistent with *Lemieux et al.* [2008b]. We evaluate the matrix permeability, k, using an exponential decay model (unlike *Lemieux et al*. [2008b]) where $k = k_0 e^{-Ad}$; where k_0 is the permeability at the top of the sediment column varied in the model through a wide hydrogeologic range, A is the same decay parameter as used before [*Jiang et al*., 2009], and d is the depth. The surface permeability, k_0, is varied from 10^{-10} to 10^{-18} m^2 in order to demonstrate a wide range of geologic materials (generally speaking, unconsolidated sand or gravel to unfractured mudrock or massive crystalline rock). The vertical stress from the ice sheet, σ_{zz}, is evaluated as $\sigma_{zz} = \rho_w g h(t)$ where ρ_w is the water density, g is the acceleration due to gravity, and $h(t)$ is the water equivalent ice sheet height at a given time. The ice sheet starts out at 0 m at 0 kyr and linearly grows to a maximum added height of 3000 m water equivalent (~3300 m of ice) at 10 kyr. After reaching the peak thickness, the ice sheet linearly shrinks back to 0 m of ice at 20 kyr ending the model simulation, consistent with *Lemieux et al*. [2008b].

As before, we modeled the numerical simulations using COMSOL Multiphysics. The domain of 3 km used a 1 m mesh size for a total of 3,000 elements. The governing equation (Eq. 3.4) was solved with the Dirichlet boundary condition of a given hydraulic head function, $h(t)$, at the top (0 km) and a source term throughout (RHS of Equation 3.4) the domain. The simulation was iterated through a partial mock glacial cycle using each of the given values of surface permeability (k_0). We used a 500-year time step in order to balance accuracy, solution time, and output data size. Again, due to COMSOL's

solving efficiency, current notebook computer performance, and the problem's single dimension with time dependence the solution time was within minutes.

3.3.3 Experimental Design and Methods – East Antarctic Areas of Higher Heat Potential and Groundwater Impact

In order to relate the previous method's results to a real-world setting of great societal interest (i.e. sea level rise component from the marine-grounded East Antarctic Ice Sheet), we created a subglacial map detailing areas where the above experiments' results may be most likely influential to ice sheet dynamics. We created this map by using current crustal thermal data, tectonic plate reconstruction, and geophysically derived geologic maps from publicly available data. Some of the surface radiogenic heat production data in Australia come from the publically available Global Heat Flow Database (http://www.heatflow.und.edu/). The heat production data in East Antarctica are from *Carson and Pittard* [2012]. We calculated the bulk of the present-day heat production data from the Australian OZCHEM surface geochemistry database [*Champion et al*., 2007] using the same method as *Carson and Pittard* [2012] used which is based on *Turcotte and Schubert* [2002]. The tectonic interpretations across East Antarctica and Australia from *Aitken et al*. [2014] serve as a rough guide to tectonic province delineation in the East Antarctic.

Aerogeophysical surveys from the University of Texas Institute for Geophysics and other collaborations [e.g. *Young et al*., 2011; *Frederick*, 2015] are principally over the Wilkes and the Aurora Subglacial Basins of East Antarctica. These surveys comprise gravimetric and ice-penetrating radar datasets among others, which we used to define sedimentary basin depth and extent. Gravity data are useful in delimiting less dense sedimentary basins and their depths from the surrounding, denser crystalline basement rock. Ice-penetrating radar data are useful not only for imaging internal ice sheet structure and ice bottom depth (Bedmap2 used; *Fretwell et al*. [2013]) but also in mapping out bed roughness [*Shepherd et al*., 2001]. The bed roughness (root mean

squared deviation of detrended bed elevation data on a 1,600 m baseline) we used here to define extents of smoother (i.e. low roughness) sedimentary terrains interpreted as softer sedimentary land surfaces or previously shallow marine settings.

We constructed a somewhat conservative and arbitrary approach to citing zones of higher probable groundwater impact (see Figure 3.8) to ice sheet dynamics by selecting only the zones of overlap of relatively low bed roughness (cutoff height of about 20 m) and areas of at least 1 km of gravity-derived sediment thickness (for higher confidence in delineation). This approach ensured that potential basin-to-regional scale groundwater flow systems could be delineated in a relatively conservative approach, relying on the combination of two independent geophysical constraints (i.e. electromagnetic and gravimetric). We used ArcGIS (ESRI, v10.2) and PaleoGIS (The Rothwell Group, L.P., v4.2), a tectonic plate reconstruction software, to interpret all of the data together. We used a plate reconstruction model to connect East Antarctica and Australia at 160 Ma, in keeping with *Aitken et al*. [2014]. Once the East Antarctic and Australian plates were reconnected, we calculated basic statistical functions (average, standard deviation, etc.) for each of the heat production groupings (see Figure 3.8 for the selected rectangular regions) delineated by data point proximity and correlation to roughly defined tectonic provenances [*Carson et al*., 2013; *Aitken et al*., 2014].

3.4 RESULTS

3.4.1 Results – Hydrothermal Model

One of the main trends in the hydrothermal model results is the grouping in temperature profiles (see Figure 3.4). As expected in the sediments and basement rock, the temperature profiles with the higher heat production (5 $\mu W/m^3$) curve upward from the linear trend expected had no heat production been added. The profiles with the lower heat production (0.5 $\mu W/m^3$) group closer to that linear trend. The modeled temperatures in the ice sheet are nearly identical for much of the ice column. The temperature profiles

for all of the results are equal at the model domain top and bottom (i.e. boundary conditions). A major slope break occurs at the ice/bed interface (at 0 km). In all but one (Q_0 = 0.5 μW/m^3 and V_0 = -10 mm/yr) of the resulting temperature profiles, the ice is above the pressure melting temperature of -2.6°C (see zoom of Figure 3.4 in Supplemental Figure S3.4). The simulated temperatures at the ice/bed interface range from about -4 to 35°C. The resulting phase change in all but one of the profiles results in the conversion of ice to water in the column. This essentially simulates a one-dimensional subglacial lake under an ice sheet where the bottom of the column is liquid water and the ice sheet is above it. The columns of basal water range in height from 32 to 220 meters (see Figure S3.5 for phase change plot).

Another prominent trend in the model results is the simulated vertical heat flux in the uppermost portion of the sedimentary basin (see Figure 3.5) where the groundwater volume flux is the dominant factor in heat advection. The highest positive vertical heat flux values (peak of ~ 440-500 mW/m^2 at 0 km elevation) correlate to the model runs using the highest positive groundwater volume fluxes (max of 10 mm/yr). Likewise, the most negative vertical heat flux (peak of ~ -300 mW/m^2 at 0 km elevation) correlates to where the heat flux is advected via groundwater downward at a max of -10 mm/yr at 0 km elevation. The values clustering in the middle of Figure 3.5 (V_0 = -1 to 1 mm/yr) span a range of about 25-125 mW/m^2. Within these, the simulated vertical heat flux values without fluid advection (i.e. volume flux = 0 mm/yr) are at roughly 60 and 85 mW/m^2 (for Q_0 = 0.5 μW/m^3 and 5.0 μW/m^3, respectively). Also within that same cluster, it is observed that a change of +/- 1 mm/yr will alter the vertical heat flux at the ice/bed interface surface by about 40 mW/m^2. Another trend in the middle clustering is that, all other things being equal, the difference in heat production choice (i.e. Q_0) results in about a 20-25 mW/m^2 difference in simulated heat flux output. The decrease in heat flux with depth is due to the exponential decrease in groundwater volume flux prescribed in the model setup, which is meant to more closely simulate assumed natural conditions.

3.4.2 Results – Hydromechanical Model

The main outputs for the hydromechanical model are subsurface pore pressure and the surface exchange, which is the groundwater volume flux at the surface (i.e. top) of the one-dimensional model. The simulated pore pressures shown in Figure 3.6 demonstrate the subsurface behavior through a portion of a mock glacial cycle (20 kyr here as in *Lemieux et al.* [2008b]) for one of the parameterizations of surface permeability (k_0 = 10^{-18} m^2). The fossil, or anomalous, pore pressure is observed as bulges of increasing pressure down to about 1.2 km in depth, which relates to the exponential drop in permeability with depth. All but one (k_0 = 10^{-10} m^2) of the parameterizations modeled exhibit similar behavior to the one shown in Figure 3.6 but with slightly less exaggeration of fossil pore pressure and are not included. Pore pressure can be converted to hydraulic head; a converted plot of Figure 3.6 is included in the Supporting materials (Figure S3.8).

The main behavior of the simulated pore pressure is that the addition of the growing ice overburden pressure adds to the top of the domain unevenly until the ice sheet shrinks leaving the pressure at the top lower than that part of the way down. This disequilibrium of pressure causes higher pore pressure in the subsurface leading to volume fluxes of water infiltrating into (recharge) or exfiltrating out of (discharge) the surface of the sediment (ice/bed interface). Figure 3.7 shows this behavior in detail for each parameterization. At the beginning (0 kyr) all of the parameterizations are essentially (with some numerical error) at zero volume flux but as the simulation time advances they quickly differ. The highest surface permeability parameters (10^{-10} and 10^{-12} m^2) quickly reach a maximum input of about -0.72 mm/yr almost instantaneously where as the rest are more or less evenly spread out (differing by about 0.2 mm/yr). As the ice sheet pressure adjusts, the parameterizations act largely (again, with some numerical error) symmetrical to the ice advance pattern. As before the highest surface permeability parameters quickly reach a maximum output of about 0.72 mm/yr almost instantaneously where as the rest are more or less evenly spread out through 20 kyr. The

magnitude of volume flux for the rest of the surface permeability parameters vary from 0.2 to 0.6 mm/yr. Given added simulation time past 20 kyr (not shown in Figure 3.7) it can take an additional few hundred to tens of thousands of years, depending on the parameterization, for the surface exchange to return to the initial condition (i.e. 0 mm/yr).

3.4.3 Results – East Antarctic Areas of Higher Heat Potential and Groundwater Impact

The mapping of the extents of this research's relevant impact to under the East Antarctic Ice Sheet is shown entirely in Figure 3.8. Our effort produced a map of the regions where groundwater flow systems may possibly be extent at the basin-to-regional scale in East Antarctica. The map is also a first attempt at trying to roughly estimate the degree of heterogeneity in the near-surface thermal properties of the East Antarctic crust by extension of known values in the previously connected continent of Australia (c. 160 Ma) via geophysical interpretation, along with some limited geochemical data from East Antarctica. The groupings of surface heat production largely cluster into the three provinces of heat flow in Australia (see the rectangular boxes A-C in Figure 3.8 and *McLaren et al*. [2003]). The average heat production in Group A is 1.08 $\mu W/m^3$ with a standard deviation of 1.53 $\mu W/m^3$. The statistical calculations for Group A used 2,044 data points from Australia and 55 data points from East Antarctica. The average heat production in Group B is 4.27 $\mu W/m^3$ with a standard deviation of 28.75 $\mu W/m^3$. The statistical calculations for Group B used 2,132 data points from Australia and 34 data points from East Antarctica. The average heat production in Group C is 1.43 $\mu W/m^3$ with a standard deviation of 2.59 $\mu W/m^3$. The statistical calculations for Group C used 9,702 data points from Australia and 224 data points from East Antarctica. Group B represents the Mawson/Gawler cratonic connection [*Carson et al*., 2013; *Aitken et al.*, 2014] with the values of heat production being tightly connected to the tectonic interpretations of *Aitken et al.* [2014] and are a part of the South Australian heat flow anomaly [see *Sandiford and McLaren et al*., 2002; *McLaren et al*., 2003; *Carson et al*., 2013]. The values in Group C largely come from a different and varied cratonic history than those in

Group A and are much younger in age on average. The areas which groundwater may have some impact on ice sheet dynamics and water budgets (see Section 3.3.3) are mostly located distal to the coastline of East Antarctica with the exception of some large, coastal outlet glacier areas containing deep sedimentary valleys. The bulk of the areas of probable groundwater impact are largely in areas presently at or below present day sea level (lying mostly within extents of the Aurora and Wilkes subglacial basins; see Figure 3.8). The largest groundwater impact areas' longest axes (specifically in the Wilkes and Aurora subglacial basins) tend to coincide with the longer tectonic interpretations of *Aitken et al*. [2014].

3.5 DISCUSSION

The one-dimensional hydrothermal model, while a highly simplified version of reality, demonstrates the basic but important impact the advection of heat flux via groundwater can contribute when added to diffusive heat flux (shown here by adding as much as 380-415 mW/m^2). The values with diffusion alone (roughly 60 and 85 mW/m^2) are consistent with those estimated by *Fox Maule et al*. [2005] with the lower value also consistent with those of *Shapiro and Ritzwoller* [2004] in East Antarctica. One main simplification inherit with one dimensional modeling is the absence of horizontal effects, in particular here, as horizontal heat flux by groundwater or ice sheet flow. This effect has been studied by *Waddington* [1987] and shown to be important. Future work should include this when extending this approach to multidimensional models. Although the simulated lake depths represent equilibrium levels (the model is unable to drain water from under the ice column), the range of lake depths (32-220 m) for all but one of the simulations (one had ice frozen to the bed) is consistent with those observed (see current inventory from *Wright and Siegert* [2012]). The results from the hydrothermal model demonstrate that even with moderately low groundwater volume flux magnitudes, the vertical heat flux magnitude under the interior of the East Antarctic Ice Sheet can be modified dramatically. This added complexity to the geothermal heat flux

parameterization for continental ice sheet models could add significant value to their usage if incorporated.

The one-dimensional hydromechanical model, while also a highly simplified version of reality, demonstrates how changes in ice sheet thickness not only alter the pressure potential of the subglacial water and groundwater but also how the timing of the change can result in unsteady subsurface pore pressures. This disequilibrium in pore pressure causes groundwater to infiltrate into the saturated sediment during ice sheet thickening and exfiltration upon ice thinning similarly observed by *Lemieux et al*. [2008b]. The magnitude of the rates of surface groundwater volume flux can reach 0.6-0.72 mm/yr which given knowledge of the previous model's results would equate to about a 24-28.8 mW/m^2 change in the heat flux magnitude. This significant alteration to the geothermal heat flux could occur at discrete locations (i.e. fault zones) or across widespread areas in the sedimentary basins underneath the East Antarctic Ice Sheet. The groundwater volume fluxes simulated here are only a fraction of those estimated by *Christoffersen et al*. [2014], which are up to roughly one order of magnitude greater, for the marine-grounded Siple Coast ice streams in West Antarctica. Currently, in much of the East Antarctic the ice sheet is generally not as dynamic as in West Antarctica although, as recent work indicates, East Antarctica experienced great changes when compared to present day activity not long ago in the geologic record [*Mackintosh et al.,* 2011; *Young et al.,* 2011; *Mengel and Levermann* 2014; *Pollard et al.,* 2015].

We sought to roughly outline the extent of probable areas where groundwater could potentially act similar to the model simulations and also roughly map the heterogeneity of surface heat production in East Antarctica in Figure 3.8. The resulting figure conservatively estimates that areas shown to have probable groundwater flow systems exist in mostly submarine areas under the East Antarctic Ice Sheet. This area is more prone to ice sheet change from climatic forcing [*Young et al.,* 2011; *Pollard et al.,* 2015] which increases the significance of groundwater as a subglacial process there. The

fact that these sedimentary basin surfaces are generally lower than their surrounding topography is not surprising but as this terrain becomes overlain by ice they are both dramatically lowered (albeit unequally due to erosional and isostatic differentials) with deeper depressions existing more inland under the thicker ice. The probable groundwater impact areas locations are significantly inland and are most likely due to this effect and the long, complicated geologic history of the intra-cratonic sedimentary basins of East Antarctica. The heat production data statistics demonstrate the heterogeneity of the geologic surface across the East Antarctic – Australian continental margin. The data, coupled with our model results, suggest that higher, heterogeneous geothermal heat fluxes are more likely throughout East Antarctica than previously estimated [e.g. *Shapiro and Ritzwoller*, 2004; *Fox Maule et al*., 2005; *Pollard et al*., 2005], especially in areas where groundwater flow systems are potentially present. While this may not be greatly significant by itself, our initial attempt to estimate the areas over which these specific processes could potentially play a role in ice sheet dynamics coupled to the deterministic model results could be very significant.

3.6 CONCLUSION

The continental ice sheet modeling community will eventually need to incorporate the effects demonstrated here when simulating ice dynamics in the interior of the East Antarctic Ice Sheet if higher accuracy estimates of future ice volume are to be calculated. While it is highly likely that the physical effects presented here are not as crucial to understand in areas of higher ice velocity (i.e. outlet glaciers), a significant fraction of the total ice sheet maybe affected by such processes and, thus, should be considered. For example, the added complexity to the geothermal heat flux parameterization for continental ice sheet models could add significant value to their usage if incorporated. Further efforts to better define the subglacial geology of the region will help resolve the great uncertainties that exist in the thermal and mechanical properties of the East Antarctic subsurface and lead to better estimations of heat flux and groundwater volume

flux rates (specifically targeting the areas denoted in Figure 3.8 as questions marks). Future efforts in continuing to test the aforementioned hypothesis should focus on coupling these processes together in multidimensional models. This work should also eventually couple these physical processes to the flow of water at the ice/bed interface, as well as, to the flow of the ice sheet above in order to gain an overall better understanding of this poorly understood, critically important natural system.

3.7 FIGURES AND TABLES

Parameter	Value	Units	Parameter Description	Model Usage	References
A	5×10^{-3}	m^{-1}	*Hydraulic conductivity decay parameter*	M, T	*Jiang et al. 2009*
b	5×10^{-3}	m^{-1}	*Porosity decay term*	T	*Sclater & Christie 1980; Jiang et al. 2010*
$C_{p,i}$	2093	J/(kg×K)	*Specific heat capacity, ice*	T	*Mellor & Kantha 1989*
$C_{p,w}$	4186	J/(kg×K)	*Specific heat capacity, water*	T	-
D	10	km	*Crustal length scale*	T	*Jaupart 1986; Waples 2001*
g	9.81	m/s^2	*Acceleration due to gravity*	M	-
H	3000	m	*Total ice sheet thickness added*	T	-
k_0	10^{-18}, 10^{-16}, 10^{-14}, 10^{-12}, 10^{-10}	m^2	*Bed surface permeability*	M	*Singhal & Gupta 2010; Gleeson et al.2011, 2014*
L	3.3×10^5	J/kg	*Latent heat, H_2O*	T	*Mellor & Kantha 1989*
m	1.317	-	*Ice accumulation parameter*	T	*Price et al. 2002*
Q_0	0.5, 5.0	$\mu W/m^3$	*Heat production, surface of basement rock*	T	*Sandiford & McLaren 2002; McLaren et al. 2003*
Q_s	1.0	$\mu W/m^3$	*Heat production, sedimentary rock*	T	*Waples 2001*
S	1.02×10^{-10}	Pa^{-1}	*Storage coefficient*	M	*Lemieux et al. 2008b*
T_b	580	°C	*Temperature, Curie depth*	T	*Fox Maule et al. 2005; Rajaram et al. 2009*
T_i	-50	°C	*Temperature, average ice sheet surface*	T	*Comiso 2000; Price et al. 2002*
T_m	-2.61	°C	*Temperature, ice-bed interface*	T	*Siegert and Dowdeswell 1996*
$u_{i,0}$	-73	mm/yr	*Ice sheet surface ice accumlation rate*	T	*Mosley-Thompson et al. 1999; Price et al. 2002*
V_0	-10, -1, 0, 1, 10	mm/yr	*Sediment surface groundwater volume flux*	T	-
ζ	0.2	-	*Loading efficiency*	M	*Lemieux et al. 2008b*
κ_b	3.2	W/(m×K)	*Thermal conductivity, basement rock*	T	*Beardsmore & Cull 2001*
κ_i	2	W/(m×K)	*Thermal conductivity, ice*	T	*Mellor & Kantha 1989*
κ_s	2.8	W/(m×K)	*Thermal conductivity, sedimentary rock*	T	*Beardsmore & Cull 2001*
κ_w	0.56	W/(m×K)	*Thermal conductivity, water*	T	-
μ	8.94×10^{-4}	Pa×s	*Viscosity, water*	M	-
ρ_i	910	kg/m^3	*Density, ice*	M (*implicit*), T	*Bamber et al. 2001*
ρ_w	1000	kg/m^3	*Density, water*	M, T	-
ϕ_0	0.2	-	*Sediment surface porosity*	T	*Gleeson et al. 2011, 2014*

Table 3.1. Parameters used in the two different numerical models with references, if applicable. Parameters designated by 'T' are used in the hydrothermal model and 'M' for those used in the hydromechanical model. Note that the accumulation rate is negative as it is directed downward.

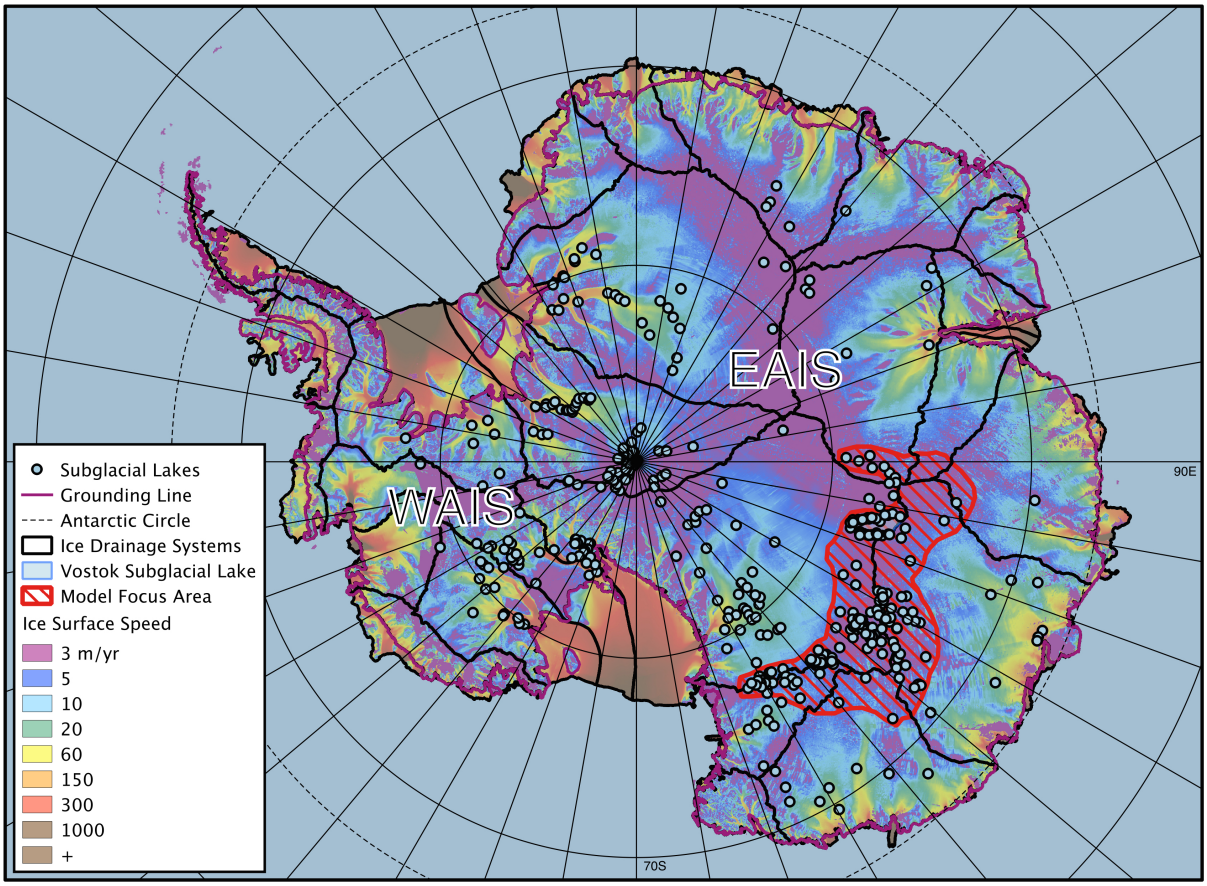

Figure 3.1. Map showing the area of modeling focus and applicability (red-hatched zone). This area was roughly determined by enclosing identified subglacial lakes ([*Wright and Siegert*, 2012] existing under very slow moving ice (surface speed from *Rignot et al.* [2011]) along the ice sheet drainage divides [*Zwally et al.*, 2012] for a large section of East Antarctica known to contain sedimentary basins. The grounding lines used are from *Bindschadler et al.* [2011]. The focus area is used to define typical parameters for the modeling. See Section 3.3 for more details about the model parameters obtained for this area. Note that the latitude and longitude graticules are all in 10° increments. The East and West Antarctic Ice Sheet are noted as EAIS and WAIS, respectively.

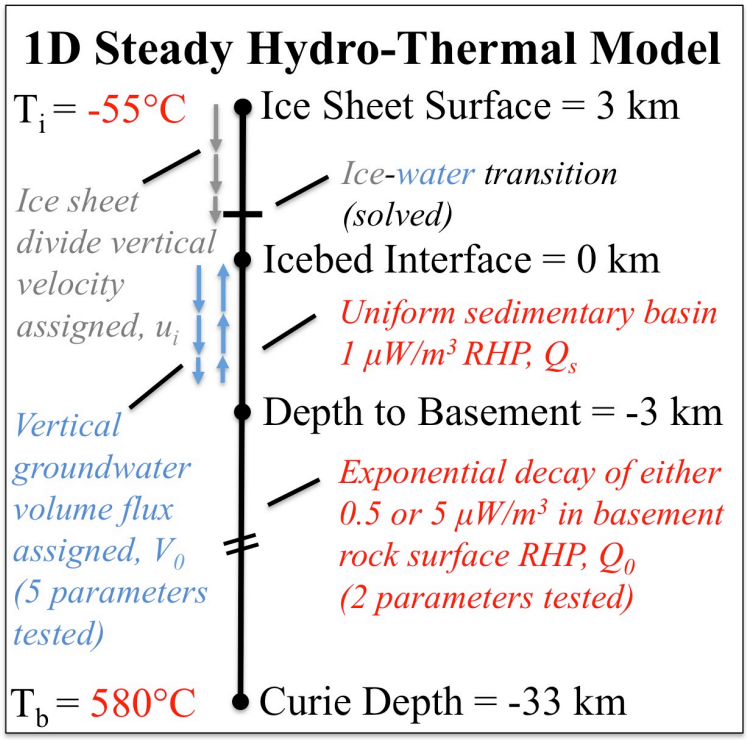

Figure 3.2. Hydrothermal model diagram with explanation. The specific details for this model can be found in Section 3.3.1. "Basement" refers to the crystalline basement rock that exists beneath the modeled sedimentary basin. "RHP" is an abbreviation for the radiogenic heat production (or generation), which naturally occurs from the decay of unstable nuclides in minerals. Note that this vertical heat flow model has two Dirichlet boundary conditions: one at the top and the other at the bottom of the model domain.

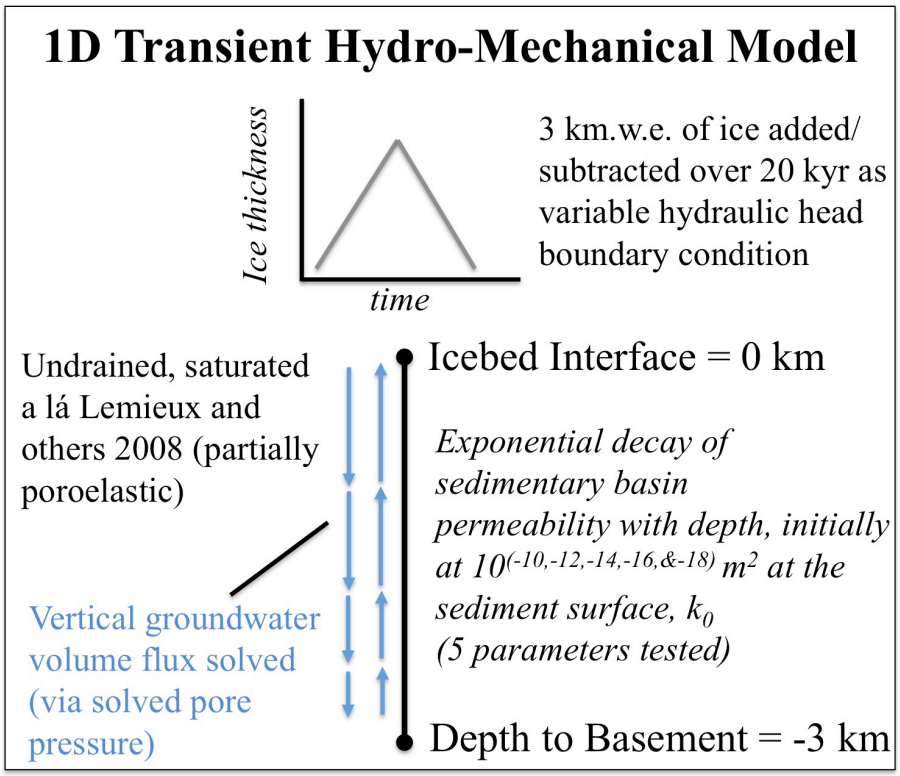

Figure 3.3. Hydromechanical model diagram with explanation. The specific details for this model can be found in Section 3.3.2. Note that the top boundary condition of this vertical groundwater flow model is a variable hydraulic head and the one at the bottom is a no flow boundary condition. Also note that km.w.e. is short for "kilometers water equivalence" in this usage.

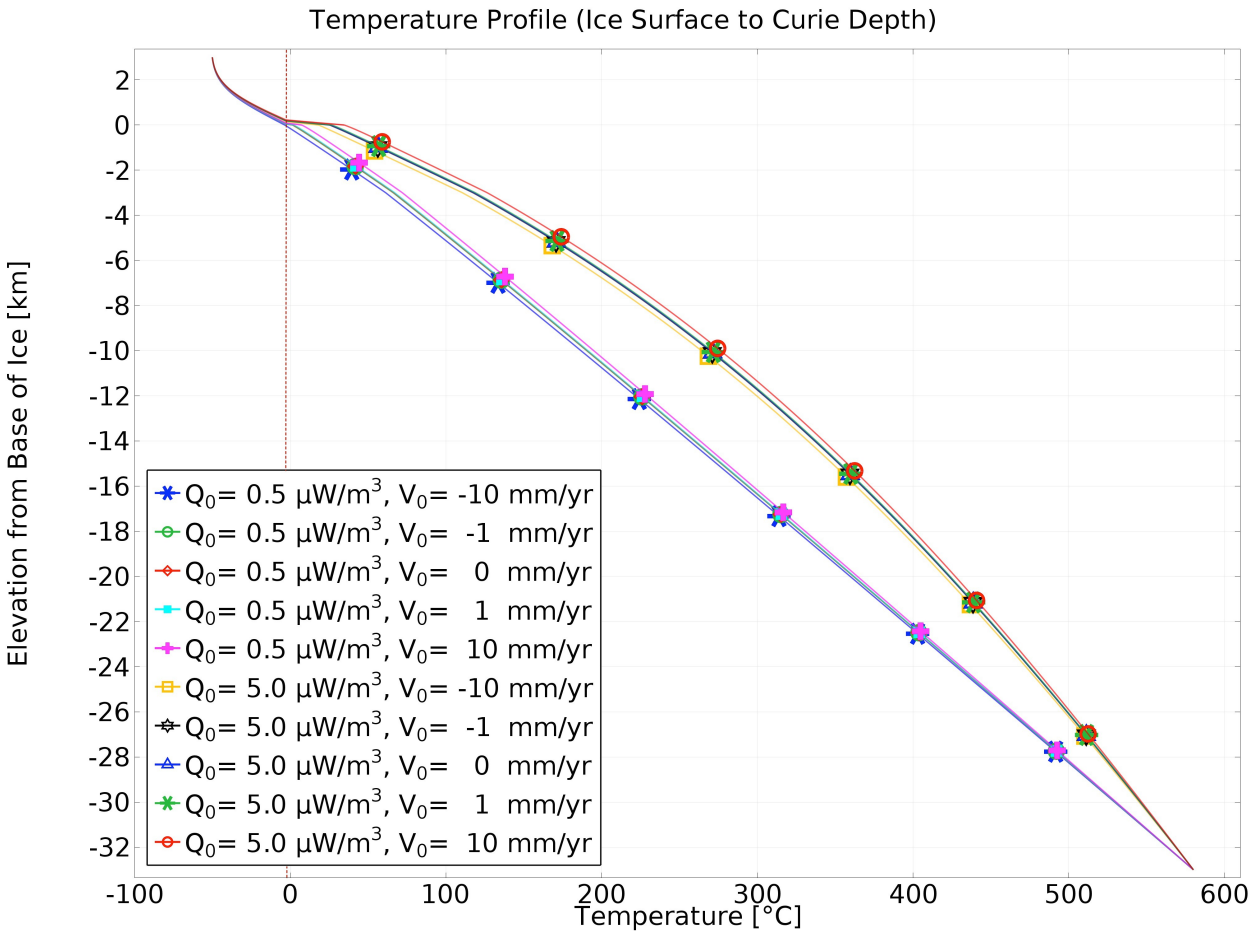

Figure 3.4. Temperature profile with depth from the steady-state 1D hydrothermal model results. The model extends from ice sheet surface (3 km) through the sedimentary basin and crystalline basement (-3 km) to the base of the magnetic crust, or Curie depth (-33 km). Basement surface radiogenic heat production, Q_0, and sediment surface groundwater volume flux, V_0, parameters are plotted. Note that the dominant factor in the two temperature groups in the deeper subsurface is the radiogenic heat production value. The dashed red line is meant to assist the reader in quickly identifying the pressure melting temperature of ice at the ice/bed interface and does not represent the pressure melting temperature in the subsurface of Earth.

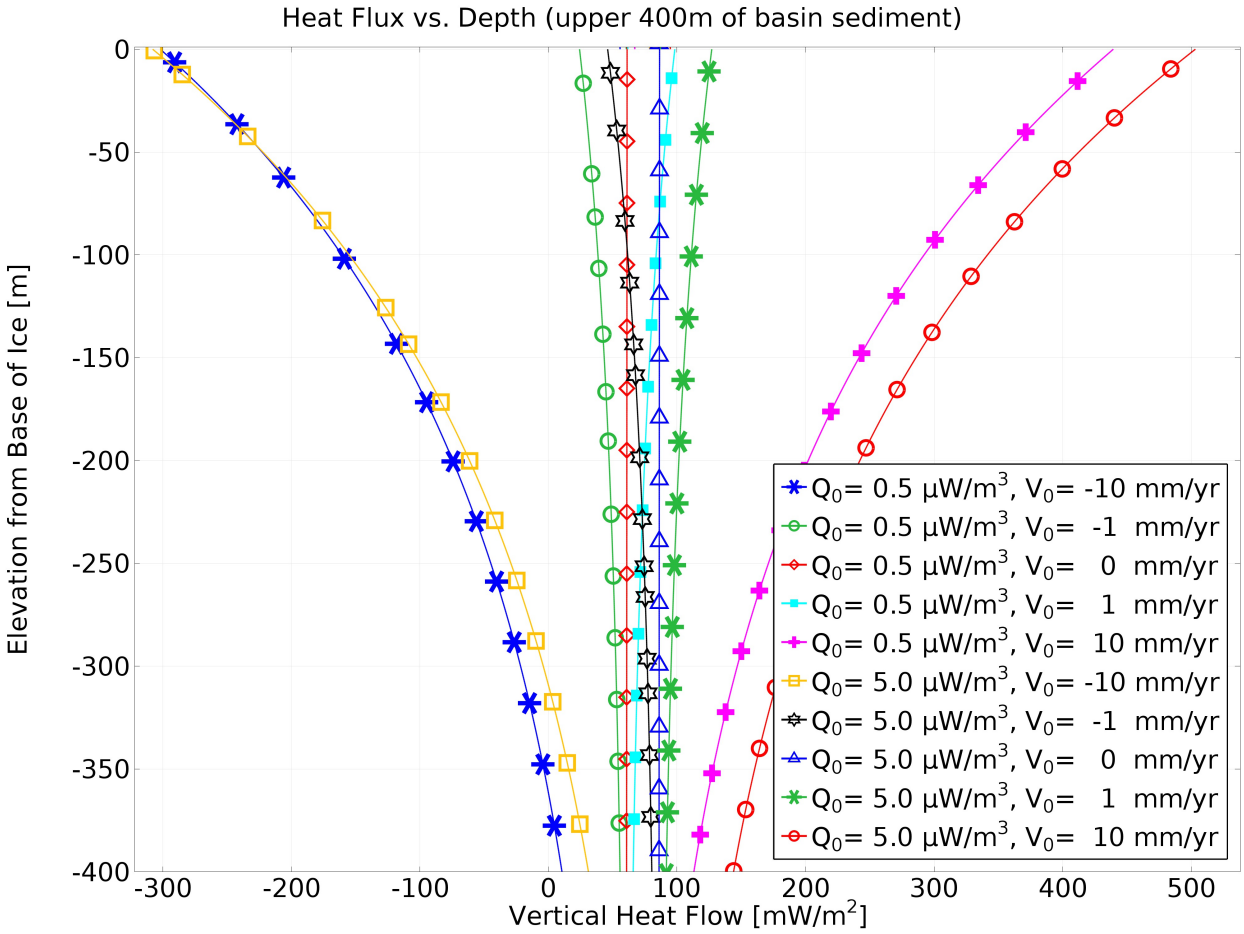

Figure 3.5. Vertical heat flux in the upper 400 meters of the sedimentary basin (0 – -0.4 km) from the steady-state 1D hydrothermal model results. Basement surface radiogenic heat production, Q_0, and sediment surface groundwater volume flux, V_0, parameters are plotted. Radiogenic heat production in the sedimentary rock (down to 1 km from the base of the ice) is uniformly 1 μW/m^3 throughout. Positive V_0 is a volume flux moving in the upward direction. Greater heat flux mostly occurs when the water volume flux is positive but heat production is also an important factor.

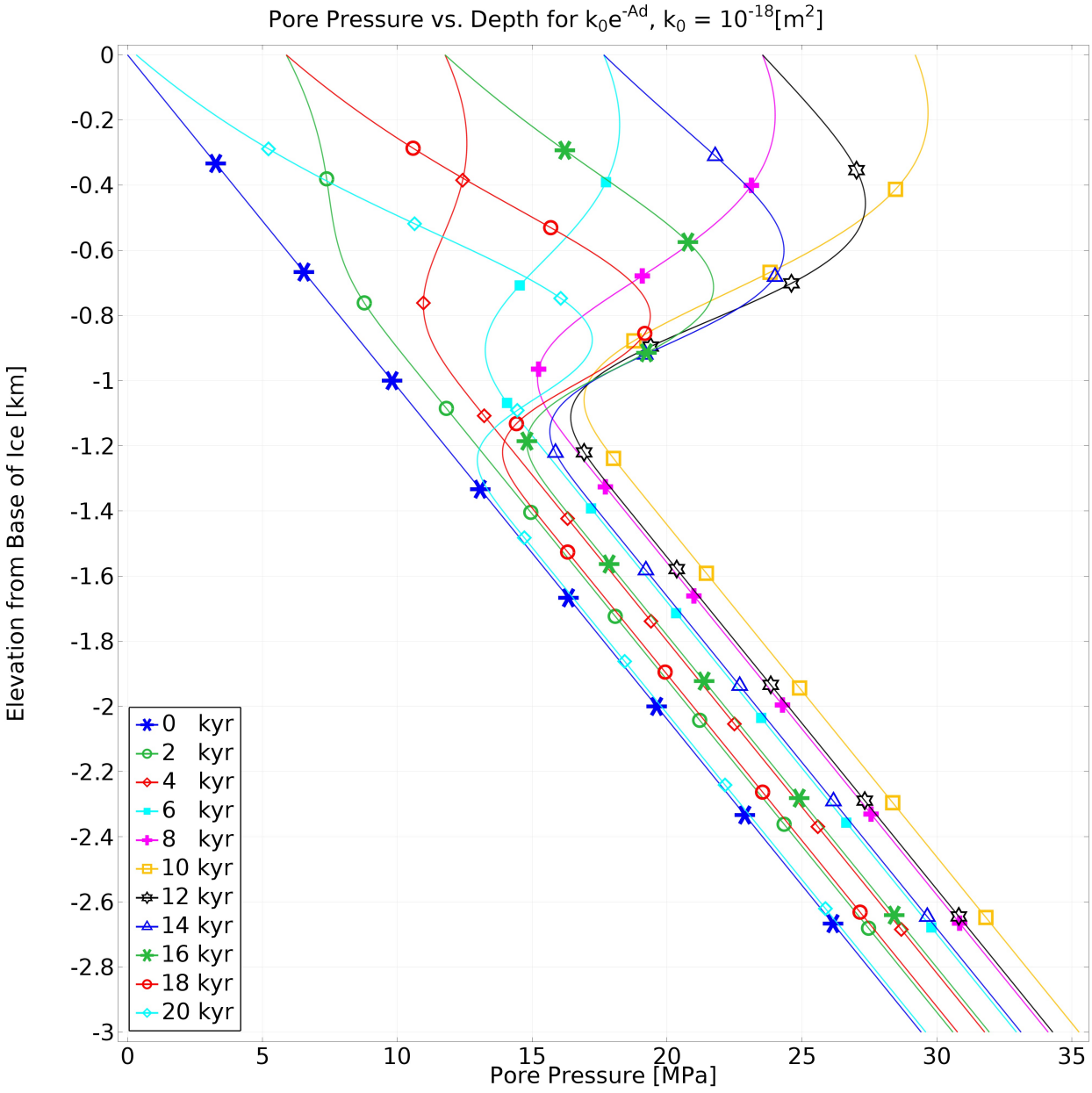

Figure 3.6. Simulated subsurface pore pressure over the partial mock glacial cycle from the transient 1D hydromechanical model results. The parameterization of permeability, k, relies on the function $k = k_0 e^{-Ad}$ where k_0 is equal to 10^{-18} m^2 in this case (see Section 3.3.2). The plot shows the increase in shallow subsurface pore pressure during ice advance and the anomalous, or fossil, pore pressure as the ice retreats.

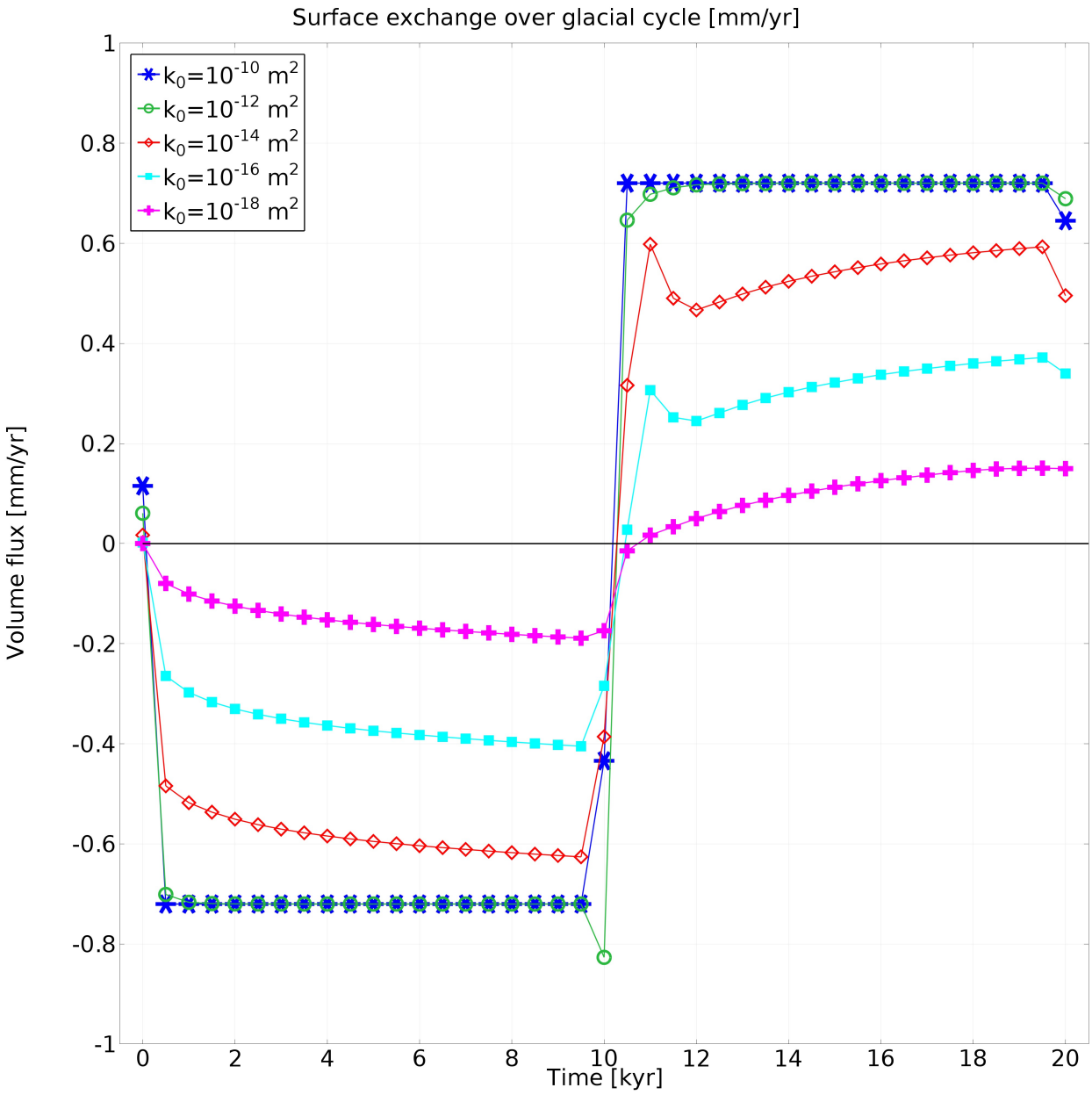

Figure 3.7. Vertical water volume flux (exchange flux) at the ice/bed interface over a simplified partial glacial cycle from the transient 1D hydromechanical model. Positive flux is upward out of the sediment surface (i.e. discharge or exfiltration). The ice sheet steadily advances leading to a maximum at 10 kyr with steady retreat following. Subsurface recharge (or infiltration) occurs during ice advance and discharge occurs with retreat. The parameterization of permeability, k, relies on the function $k = k_0 e^{-Ad}$ (see Section 3.3.2).

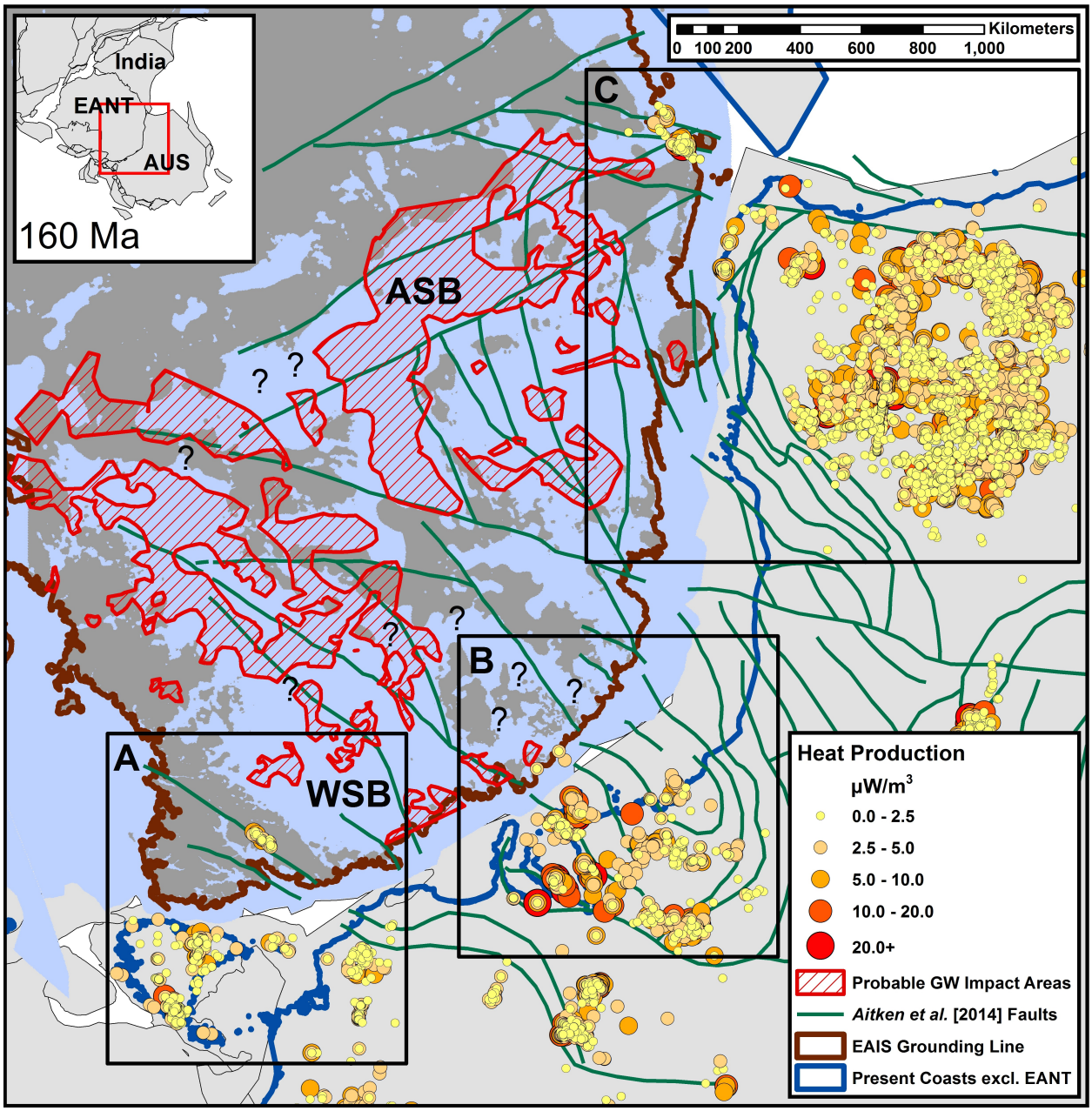
India
EANT
AUS
160 Ma
Kilometers
0 100 200 400 600 800 1,000
ASB
WSB
A
B
C
Heat Production
μW/m3
0.0 - 2.5
2.5 - 5.0
5.0 - 10.0
10.0 - 20.0
20.0+
Probable GW Impact Areas
Aitken et al. [2014] Faults
EAIS Grounding Line
Present Coasts excl. EANT

Figure 3.8. Map of the reconstructed assemblage of the East Antarctic (EANT) and Australian (AUS) plates at 160 Ma with present day, surface radiogenic heat production values (calculated mainly from *Champion et al*. [2007] and *Carson and Pittard* [2012]). The relative global tectonic plate (plates in light gray) assemblage at 160 Ma and the extent of the study area are shown in the inset map. The grouping extents used for the heat production statistics are in each of the lettered boxes. The averages for the heat production groupings are 1.08 (standard deviation 1.53), 4.27 (std. 28.75), and 1.43 (std. 2.59) $\mu W/m^3$ for boxes A, B, and C, respectively. The geophysically derived fault and tectonic interpretations from *Aitken et al*. [2014] are shown with green lines. The Wilkes Subglacial Basin (WSB) covers much of the area at or below sea level from the coast towards the South Pole. The Aurora Subglacial Basin (ASB) extends in a similar manner to the WSB but from a different direction; it also terminates near the WSB's terminus. Probable groundwater impact areas (see Section 3.3.3) are included as red-hatched zones. Areas where the present-day bed elevation from *Fretwell et al*. [2013] is at or below mean sea level are colored blue and those above are in dark gray. Locations where geophysical data availability is limited or non-existent and are of added hydrogeological and geochemical interest in line with this study for future aerogeophysical surveying are designated with question marks (?). The present-day East Antarctic Ice Sheet (EAIS) grounding line from *Bohlander and Scambos* [2007] is included in brown. Present-day coastlines [*Wessel and Smith*, 1996; v2.3.3] on other plates are shown as blue lines.

3.8 REFERENCES

Aitken, A. R. A., D. A. Young, F. Ferraccioli, P. G. Betts, J. S. Greenbaum, T. G. Richter, J. L. Roberts, D. D. B., and M. J. Siegert (2014), The subglacial geology of Wilkes Land, East Antarctica, Geophys. Res. Lett., 41, 2390–2400.

Alley, R. B. (1989), Water-pressure coupling of sliding and bed deformation: I. Water system, J. Glaciol., 35(119), 108–118.

Athy, L. F. (1930), Density, porosity, and compaction of sedimentary rocks, AAPG Bulletin, 14(1), 1-24.

Bamber, J. L., R. L. Layberry, and S. P. Gogineni (2001), A new ice thickness and bed data set for the Greenland ice sheet: 1. Measurement, data reduction, and errors, J. Geophys. Res., 106(D24), 33773-33780.

Beardsmore, G. R., and J. P. Cull (2001), Crustal heat flow: a guide to measurement and modelling. Cambridge University Press.

Bense, V. F., and M. A. Person (2008), Transient hydrodynamics within intercratonic sedimentary basins during glacial cycles, J. Geophys. Res., 113, F04005, doi:10.1029/2007JF000969.

Bindschadler, R., H. Choi, and ASAID Collaborators (2011), High-resolution Image-derived Grounding and Hydrostatic Lines for the Antarctic Ice Sheet, National Snow and Ice Data Center, Boulder, Colo., doi:10.7265/N56T0JK2.

Blankenship, D. D., C. R. Bentley, S. T. Rooney, and R. B. Alley (1986), Seismic measurements reveal a saturated porous layer beneath an active Antarctic ice stream, Nature, 322, 54–57.

Blankenship, D. D., R. E. Bell, S. M. Hodge, J. M. Brozena, J. C. Behrendt, and C. A. Finn (1993), Active volcanism beneath the West Antarctic ice sheet and implications for ice-sheet stability, Nature, 361, 526–529.

Blankenship, D. D., D. L. Morse, C. A. Finn, R. E. Bell, M. E. Peters, S. D. Kempf, S. M. Hodge, M. Studinger, J. C. Behrendt, and J. M. Brozena (2001), Geologic Controls on the Initiation of Rapid Basal Motion for West Antarctic Ice Streams: A Geophysical Perspective Including New Airborne Radar Sounding and Laser Altimetry Results, in The West Antarctic Ice Sheet: Behavior and Environment (eds R. B. Alley and R. A. Bindschadler), American Geophysical Union, Washington, D. C.

Bohlander, J., and T. Scambos (2007), Antarctic coastlines and grounding line derived from MODIS Mosaic of Antarctica (MOA), Boulder, Colorado USA: National Snow and Ice Data Center, Digital media

Boulton, G. (2010), Drainage pathways beneath ice sheets and their implications for ice sheet form and flow: the example of the British Ice Sheet during the Last Glacial Maximum. J. Quaternary Sci., 25: 483–500.

Carson, C. J., and M. Pittard (2012), A Reconaissance Crustal Heat Production Assessment of the Australian Antarctic Territory (AAT). Geoscience Australia.

Carson, C. J., S. McLaren, J. L. Roberts, S. D. Boger, and D. D. Blankenship (2013), Hot rocks in a cold place: high sub-glacial heat flow in East Antarctica, J. Geol. Soc. London., 171(1), 9–12.

Champion, D. C., A. R. Budd, M. S. Hazell, and A. Sedgmen, (2007), OZCHEM National Whole Rock Geochemistry Dataset, Geoscience Australia.

Christoffersen, P., M. Bougamont, S. P. Carter, H. A. Fricker, and S. Tulaczyk (2014), Significant groundwater contribution to Antarctic ice streams hydrologic budget, Geophys. Res. Lett., 41, 1–8.

Clarke, G. K. C., S. G. Collins, and D. E. Thompson (1984), Flow, thermal structure, and subglacial conditions of a surge-type glacier, Can. J. Earth Sci., 21, 232–240.

Comiso, J. C. (2000), Variability and trends in Antarctic surface temperatures from in situ and satellite infrared measurements. Journal of Climate, 13(10), 1674-1696.

Cutler, P. M., D. R. MacAyeal, D. M. Mickelson, B. R. Parizek, and P. M. Colgan (2000), A numerical investigation of ice-lobe-permafrost interaction around the southern Laurentide ice sheet, J. Glaciol., 46(153), 311–325.

Drewry, D. (1976), Sedimentary basins of the East Antarctic craton from geophysical evidence. Tectonophysics, 36(1), 301-314.

Echelmeyer, K. (1987), Anomalous heat flow and temperatures associated with subglacial water flow, The Physical Basis of Ice Sheet Modelling (Proceedings of the Vancouver Symposium, August 1987). IAHS Publ. no. 170.

Ferraccioli, F., E. Armadillo, T. Jordan, E. Bozzo, and H. Corr (2009), Aeromagnetic exploration over the East Antarctic Ice Sheet: A new view of the Wilkes Subglacial Basin, Tectonophysics, 478(1-2), 62–77.

Flowers, G. E., S. J. Marshall, H. Björnsson, and G. K. C. Clarke (2005), Sensitivity of Vatnajökull ice cap hydrology and dynamics to climate warming over the next 2 centuries, J. Geophys. Res. Earth Surf., 110(F2), F02011.

Fox Maule, C., M. E. Purucker, N. Olsen, and K. Mosegaard (2005), Heat flux anomalies in Antarctica revealed by satellite magnetic data., Science, 309(5733), 464–467.

Frederick, B. C. (2015), Submarine Sedimentary Basin Analyses for the Aurora and Wilkes Subglacial Basins and the Sabrina Coast Continental Shelf, East Antarctica, Ph.D. dissertation, Univ. of Texas, Austin, Texas, USA.

Fretwell, P., et al. (2013), Bedmap2: Improved ice bed, surface and thickness datasets for Antarctica, Cryosphere, 7(1), 375–393.

Gleeson, T., L. Smith, N. Moosdorf, J. Hartmann, H. H. Dürr, A. H. Manning, L. P. H. van Beek, and A. M. Jellinek (2011), Mapping permeability over the surface of the Earth, Geophys. Res. Lett., 38, L02401.

Gleeson, T., N. Moosdorf, J. Hartmann, and L. P. H. van Beek (2014), A glimpse beneath earth's surface: GLobal HYdrogeology MaPS (GLHYMPS) of permeability and porosity, Geophys. Res. Lett., 41, 3891–3898.

Grasby, S., K. Osadetz, R. Betcher, and F. Render (2000), Reversal of the regional-scale flow system of the Williston basin in response to Pleistocene glaciation, Geology, 28(1986), 635–638.

Grasby, S. E., and Z. Chen (2005), Subglacial recharge into the western Canada sedimentary basin—Impact of Pleistocene glaciation on basin hydrodynamics, Geol. Soc. Am. Bull., 117(3/4), 500–514.

Hughes, T., A. Sargent, and J. Fastook (2011), Ice-bed coupling beneath and beyond ice streams: Byrd Glacier, Antarctica, J. Geophys. Res. Earth Surf., 116(F3), 1–17.

Huybrechts, P., and J. Oerlemans (1988), Evolution of the East Antarctic ice sheet: A numerical study of thermo-mechanical response patterns with changing climate, Ann. Glaciol., 11, 52–59.

Ingebritsen, S. E., C. E. Neuzil, and W. E. Sanford (2006), Groundwater in geologic processes, Cambridge University Press.

Jaupart, C. (1986), On the average amount and vertical distribution of radioactivity in the continental crust, in Burrus, J., ed., Thermal Modeling in Sedimentary Basins: ´Editions Technip, Paris, 33–47.

Jiang, X. W., L. Wan, X. S. Wang, S. Ge, and J. Liu (2009), Effect of exponential decay in hydraulic conductivity with depth on regional groundwater flow, Geophys. Res. Lett., 36, L24402.

Jiang, X. W., L. Wan, M. B. Cardenas, S. Ge, and X. S. Wang (2010), Simultaneous rejuvenation and aging of groundwater in basins due to depth-decaying hydraulic conductivity and porosity, Geophys. Res. Lett., 37, L05403.

Jordan, T. A., F. Ferraccioli, E. Armadillo, and E. Bozzo (2013), Crustal architecture of the Wilkes Subglacial Basin in East Antarctica, As revealed from airborne gravity data, Tectonophysics, 585, 196–206.

Lachenbruch, A. H. (1970), Crustal temperature and heat production: Implications of the linear heat-flow relation, J. Geophys. Res., 75(17), 3291-3300.

Lemieux, J. M., E. A. Sudicky, W. R. Peltier, and L. Tarasov (2008a), Dynamics of groundwater recharge and seepage over the Canadian landscape during the Wisconsinian glaciation, J. Geophys. Res. Earth Surf., 113(F1), F01011.

Lemieux, J. M., E. A. Sudicky, W. R. Peltier, and L. Tarasov (2008b), Simulating the impact of glaciations on continental groundwater flow systems: 1. Relevant processes and model formulation, J. Geophys. Res. Earth Surf., 113, F03017.

Lowe, A. L., and J. B. Anderson (2003), Evidence for abundant subglacial meltwater beneath the paleo-ice sheet in Pine Island Bay, Antarctica, J. Glaciol., 49(164), 125–138.

Mackintosh, A., et al. (2011), Retreat of the East Antarctic ice sheet during the last glacial termination, Nat. Geosci., 4(3), 195–202.

McIntosh, J. C., G. Garven, and J. S. Hanor (2011), Impacts of Pleistocene glaciation on large-scale groundwater flow and salinity in the Michigan Basin, Geofluids, 11(1), 18–33.

McKenna, T. E., and J. M. Sharp Jr. (1998), Radiogenic heat production in sedimentary rocks of the gulf of Mexico basin, south Texas, AAPG Bull., 82, 484–496.

McLaren, S., M. Sandiford, M. Hand, N. Neumann, L. Wyborn, and I. Bastrakova (2003), The hot southern continent; heat flow and heat production in Australian Proterozoic terranes, Spec. Pap. - Geol. Soc. Am., 372, 157–167.

Mellor, G. L., and L. Kantha (1989), An ice-ocean coupled model, J. Geophys. Res., 94(89), 10937–10954.

Mengel, M., and A. Levermann (2014), Ice plug prevents irreversible discharge from East Antarctica, Nat. Clim. Chang., 4(May), 451–455.

Mosley-Thompson, E., J. F. Paskievitch, A. J. Gow, and L. G. Thompson (1999), Late 20th Century increase in South Pole snow accumulation, J. Geophys. Res., 104, 3877-3886.

Neuzil, C. E. (2012), Hydromechanical effects of continental glaciation on groundwater systems, Geofluids, 12(1), 22-37.

Neuzil, C. E. (2015), Interpreting fluid pressure anomalies in shallow intraplate argillaceous formations. Geophys. Res. Lett., 42, 4801–4808. doi: 10.1002/2015GL064140.

Pattyn, F. (2008), Investigating the stability of subglacial lakes with a full Stokes ice-sheet model, J. Glaciol., 54(185), 353–361.

Pattyn, F. (2010), Antarctic subglacial conditions inferred from a hybrid ice sheet/ice stream model, Earth Planet. Sci. Lett., 295(3-4), 451–461.

Person, M., J. McIntosh, V. Bense, and V. H. Remenda (2007), Pleistocene hydrology of North America: The role of ice sheets in reorganizing groundwater flow systems, Rev. Geophys., 45(3), RG3007.

Person, M., V. Bense, D. Cohen, and A. Banerjee (2012), Models of ice-sheet hydrogeologic interactions: A review, Geofluids, 12(1), 58–78.

Petrunin, A. G., I. Rogozhina, A. P. M. Vaughan, I. T. Kukkonen, M. K. Kaban, I. Koulakov, and M. Thomas (2013), Heat flux variations beneath central Greenland's ice due to anomalously thin lithosphere, Nat. Geosci., 6, 746–750, doi:10.1038/ngeo1898.

Piotrowski, J. (2006), Groundwater under ice sheets and glaciers, Glacier Sci. Environ. Chang., 50–60.

Piotrowski, J. A., P. Hermanowski, and A. M. Piechota (2009), Meltwater discharge through the subglacial bed and its land-forming consequences from numerical experiments in the Polish lowland during the last glaciation, Earth Surf. Process. Landforms, 34, 481–492.

Pollard, D., R. M. DeConto, and A. A. Nyblade (2005), Sensitivity of Cenozoic Antarctic ice sheet variations to geothermal heat flux, Glob. Planet. Change, 49(1-2), 63–74.

Pollard, D., R. M. Deconto, and R. B. Alley (2015), Potential Antarctic Ice Sheet retreat driven by hydrofracturing and ice cliff failure, Earth Planet. Sci. Lett., 412, 112–121.

Price, P. B., O. V Nagornov, R. Bay, D. Chirkin, Y. He, P. Miocinovic, A. Richards, K. Woschnagg, B. Koci, and V. Zagorodnov (2002), Temperature profile for glacial ice at the South Pole: implications for life in a nearby subglacial lake., Proc. Natl. Acad. Sci. U. S. A., 99(12), 7844–7847.

Rajaram, M., S. P. Anand, K. Hemant, and M. E. Purucker (2009), Curie isotherm map of Indian subcontinent from satellite and aeromagnetic data, Earth Planet. Sci. Lett., 281(3-4), 147–158.

Rignot, E., J. Mouginot, and B. Scheuchl (2011), Ice flow of the Antarctic Ice Sheet, Science, 333, 1427–1430.

Sandiford, M., and S. McLaren (2002), Tectonic feedback and the ordering of heat producing elements within the continental lithosphere, Earth Planet. Sci. Lett., 204, 133–150.

Schroeder, D. M., D. D. Blankenship, D. A. Young, and E. Quartini (2014), Evidence for elevated and spatially variable geothermal flux beneath the West Antarctic Ice Sheet, Proc. Natl. Acad. Sci., 111(25), 9070-9072.

Sclater, J. G., and P. Christie (1980), Continental stretching: An explanation of the post-mid-cretaceous subsidence of the central North Sea basin, J. Geophys. Res. Solid Earth, 85(B7), 3711-3739.

Shapiro, N. M., and M. H. Ritzwoller (2004), Inferring surface heat flux distributions guided by a global seismic model: Particular application to Antarctica, Earth Planet. Sci. Lett., 223(1-2), 213–224.

Shepard, M. K., B. A. Campbell, M. H. Bulmer, T. G. Farr, L. R. Gaddis, and J. J. Plaut (2001), The roughness of natural terrain: A planetary and remote sensing perspective, J. Geophys. Res., 106, 32777-32795.

Siegel, J., D. Lizarralde, B. Dugan, and M. Person (2014), Glacially generated overpressure on the New England continental shelf: Integration of full-waveform inversion and overpressure modeling, J. Geophys. Res, 119, 3393–3409.

Siegert, M. J., and J. A. Dowdeswell (1996), Spatial variations in heat at the base of the Antarctic ice sheet from analysis of the thermal regime above subglacial lakes, J. Glaciol., 42(142), 501–509.

Singhal, B. B. S., and R. P. Gupta (2010), Applied hydrogeology of fractured rocks (Vol. 430). New York: Springer.

Stauffer, P. H. (2006), Flux flummoxed: A proposal for consistent usage, Ground Water, 44(2), 125–128.

Studinger, M., R. E. Bell, W. R. Buck, G. D. Karner, and D. D. Blankenship (2004), Sub-ice geology inland of the Transantarctic Mountains in light of new aerogeophysical data, Earth Planet. Sci. Lett., 220(3-4), 391–408.

Sun, B., J. C. Moore, T. Zwinger, L. Zhao, D. Steinhage, X. Tang, D. Zhang, X. Cui, and C. Martín (2014), How old is the ice beneath Dome A, Antarctica?, The Cryosphere, 8, 1121–1128.

Thoma, M., K. Grosfeld, C. Mayer, and F. Pattyn (2012), Ice-flow sensitivity to boundary processes: A coupled model study in the Vostok Subglacial Lake area, Antarctica, Ann. Glaciol., 53(60), 173-180.

Turcotte, D. L., and G. Schubert (2002), Geodynamics, Cambridge University Press.

Van Liefferinge, B., and F. Pattyn (2013), Using ice-flow models to evaluate potential sites of million year-old ice in Antarctica, Clim. Past, 9(5), 2335–2345.

Waddington, E. (1987), Geothermal heat flux beneath ice sheets, The Physical Basis of Ice Sheet Modelling (Proceedings of the Vancouver Symposium, August 1987), IAHS Publ. no. 170.

Waples, D. W. (2001), A New Model for Heat Flow in Extensional Basins: Radiogenic Heat, Asthenospheric Heat, and the McKenzie Model, Nat. Resour. Res., 10(2), 227–238.

Wessel, P., and W. H. F. Smith (1996), A global, self-consistent, hierarchical, high-resolution shoreline database, J. Geophys. Res., 101(B4), 8741–8743.

Wilch, E., and T. J. Hughes (2000), Calculating basal thermal zones beneath the antarctic ice sheet, J. Glaciol., 46(153), 297-310.

Winkelmann, R., M. A. Martin, M. Haseloff, T. Albrecht, E. Bueler, C. Khroulev, and A. Levermann (2011), The Potsdam Parallel Ice Sheet Model (PISM-PIK) - Part 1: Model description, Cryosphere, 5(3), 715-726.

Wright, A., and M. Siegert (2012), A fourth inventory of Antarctic subglacial lakes, Antarct. Sci., 24(6), 659-664.

Young, D. A., et al. (2011), A dynamic early East Antarctic Ice Sheet suggested by ice-covered fjord landscapes, Nature, 474(7349), 72–75.

Zwally, H. J., M. B. Giovinetto, M. A. Beckley, and J. L. Saba (2012), Antarctic and Greenland drainage systems, GSFC Cryospheric Sciences Laboratory.

3.9 SUPPLEMENTARY FIGURES

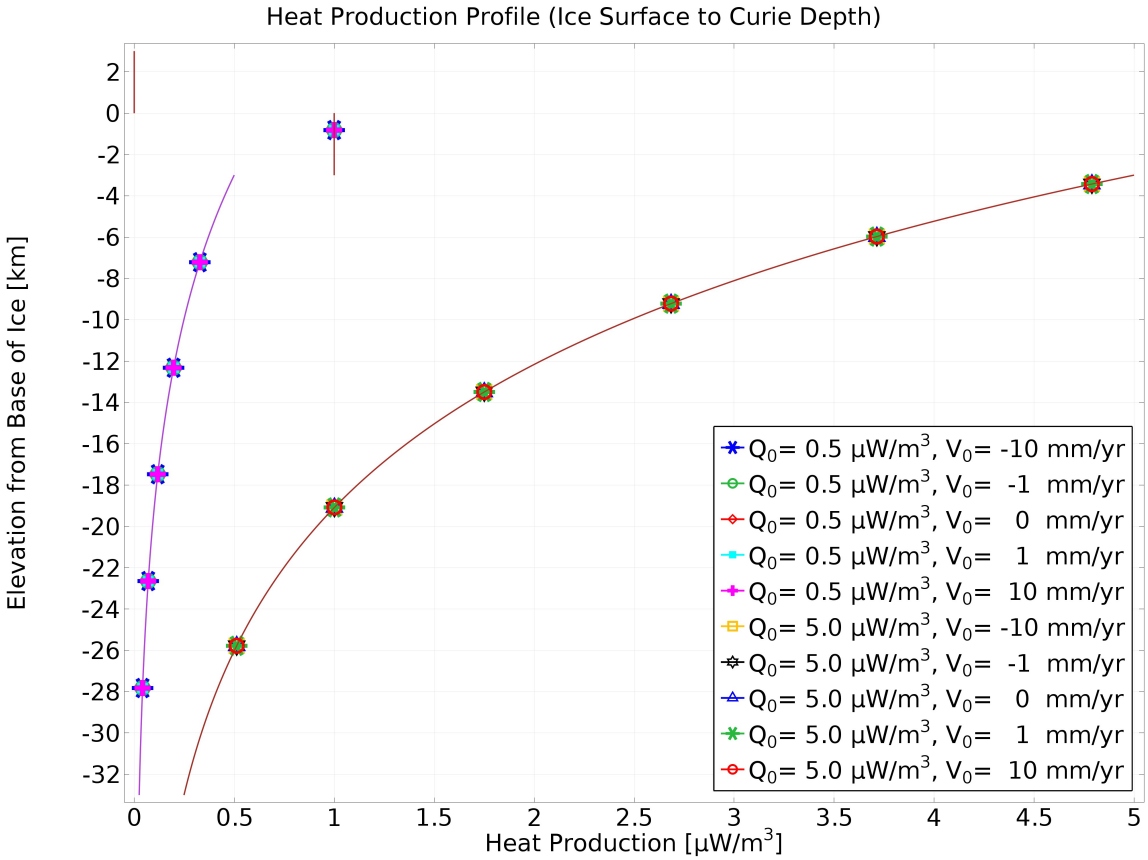

Figure S3.1. The radiogenic heat production used in the steady-state 1D hydrothermal model. The sedimentary basin fill is assigned a uniform value of 1 $\mu W/m^3$ for all simulations which is an average used in most sedimentary fills [*Waples*, 2001]. The basement rock heat production is varied between two different exponential functions, a lower crustal average (Q_0 = 0.5 $\mu W/m^3$) and a higher one (Q_0= 5 $\mu W/ m^3$) that more closely exhibits Australian analogs [*Sandiford and McLaren*, 2002; *McLaren et al*., 2003; *Carson et al*., 2013]. The ice sheet is not given a value.

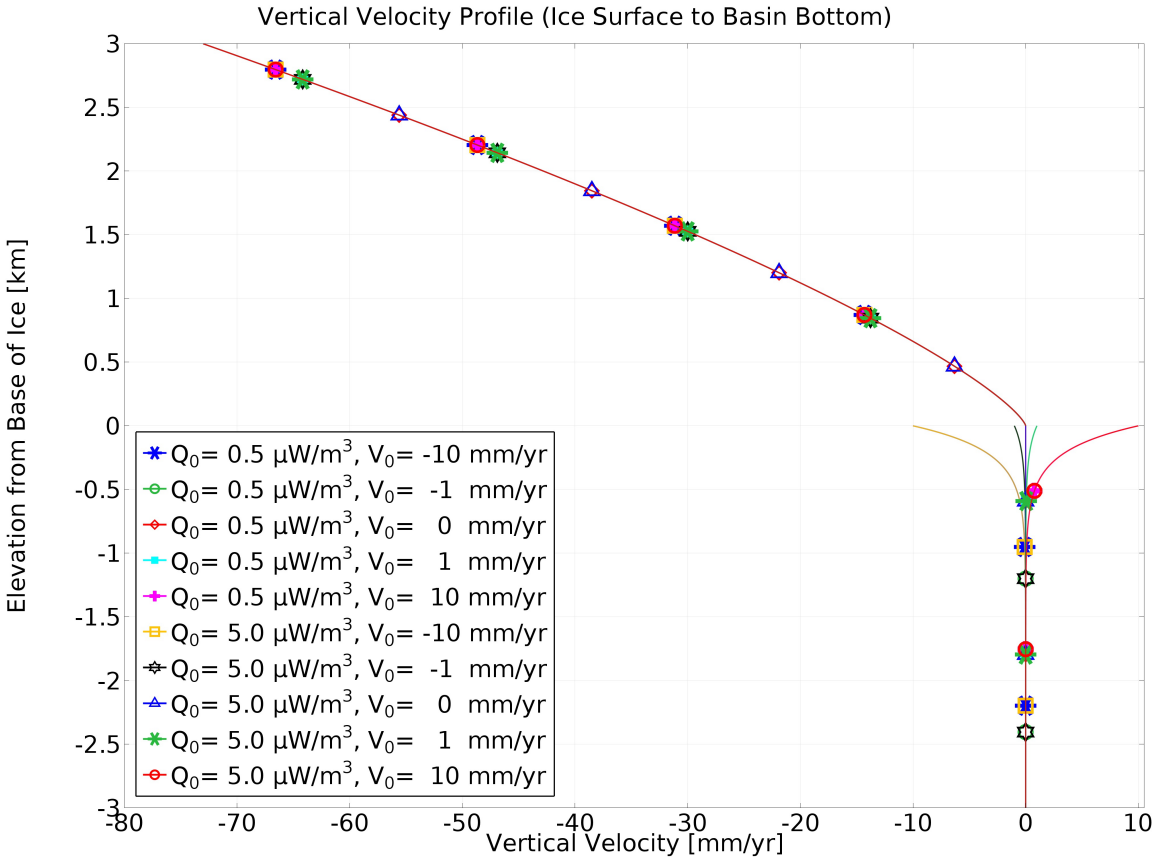

Figure S3.2. The assigned vertical velocity for the ice and groundwater fluxes in the steady-state 1D hydrothermal model. Note this is for the ice sheet (3 – 0 km) and sedimentary basin (0 – -3 km) domains of the model; no fluid movement was modeled in the basement domain (-3 – -33 km).

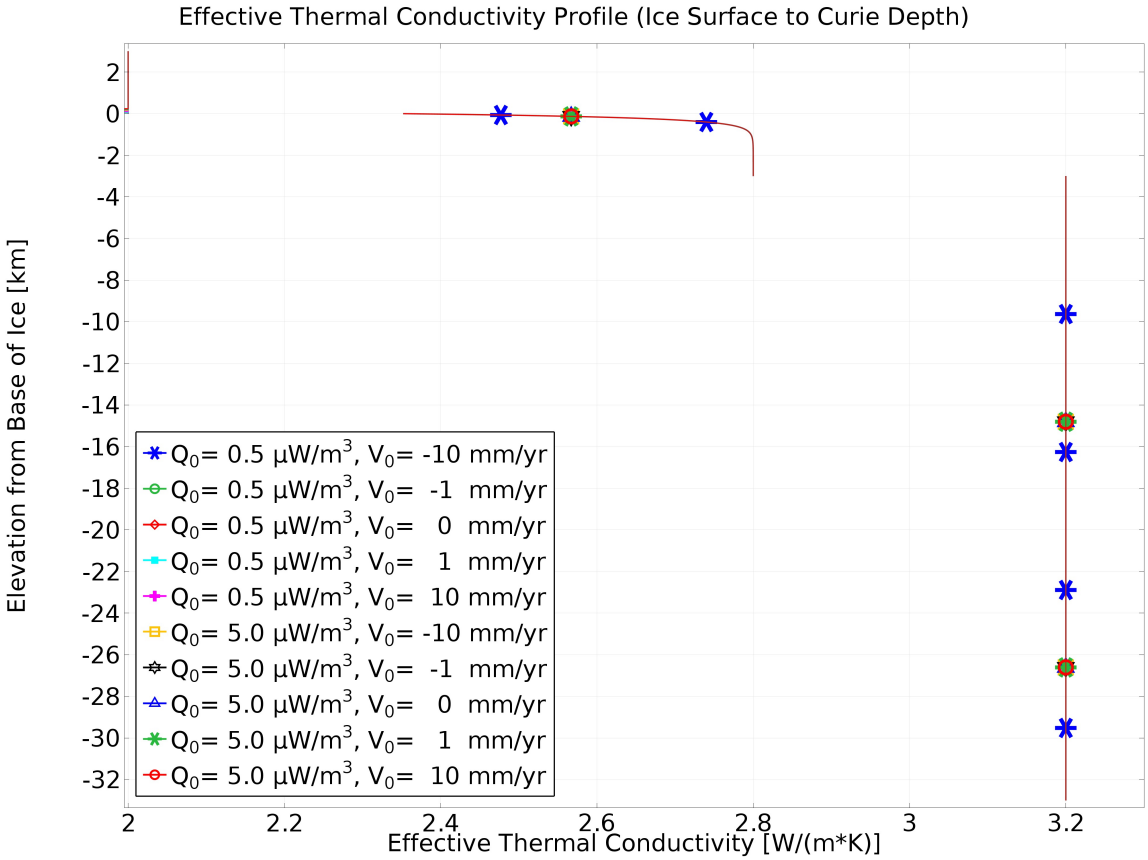

Figure S3.3. Thermal conductivity, $\varkappa$, assigned throughout the steady-state 1D hydrothermal model for all simulations. Ice and basement are assigned a constant value of 2 W/(mK) and 3.2 W/(mK). Thermal conductivity in the sedimentary basin is an effective value based on a weighted average of water and rock content. The relationship is due to an exponential decay in porosity.

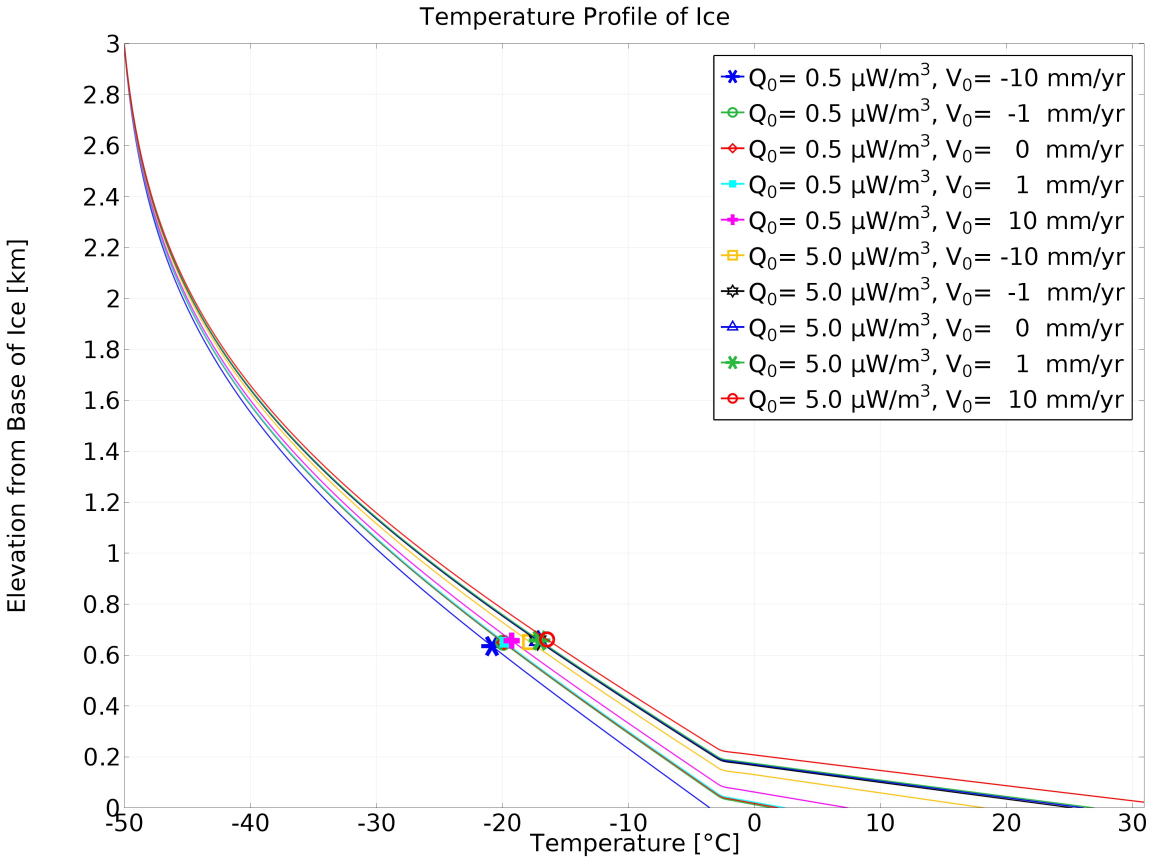

Figure S3.4. Simulated temperature profile results of the ice sheet from the steady-state 1D hydrothermal model. Through most of the ice column the temperatures are mostly the same for all parameterizations. In the lower few hundred meters the temperatures start to vary from one another. The slope breaks occur due to a phase change from ice to water at the pressure melting temperature (-2.61 °C) except for one that does not reach the melting point.

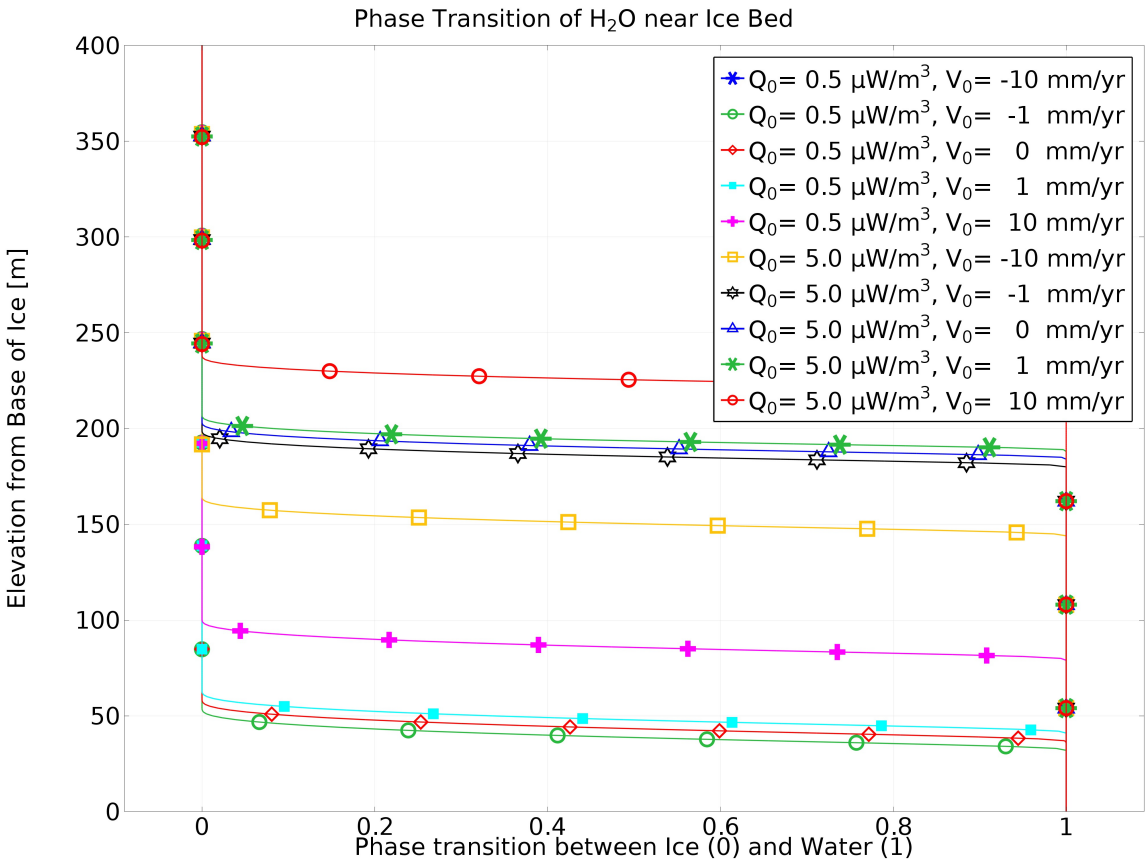

Figure S3.5. Phase plot of the transition of ice (0) to water (1) in the bottom of the simulated ice column from the steady-state 1D hydrothermal model. The steady-state 1D column of water is essentially a one-dimensional subglacial lake ranging here from ~50 – 250 m in depth. All but one of the parameterizations (Q_0 = 0.5 μW/m^3, V_0 = -10 mm/yr) reached the melting point above the ice-sediment interface. Where parameterizations group closely are where they share a radiogenic heat production value in the basement rock.

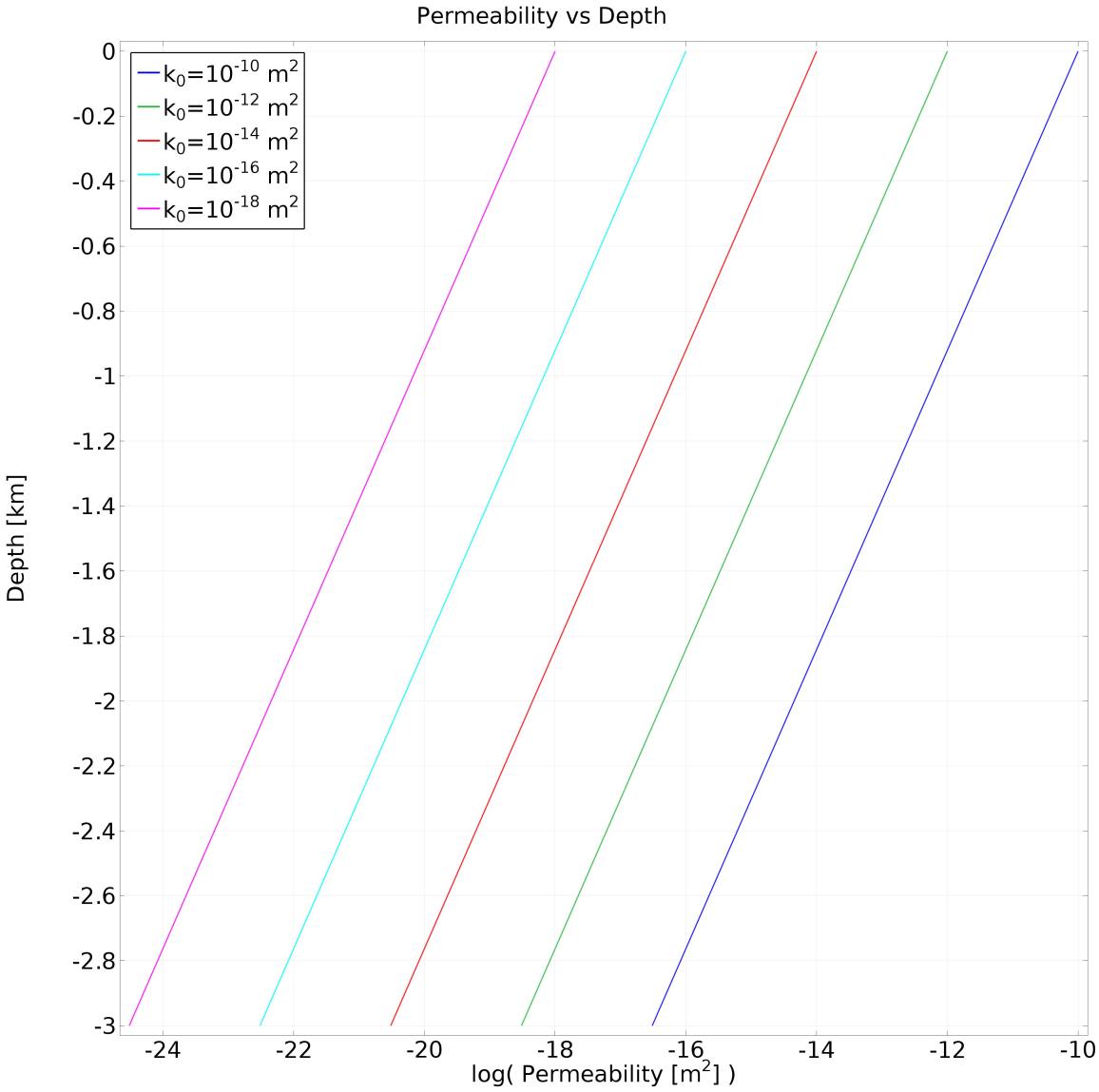

Figure S3.6. Permeability as a function of depth for different parameterizations used in the transient 1D hydromechanical model. The decay in permeability, k, with depth is exponential according to the function $k = k_0 e^{-Ad}$ where k_0 is equal to $10 - 18$ m^2 in this case and d is the depth. Note that the horizontal axis is logarithmic.

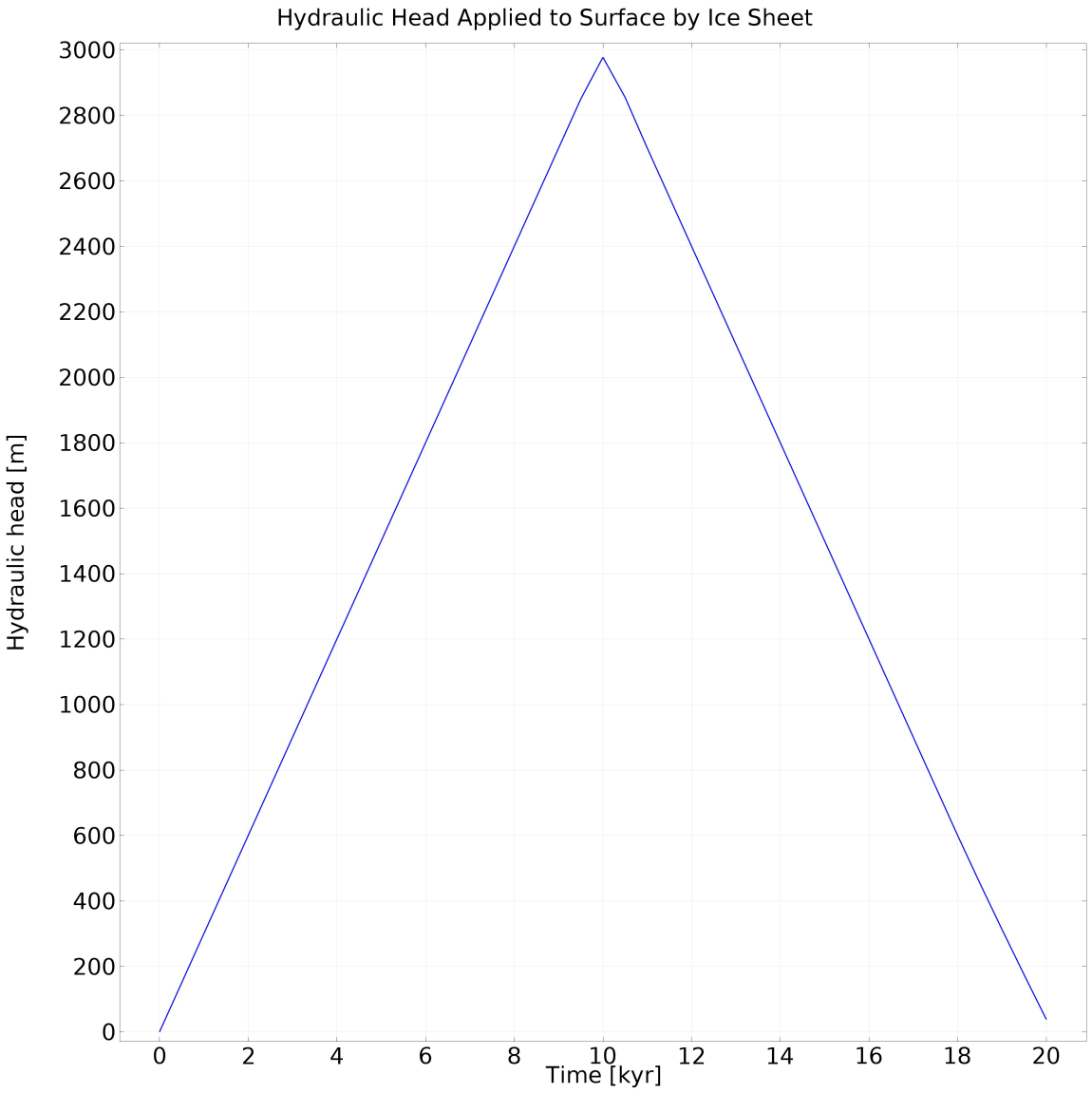

Figure S3.7. Hydraulic head function, h(t), applied to the sediment surface from a simulated water equivalent ice sheet over a partial mock glacial cycle. The ice sheet initiates at 0 kyr and steadily grows a maximum thickness (~3300 m of ice) at 10 kyr then shrinks to the initial state at 20 kyr.

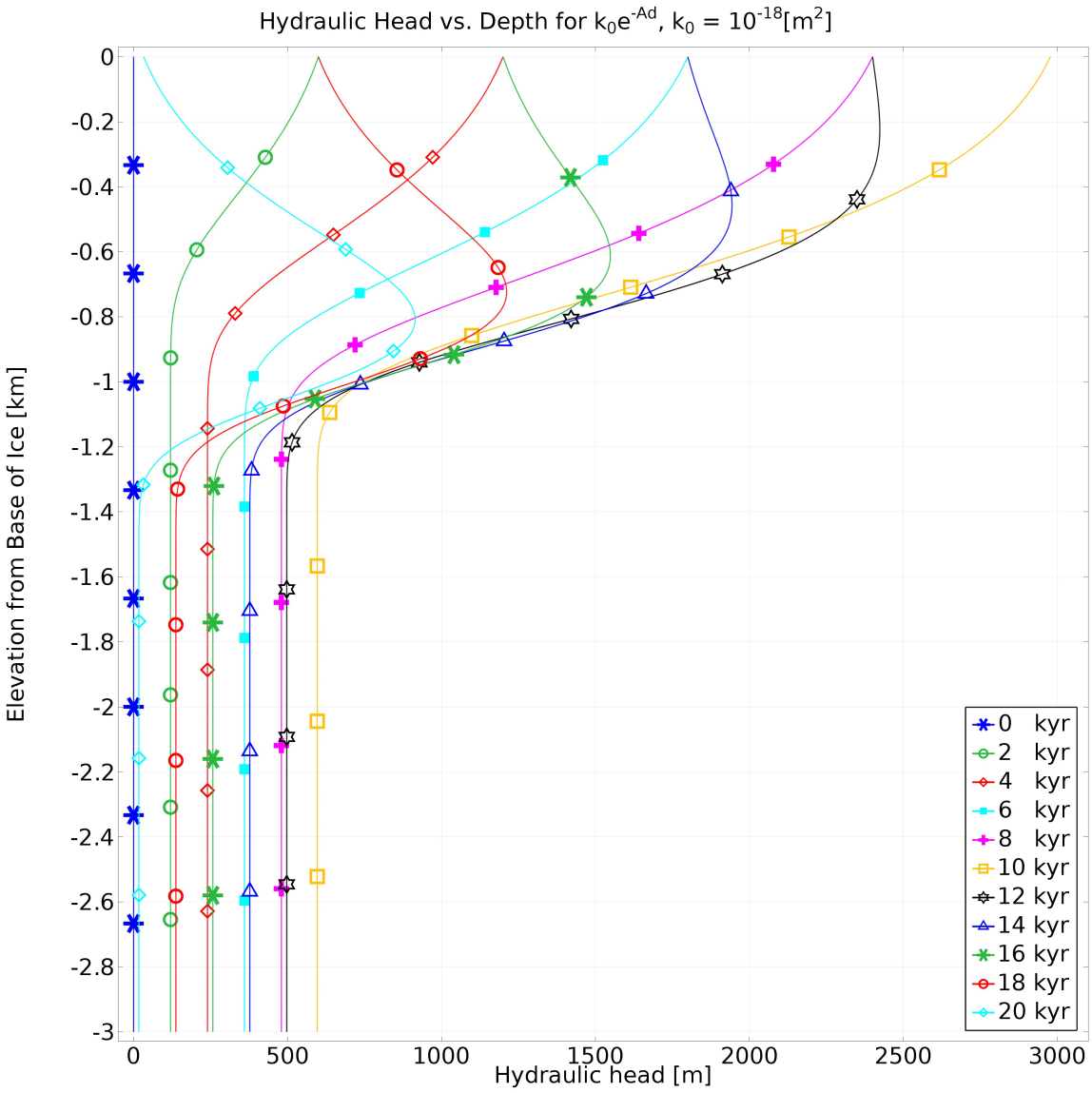

Figure S3.8. Same as Figure 3.6 but with pore pressure converted to hydraulic head.

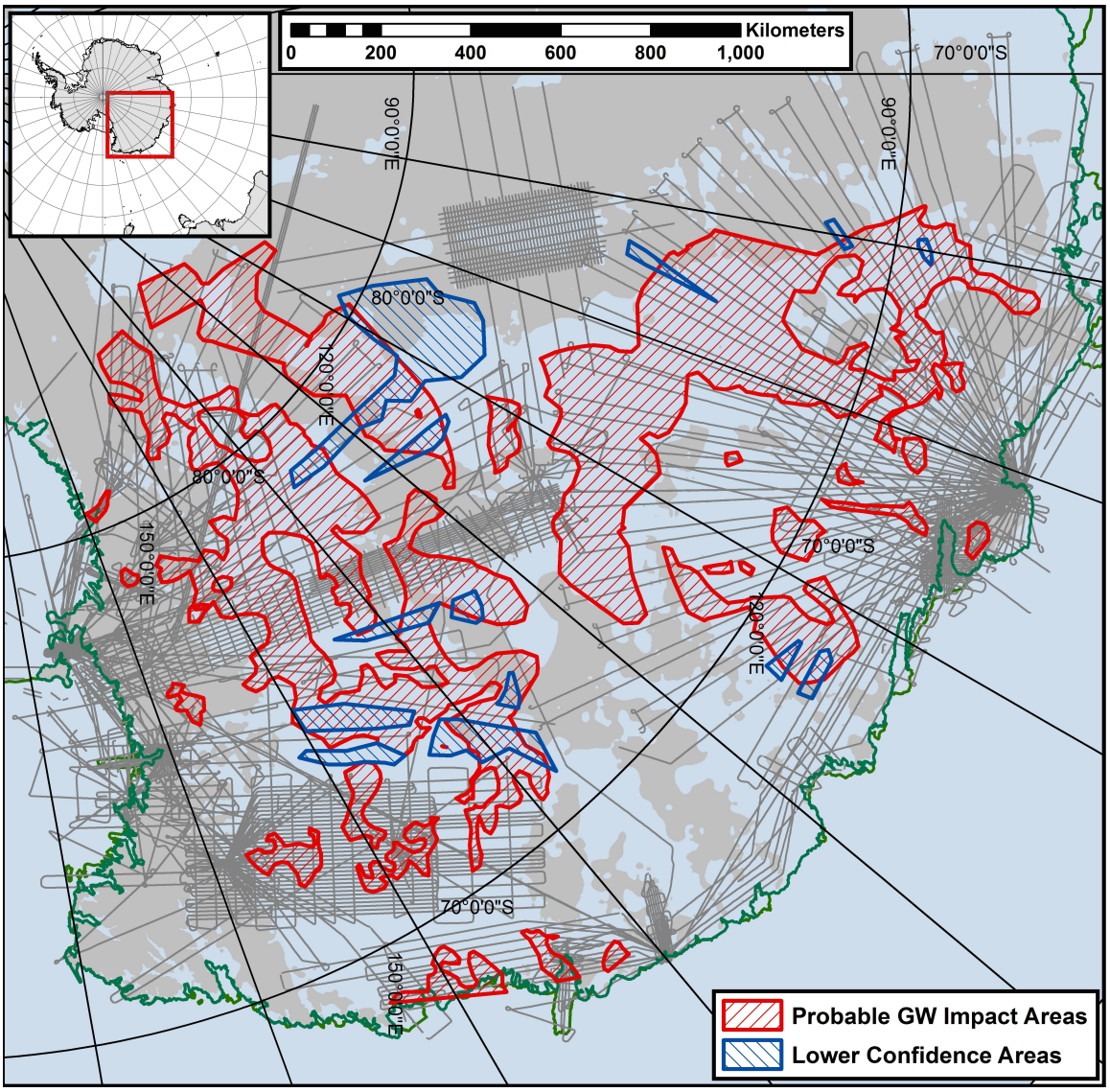

Figure S3.9. Flight lines of the University of Texas Institute for Geophysics-affiliated aerogeophysical data surveys over East Antarctica used in this research. Probable groundwater impact area interpretations from Figure 3.8 are included in red. Specific areas which neither radar-derived bed roughness nor gravity-derived sedimentary basin thickness coverage exist are labeled as lower confidence areas in blue. Areas where the bed elevation from *Fretwell et al*. [2013] is at or below mean sea level are colored blue and those above are in gray. The grounding line and coastline from *Bohlander and Scambos* [2007] are also included.

3.10 SUPPLEMENTARY REFERENCES

Bohlander, J., and T. Scambos (2007), Antarctic coastlines and grounding line derived from MODIS Mosaic of Antarctica (MOA), Boulder, Colorado USA: National Snow and Ice Data Center, Digital media.

Carson, C. J., S. McLaren, J. L. Roberts, S. D. Boger, and D. D. Blankenship (2013), Hot rocks in a cold place: high sub-glacial heat flow in East Antarctica, J. Geol. Soc. London., 171(1), 9–12.

Fretwell, P., et al. (2013), Bedmap2: Improved ice bed, surface and thickness datasets for Antarctica, Cryosphere, 7(1), 375–393.

McLaren, S., M. Sandiford, M. Hand, N. Neumann, L. Wyborn, and I. Bastrakova (2003), The hot southern continent; heat flow and heat production in Australian Proterozoic terranes, Spec. Pap. - Geol. Soc. Am., 372, 157–167.

Sandiford, M., and S. McLaren (2002), Tectonic feedback and the ordering of heat producing elements within the continental lithosphere, Earth Planet. Sci. Lett., 204, 133–150.

Waples, D. W. (2001), A New Model for Heat Flow in Extensional Basins: Radiogenic Heat, Asthenospheric Heat, and the McKenzie Model, Nat. Resour. Res., 10(2), 227–238.

Chapter 4: Groundwater impact on the Totten Glacier Catchment basal water system: Results of a thermomechanical ice sheet model[3]

Abstract

We hypothesize that recent geophysical investigations' discoveries of large sedimentary basins under the potentially unstable Totten Glacier Catchment of East Antarctica may play a crucial role (via groundwater systems) in the subglacial water transport, basal processes, and dynamics of the ice sheet (rheological and sliding behavior). Given recent observations and our hypothesis, we construct numerical models that link lithospheric heat generation and transport, subsurface fluid and heat transport, and Stokes-flow ice dynamics to various groundwater-forcing functions. We design these models for an ice flowline that runs the centerline of the catchment from the ice divide in central East Antarctica to the grounding line at Totten Glacier. We find that, given some specific assumptions about the base of the ice sheet, groundwater forcing applied under the ice sheet showed measurable differences in the ice sheet's dynamics and rheological structure; although, the link between the change in the internal thermal structure of the ice sheet and the heat transfer from the advection of groundwater in the basin is not clear and requires further work. However, the groundwater did have a direct impact heavily on the subglacial hydrological system that lead to very measurable differences in the sliding speed of the modeled ice flowline. From these results we assert that groundwater systems under the Totten Glacier Catchment should be given further consideration in future ice sheet modeling assessments pending further geophysical and geological exploration to better define the basins.

[3] A version of this chapter will be submitted as Gooch, B.T., M. Rückamp, D.A. Young, and D.D. Blankenship (in preparation), Groundwater impact on the Totten Glacier Catchment basal water system: Results of a thermomechanical ice sheet model, *Journal of Geophysical Research*.

4.1 OBSERVATIONS – TOTTEN GLACIER CATCHMENT AND SEDIMENTARY BASINS, EAST ANTARCTICA

Recent observations of the Totten Glacier Catchment in East Antarctica (Figure 4.1) have shown its recent and long-term history of variability to be more dynamic than initially thought [e.g. *Chen et al.*, 2009; *Young et al.*, 2011; *Pritchard et al.*, 2012; *Greenbaum et al.*, 2015; *Pollard et al.*, 2015; *Li et al.*, 2015; *Aitken et al.*, in rev.]. With recent increased interest in its dynamics and in its potential contribution to sea level rise (3-7 m; *Greenbaum et al.* [2015]), the Totten Glacier Catchment is becoming an important target for ice sheet modeling for future ice volume change estimates. One of the greatest challenges for better understanding this ice sheet system is increasing knowledge of the basal geologic and hydrologic systems that underlie the ice [cf. *Taylor et al.*, 2004; *Bamber et al.*, 2006; *White*, 2013]. While there has been research into the subglacial hydraulic and geologic nature of the bed in this area of East Antarctica [e.g. *Siegert et al.*, 2007; *Wright et al.*, 2012; *Aitken et al.*, 2014, in rev.; *Frederick*, 2015; *Gooch et al.*, 2016], there are still considerable uncertainties in the data and relations of how basal processes affect this ice catchment's dynamics need to be addressed before further usage of prognostic ice sheet models can take place.

The geothermal heat flux in the Totten catchment and surrounding area is one largely unknown basal forcing that is required as input to numerical ice sheet models. Most all of the estimates for the region are from continental-scale datasets derived from seismic tomography [*Shapiro and Ritzwoller*, 2004; *An et al.*, 2015b], satellite magnetic data inversion [*Fox Maule et al.*, 2005], geologic data [*Pollard et al.*, 2005], or a combination of various estimates blended with subsurface data [*Pattyn*, 2010]. While some approaches may yield closer versions to reality than others for certain areas of Antarctica, they all still need to be continually refined.

The model of the geologic material at the base of the Totten catchment is continuing to be refined. The most recent work has been from *Young et al.* [2011],

Aitken et al. [2014], and *Frederick* [2015], which utilized much of the same geophysical datasets. Generally, there are two main basins – the Aurora and Sabrina Subglacial Basins (Figure 4.1), each with varying amounts of sedimentary basin fill of what is believed to be intracratonic erosive materials [*Drewry*, 1976] of pre- and post-glacial deposition. These sedimentary basins likely play host to a variety of subglacial hydrological processes including distributed and possibly some channelized systems of water flow at the bed as well as in the porous space within the basin fill (i.e. groundwater).

4.2 HYPOTHESIS – GROUNDWATER FLUX IMPACT ON TOTTEN GLACIER CATCHMENT ICE DYNAMICS

From previous work that included groundwater components in models of ice dynamics in other glaciated terrains [e.g. *Cutler et al.*, 2000; *Boulton and Hartikainen*, 2004; *Flowers et al.*, 2005;] or just subglacial hydrological models [*Boulton et al.*, 2007; *Flowers*, 2008; *Gooch et al.*, 2016], it seems to us that groundwater may be important to include in models of the ice dynamics of the Totten Glacier Catchment due to the significant sediment presence there. The importance in the coupling of groundwater advection to heat flux has been shown to be significant in many glacial settings underlain by sedimentary systems as well [*Clarke et al*., 1984; *Echelmeyer*, 1987; *Gooch et al.*, 2016]. We hypothesize that the probable groundwater systems that likely exist under the Totten Glacier Catchment and surrounding area have measureable impact on the overlying ice dynamics. In this particular work, we seek to generally test the hypothesis using available data and conservative approximations of the subsurface. We do this by constructing a thermomechanical ice sheet flowline model with subglacial hydrology that is capable of testing thermal and mechanical impacts to the ice sheet by various groundwater forcings. We intend this work to be a first approach to understanding the very complex nature of groundwater-ice sheet interaction for the Totten Glacier Catchment of East Antarctica.

4.3 EXPERIMENTAL DESIGN AND METHODS

Building mainly on the work of *Wilkens* [2014], *Wilkens et al.* [2015], and *Gooch et al.* [2016, in rev.], we designed deterministic, diagnostic numerical models to test different physical aspects of our hypothesis using COMSOL Multiphysics (COMSOL, Inc.), an automated partial differential equations solver utilizing the finite element method. We chose the ice sheet modeling approach from *Wilkens* [2014] and *Wilkens et al.* [2015] as it allowed us to couple a steady-state Stokes ice flow model to preexisting groundwater flow and heat transport work built within the COMSOL environment [i.e. *Gooch et al.*, 2016, in rev.]. While this region of East Antarctica is not indefinitely in a steady state, we chose this approach as it simplifies the work and is a reasonable assumption in order to start testing our hypothesis about this region's potential impact from groundwater. Our goal with this diagnostic model was to simply observe the behavior of a Stokes fluid mimicking ice sheet behavior while being coupled to different groundwater forcings under reasonable assumptions. The model domain stretches up from the base of the thermal lithosphere, where the temperature is defined (although the depth is estimated by *An et al.* [2015b]), to the sedimentary basins (derived geophysically by *Frederick* [2015]) at the geologic surface and then into the ice sheet at the top (geometry is from Bedmap2 [*Fretwell et al.*, 2013]); see Figures 4.1 and 4.2 for the location and a graphic of the model domain. A water sheet (or film) exists along the one-dimensional boundary between the base of the ice sheet and ice/bed interface (see Figure 4.3). *Flowers* [2015] provides an excellent review of the various subglacial hydrological models that currently exist, including the water sheet which is applicable to large-scale East Antarctic transport. We will discuss the various subdomain components in detail in the following subsections. Table 4.1 lists the various parameters and their values used throughout the model; we provide references for each of these where needed. Throughout our design of the model we chose parameters that are based on data from this area, published estimates, or conservative values in order to test our hypothesis.

The flowline shown in Figure 4.1 was selected by first calculating the hydraulic pressure potential at the base of the Totten Glacier Catchment and surrounding area. The pressure potential is defined as $\Phi = \rho_i g H + \rho_w g z_b$ [*Shreve*, 1972], where ρ_i is the density of ice (assumed here and throughout this work as a constant), g is the acceleration due to gravity, H is the thickness of ice, ρ_w is density of water (also assumed to be a constant in this work), and z_b is the ice bed elevation. We used the hydraulic pressure potential to determine the subglacial water flow routing possible for water for the area of interest under the ice sheet [e.g. *Wright et al.*, 2008]. We then used the hydraulic pressure potential to create a hypothetical subglacial water flow accumulation map, which we then used to locate the largest flow system that crossed the Totten ice stream at the grounding line back to its potential origin at the ice divide in central East Antarctica. We chose this route as it roughly parallels the ice sheet surface movement and is the centerline for the ice catchment (see Figure 4.1), which is an important assumption for a 2D ice sheet flowline model. The coordinate system we chose for the model uses *x* for the horizontal and *z* for the vertical dimension. The flowline coordinate, *x*, increases from zero at the ice divide (X; see Figure 4.1) to 1,363 km at the grounding line (X'). The vertical coordinate *z* is the elevation above present sea level so, as our model extends to the top of the asthenosphere (~200 km below present sea level), most of the *z* coordinates are negative.

4.3.1 Experimental Design and Methods – Ice Sheet Model Subdomain

The numerical ice sheet model we used is a 2D flowline version we developed from the 3D thermomechanical full-Stokes model COMice (a finite-element model built with COMSOL; *Wilkens* [2014]). The model contains a formulation for non-Newtonian ice rheology with governing equations for mass and momentum solving for ice velocity ($\mathbf{u_i}=[u_{i,x}\ u_{i,z}]^T$) and ice pressure ($p_i$), as well as, energy by solving for temperature (T). We will give an overview of their model with explanation of our implementation of it for

this work but refer the reader to the work of *Wilkens* [2014] and *Wilkens et al.* [2015] for more specific information.

The governing equation for the conservation of mass is

$$\nabla \cdot \boldsymbol{u_i} = -\frac{u_{i,x}}{\omega}\frac{\partial \omega}{\partial x} \tag{4.1}$$

where the term on the right hand side approximates the effect of out-of-plane ice velocity from an assumed axisymmetric flow width, ω (*Pattyn* [2002]; ω is displayed as a function of x in Figure S4.1). This assumption, while not precisely valid for the Totten catchment, attempts to better approximate reality. This approach is not in *Wilkens* [2014] or *Wilkens et al.* [2015] as they construct a fully 3D model while we do not. The governing equation for the conservation of linear momentum is

$$\nabla \cdot \boldsymbol{\sigma} = -\rho_i \boldsymbol{g} \tag{4.2}$$

where $\boldsymbol{\sigma}$ is the stress tensor and $\mathbf{g} = [0\ -g]^T$ which is the acceleration due to gravity; the right hand side of (4.2) is the volume force applied to the ice sheet. The stress tensor, $\boldsymbol{\sigma}$, is equal to $\boldsymbol{\tau}$-$p_i\mathbf{I}$, where $\boldsymbol{\tau}$ is the deviatoric stress and $\mathbf{I}$ is the identity matrix. The deviatoric stress is defined as $\boldsymbol{\tau} = 2\mu\dot{\boldsymbol{\varepsilon}}$ where μ is the dynamic viscosity and $\dot{\boldsymbol{\varepsilon}}$ is the strain-rate tensor. The effective strain rate is defined as

$$\dot{\varepsilon}_e = \sqrt{\mathrm{tr}(\dot{\boldsymbol{\varepsilon}}^2)/2}. \tag{4.3}$$

The dynamic viscosity is dependent on the effective stress rate and the rate factor formulated as

$$\mu_i(T', \dot{\varepsilon}_e) = \tfrac{1}{2}\alpha(T')^{(-1/n)}\dot{\varepsilon}_e^{\,1-n/n} \tag{4.4}$$

after Glen [1955] and Nye [1957] where $\alpha(T')$ is the rate factor, n is the stress exponent, and T' is the temperature relative to the pressure-melting temperature. This temperature is equal to $\mathrm{T} + \beta_c p_i$ where β_c is the Clausius-Clapeyron constant for air-saturated ice [*Hooke*, 2005; *Greve and Blatter*, 2009]. The rate factor, $\alpha(T')$, is equal to $\alpha_0 e^{-E/RT'}$ where R is the gas constant, α_0 is a pre-exponential constant, E is creep activation energy (the latter two are used the same as in *Cuffey and Paterson* [2010], *Wilkens* [2014], and *Wilkens et al.* [2015]).

The governing equation for the conservation of energy is the heat transfer equation

$$\rho_i C_{p,i}(T)\boldsymbol{u_i}\nabla T - \nabla \cdot (\kappa_i(\mathrm{T})\nabla \mathrm{T}) = Q_i \tag{4.5}$$

where $C_{p,i}(T)$ is the temperature-dependent specific heat capacity of ice and $\kappa_i(\mathrm{T})$ is the temperature-dependent thermal conductivity of ice; both of which are used here the same as in *Cuffey and Paterson* [2010] and *Wilkens et al.* [2015]. The viscous dissipative heat source from internal deformation of the ice sheet, Q_i, is equal to $\boldsymbol{\tau}:\dot{\boldsymbol{\varepsilon}}$ (which is the same as $4\mu_i \dot{\varepsilon}_e{}^2$). As the ice sheet geometry is fixed, we do not account for melt or refreezing at the base of the ice sheet but do account for the potential impacts in the basal water sheet as a forcing function on the ice sheet's dynamics.

The boundary conditions we chose for the steady (i.e. no change in ice thickness) ice sheet flowline model are similar to those used in *Wilkens* [2014] or *Wilkens et al.* [2015] with slight deviation. For the ice sheet surface we apply a normal pressure equal to atmospheric pressure ($P_a = \boldsymbol{\sigma} \cdot \boldsymbol{n}$). At the ice divide (left hand side; see Figure 4.2) we apply a symmetry (or mirror) condition where $\boldsymbol{u_i} \cdot \boldsymbol{n} = 0$ and $\boldsymbol{\tau n} - (\boldsymbol{\tau n} \cdot \boldsymbol{n})\boldsymbol{n} = 0$, where **n** is the vector normal to the boundary. This condition means that there is no flow across

the ice divide boundary and that the tangential stresses disappear. The right hand side of the ice sheet is the Totten Glacier at the grounding line and is given a normal stress condition where the pressure is set to equal $\rho_i g(z_s(x) - z)$ where $z_s(x)$ is the ice surface elevation which is an assigned function. We varied the boundary conditions at the bottom of the ice sheet in two different ways. We first set the base of the ice sheet to a no slip condition where $\mathbf{u_{i,b}} = 0$. This is a simple method that allowed us to observe changes within the ice sheet but not at the basal layer as realistically would be with a sliding function. Next, we chose a sliding function that would enable us to calibrate modeled surface ice speed to observed surface speed. We drew from the work of *Budd and Jensen* [1987], *Alley* [1996], and *Le Brocq et al.* [2009] to establish a sliding function. The main difference for our function is that instead of applying a basal velocity as in *Le Brocq et al.* [2009], we apply a stress at the bed that is dependent on the water sheet thickness (discussed in the next section) along the flowline. We invert the sliding parameter relation used in *Le Brocq et al.* [2009; Figure 4.4] as we wanted an inverse relation to water sheet thickness (i.e. more water, less resisting stress; see Figure S4.5). The final form of the sliding function we used is $\boldsymbol{u_i} \cdot \boldsymbol{n} = 0$ and $\boldsymbol{\tau n} - (\boldsymbol{\tau n} \cdot \boldsymbol{n})\boldsymbol{n} = c_f f(b)\boldsymbol{u_i} \cdot \boldsymbol{t}$, where c_f is the forming coefficient used to calibrate the model, $f(b)$ is the inverse function of that in Figure 4.4 of *Le Brocq et al.* [2009], and **t** is the tangential vector to the bed. We calibrated the modeled ice surface speed to the observed surface speed from data from *Rignot et al.* [2011] sampled along the flowline. We calibrated the model to the higher groundwater forcing level (of two total: "high" and "low" groundwater; discussed later) to keep the values of each within reason. We did this purely to compare the difference between the varying levels of groundwater flux, making sure that the modeled surface speed was not faster than observed.

The temperature boundary conditions we used for the model are the average surface temperatures from *Comiso* [2000] (see Figure S4.2) sampled along the flowline and a fixed pressure-melting temperature at the base of the ice (i.e. $T_{pmp} = 0℃ - \beta_c \rho_i g H$). While the surface assumption is reasonable, the basal assumption of

temperature is not entirely valid for the entire length of the flowline although *Siegert et al.* [2007] and *Pattyn* [2010] demonstrate that the majority of this flowline is likely warm-based (mostly along the first and later thirds of the flowline; the middle is probably scattered between warm- and cold-based). However, our simplification simplifies the groundwater thermodynamics in the sedimentary basin greatly (discussed in detail in Section 4.3.3). We believe that eventually removing this fixed temperature at the basal boundary, even though it adds a great amount of complexity to this problem, will be of added benefit to the ice sheet modeling discipline but for now we proceed with this assumption. Finally, the lateral sides of this subdomain (and all other subdomains) are given insulation boundary conditions for temperature.

In addition to a boundary condition at the base of the ice sheet, we placed a few boundary heat source terms at the ice base to help mimic reality. We added a frictional heat term $\boldsymbol{u_{i,b}\tau_b}$ where $\boldsymbol{\tau_b}$ is the basal shear stress (both terms come from the numerical solution) and also a term to account for latent heat loss at the bed for constant meltwater generation. This latent heat loss is derived by rearranging Equation 9.38 from *Cuffey and Paterson* [2010] so that the calculated basal melt (described in the next section) is related to the latent heat loss at the bed (F_L) equaling $-(\boldsymbol{u_{i,b}\tau_b} + F_{v,b})$, where $F_{v,b}$ is the total vertical heat flux at the ice base accounting for both advective and conductive components. This boundary source is solved iteratively by COMSOL during simulation. A final heat source/sink placed at the ice/bed interface is the heat gained or lost from the moving water at the ice/bed interface which will be described in detail in the in the next section.

4.3.2 Experimental Design and Methods – Basal Water Sheet Model Subdomain

We chose to model the basal hydrology of the model using a water sheet (*Weertman* [1966]; distributed water system) approach similar to *Le Brocq et al.* [2009] and coupled to a groundwater system [*Gooch et al.*, in rev.]. The approach is valid for

systems at this large scale; for glacier-scale problems a more efficient drainage system should probably be chosen (see *Flowers et al.* [2015] for a review of these systems). We chose to make this subdomain a one-dimensional boundary system, as opposed to the others, which are two-dimensional. This is because the water sheet thickness is much less than the dimensions of the model (mm's vs. km's; see Figure 4.3), which simplifies our model design significantly. The thickness of the water sheet (d) is unknown and solved by our model. Subglacial lakes are not modeled by this particular paradigm although one large subglacial lake intersects the flowline (Totten_2; see Figure 4.1). In solving for this, we are able to estimate the flow of water and transport of heat along this sheet (similar to a fracture aperture). The governing equation for the steady water sheet thickness is

$$-\nabla_x \cdot \left(\frac{d^3}{12\mu_w}\nabla_x p_w\right) = \dot{b} + G \tag{4.6}$$

where μ_w is the viscosity of water, p_w is the pressure of water which is equal to the ice overburden (i.e. $\rho_i g(z_s - z_b) + \rho_w g z_b$; which is a reasonable assumption for our purposes here), $\dot{b}$ is the melt component from the basal ice, and G is the source/sink term of groundwater flux normal to the ice/bed interface (discussed in the next section). The basal melt ($\dot{b}$) is equal to the basal ice friction ($\boldsymbol{u_{i,b}\tau_b}/\rho_w L$) and total vertical heat flux ($F_{v,b}/\rho_w L$) components where L is the latent heat of water. We choose to use the total vertical heat flux here, as it is similar to the approach of ice sheet models using geothermal heat flux, although it is likely that the full total heat flux vector (i.e. horizontal + vertical) is important for future investigation. It is important to note that the ice sheet has a fixed geometry throughout the simulations; we are not considering mass balance as part of these diagnostic simulations so this melt rate does not impact the overall geometry of the ice sheet. We set a boundary condition of zero sheet thickness at the ice divide and do not condition the water sheet elsewhere.

The inner term of the left hand side of (4.6) contains the average velocity of the water ($\overline{\boldsymbol{u}}_{\boldsymbol{ws}}$; laminar flow between parallel plates) which is equal to $-d^2/12\mu_w \nabla_x p_w$ which we use in our model to drive heat advected by the water sheet at the ice/bed interface. The boundary heat source term applied to the water sheet along the ice/bed interface is

$$F_w = -d\rho_w C_{p,w} \overline{\boldsymbol{u}}_{\boldsymbol{ws}} \cdot \nabla_x T \tag{4.7}$$

where $C_{p,w}$ is the specific heat capacity of water and $\nabla_x T$ is the horizontal temperature gradient. Given that this water is not allowed to refreeze by our model assumption (although negative sources from heat flux "refreezing" or negative groundwater flux are subtracted from the sheet thickness), we implicitly approximate reality of heat transfer to and from the surrounding subdomains from the positive and negative behavior of the horizontal temperature gradient. This oscillation causes the heat carried by the water to "interact" with its surroundings by adding and subtracting heat along the flowline. While this is not an ideal model of this system, but it simplifies the model design and allows some advancement toward reality (i.e. by allowing the natural thermal gradient to dictate how the advected water interacts with its surroundings) until later improvements will enable a more proper method of water sheet heat transport and phase change at the base of the ice sheet.

4.3.3 Experimental Design and Methods – Sedimentary Basin Groundwater Model Subdomain

We define the sedimentary basin subdomain geometry largely through geophysically derived estimates for the area and the hydraulic properties purely in a theoretical nature designed to test a large range of possibilities. We use existing estimates for sedimentary basin depth [*Frederick*, 2015]. While there are places along the flowline where the crystalline basement rock (modeled as impermeable here) that

underlies the sedimentary rock comes close to the bed surface, the ice/bed interface is mostly lined with porous material (see Figure 4.2b). In only two short segments does the crystalline basement rock come in contact with the ice base, creating three separate groundwater zones along the flowline. In reality, these zones are likely connected out-of-plane. The groundwater system we formulated in this model does not represent the actual subsurface hydraulic system but rather approximates conservative estimates (a "high" and "low" scenario; discussed later in this section) of the possible hydrologic forcing that could be applied to the base of the Totten Glacier Catchment. We assume that the subsurface is fully saturated, which is likely [e.g. *Huybrechts*, 1993; *Siegert et al.*, 2005; *Young et al.*, 2011]. In order to provide flux of water through the bed, we apply a constant hydraulic head pressure to solve for the groundwater flux (the forcing we are using to test our hypothesis); otherwise applying a method based on the melt rate would overwrite this hydraulic forcing. This hypothetical regional groundwater system also advects heat in a realistic manner, which is currently (to our knowledge) not incorporated into ice sheet models. The following approach we take closely follows the work of *Gooch et al.* [2016, in rev.] which are both diagnostic in nature, as is this work.

The governing equation for the steady flow of groundwater in the fully saturated sedimentary basin is

$$-\nabla \cdot \left(\frac{k(z)}{\mu_w}\nabla p_{gw} + \rho_i g \nabla z\right) = 0 \tag{4.8}$$

where $k(z)$ is the permeability of the porous sedimentary basin and ∇p_{gw} is the pressure gradient of the groundwater. The second term with the parentheses is the gravitational component of groundwater flow. All the terms within the parentheses makeup the groundwater volume flux, $\boldsymbol{u_{gw}}$ [*Stauffer*, 2006]. The permeability is a function of depth; $k(z) = k_0 e^{-A(z_b - z)}$, where k_0 is the initial sediment surface permeability in the bed and A is an exponential decay factor we tuned to a more aggressive, but realistic value to

make our groundwater argument more conservative (see Table 4.1). The decay function with depth is a simple relationship long used in the absence of actual drilling data of sediment porosity (and permeability; after *Athy* [1930], *Sclater and Christie* [1980], and *McKenna and Sharp* [1998]). The sole parameterization of the groundwater-forcing factor in our model is the choice of the initial sediment surface permeability. We chose two values to represent a very large span of the parameter space of geologic materials. For the "high" groundwater case, we chose a value of 10^{-11} m^2 that represents a sandy unconsolidated material or fractured (or karstic) lithified rock (see Table 8.2; *Singhal and Gupta* [2010]). For the "low" groundwater case we chose 10^{-18} m^2 that represents unfractured shale or crystalline rock, which is essentially having no groundwater flow. With these realistic end-member values for surface properties we assume that reality most likely would exist between the two with the understanding that our aggressive decay function would also provide some amount of realism critical to testing our hypothesis. The boundary condition for the top of the sedimentary basin is a constant hydraulic head boundary that is equal to the ice/bed interface water pressure (p_w).

The governing equation for steady heat transfer in the sedimentary basin is

$$\rho_w C_{p,w} \boldsymbol{u_{gw}} \cdot \nabla T = \nabla \cdot \left(\kappa_{eq} \nabla T\right) + Q_s \tag{4.9}$$

where κ_{eq} is the equivalent thermal conductivity for the basin (see Figure S4.4) and Q_s is the heat produced by the radiogenic elements in the sediment (see Figure 4.2). The equivalent thermal conductivity is evaluated as $\kappa_{eq} = \phi\kappa_w + (1-\phi)\kappa_s$, where κ_w is the thermal conductivity of water, κ_s is a typical sedimentary rock thermal conductivity [*Beardsmore and Cull*, 2001], and ϕ is the porosity (see Figure S4.3). The porosity, ϕ, is evaluated as $\phi = \phi_0 e^{-b(z_b - z)}$ [*Athy*, 1930; *Sclater and Christie*, 1980; *McKenna and Sharp*, 1998], where ϕ_0 is the surface porosity of a typical crustal value [*Gleeson et al.*, 2011, 2014], and b is a porosity decay term appropriate for this kind of setting [see Table

4.1; *Sclater and Christie*, 1980; *Jiang et al*., 2010]. Our choice of heat production in the sediment is an average continental crustal value for sediment [*Waples*, 2001]. For the thermal boundary condition at the top of the sedimentary basin, the temperature is set to the pressure-melting temperature.

4.3.4 Experimental Design and Methods – Remaining Lithosphere Model Subdomain

The remaining subdomains in our model are the (continental) crust and lithospheric mantle (see Figure 4.2). We chose each of their bottom boundary depths based on the most recent estimates from *An et al.* [2015a; 2015b]. For selection of each of their thermal properties, we relied heavily on the works of *Sandiford and McLaren* [2002], *McLaren et al.* [2003], *Carson et al.* [2013], and *Gooch et al.* [2016]. We include each of these subdomains only to extrapolate temperature and heat flux from a known temperature [*Beardsmore and Cull*, 2001; *An et al.*, 2015b] at the lithosphere-asthenosphere boundary (a lá *Petrunin et al.* [2013]), so the governing equations are simple and straightforward.

The governing equations in the crust is the steady heat conduction equation

$$0 = \nabla \cdot (\kappa_b \nabla T) + Q_b \tag{4.10}$$

where κ_b is the thermal conductivity of crystalline basement rock (see Figure S4.4) and Q_b is the heat produced by the radiogenic elements in the crystalline basement rock (see Figure 4.2). The value we chose for the heat production is represented by the exponential function $Q_b = Q_0 e^{-(z_b - z)/D}$ [*Lachenbruch*, 1970], where Q_0 is the heat production at the top of the crystalline basement rock and D is a characteristic length scale typical for this kind of setting [see Table 4.1; *Jaupart*, 1986; *Waples*, 2001]. The value of the basement rock surface heat production is typical of Australian crust [once connected to East Antarctica in the Mesozoic; *Sandiford and McLaren*, 2002; *McLaren et al*., 2003] and in

keeping with *Carson et al.* [2013] except that instead of placing a few small high heat-producing granitic bodies in the near surface, we place a lower value broadly across the basement surface (that decays rapidly) after *Gooch et al.* [2016].

The governing equation for the lithospheric mantle is the steady heat conduction equation

$$0 = \nabla \cdot (\kappa_m \nabla T) + Q_m \tag{4.11}$$

where κ_m is the thermal conductivity of the lithospheric mantle and Q_m is the heat produced by the radiogenic elements in the lithospheric mantle (see Table 4.1 and Figure 4.2). We selected both of these values based on those used from *Carson et al.* [2013]. The bottom boundary condition is the fixed temperature, T_b, along the entire lithosphere-asthenosphere boundary. This is also the bottom temperature condition for the entire model. In summary, we set the temperature at the ice surface, the ice base, and the bottom of the lithosphere; in all other sections of the model, the temperature is calculated during the simulation.

4.4 RESULTS

We ran four main simulations in total: a high ($k_0 = 10^{-11}$ m^2) and low ($k_0 = 10^{-18}$ m^2) groundwater scenario each with sliding on (calibrated to the high groundwater case; $c_f = 5.25\times10^{13}$ for $k_0 = 10^{-11}$ m^2) and off. These various simulation results (i.e. pressure, temperature, and velocity) and derived values (e.g. heat flux or pressure gradient) are shown in Figures 4.4-4.9, S4.4, and S4.6-S4.19. We also ran a high ($k_0 = 10^{-11}$ m^2) and low ($k_0 = 10^{-18}$ m^2) groundwater scenario each with sliding calibrated to the low groundwater case ($c_f = 2\times10^{12}$ for $k_0 = 10^{-18}$ m^2) just to observe the results for the low case, as the high groundwater case's results were unrealistic (Figures S4.19-4.21). For all the simulations we ran, the most notable trend is that most all of the main

results except for the high groundwater case with sliding are essentially the same. This is especially apparent when looking at the modeled ice surface velocities (Figure 4.4b) and ice sheet and sedimentary basin temperatures (Figures 4.6c, S4.8). However, the water sheet thickness trends, which sliding speeds are based on, do not follow this trend. The other major trend in the modeled temperature results is the behavior of the temperature in the ice sheet. For results that are not specifically calibrated to the surface ice speed or those that do not have slip, the horizontal temperature trends are not as smooth (Figures 4.6, S4.8, S4.20). While developing this model, we noticed that the solution did not change much when turning off the contribution from the out-of-plane ice sheet dimension but decided to continue to include this in order to incorporate as much realistic behavior as possible.

The modeled pressure in the ice sheet is essentially the same for all simulations (see Figures 4.5, S4.6, S4.7); the groundwater system has the same pressure solution in every simulation, which we expected. Figure 4.5 shows the horizontal pressure gradient in the ice sheet and groundwater system; the dominant force direction in both is horizontal, which we expected. This results in the dominant velocity also being horizontal (Figures S4.12, S4.13). However, the groundwater system does display some vertical volume flux (Figure 4.5) that interacts with the water sheet. The strongest pressure gradients in the ice sheet and groundwater systems are proximal to the grounding line where the ice surface slopes are the greatest. Within the groundwater system, especially where the ice surface slopes are lowest near the ice divide, there are small flow systems that flow toward the interior of the continent associated with steep localized sub-ice bed topography.

The water sheet thickness results for all simulations group into two groups (Figure 4.4a). These groups are associated by the groundwater forcing scenarios (either high or low) and not by the sliding function. The general trend for the water sheet results for the low groundwater scenario start at the ice divide (X) at zero thickness with a rapid growth

to over 4 mm within the first 50 km and then a slower growth to about 7 mm at the grounding line (X'). For the results with the high groundwater forcing scenario, the water sheet exhibits a different trend. The sheet stays at zero for over the first 10 km and then rapidly increases to about 13-14 mm over the next roughly 10 km. It then drops quickly by 1-2 mm in a few kilometers to about 11-12 mm and then steadily grows (with some minor oscillations) to about 13-14 mm at the grounding line (X').

The modeled ice sheet strain rates and the resulting heat generation (viscous dissipation) values from the internal strain are similar in all simulations (Figure 4.7, S14). The main difference in their grouping is the rate of sliding, not the level of groundwater volume flux (although, when sliding is turned on, the higher groundwater scenario causes a large water sheet depth that leads to an increase in overall sliding speed). The low groundwater scenario with sliding has a very low sliding speed, which is not very different from zero (Figure 4.4b), so its dissipative heat generation is not very dissimilar to either of the simulations where sliding is off. The simulations where the sliding is on is faster and has less range of (and lower maximum) heat generation than those with a slower sliding speed (also less overall strain rate range). The overall averages of heat generation for the whole ice sheet for the simulations with little to no sliding speed are from about 32 to 37 $\mu W/m^3$ (maximum of about 89,000 $\mu W/m^3$) whereas the high groundwater scenario with sliding on (i.e. $c_f = 5.25\times10^{13}$ for $k_0 = 10^{-11}$ m^2) has an average heat generation of about 11 $\mu W/m^3$ (maximum of about 19,000 $\mu W/m^3$). For reference, these values are roughly double to seven times the surface heat generation of the crystalline basement rock (at 5 $\mu W/m^3$). The largest of these values are nearest the bed and proximal to the grounding line (X') which is to be expected.

The vertical heat fluxes at the bed are similar for the simulations with and without slip (Figure 4.8). The main correlation for the vertical heat flux is the level of groundwater forcing. The high groundwater forcing scenarios with and without slip have average vertical heat fluxes of 840.16 and 758.17 and mW/m^2, respectively, while the

low groundwater forcing scenarios with and without slip have average vertical heat fluxes of 49.28 and 48.49 mW/m^2, respectively. One other trend is that the vertical heat flux values associated with the high groundwater scenario have large changes in orders of magnitude (~2-3) and sign (direction) at a high frequency along the flowline. The low groundwater forcing simulations have vertical heat fluxes that vary much less and stay positive (flux upward) along the flowline; however, there are some larger deviations to this behavior proximal to the grounding line. Also, the vertical heat with the low groundwater forcing has a similar behavior to the published estimates of geothermal heat flux along this flowline [*Shapiro and Ritzroller*, 2004; *Fox Maule et al.*, 2005; and *An et al.*, 2015b]. However, when the sliding model is calibrated to the ice surface speed for the low groundwater scenario (Figure S4.20), the vertical heat flux starts to behave more like that of the high groundwater forcing scenario with more oscillations in flux direction (i.e. sign) and spreading over a few orders of magnitude. Although, the average vertical heat flux of this simulation is still not much higher (at 94 mW/m^2) than the published values along the flowline (roughly 40-60 mW/m^2).

The modeled water sheet in all simulations gained (or lost) water from the groundwater volume flux normal to the ice/bed interface and the meltwater from the bottom of the ice sheet due to the total heat flux. However, the input from frictional melt from basal shear only came from the simulations with sliding enabled (Figures 4.9, S4.16, S4.18, S4.21). The groundwater volume flux for the high groundwater scenario produces a highly oscillatory pattern of positive and negative fluxes with peak magnitudes past 1 m/yr for an average of about 347 mm/yr to the water sheet. The low groundwater scenario is meant to essentially have no significant flux contributing to the water sheet but does have an average contribution of about 3.47×10^{-5} mm/yr, which is seven orders of magnitude less than the high scenario average (this is not surprising as 10^{-11} (m^2) - 10^{-18} (m^2) = 7). The contribution of the frictional melt component for both scenarios is minimal for most of the flowline except that nearest to the grounding line (X'). The meltwater component from the total heat flux for the high groundwater

scenario varies similarly to the high groundwater forcing flux with water coming into and out of the water sheet for an average contribution of about 85 mm/yr into the water sheet system. The meltwater due to the total heat flux from the low forcing scenario is positive and steady along most of the flowline (except for some increasing fluctuation near the grounding line) contributing an average of about 4.9 mm/yr to the water sheet. Considering that most of the frictional melt components are much less than the other sources of water to the sheet, their absence in the simulations do not change the resulting thicknesses much hence the trends in thickness looking similar to those shown in Figure 4.4a.

4.5 DISCUSSION

We most notably observed from our model results that groundwater flux does have some impact at the base of our steady flowline representation of the Totten Glacier catchment section of the East Antarctic Ice Sheet. The vertical heat flux for this specific ice catchment is very dependent on the advection of groundwater near the ice/bed interface as has been observed in other glacial settings [e.g. *Clarke et al.*, 1984; *Echelmeyer*, 1987]. The heat flux is directly tied to the melt rate and accretion of basal ice and our results suggest that with the larger and fluctuating heat flux from a higher groundwater forcing, the ice sheet response would be noticeable and significant (Figures 4.8, 4.9). The actual direct impact from groundwater-enhanced heat flux in the thermal structure of the ice sheet is not as clear from our results. Although, it is clear from our results that the strength of advection of heat in the more shallow subsurface of the sedimentary basin with higher permeability is on par with the strength of heat advection in the ice sheet (Figure S4.15). However, we do assert the vague nature of the enhanced groundwater thermal effect on ice because the results for the simulations where sliding was turned off resulted in essentially the same results independent of the groundwater forcing level (Figures 4.4b, S4.8). Even removing the only other strong heat source at the bed, the water sheet heat transport (Figure S4.16), the observed behaviors persisted. We

believe this is due to the strong heat source from viscous dissipation in the lower part of the ice sheet which overwhelms other heat sources (Figure 4.7).

Our results demonstrate that the temperatures (Figures 4.6, S4.8, S4.20) above the larger sedimentary basins along our flowline where ice velocity is low (mainly in the Aurora Subglacial Basin; see Figure 4.1) are increased from areas with less sedimentary thickness; the same trend shows in the modeled thermal conductivity values of the ice as well (Figures S4). However, the actual modeled heat flux (vertical and horizontal; Figures S4.9, S4.10) in the ice sheet shows a decrease in these places and the strain rates in the ice and the associated viscous dissipative heat generation does not show elevated heat generation or strain in these places either. The result is likely the effect of conductive heat flow as the modeled thermal conductivity in the ice sheet also demonstrates this pattern (Figure S4.4). This correlation leads us to believe that the presence of the sedimentary basins below the Totten Glacier catchment might alter the thermal structure of the slower moving ice sheets above them; however, as this experiment was not applied at addressing this specific claim, we advise that further investigation is needed. However, the behavior of the conductive component of the vertical heat flow at the ice base (Figures S4.11, S4.20) is most likely (or at least partly) associated with the thickness of the sedimentary basin along the flowline. We attempt to validate this claim because the thicker package of sedimentary rock would contribute to a lower overall thermal conductivity thus lowering the conductive heat flux. This may feedback to the ice sheet causing an area of decreased temperature and thus decreased thermal conductivity, which iteratively would heat up as the heat would leave the system more slowly but this would need further analysis to prove conclusively. The presence of a large subglacial lake, $Totten_2$, (not modeled here) may also provide insight into the nature of sediment-water interaction along the flowline near the entrance of a subglacial fjord (see Figure 4.1). The pooling nature of the water subglacially may indicate that saturated sediments outside the fjord entrance are releasing water along the flowpath

before the bed geology transitions to crystalline basement rock (i.e. less permeable and porous; see Figure 4.2).

The impact of groundwater directly and indirectly on the water sheet is significant (Figures 4.4a, 4.9). In the initial water sheet formation at the ice divide, the high groundwater forcing (downward; Figures 4.5, S4.7, S4.14) dramatically drains the bed until enough water is produced along the next 10 km to rapidly raise the sheet to a maximum of about 13-14 mm and then quickly shrinks it by about 2 mm over another 10 kilometers. After this point the meltwater from the vertical heat flux becomes co-dominant (Figure 4.9) and the gradual upwinded water along the bed gradually raises (with some oscillation due to groundwater flux changes and reversed horizontal temperature gradients) the water sheet by about 2 mm at the grounding line. For the system with the low groundwater forcing, the water sheet is essentially not directly impacted by the groundwater flux at the ice/bed interface because its magnitude is inconsequential (about 5 orders of magnitude less than that of the meltwater; see Figures 4.9, S4.1, S4.21). The water sheet system can be directly impacted by the addition or subtraction of water depending on the groundwater flow direction and indirectly impacted by groundwater altering the heat flux direction and magnitude which affects the amount of melting or refreezing. The groundwater also indirectly impacts the meltwater rate from basal friction depending on the formulation of sliding law chosen (Figures 4.9, S4.18, S4.21).

As the sliding function we use here is in the approach of *Budd and Jensen* [1987], *Alley* [1996], and *Le Brocq et al.* [2009] that takes into account many factors at the ice/bed interface and into the shallow subsurface (i.e. till deformation), we note that it is this area that groundwater most likely effects the dynamics of the Totten Glacier Catchment of the East Antarctic Ice Sheet. Our results demonstrate that differences in groundwater forcing lead to differing effects to the water sheet at the base of the ice sheet (Figure 4.4). Even though our sliding function directly couples to the thickness of the

water sheet, this addition of groundwater could impact the friction parameters of other sliding function implemented at similar ice sheet scales [e.g. *Pattyn et al.* (2012); *Wilkens et al.* (2015)]. While our sliding function can be calibrated to the low groundwater forcing ice surface speed to match well to the observed ice surface speed (Figure S4.19), we still argue that high groundwater forcings would affect the water sheet in such a way that cannot be overlooked. This might also be important for other subglacial hydrological system models [e.g. *Kyrke-Smith and Fowler*, 2014]. While we demonstrate groundwater flux as a constant function of ice overburden pressure here, it would be worthwhile to also look at a numerical simulation similar to this where the groundwater boundary condition is based on the melt rate of basal ice. We posit that groundwater systems would likely affect those water sheet systems but possibly in a more dramatic way but this is beyond our scope of work here.

4.6 CONCLUSION

Through our novel methodology linking groundwater forcing to a steady thermomechanical ice sheet flowline model with basal hydrology, we have initially assessed diagnostically whether groundwater flux at the ice/bed interface has a measurable effect on ice dynamics for the Totten Glacier catchment of East Antarctica. While it is currently unclear whether the hypothetical groundwater forcing on the modeled heat flux and thermal structure of the ice sheet is direct, the potential impact on the subglacial hydrological system may have more direct impact on the actual dynamics of the Totten Glacier Catchment system of East Antarctica. We assert this as the groundwater forcing has a direct effect on the water system at the ice/bed interface, which does have an effect on the ice sliding velocity for our sliding function and most likely for other sliding functions. We also note that just the presence of the geophysically estimated sedimentary basins underlying the ice base along our model flowline alone has an effect on the thermal structure of the ice sheet but requires further analysis to determine the relationship better.

While this methodology is not a fully comprehensive way to determine groundwater's potential impact to this study area, we do however believe that this work is a foundation for other studies to build upon and a guide to those interested in better understanding the complexities of the Totten Glacier Catchment portion of the East Antarctica Ice Sheet. We believe that given future geophysical and eventually geologic research in critical submarine basins of East Antarctica, particularly the Aurora and Sabrina subglacial basins, that it will be feasible to incorporate more realistic groundwater systems into the ice sheet models utilized for the area.

Future efforts based on this work would likely need to investigate the effect of leaving the ice base temperature as part of the numerical solution (instead of fixing the temperature), finding a way to base groundwater flux from melt at the ice/bed interface rather than assumed overburden pressure, and adding control of permafrost formation for where the modeled temperatures in the sedimentary basins go below the pressure-melting temperature and cause groundwater to slowdown or freeze. Extending the model to a fully three dimensional model domain would enable the ability to test whether groundwater flow systems behaved identically to the water sheet systems or whether they may flow in different directions possibly leading to anomalous water at the bed. Future work should also incorporate transient behavior in the ice sheet thickness development and the pore pressure as some transient effects in the groundwater system could linger as the ice sheet evolves (such as in *Bense and Person* [2008], *Lemieux et al.* [2008], or *Gooch et al.* [2016]). The result of these holistic analyses would yield a better, more realistic ice sheet model of the Totten Glacier Catchment system that better meets the needs of those needing to assess future ice sheet outlet contributions to sea level from East Antarctica.

4.7 FIGURES AND TABLES

Parameter	Value	Units	Parameter Description	References
A	5×10^{-3}	m^{-1}	*Hydraulic decay parameter*	*Jiang et al. 2009*
b	5×10^{-3}	m^{-1}	*Porosity decay term*	*Sclater & Christie 1980; Jiang et al. 2010*
c_f	5.25×10^{13}, 2×10^{12}	-	*Sliding law forming coefficient (high, low)*	-
$C_{p,s}$	0.93	kJ/(kg×K)	*Specific heat capacity, sedimentary rock*	*Beardsmore & Cull 2001*
$C_{p,w}$	4.186	kJ/(kg×K)	*Specific heat capacity, water*	-
D	10	km	*Crustal length scale*	*Jaupart 1986; Waples 2001*
g	9.81	m/s^2	*Acceleration due to gravity*	-
k_0	10^{-11}, 10^{-18}	m^2	*Sedimentary surface permeability (high, low)*	*Singhal & Gupta 2010; Gleeson et al.2011, 2014*
L	333	kJ/kg	*Latent heat, H_2O*	*Mellor & Kantha 1989*
n	3	-	*Glen's flow law stress exponent*	*Cuffey & Paterson 2010*
Q_0	5.0	$\mu W/m^3$	*Heat production, surface of basement rock*	*Sandiford & McLaren 2002; McLaren et al. 2003*
Q_s	1.0	$\mu W/m^3$	*Heat production, sedimentary rock*	*Waples 2001*
Q_s	0.02	$\mu W/m^3$	*Heat production, mantle*	*Furlong & Chapman 2013; Carson et al. 2014*
R	8.31	J/(mol×K)	*Gas constant*	-
T_b	1,330	°C	*Temperature, lithosphere bottom boundary*	*Beardsmore & Cull 2001; An et al.2015b*
β_c	9.8×10^{-8}	K/Pa	*Clausius-Clapeyron constant*	*Greve & Blatter 2009; Wilkens 2014*
κ_b	2.5	W/(m×K)	*Thermal conductivity, basement rock*	*Carson et al. 2014*
κ_m	3	W/(m×K)	*Thermal conductivity, mantle*	*Carson et al. 2014*
κ_s	2.3	W/(m×K)	*Thermal conductivity, sedimentary rock*	*Beardsmore & Cull 2001*
κ_w	0.56	W/(m×K)	*Thermal conductivity, water*	-
μ_w	8.94×10^{-4}	Pa×s	*Viscosity, water*	-
ρ_i	918	kg/m^3	*Density, ice*	*Le Brocq et al. 2009; Wilkens et al. 2015*
ρ_w	1,000	kg/m^3	*Density, water*	-
ρ_s	2,369	kg/m^3	*Density, sedimentary rock matrix*	*Frederick 2015*
ρ_b	2,670	kg/m^3	*Density, crust*	*Frederick 2015*
ρ_m	3,250	kg/m^3	*Density, mantle*	*Petrunin et al. 2013; Frederick 2015*
ϕ_0	0.2	-	*Sedimentary surface porosity*	*Gleeson et al. 2011, 2014*

Table 4.1. Parameters used in the numerical model with references, if applicable.

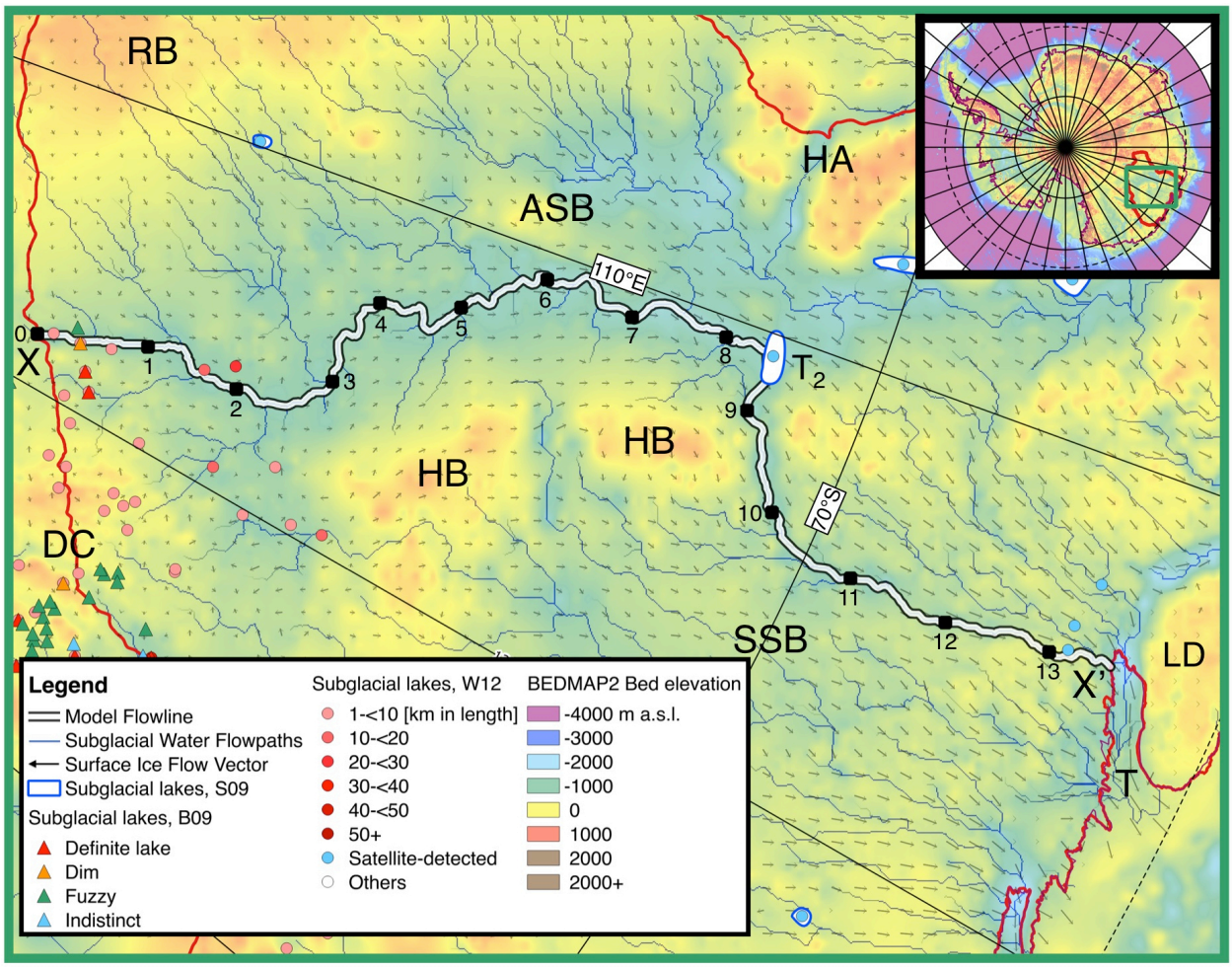
RB
HA
ASB
110°E
70°S
HB
HB
DC
SSB
LD
X
X'
T
T2
0
1
2
3
4
5
6
7
8
9
10
11
12
13
Legend
Model Flowline
Subglacial Water Flowpaths
Surface Ice Flow Vector
Subglacial lakes, S09
Subglacial lakes, B09
Definite lake
Dim
Fuzzy
Indistinct
Subglacial lakes, W12
1-<10 [km in length]
10-<20
20-<30
30-<40
40-<50
50+
Satellite-detected
Others
BEDMAP2 Bed elevation
-4000 m a.s.l.
-3000
-2000
-1000
0
1000
2000
2000+

Figure 4.1. Map of the Totten Glacier and surrounding ice sheet catchment emptying along the Sabrina Coast in East Antarctica with the model flowline (X to X'; 1,363 km in total length with 100 km segments noted) discussed in this article. Important places or those discussed in this article are highlighted; ASB – Aurora Subglacial Basin, DC – Dome C, HA – Highland A, HB – Highland B, LD – Law Dome, RB – Ridge B, SSB – Sabrina Subglacial Basin, T_2 – subglacial lake $Totten_2$, and T – Totten Glacier. The red outline represents the larger ice catchment boundaries [*Zwally et al.,* 2012] and, where at the coast, represents overlap with the grounding line [*Bindschadler et al.,* 2011]; the precise catchment for Totten Glacier was measured and is displayed as a function of flowline coordinate in Figure S4.1. Surface ice flow speeds and direction are from the MEaSUREs dataset [*Rignot et al.,* 2011]. The subglacial water flowpaths and the bed elevation are based on the Bedmap2 dataset [*Fretwell et al.,* 2013]. All latitude and longitude graticules in the inset and main figure are in 10° increments with the Antarctic Circle shown as a dashed line. The subglacial lake inventory references are: B09 – *Blankenship et al.* [2009], S09 – *Smith et al.* [2009], and W12 – *Wright and Siegert* [2012]. A version of this map with the background indicating measured ice surface speed instead of bed elevation is given in Figure S4.22.

Model Domain with Key Sedimentary Basin & Lithospheric Parameterizations

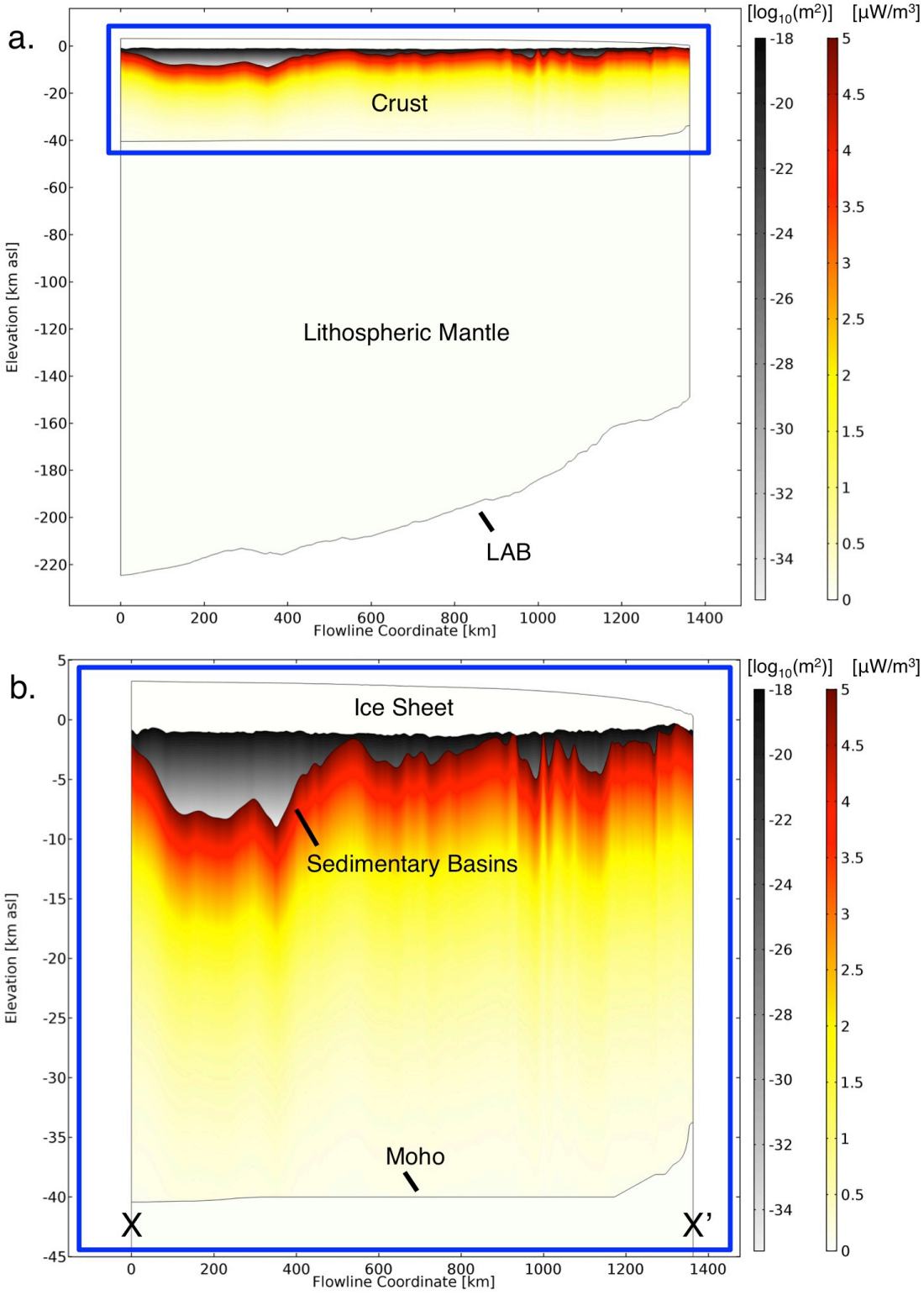

Figure 4.2. Flowline (X-X'; see Figure 4.1 for location) model domain with (a) the larger extent encompassing the entire lithospheric and cryospheric model section with the inset (b) showing the more critical subdomains of the numerical model along with the main parameterization focus of the model. The elevation is in km above present sea level (asl). The LAB (Lithosphere-Asthenosphere Boundary) and the Moho are from *An et al*. [2015a, 2015b]. The ice sheet surface and bed elevations are from Bedmap2 [*Fretwell et al*., 2013]; sedimentary basin depths are from *Frederick* [2015]. Permeability shown here is from the $k_0 = 10^{-18}$ m^2 parameterization which quickly decays to below 10^{-34} m^2 at the base of the deepest basin. The color bar for the $k_0 = 10^{-11}$ m^2 parameterization (not shown) would decay similarly, starting at 10^{-11} m^2 and end below 10^{-27} m^2. The input of radiogenic heat production in the sedimentary basins is uniformly set to 1 $\mu W/m^3$ for both parameterizations [*Waples*, 2001]. The crystalline basement subdomain (between the Moho and sedimentary base) is set with an exponentially decaying function starting at 5 $\mu W/m^3$ for both parameterizations [*Sandiford and McLaren*, 2002; *McLaren et al*., 2003] while the lithospheric mantle is set to 0.02 $\mu W/m^3$ for both parameterizations [*Furlong and Chapman*, 2013; *Carson et al*., 2013]. The viscous dissipative heating from the internal deformation of the ice (a result of simulation) is shown in Figure 4.7.

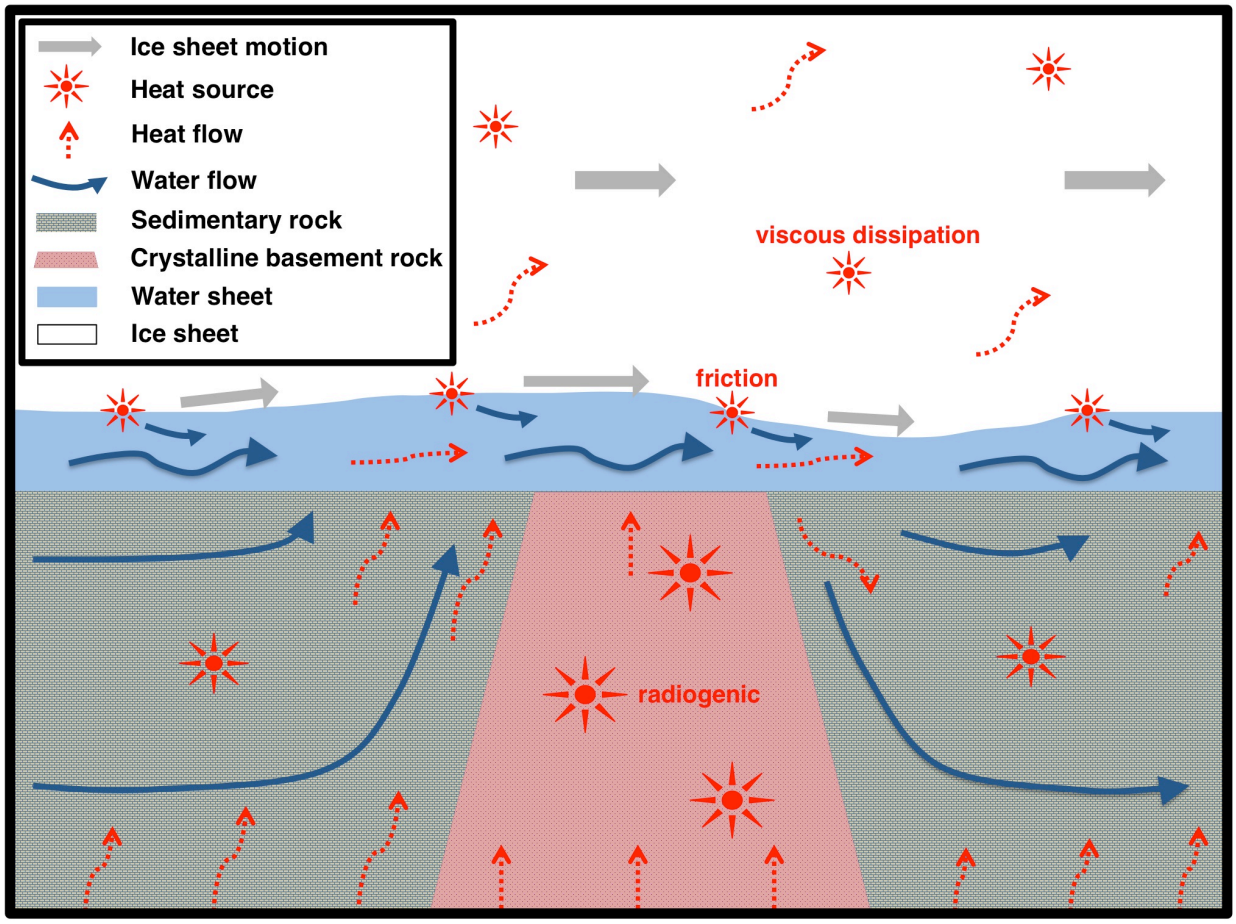

Figure 4.3. Components involved in the critical zone (proximal to the ice/bed interface) of the numerical model presented in this article. All arrows represent the general flow patterns of heat and water. The graphic is not to any particular scale however the horizontal dimension could represent 1 to 10's of kilometers or more and the vertical dimension could represent 1 to 10's of centimeters or more as long as the water sheet in the middle does not exceed ~1-2 centimeters. The heat sources shown explicitly here are from viscous dissipation (internal deformation) in the ice sheet, friction at the base of the ice from sliding along the bed, and from radiogenic elements in the sediments and crystalline basement rock. The ice motions are shown as both basal sliding and internal deformation creep.

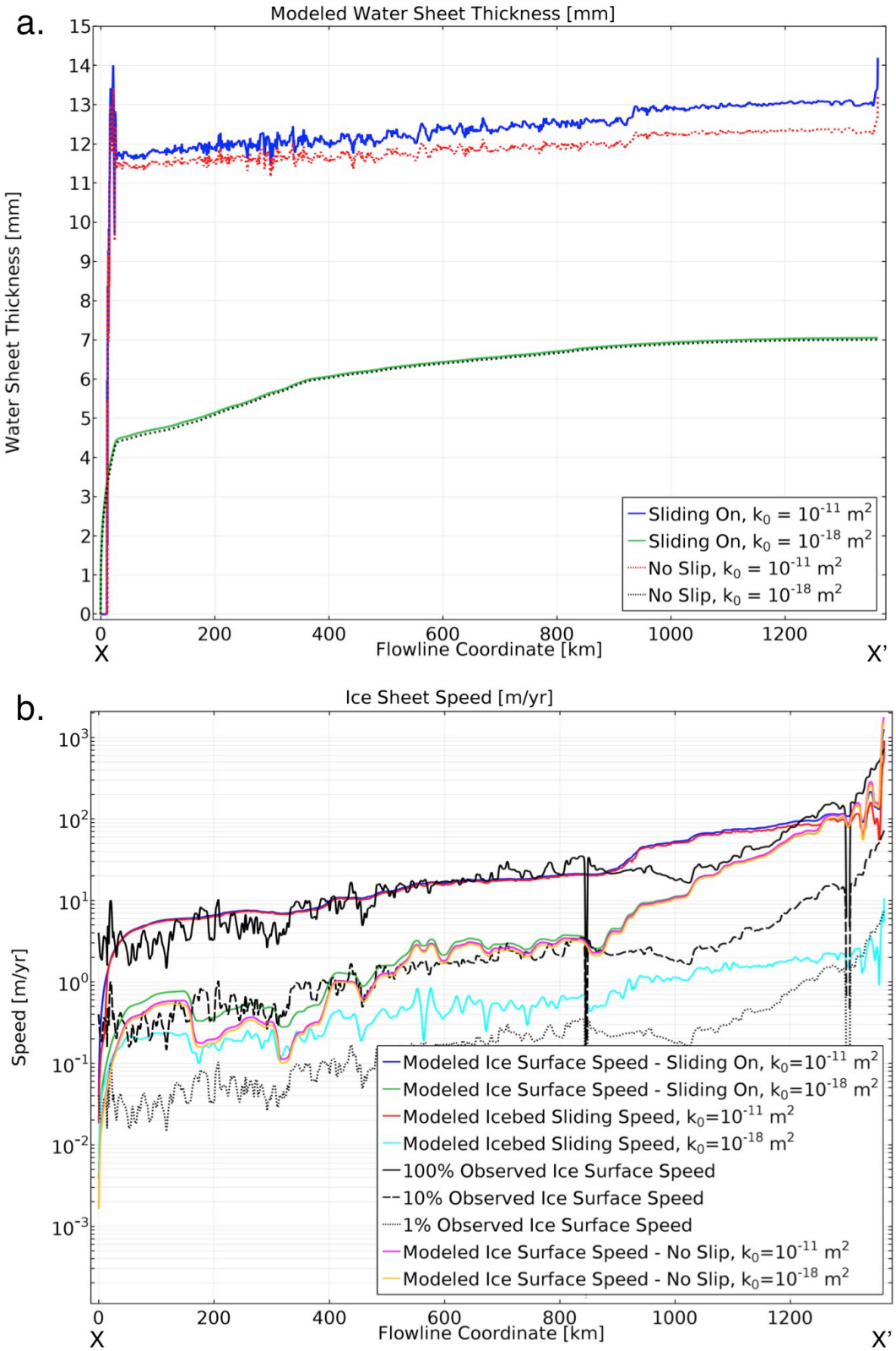
a.
Modeled Water Sheet Thickness [mm]
Water Sheet Thickness [mm]
Flowline Coordinate [km]
X
X'
Sliding On, k0 = 10-11 m2
Sliding On, k0 = 10-18 m2
No Slip, k0 = 10-11 m2
No Slip, k0 = 10-18 m2
b.
Ice Sheet Speed [m/yr]
Speed [m/yr]
Flowline Coordinate [km]
X
X'
Modeled Ice Surface Speed - Sliding On, k0=10-11 m2
Modeled Ice Surface Speed - Sliding On, k0=10-18 m2
Modeled Icebed Sliding Speed, k0=10-11 m2
Modeled Icebed Sliding Speed, k0=10-18 m2
100% Observed Ice Surface Speed
10% Observed Ice Surface Speed
1% Observed Ice Surface Speed
Modeled Ice Surface Speed - No Slip, k0=10-11 m2
Modeled Ice Surface Speed - No Slip, k0=10-18 m2

Figure 4.4. (a) Modeled basal water sheet thickness and (b) ice surface and bed speeds along the model flowline (see Figures 4.1 and S4.22) for all simulations discussed in this article (i.e. high ($k_0 = 10^{-11}$ m^2) and low ($k_0 = 10^{-18}$ m^2) groundwater scenarios, with and without sliding). Where slip is applied it is calibrated to the high groundwater scenario ($c_f = 5.25\times10^{13}$). The full (100%) and partial (10% and 1%) observed ice surface speeds [*Rignot et al.*, 2011] are included for comparison. The sliding simulations were calibrated by iteratively matching the high groundwater parameterization's results of ice surface speed to the observed values.

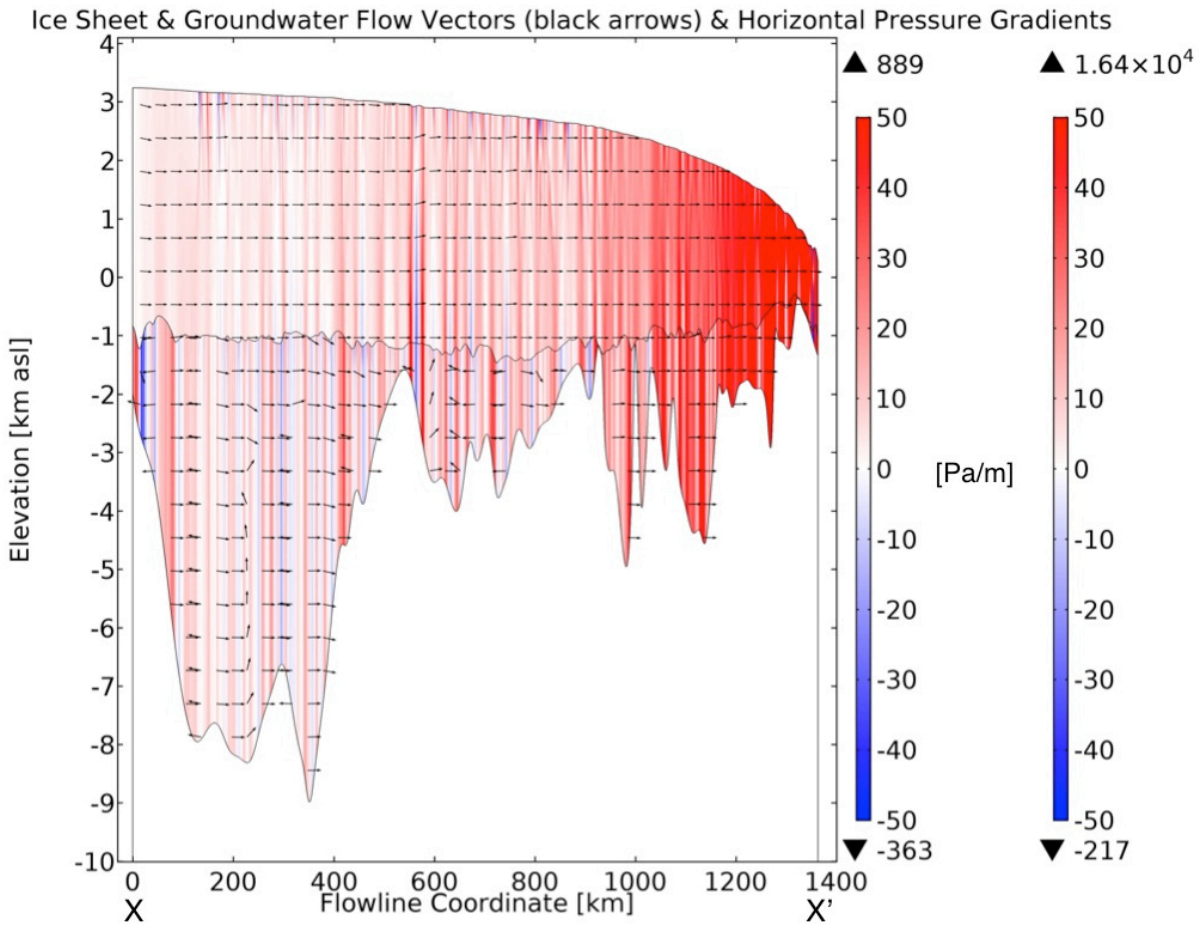
Ice Sheet & Groundwater Flow Vectors (black arrows) & Horizontal Pressure Gradients
Elevation [km asl]
4
3
2
1
0
-1
-2
-3
-4
-5
-6
-7
-8
-9
-10
0
200
400
600
800
1000
1200
1400
Flowline Coordinate [km]
X
X'
▲ 889
50
40
30
20
10
0
-10
-20
-30
-40
-50
▼ -363
[Pa/m]
▲ 1.64×10^4
50
40
30
20
10
0
-10
-20
-30
-40
-50
▼ -217

Figure 4.5. Computed horizontal pressure gradient solutions ($k_0 = 10^{-18}$ m^2) for the permeable sediment and the ice sheet subdomains of the numerical model with sliding. A positive (in red) pressure gradient represents horizontal flow to the right (toward X', the grounding line) whereas a negative (in blue) gradient represents a reversed flow direction upstream (toward X, the ice divide). The arrow vectors show the direction of flow of groundwater and the ice sheet, which are largely horizontal except for some vertical deviations, mostly in the groundwater. Places where groundwater flow is reversed exist due to the topographic component of the pressure potential. The largest magnitudes of the pressure gradient are proximal to the grounding line as the greatest changes in ice surface slope (the dominant component of flow for ice and groundwater) occur there. The maximum and minimum values for the ice sheet and groundwater are posted above and below their respective color bars (groundwater, left; ice sheet, right). The same results for parameterization $k_0 = 10^{-11}$ m^2 are nearly identical to these but are shown in Figure S4.7.

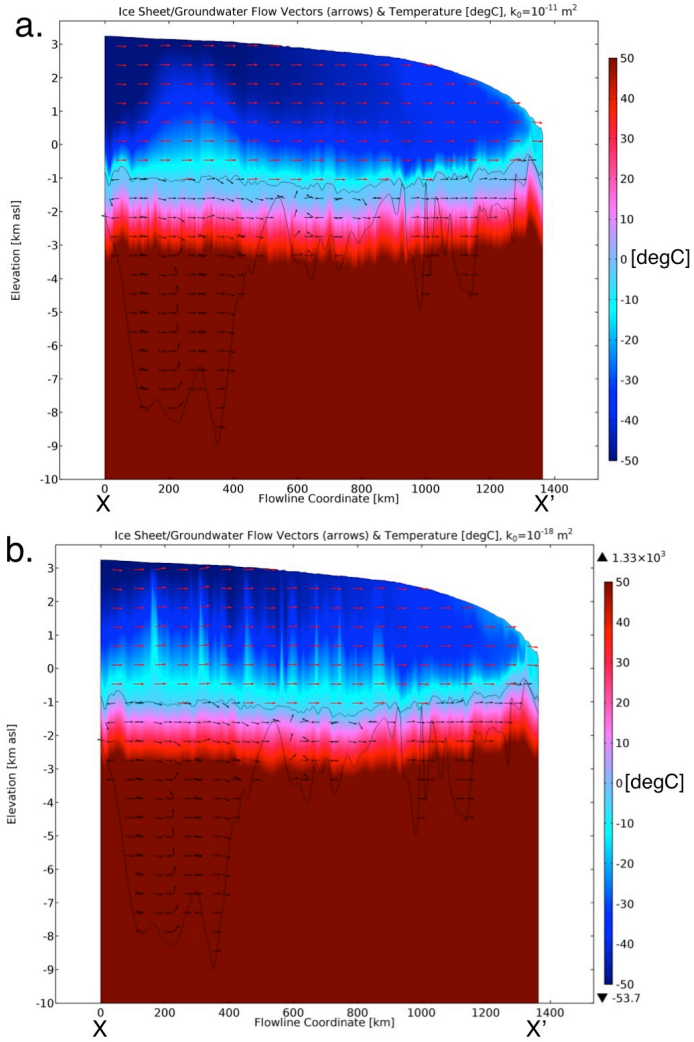
a.
Ice Sheet/Groundwater Flow Vectors (arrows) & Temperature [degC], k0=10-11 m2
Elevation [km asl]
Flowline Coordinate [km]
X
X'
[degC]
b.
Ice Sheet/Groundwater Flow Vectors (arrows) & Temperature [degC], k0=10-18 m2
▲ 1.33×10^3
▼ -53.7
c.
Ice Sheet Lateral Boundary Temperature Profiles
Ice Divide, Sliding On, k0=10-11 m2
Ice Divide, Sliding On, k0=10-18 m2
Ice Stream, Sliding On, k0=10-11 m2
Ice Stream, Sliding On, k0=10-18 m2
Ice Divide, No Slip, k0=10-11 m2
Ice Divide, No Slip, k0=10-18 m2
Ice Stream, No Slip, k0=10-11 m2
Ice Stream, No Slip, k0=10-18 m2
Temperature [degC]

Figure 4.6. Computed temperatures from the numerical model for (a) the high groundwater and (b) low groundwater parameterizations of the sliding model. (c) Represents the lateral boundary temperatures of all simulations (i.e. high/low groundwater and sliding on/off). Note that all but the high groundwater parameterization with slip have roughly the same results (also see Figure S4.8 for all simulations' temperature results compared). Also note that the pressure melting temperature ranges from 0° to about -4° Celsius (see Figure S4.2).

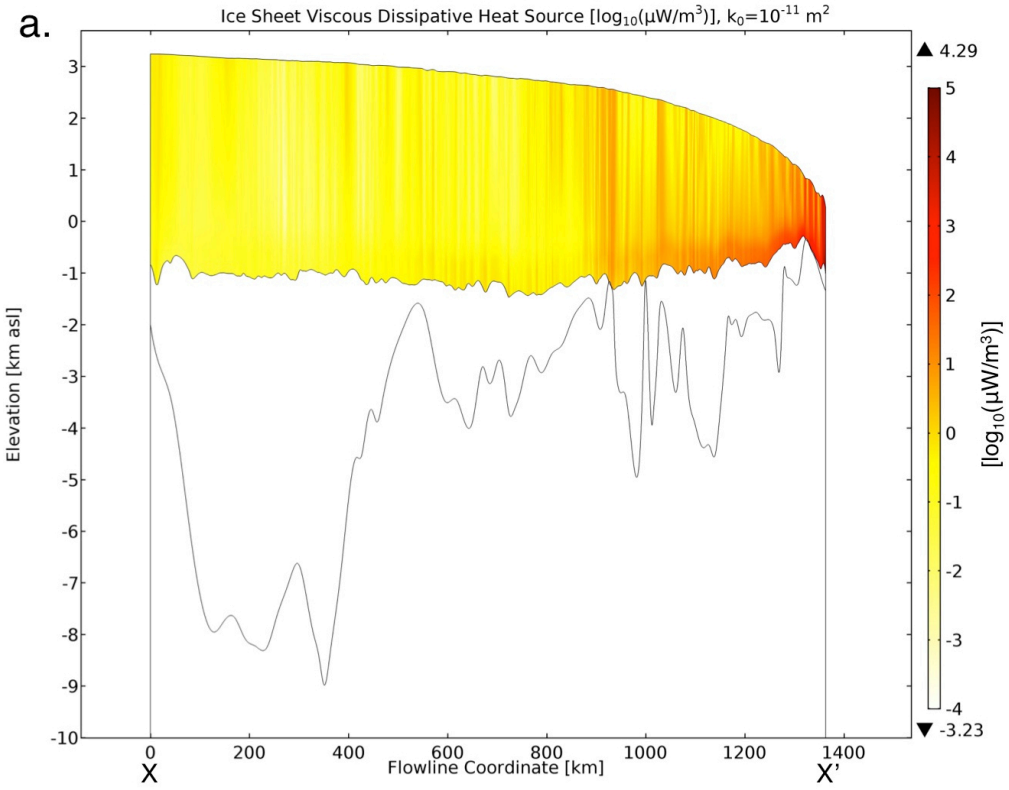
a.
Ice Sheet Viscous Dissipative Heat Source [log10(μW/m3)], k0=10-11 m2
Elevation [km asl]
Flowline Coordinate [km]
X
X'
[log10(μW/m3)]
▲ 4.29
▼ -3.23

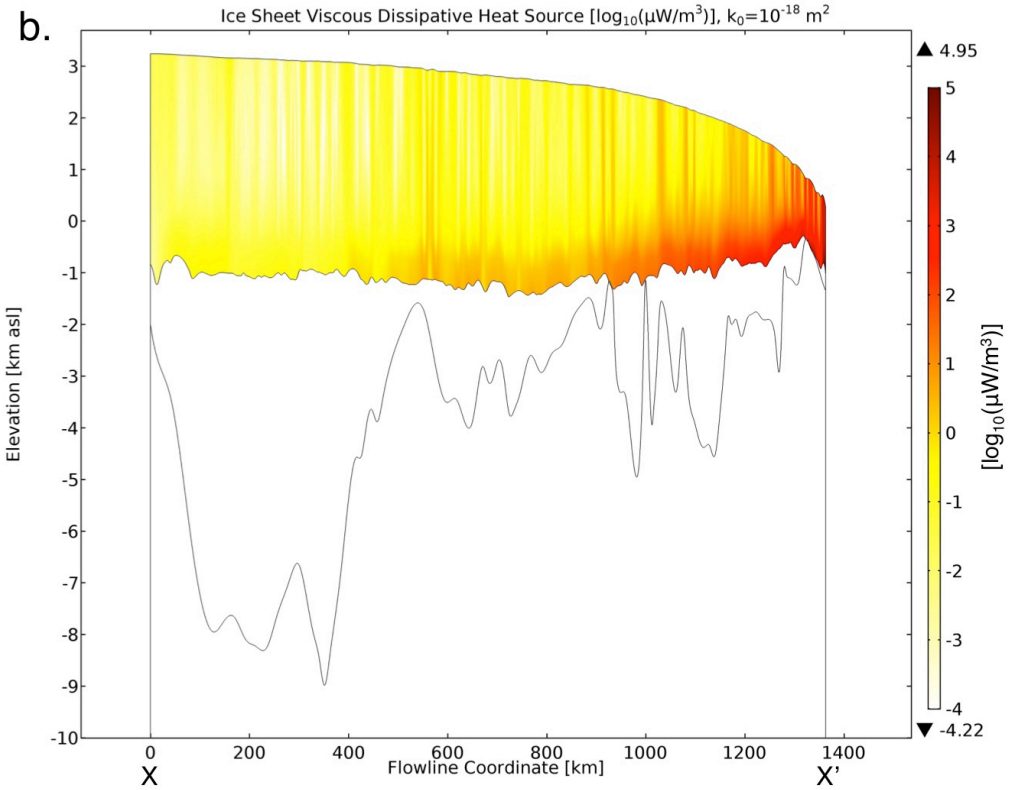
b.
Ice Sheet Viscous Dissipative Heat Source [log10(μW/m3)], k0=10-18 m2
Elevation [km asl]
Flowline Coordinate [km]
X
X'
[log10(μW/m3)]
▲ 4.95
▼ -4.22

Figure 4.7. Computed viscous dissipative heat from the internal deformation of ice from the numerical model for (a) the high groundwater and (b) low groundwater parameterizations of the sliding model. Note that the scale is in powers of ten (of $\mu W/m^3$); also that the maximum and minimum values are listed above and below (respectively) each color bar.

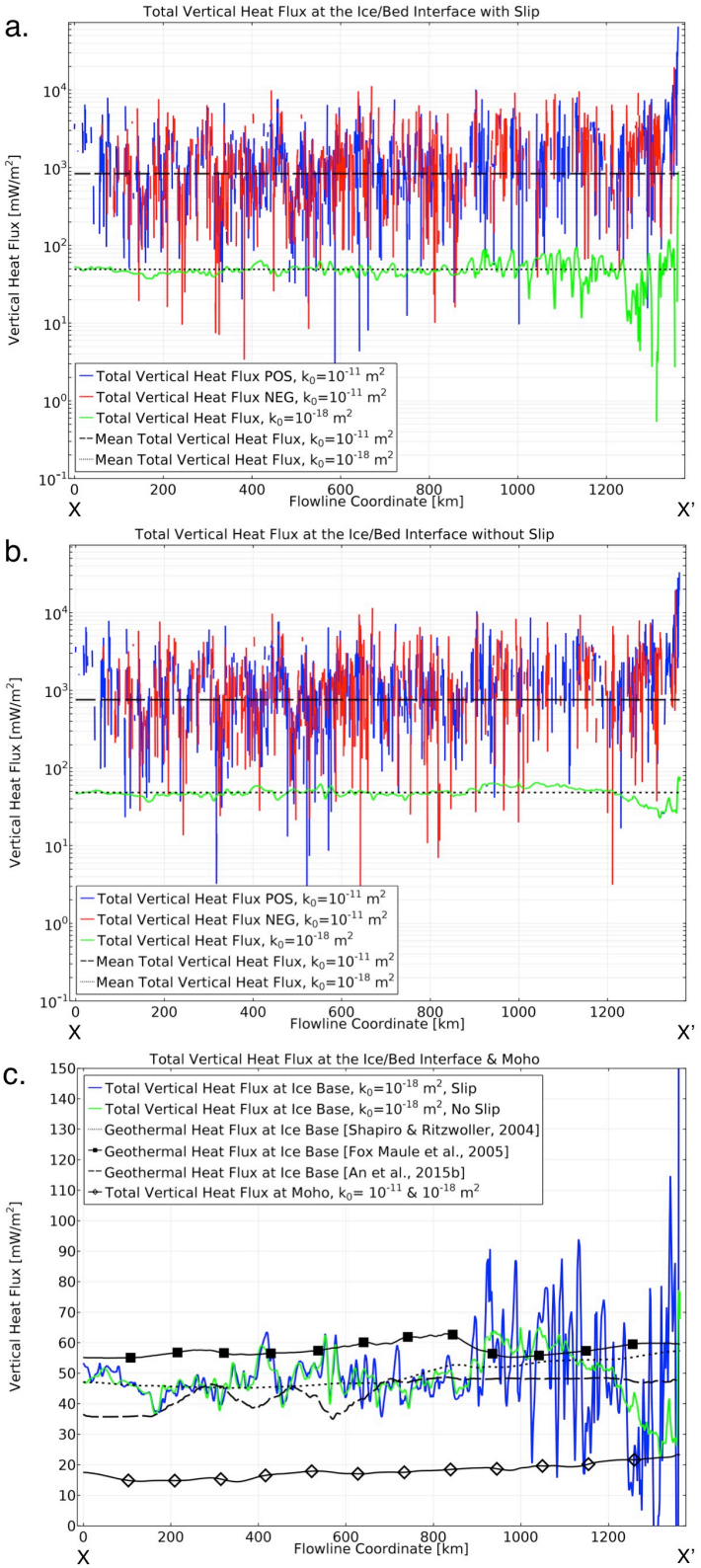
a.
Total Vertical Heat Flux at the Ice/Bed Interface with Slip
Vertical Heat Flux [mW/m^2]
Flowline Coordinate [km]
X
X'
Total Vertical Heat Flux POS, k_0=10^{-11} m^2
Total Vertical Heat Flux NEG, k_0=10^{-11} m^2
Total Vertical Heat Flux, k_0=10^{-18} m^2
Mean Total Vertical Heat Flux, k_0=10^{-11} m^2
Mean Total Vertical Heat Flux, k_0=10^{-18} m^2
b.
Total Vertical Heat Flux at the Ice/Bed Interface without Slip
Vertical Heat Flux [mW/m^2]
Flowline Coordinate [km]
X
X'
Total Vertical Heat Flux POS, k_0=10^{-11} m^2
Total Vertical Heat Flux NEG, k_0=10^{-11} m^2
Total Vertical Heat Flux, k_0=10^{-18} m^2
Mean Total Vertical Heat Flux, k_0=10^{-11} m^2
Mean Total Vertical Heat Flux, k_0=10^{-18} m^2
c.
Total Vertical Heat Flux at the Ice/Bed Interface & Moho
Vertical Heat Flux [mW/m^2]
Flowline Coordinate [km]
X
X'
Total Vertical Heat Flux at Ice Base, k_0=10^{-18} m^2, Slip
Total Vertical Heat Flux at Ice Base, k_0=10^{-18} m^2, No Slip
Geothermal Heat Flux at Ice Base [Shapiro & Ritzwoller, 2004]
Geothermal Heat Flux at Ice Base [Fox Maule et al., 2005]
Geothermal Heat Flux at Ice Base [An et al., 2015b]
Total Vertical Heat Flux at Moho, k_0= 10^{-11} & 10^{-18} m^2

Figure 4.8. Total vertical heat flux (in mW/m^2) at the ice/bed interface comparisons of the different parameterizations for the models with (a) sliding enabled and (b) no slip at the ice/bed interface along the model flowline shown in Figure 4.1. Note that the values for the high groundwater parameterization ($k_0 = 10^{-11}$ m^2; with and without slip) yields values spanning many orders of magnitude above and below zero so it has to be split into positive (POS) and negative (NEG) components for proper comparison. A mean of all heat flux results for each of the parameterizations of groundwater is shown as a solid horizontal bar. The means for the high and low groundwater parameterizations with slip are 840.16 and 49.28 mW/m^2, respectively. The means for the high and low groundwater parameterizations without slip are 758.17 and 48.49 mW/m^2, respectively. (c) Recently published vertical geothermal heat flux datasets at the ice/bed interface for East Antarctica [*Shapiro and Ritzroller*, 2004; *Fox Maule et al*., 2005; and *An et al*., 2015b], sampled along the model flowline, have been plotted for comparison with the low groundwater parameterization ($k_0 = 10^{-18}$ m^2) heat flux results with and without slip. All simulations essentially produced the same heat flux at the Moho (plotted for comparison).

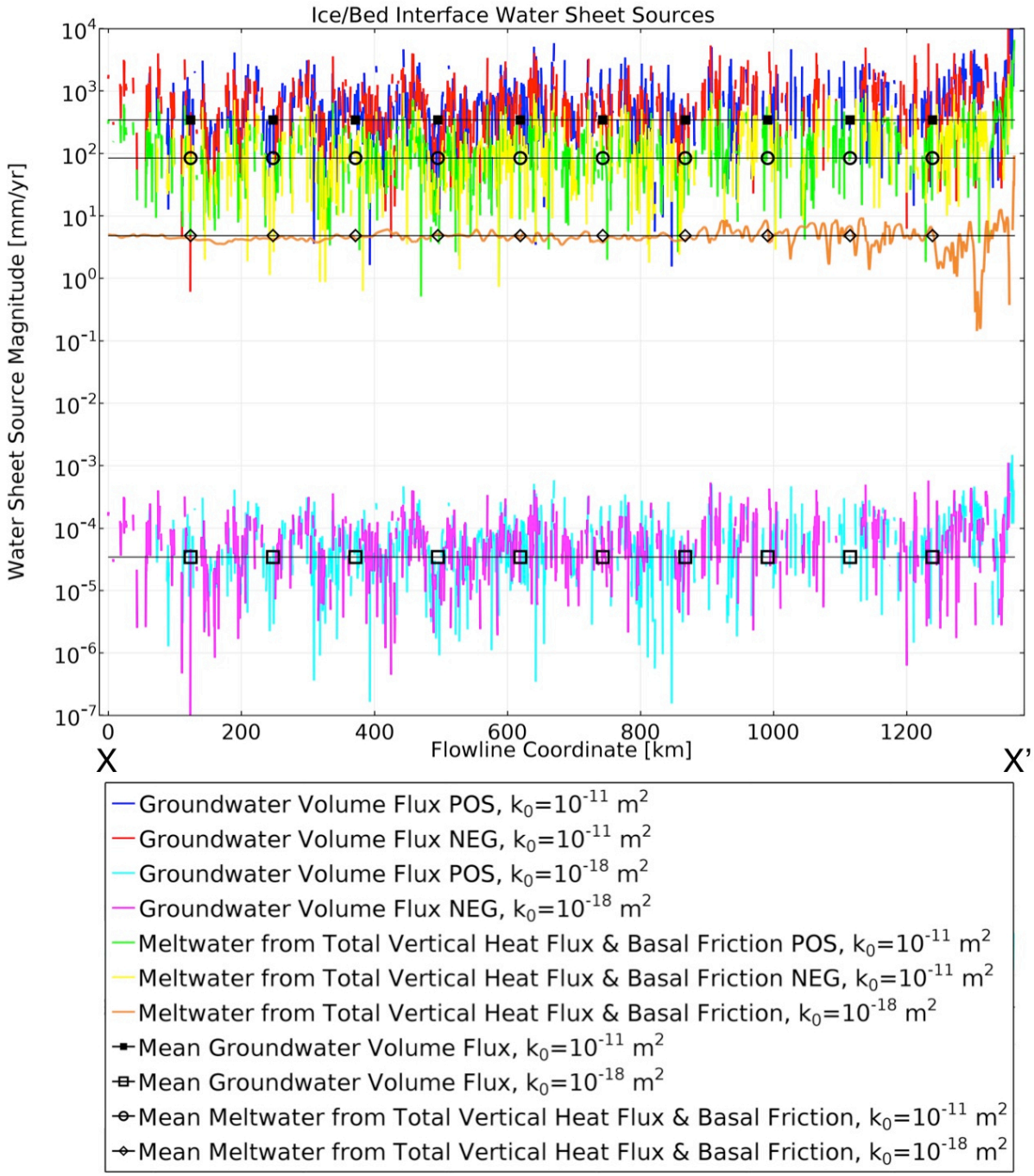
Ice/Bed Interface Water Sheet Sources
Water Sheet Source Magnitude [mm/yr]
10^{4}
10^{3}
10^{2}
10^{1}
10^{0}
10^{-1}
10^{-2}
10^{-3}
10^{-4}
10^{-5}
10^{-6}
10^{-7}
0
200
400
600
800
1000
1200
Flowline Coordinate [km]
X
X'
Groundwater Volume Flux POS, $k_0=10^{-11}$ m^2
Groundwater Volume Flux NEG, $k_0=10^{-11}$ m^2
Groundwater Volume Flux POS, $k_0=10^{-18}$ m^2
Groundwater Volume Flux NEG, $k_0=10^{-18}$ m^2
Meltwater from Total Vertical Heat Flux & Basal Friction POS, $k_0=10^{-11}$ m^2
Meltwater from Total Vertical Heat Flux & Basal Friction NEG, $k_0=10^{-11}$ m^2
Meltwater from Total Vertical Heat Flux & Basal Friction, $k_0=10^{-18}$ m^2
Mean Groundwater Volume Flux, $k_0=10^{-11}$ m^2
Mean Groundwater Volume Flux, $k_0=10^{-18}$ m^2
Mean Meltwater from Total Vertical Heat Flux & Basal Friction, $k_0=10^{-11}$ m^2
Mean Meltwater from Total Vertical Heat Flux & Basal Friction, $k_0=10^{-18}$ m^2

Figure 4.9. Basal water sheet sources (and sinks, if negative) along the ice sheet base of the model flowline shown in Figure 4.1 for the simulation including sliding. For fluxes ranging many orders of magnitude above and below zero, the positive (POS) and negative (NEG) components are shown separately. Also, where the values are split into the two components, an average is displayed for all values in order to define the overall sign and magnitude of the flux. The means for the high groundwater ($k_0 = 10^{-11}$ m^2), low groundwater ($k_0 = 10^{-18}$ m^2), combined high (groundwater) total vertical heat flux and basal friction melt, and combined low (groundwater) total vertical heat and basal friction flux melt are 346.83, 3.46×10^{-5}, 85.02, and 4.88 mm/yr, respectively. As the groundwater properties are the same in the simulation without sliding (not shown), their mean values are the same. The mean for the high total vertical heat flux melt plus basal friction melt from the simulation without sliding (not shown) is 72.5 mm/yr; and for the low total value, 4.64 mm/year. The average net input to the water sheet (not shown) for model with sliding is 429.11 mm/yr for the high groundwater value and 4.88 mm/yr for the low groundwater value. The average net input to the water sheet for model without sliding is 416.59 mm/yr for the high groundwater value and 4.64 mm/yr for the low groundwater value. Figure S4.18 has the separated components of the combined melt rates shown separately.

4.8 REFERENCES

Aitken, A. R. A., D. A. Young, F. Ferraccioli, P. G. Betts, J. S. Greenbaum, T. G. Richter, J. L. Roberts, D. D. B., and M. J. Siegert (2014), The subglacial geology of Wilkes Land, East Antarctica, Geophys. Res. Lett., 41, 2390–2400.

Aitken, A. R. A., et al. (in rev.) East Antarctic Ice Sheet bed erosion indicates repeated large-scale retreat and advance events, Nature.

Alley, R. B. (1996), Toward a hydrologic model for computerized ice-sheet simulations, Hydrol. Proc., 10, 649–660.

An, M., D. A. Wiens, Y. Zhao, M. Feng, A. A. Nyblade, M. Kanao, Y. Li, A. Maggi, and J. Lévêque (2015a), S-velocity model and inferred Moho topography beneath the Antarctic Plate from Rayleigh waves, J. Geophys. Res. Solid Earth, 120, 359–383, doi:10.1002/2014JB011332.

An, M., D. A. Wiens, Y. Zhao, M. Feng, A. Nyblade, M. Kanao, Y. Li, A. Maggi, and J.-J. Lévêque (2015b), Temperature, lithosphere-asthenosphere boundary, and heat flux beneath the Antarctic Plate inferred from seismic velocities, J. Geophys. Res. Solid Earth, 120, 8720–8742, doi:10.1002/2015JB011917.

Athy, L. F. (1930), Density, porosity, and compaction of sedimentary rocks, AAPG Bulletin, 14(1), 1-24.

Bamber, J. L., F. Ferraccioli, I. Joughin, T. Shepherd, D. M. Rippin, M. J. Siegert, and D. G. Vaughan (2006), East Antarctic ice stream tributary underlain by major sedimentary basin, Geology, 34, 33–36.

Beardsmore, G. R., and J. P. Cull (2001), Crustal heat flow: a guide to measurement and modelling. Cambridge University Press.

Bense, V. F., and M. A. Person (2008), Transient hydrodynamics within intercratonic sedimentary basins during glacial cycles, J. Geophys. Res., 113, F04005, doi:10.1029/2007JF000969.

Bindschadler, R., H. Choi, and ASAID Collaborators (2011), High-resolution Image-derived Grounding and Hydrostatic Lines for the Antarctic Ice Sheet, National Snow and Ice Data Center, Boulder, Colo., doi:10.7265/N56T0JK2.

Blankenship, D.D., S. P. Carter, J. W. Holt, D. L. Morse, M. E. Peters, and D. A. Young (2009), Antarctic Subglacial Lake Classification Inventory, Boulder, Colorado USA, National Snow and Ice Data Center, http://dx.doi.org/10.7265/N5CN71VX.

Boulton, G., & J. Hartikainen (2004), Thermo-hydro-mechanical impacts of coupling between glaciers and permafrost, Elsevier Geo-Engineering Book Series, 2, 293-298.

Boulton, G.S., R. Lunn, P. Vidstrand, and S. Zatsepin (2007), Subglacial drainage by groundwater–channel coupling, and the origin of esker systems: Part 2 – theory and simulation of a modern system, Quat. Sci. Rev., 26, 1091–1105.

Budd, W. F., and D. Jenssen (1987), Numerical modelling of the large-scale basal water flux under the West Antarctic Ice Sheet, in Dynamics of the West Antarctic Ice Sheet, edited by C. J. van der Veen, and J. Oerlemans, pp. 293–320, D. Reidel, Norwell, Mass.

Carson, C. J., S. McLaren, J. L. Roberts, S. D. Boger, and D. D. Blankenship (2013), Hot rocks in a cold place: high sub-glacial heat flow in East Antarctica, J. Geol. Soc. London., 171(1), 9–12.

Chen, J. L., C. R. Wilson, D. D. Blankenship, and B. D. Tapley (2009), Accelerated Antarctic ice loss from satellite gravity measurements, Nat. Geosci., 2(12), 859–862.

Clarke, G. K. C., S. G. Collins, and D. E. Thompson (1984), Flow, thermal structure, and subglacial conditions of a surge-type glacier, Can. J. Earth Sci., 21, 232–240.

Comiso, J. C. (2000), Variability and trends in Antarctic surface temperatures from in situ and satellite infrared measurements. Journal of Climate, 13(10), 1674-1696.

Cuffey, K., and W. S. B. Paterson (2010), The Physics of Glaciers, 4th ed., Elsevier, Burlington, Mass.

Cutler, P. M., D. R. MacAyeal, D. M. Mickelson, B. R. Parizek, and P. M. Colgan (2000), A numerical investigation of ice-lobe-permafrost interaction around the southern Laurentide ice sheet, J. Glaciol., 46(153), 311–325.

Drewry, D. (1976), Sedimentary basins of the East Antarctic craton from geophysical evidence. Tectonophysics, 36(1), 301-314.

Echelmeyer, K. (1987), Anomalous heat flow and temperatures associated with subglacial water flow, The Physical Basis of Ice Sheet Modelling (Proceedings of the Vancouver Symposium, August 1987). IAHS Publ. no. 170.

Flowers, G. E., S. J. Marshall, H. Björnsson, and G. K. C. Clarke (2005), Sensitivity of Vatnajökull ice cap hydrology and dynamics to climate warming over the next 2 centuries, J. Geophys. Res. Earth Surf., 110(F2), F02011.

Flowers, G. E. (2008), Subglacial modulation of the hydrograph from glacierized basins, Hydrol. Processes, 22, 3903–3918, doi:10.1002/hyp.7095.

Flowers, G. E. (2015), Modelling water flow under glaciers and ice sheets, Proc. A, (471).

Fox Maule, C., M. E. Purucker, N. Olsen, and K. Mosegaard (2005), Heat flux anomalies in Antarctica revealed by satellite magnetic data., Science, 309(5733), 464–467.

Frederick, B. C., (2015), Submarine Sedimentary Basin Analyses for the Aurora and Wilkes Subglacial Basins and the Sabrina Coast Continental Shelf, East Antarctica, Ph.D. dissertation, Univ. of Texas, Austin, Texas, USA.

Fretwell, P., et al. (2013), Bedmap2: Improved ice bed, surface and thickness datasets for Antarctica, Cryosphere, 7(1), 375–393.

Furlong, K.P., and D. S. Chapman (2013) Heat Flow, Heat Generation, and the Thermal State of the Lithoshpere. Annu. Rev. Earth Planet. Sci., 05/2012. 41, 345–410.

Gleeson, T., L. Smith, N. Moosdorf, J. Hartmann, H. H. Dürr, A. H. Manning, L. P. H. van Beek, and A. M. Jellinek (2011), Mapping permeability over the surface of the Earth, Geophys. Res. Lett., 38, L02401.

Gleeson, T., N. Moosdorf, J. Hartmann, and L. P. H. van Beek (2014), A glimpse beneath earth's surface: GLobal HYdrogeology MaPS (GLHYMPS) of permeability and porosity, Geophys. Res. Lett., 41, 3891–3898.

Glen, J. W. (1955), The creep of polycrystalline ice, Proc. Roy. Soc., Ser. A, 228, 519–538.

Gooch, B. T., D. A. Young, and D. D. Blankenship (2016), Potential groundwater and heterogeneous heat source contributions to ice sheet dynamics in critical submarine basins of East Antarctica, Geochem. Geophys. Geosyst., 17, doi:10.1002/2015GC006117.

Gooch, B. T., S. P. Carter, O. Ghattas, D. A. Young, and D. D. Blankenship (in review), Groundwater dominance in the subglacial hydrology of ice sheet interiors: example at Dome C, East Antarctica, The Cryosphere Discuss.

Greenbaum, J. S., et al. (2015), Ocean access to a cavity beneath Totten Glacier in East Antarctica, Nat. Geosci., 8, 294–298.

Greve, R., and H. Blatter (2009), Dynamics of Ice Sheets and Glaciers, Springer, Dordrecht, Netherlands.

Hooke, R. L. (2005), Principles of Glacier Mechanics, 2nd ed., Cambridge Univ. Press, New York.

Huybrechts, P. (1993), Glaciological modelling of the late cenozoic East Antarctic Ice Sheet: Stability or dynamism?, Geogr. Ann., 75A(4), 221–238.

Jaupart, C. (1986), On the average amount and vertical distribution of radioactivity in the continental crust, in Burrus, J., ed., Thermal Modeling in Sedimentary Basins: ´Editions Technip, Paris, 33–47.

Jiang, X. W., L. Wan, X. S. Wang, S. Ge, and J. Liu (2009), Effect of exponential decay in hydraulic conductivity with depth on regional groundwater flow, Geophys. Res. Lett., 36, L24402.

Kyrke-Smith, T. M., and A. C. Fowler (2014), Subglacial swamps, Proc. R. Soc. A, 470, 20140340, doi:10.1098/rspa.2014.0340.

Lachenbruch, A. H. (1970), Crustal temperature and heat production: Implications of the linear heat-flow relation, J. Geophys. Res., 75(17), 3291-3300.

Le Brocq, A., A. Payne, M. Siegert, and R. Alley (2009), A subglacial water-flow model for West Antarctica, J. Glaciol., 55(193), 879–888.

Lemieux, J.-M., E. Sudicky, W. Peltier, and L. Tarasov (2008), Dynamics of groundwater recharge and seepage over the Canadian landscape during the Wisconsinian glaciation, J. Geophys. Res., 113, F01011, doi:10.1029/2007JF000838.

Li, X., E. Rignot, M. Morlighem, J. Mouginot, and B. Scheuchl (2015), Grounding line retreat of Totten Glacier, East Antarctica, 1996 to 2013, Geophys. Res. Lett., 42, 8049–8056, doi:10.1002/2015GL065701.

McKenna, T. E., and J. M. Sharp Jr. (1998), Radiogenic heat production in sedimentary rocks of the gulf of Mexico basin, south Texas, AAPG Bull., 82, 484–496.

McLaren, S., M. Sandiford, M. Hand, N. Neumann, L. Wyborn, and I. Bastrakova (2003), The hot southern continent; heat flow and heat production in Australian Proterozoic terranes, Spec. Pap. - Geol. Soc. Am., 372, 157–167.

Mellor, G. L., and L. Kantha (1989), An ice-ocean coupled model, J. Geophys. Res., 94(89), 10937–10954.

Nye, J. F. (1957), The distribution of stress and velocity in glaciers and ice sheets, Proc. R. Soc. London, Ser. A, 239, 113–133.

Pattyn, F. (2002), Transient glacier response with a higher-order numerical ice-flow model, J. Glaciol., 48, 467–477.

Pattyn, F. (2010), Antarctic subglacial conditions inferred from a hybrid ice sheet/ice stream model, Earth Planet. Sci. Lett., 295(3-4), 451–461.

Pattyn, F., et al. (2012), Results of the Marine Ice Sheet Model Intercomparison Project, MISMIP, Cryosphere Discuss., 6, 267–308, doi:10.5194/tcd-6-267-2012.

Petrunin, A. G., I. Rogozhina, A. P. M. Vaughan, I. T. Kukkonen, M. K. Kaban, I. Koulakov, and M. Thomas (2013), Heat flux variations beneath central Greenland's ice due to anomalously thin lithosphere, Nat. Geosci., 6, 746–750, doi:10.1038/ngeo1898.

Pollard, D., R. M. DeConto, and A. A. Nyblade (2005), Sensitivity of Cenozoic Antarctic ice sheet variations to geothermal heat flux, Glob. Planet. Change, 49(1-2), 63–74.

Pollard, D., R. M. Deconto, and R. B. Alley (2015), Potential Antarctic Ice Sheet retreat driven by hydrofracturing and ice cliff failure, Earth Planet. Sci. Lett., 412, 112–121.

Pritchard, H. D., S. R. M. Ligtenberg, H. A. Fricker, D. G. Vaughan, M. R. van den Broeke, and L. Padman (2012), Antarctic ice-sheet loss driven by basal melting of ice shelves, Nature, 484(7395), 502–505.

Rignot, E., J. Mouginot, and B. Scheuchl (2011), Ice flow of the Antarctic Ice Sheet, Science, 333, 1427–1430.

Sandiford, M., and S. McLaren (2002), Tectonic feedback and the ordering of heat producing elements within the continental lithosphere, Earth Planet. Sci. Lett., 204, 133–150.

Sclater, J. G., and P. Christie (1980), Continental stretching: An explanation of the post-mid-cretaceous subsidence of the central North Sea basin, J. Geophys. Res. Solid Earth, 85(B7), 3711-3739.

Shapiro, N. M., and M. H. Ritzwoller (2004), Inferring surface heat flux distributions guided by a global seismic model: Particular application to Antarctica, Earth Planet. Sci. Lett., 223(1-2), 213–224.

Shreve, R. L. (1972), Movement of water in glaciers, J. Glaciol., 11(62), 205–214.

Siegert, M. J., J. P. Taylor, and J. Antony (2005), Spectral roughness of subglacial topography and implications for former ice-sheet dynamics in East Antarctica, Global Planet. Change, 45, 249–263.

Siegert, M. J., A. Le Brocq, and A. J. Payne (2007), Hydrological connections between Antarctic subglacial lakes and the flow of water beneath the East Antarctic Ice Sheet, in Glacial Sedimentary Processes and Products, Spec. Publ., vol 39, edited by M. J. Hambrey et al., pp. 3–10, Int. Assoc. of Sedimentol., Malden, Mass.

Singhal, B. B. S., and R. P. Gupta (2010), Applied hydrogeology of fractured rocks (Vol. 430). New York: Springer.

Smith, B. E., H. A. Fricker, I. R. Joughin, and S. Tulaczyk (2009), An inventory of active subglacial lakes in Antarctica detected by ICESat (2003–2008), J. Glaciol., 55, 573–595, doi:10.3189/002214309789470879.

Stauffer, P. H. (2006), Flux flummoxed: A proposal for consistent usage, Ground Water, 44(2), 125–128.

Taylor, J., M. J. Siegert, A. J. Payne, M. J. Hambrey, P. E. O'Brien, A. K. Cooper, and G. Leitchenkov (2004), Topographic controls on post-Oligocene changes in ice-sheet dynamics, Prydz Bay region, East Antarctica, Geology, 32, 197–200, doi:10.1130/G20275.1.

Waples, D. W. (2001), A New Model for Heat Flow in Extensional Basins: Radiogenic Heat, Asthenospheric Heat, and the McKenzie Model, Nat. Resour. Res., 10(2), 227–238.

Weertman, J. (1966), Effect of a basal water layer on the dimensions of ice sheets, J. Glaciol., 6(44), 191–207.

White, D. A. (2013), Cenozoic landscape and ice drainage evolution in the Lambert Glacier–Amery Ice Shelf system, Geological Society, London, Special Publications, 381(1), 151-165.

Wilkens, N. (2014), Pine Island Glacier-a 3D full-Stokes model study, Ph.D. dissertation, University of Hamburg, Hamburg, Germany.

Wilkens, N., J. Behrens,T. Kleiner, D. Rippin, M. Rückamp, and A. Humbert (2015), Thermal structure and basal sliding parametrisation at Pine Island Glacier–a 3-D full-Stokes model study, The Cryosphere, 9(2), 675-690.

Wright, A. P., M. J. Siegert, A. M. Le Brocq, and D. B. Gore (2008), High sensitivity of subglacial hydrological pathways in Antarctica to small ice sheet changes, Geophys. Res. Lett., 35, L17504, doi:10.1029/2008GL034937.

Wright, A., and M. Siegert (2012), A fourth inventory of Antarctic subglacial lakes, Antarct. Sci., 24(6), 659-664.

Wright, A. P., et al. (2012), Evidence of a hydrological connection between the ice divide and ice sheet margin in the Aurora Subglacial Basin, East Antarctica, J. Geophys. Res., 117, F01033, doi:10.1029/2011JF002066.

Young, D. A., et al. (2011), A dynamic early East Antarctic Ice Sheet suggested by ice-covered fjord landscapes, Nature, 474(7349), 72–75.

Zwally, H. J., M. B. Giovinetto, M. A. Beckley, and J. L. Saba (2012), Antarctic and Greenland drainage systems, GSFC Cryospheric Sciences Laboratory.

4.9 SUPPLEMENTARY FIGURES

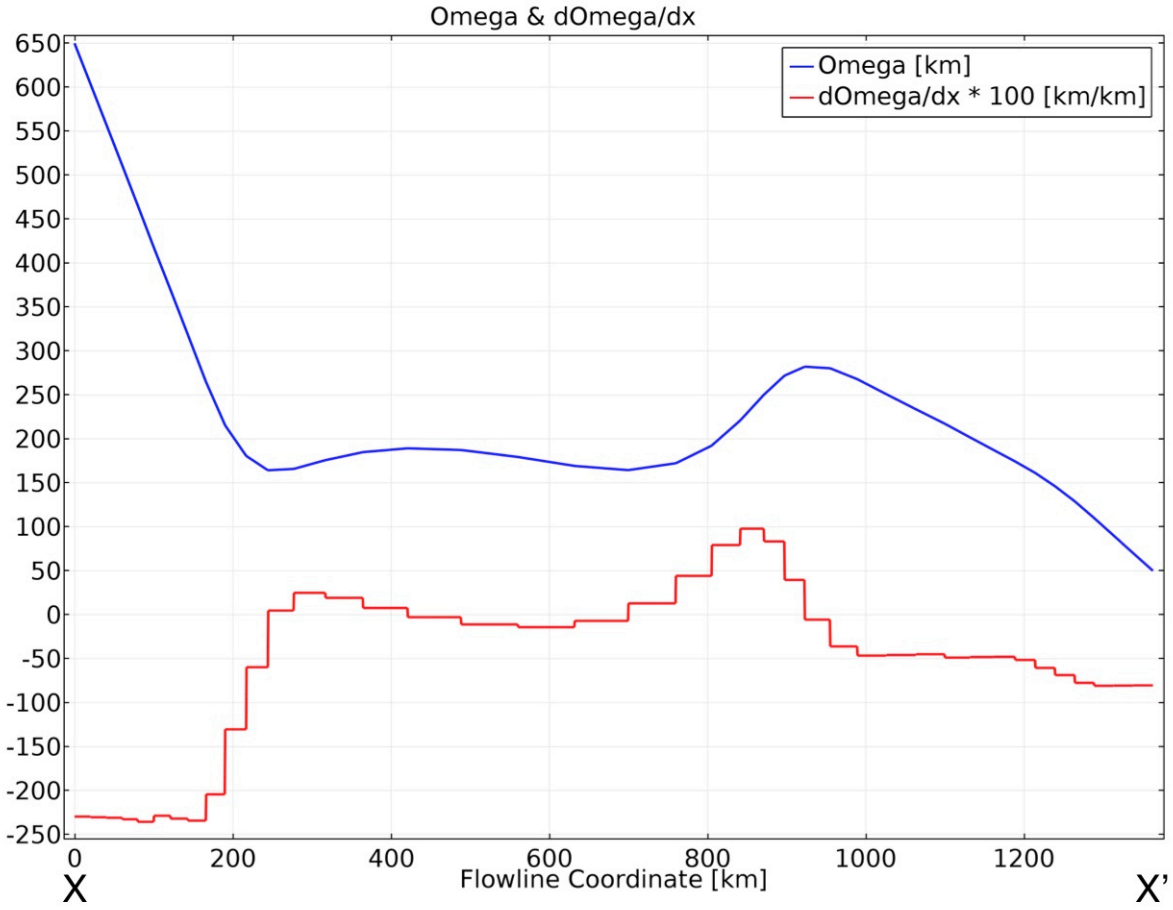

Figure S4.1. The value of ice catchment width, ω, along with its first derivative with respect to the flowline coordinate, x (see Figure 4.1).

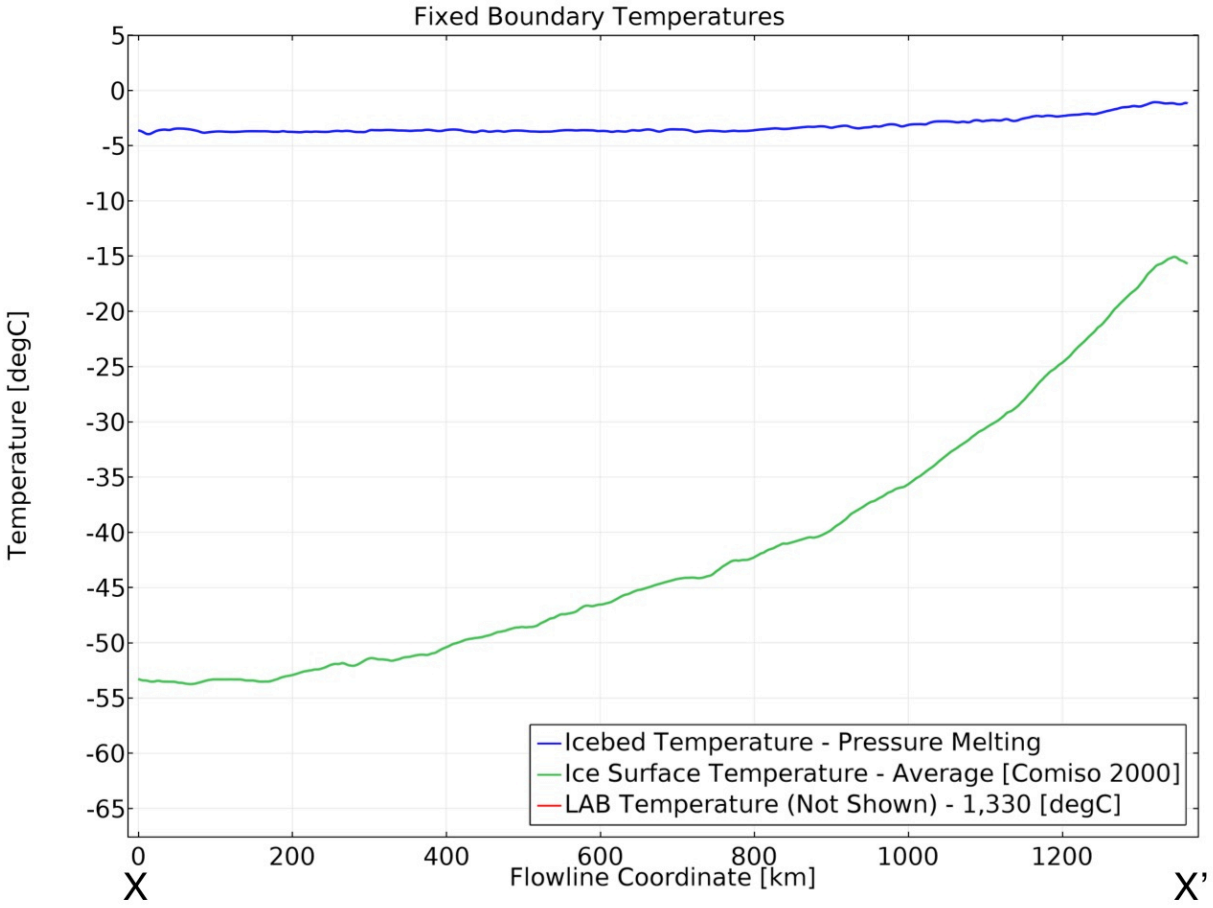

Figure S4.2. Temperature boundary conditions as a function of flowline coordinate applied to all simulations (see Figure 4.1 for model geometry). The pressure melting temperature of ice at the base of the ice sheet is a function described in the main text of the article. The average annual surface temperature is from *Comiso* [2000]. The temperature at the bottom of the model domain, the LAB (Lithosphere-Asthenosphere Boundary), is not shown here but mentioned.

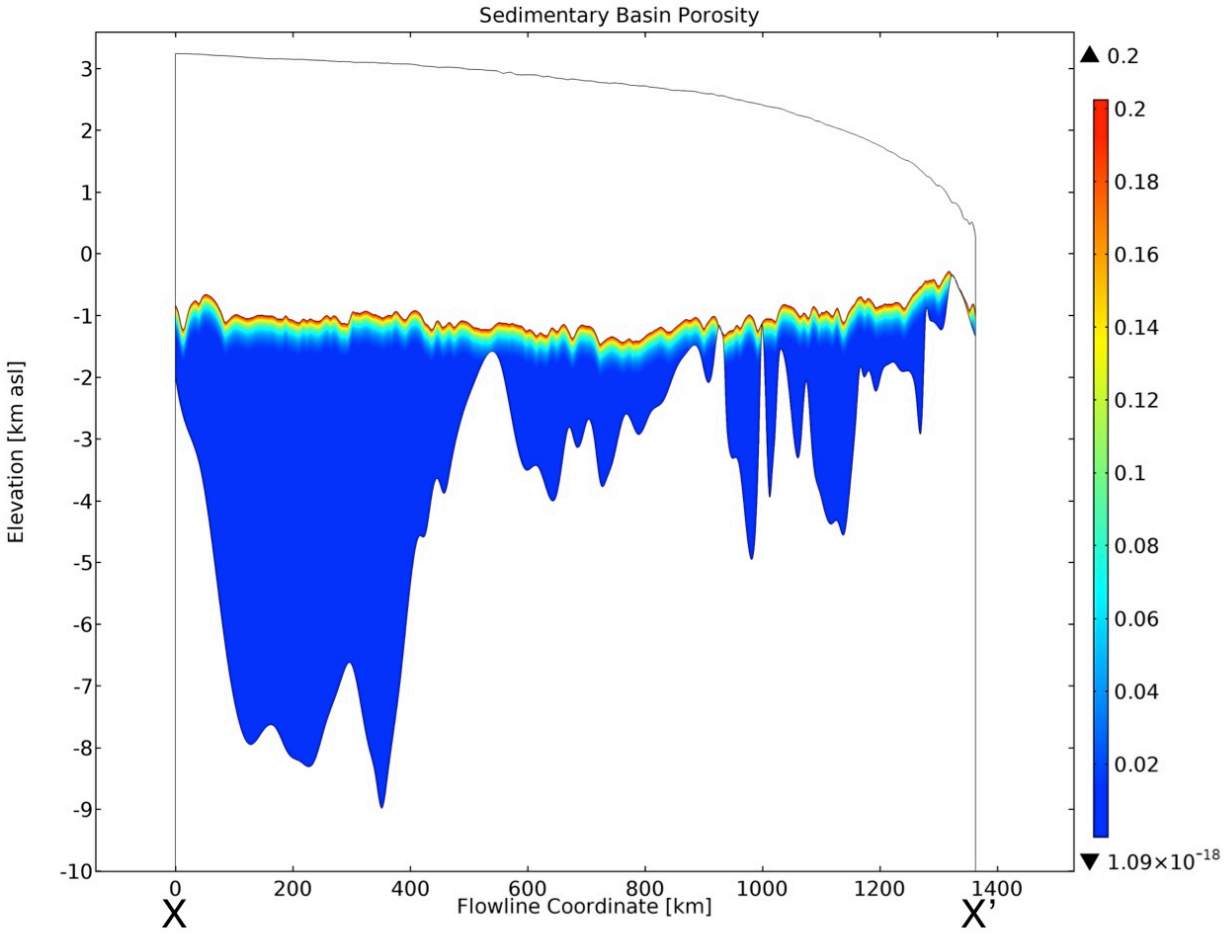

Figure S4.3. Sedimentary basin porosity decay model used in all simulations; the specifics of the model are described in the main text of the article. The maximum and minimum values of the model are shown above and below the color bar, respectively. The average porosity value of the model is about 0.01.

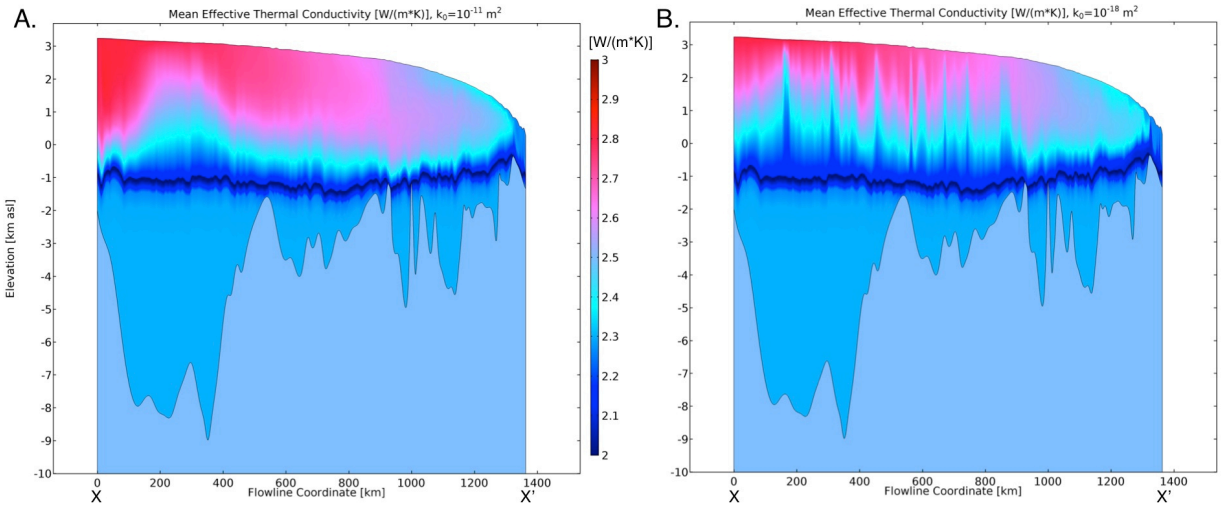

Figure S4.4. Effective thermal conductivity of the (a) high and (b) low groundwater parameterizations for the simulation including sliding. Both of the parameterizations' results for the simulation without sliding look the same as Figure S4.4b. Effective thermal conductivity in the ice sheet is a result of the simulation while the values in the sedimentary basin (accounting for the water-saturated porosity decay model) and crystalline basement rock, as well as, the lithospheric mantle (not shown) are assigned *a priori*.

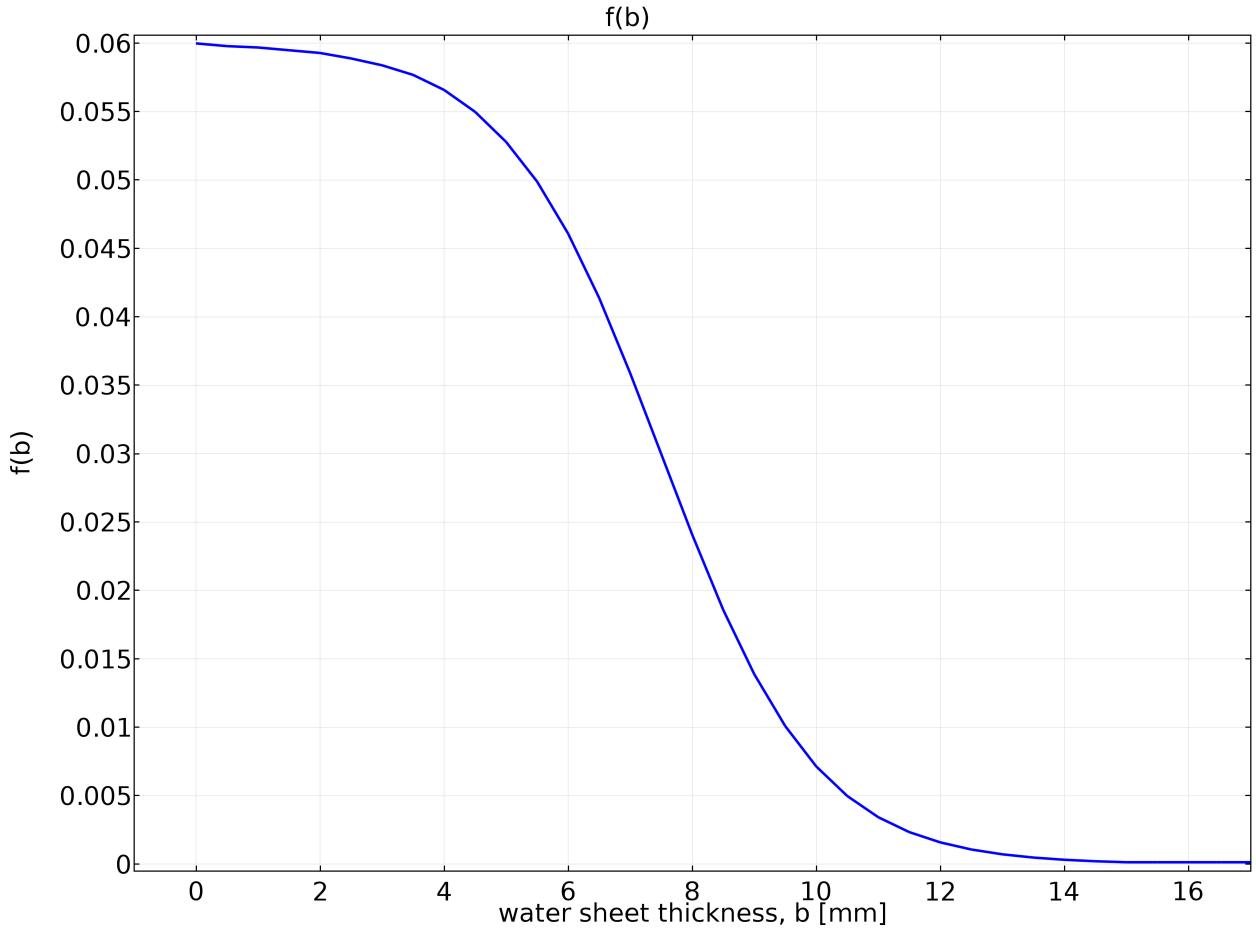

Figure S4.5. Inverse function used to relate the basal water sheet thickness to a sliding relation. It is based on the inverse published in *Le Brocq et al*. [2009] where thicker sheets produce larger values, capped at 15 millimeters. Its usage appears in the main text of this article.

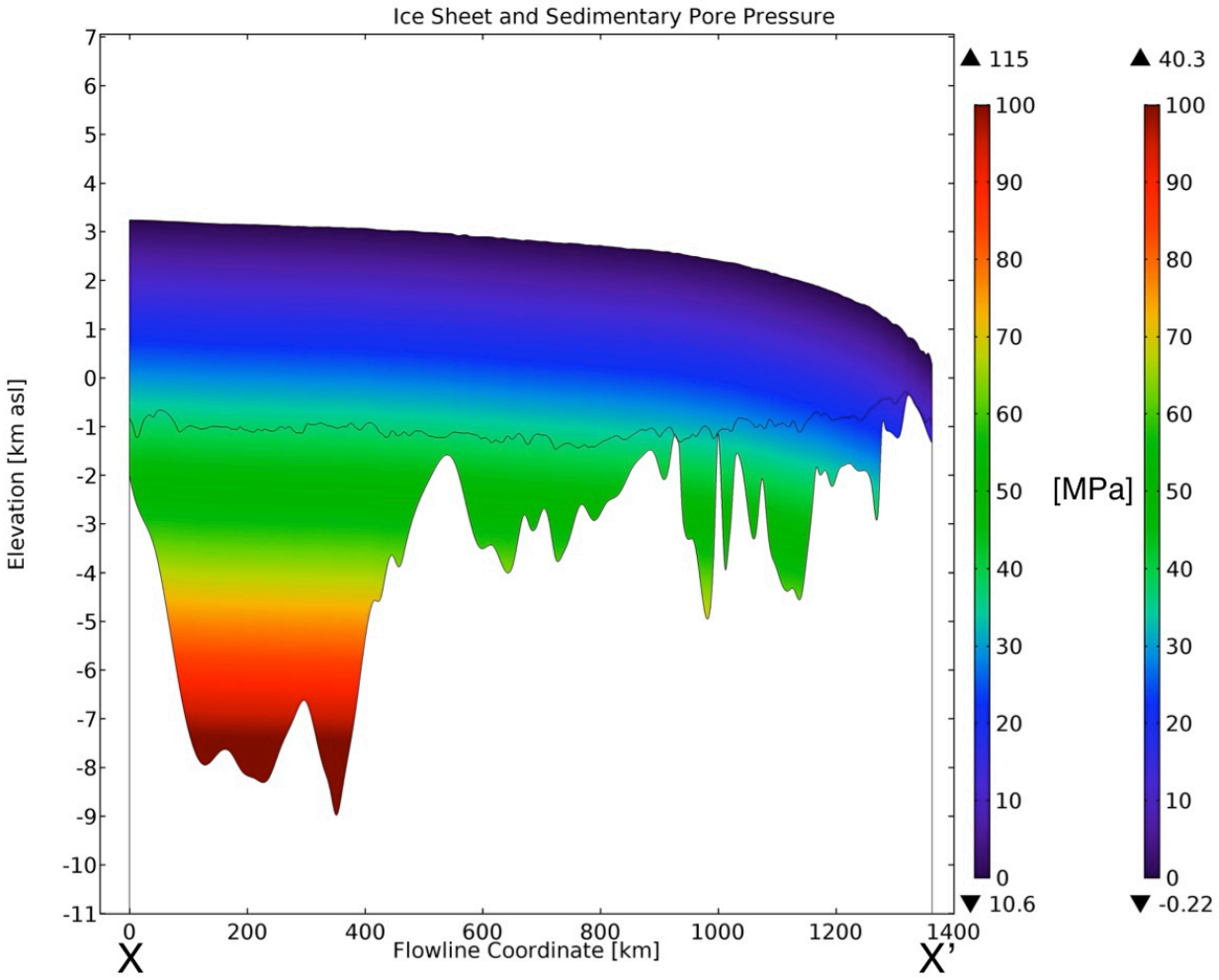

Figure S4.6. Numerical model output of ice sheet pressure and pore pressure in the sedimentary basins along the model flowline X-X' (see Figure 4.1). The color bar on the left is for the pore pressure and the color bar on the right is for the ice sheet. Maximum and minimum values are displayed at the top and bottom of the color bars, respectively.

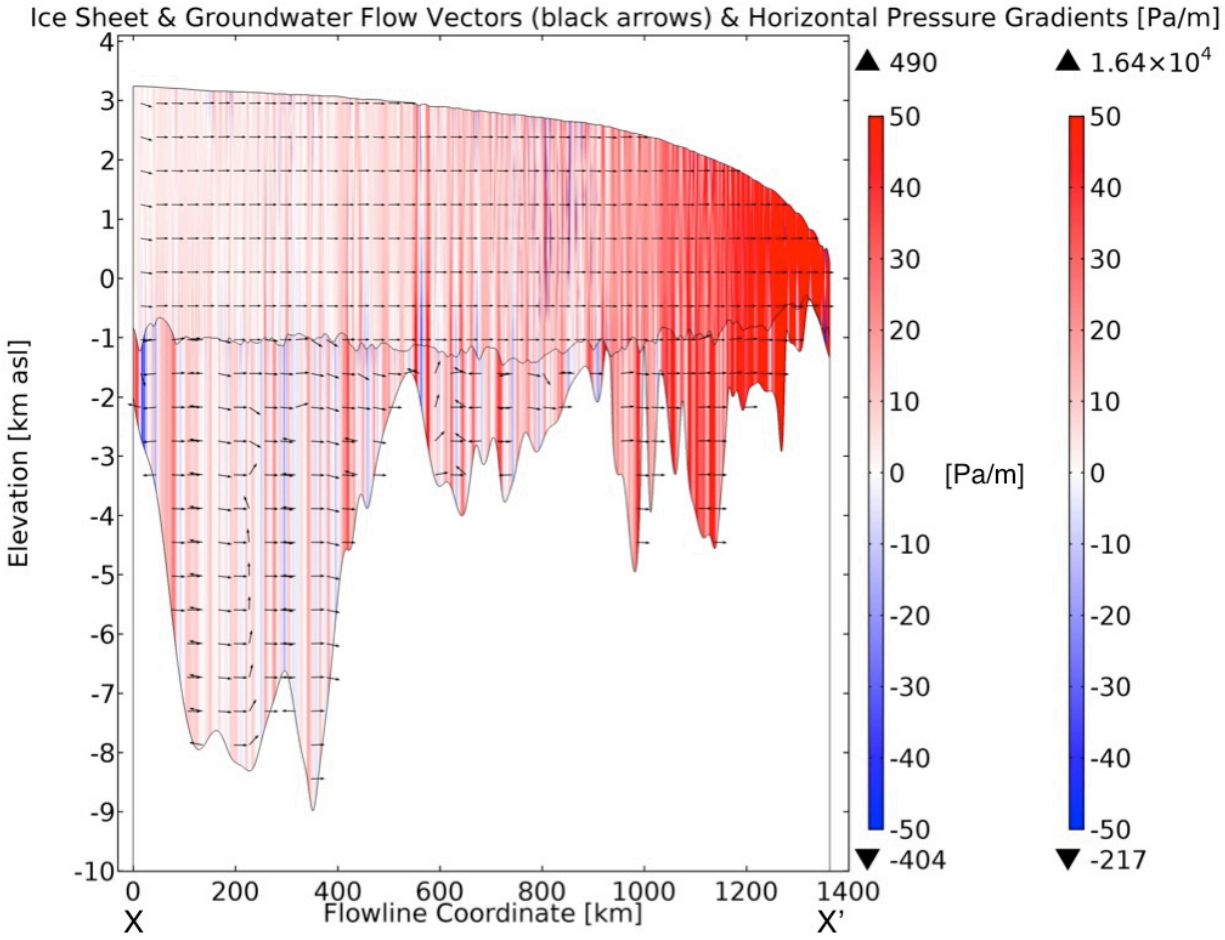
Ice Sheet & Groundwater Flow Vectors (black arrows) & Horizontal Pressure Gradients [Pa/m]
Elevation [km asl]
4
3
2
1
0
-1
-2
-3
-4
-5
-6
-7
-8
-9
-10
0
200
400
600
800
1000
1200
1400
X
X'
Flowline Coordinate [km]
▲ 490
50
40
30
20
10
0
-10
-20
-30
-40
-50
▼ -404
[Pa/m]
▲ 1.64×10^4
50
40
30
20
10
0
-10
-20
-30
-40
-50
▼ -217

Figure S4.7. Computed horizontal pressure gradient solutions ($k_0 = 10^{-11}$ m^2) for the permeable sediment and the ice sheet subdomains of the numerical model with sliding. A positive (in red) pressure gradient represents horizontal flow to the right (toward X', the grounding line) whereas a negative (in blue) gradient represents a reversed flow direction upstream (toward X, the ice divide). The arrow vectors show the direction of flow of groundwater and the ice sheet, which are largely horizontal except for some vertical deviations in the groundwater. Places where groundwater flow is reversed exist due to the topographic component of the pressure potential. The largest magnitudes of pressure gradient are proximal to the grounding line as the greatest changes in ice surface slope (the dominant component of flow for ice and groundwater) occur there. The maximum and minimum values for the ice sheet and groundwater are posted above and below their respective color bars (groundwater, left; ice sheet, right). The same results for parameterization $k_0 = 10^{-18}$ m^2 are nearly identical to these but are shown in Figure 4.5.

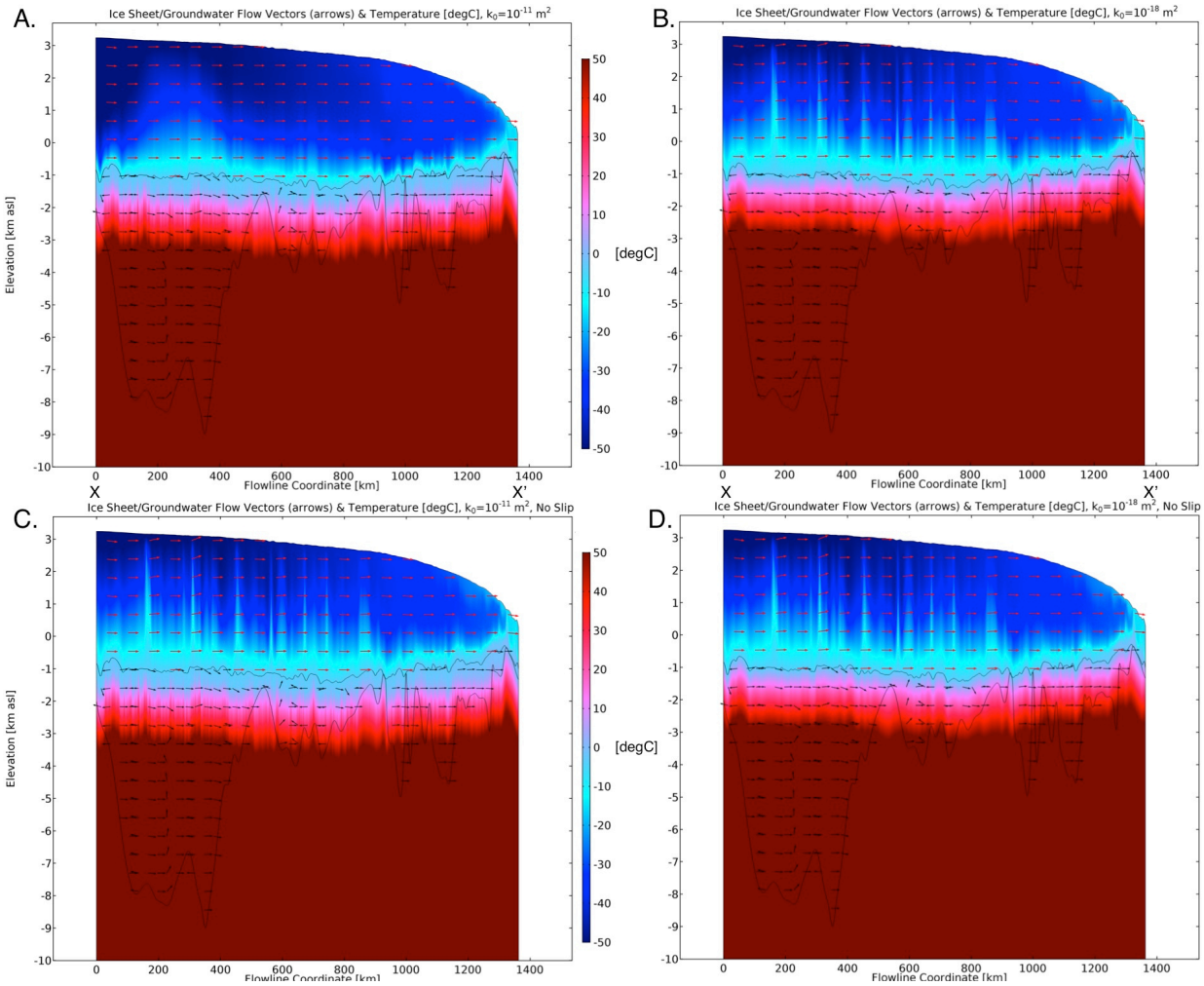

Figure S4.8. Computed temperatures from the numerical model for (a) the high groundwater and (b) low groundwater parameterizations of the sliding model. (c) the high groundwater and (d) low groundwater parameterizations of the model without sliding. Note that all but the high groundwater parameterization with sliding have roughly the same results for all simulations temperature results compared (as mentioned in Figure 4.6). Also note that the pressure melting temperature ranges from 0° to about -4° Celsius (see Figure S4.2).

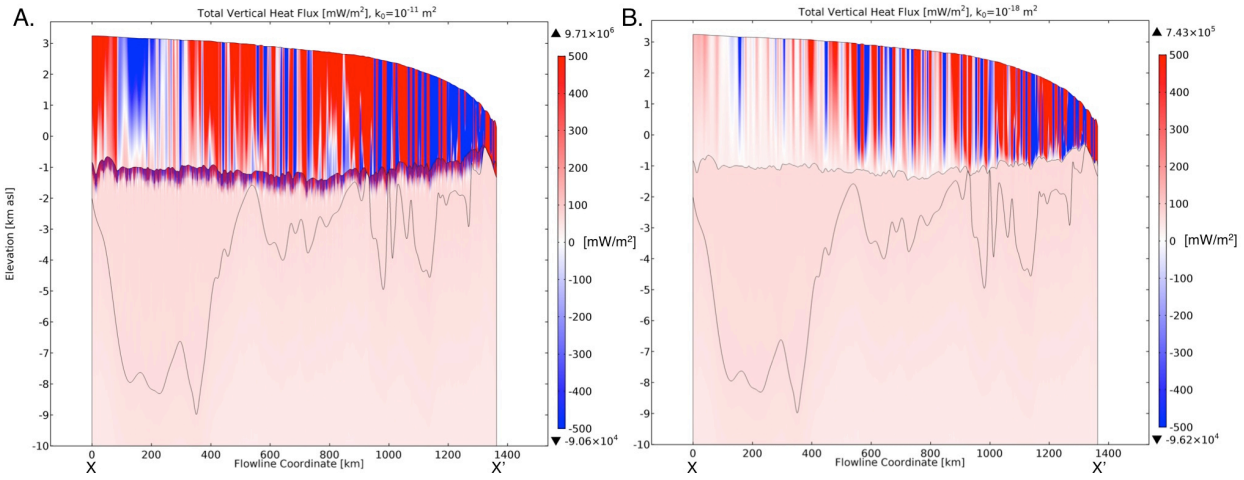

Figure S4.9. The vertical heat flux component (in powers of ten of mW/m^2) in the ice sheet, sedimentary basin, and crystalline basement rock subdomains for the (a) high and (b) low groundwater parameterizations. The maximum and minimum values above and below (respectively) the color bar are relevant to the subdomains pictured. The main component in the total heat flux is the convective component (cf. the conductive; see Figure S4.15). The main difference between the two is the effect groundwater has in the upper part of the sedimentary basin and the behavior of the ice sheet proximal to the ice divide (X) for the high groundwater parameterization. A negative (blue) vertical heat flux is down while a positive (red) is up. The maximum and minimum values are posted above and below the color bars.

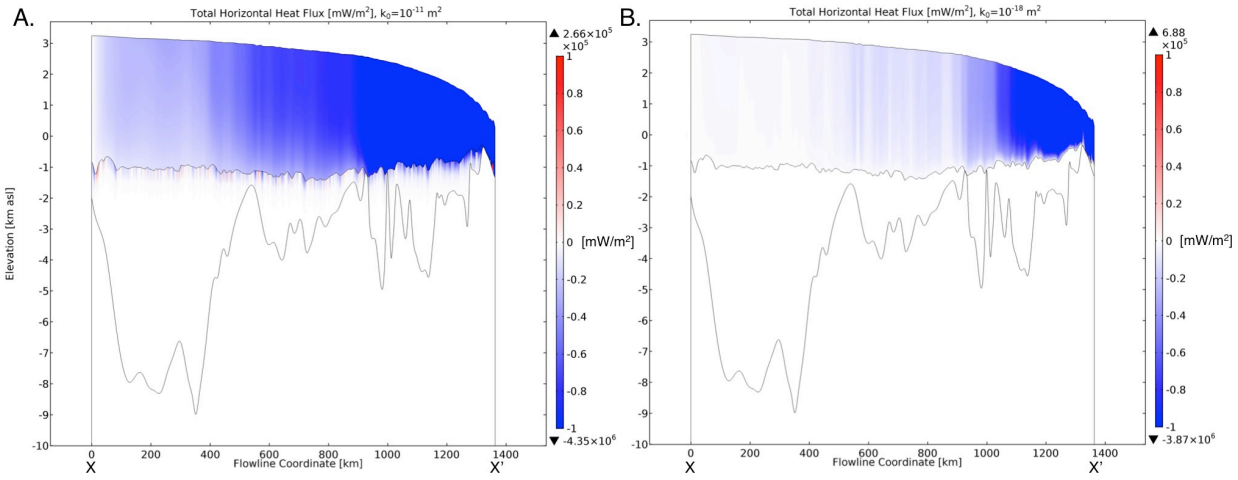

Figure S4.10. The horizontal heat flux component (in powers of ten of mW/m^2) in the ice sheet, sedimentary basin, and crystalline basement rock subdomains for the (a) high and (b) low groundwater parameterizations. The maximum and minimum values above and below (respectively) the color bar are relevant to the subdomains pictured. The main difference between the two is the effect groundwater has in the upper part of the sedimentary basin and the behavior of the ice sheet proximal to the ice divide (X) and the central portion of the profile for the high groundwater parameterization.

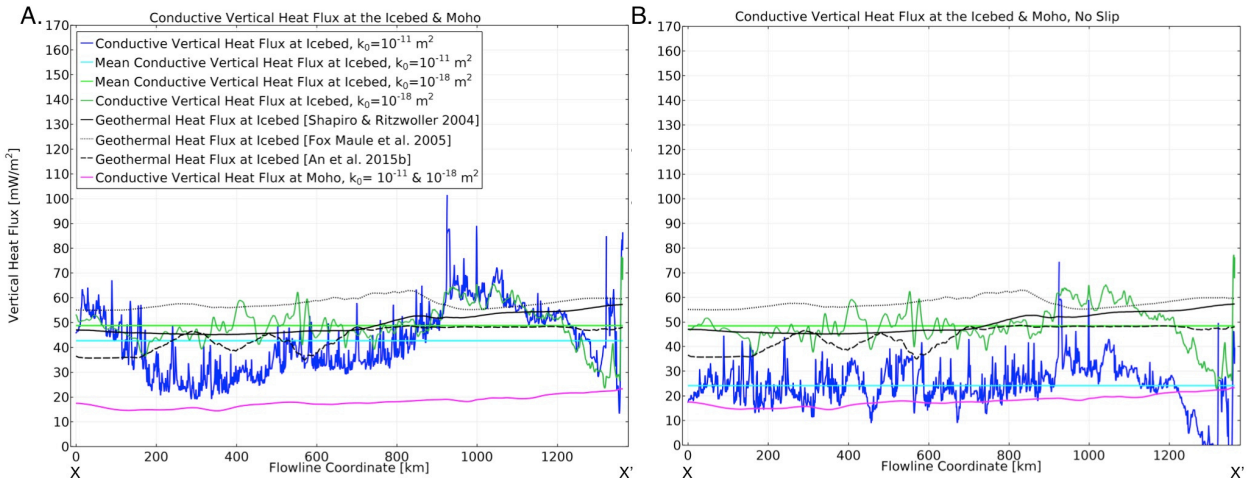

Figure S4.11. Similar to Figure 4.8 in the main text, these plots show only the vertical conductive component of the heat flux (in mW/m^2) for the different parameterizations for the models with (a) sliding enabled and (b) no slip at the ice/bed interface and Moho along the model flowline shown in Figure 4.1. The means for the high and low groundwater parameterizations with slip are 42.73 and 48.86 mW/m^2, respectively. The means for the high and low groundwater parameterizations with no slip are 24.17 and 48.49 mW/m^2, respectively. The three most commonly used, recent vertical geothermal heat flux datasets for East Antarctica [*Shapiro and Ritzroller*, 2004; *Fox Maule et al.*, 2005; and *An et al.*, 2015b], sampled along the model flowline, have been plotted for comparison, as in Figure 4.8.

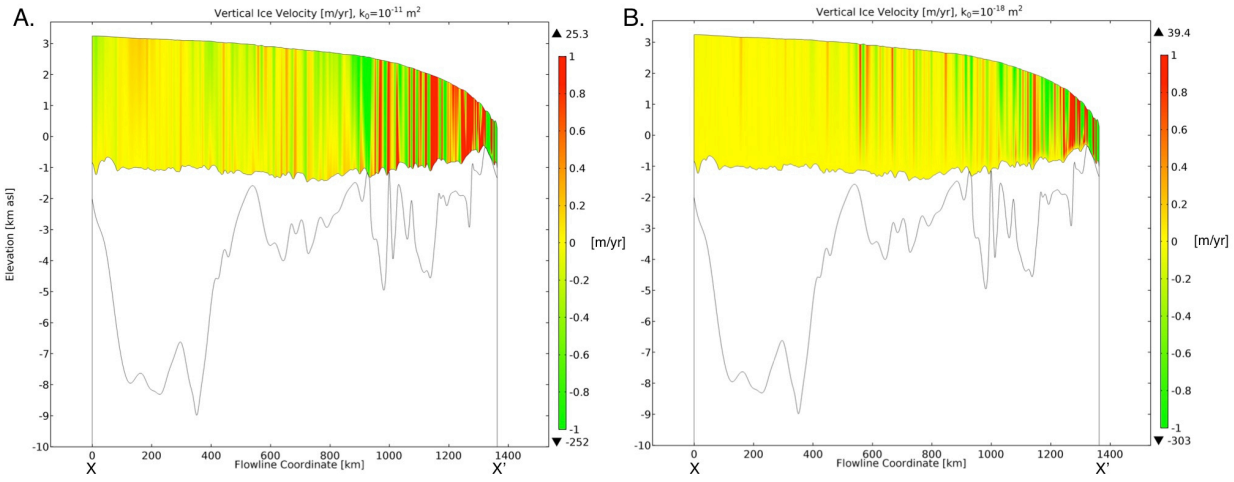

Figure S4.12. Vertical component of ice velocity (in m/yr) of the (a) high and (b) low groundwater parameterizations of the flowline model. The maximum and minimum values are above and below (respectively) the color bar.

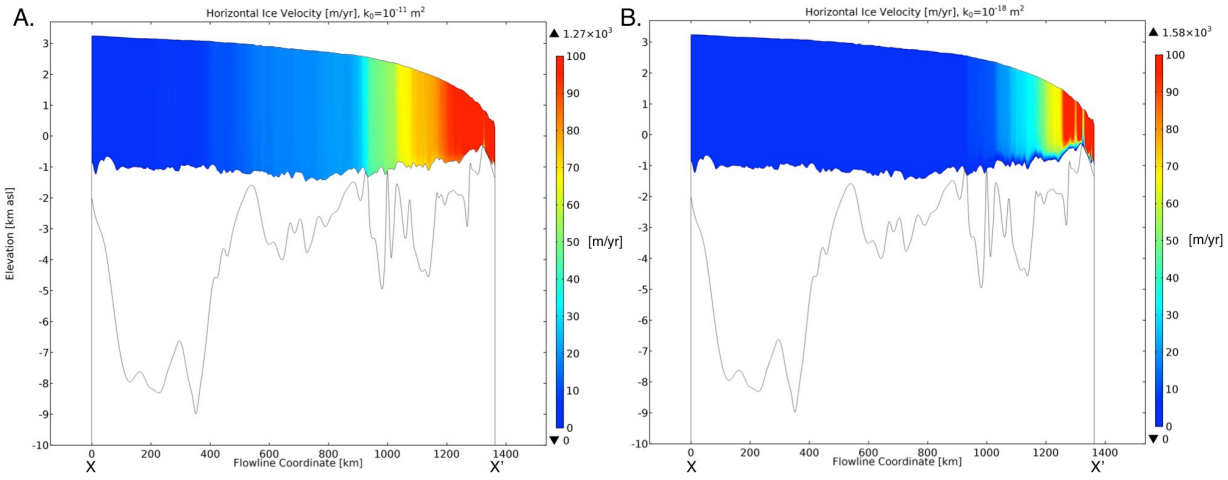

Figure S4.13. Horizontal component of ice velocity (in m/yr) of the (a) high and (b) low groundwater parameterizations of the flowline model sliding. The maximum and minimum values are above and below (respectively) the color bar. The ice surface and bed values of these plots are plotted in Figure 4.4. The increase in horizontal speed in (a) is largely due to the enhanced sliding.

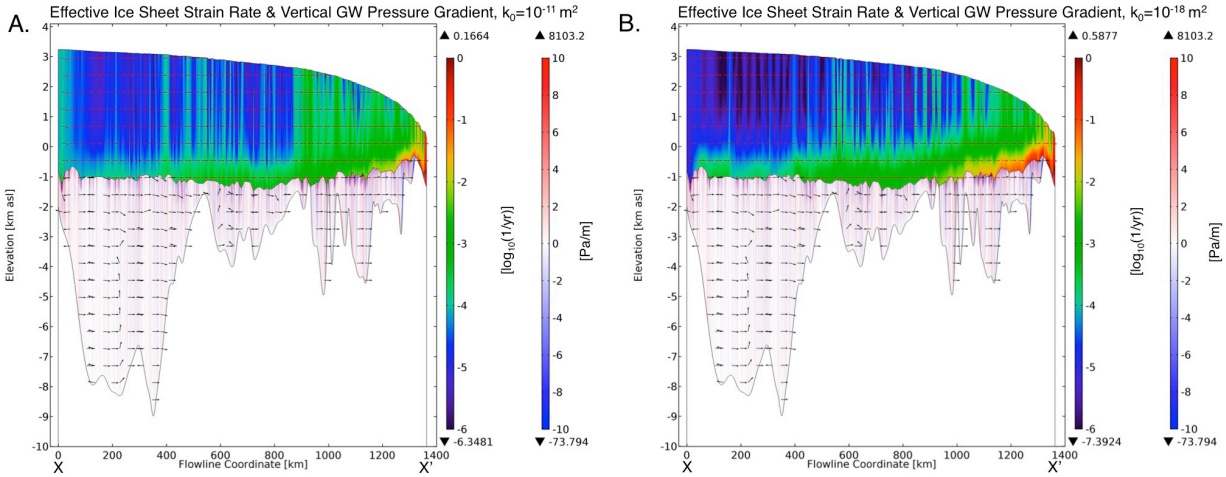

Figure S4.14. Effective ice sheet strain rates (in powers of ten of 1/yr) and vertical sedimentary pore pressure gradients of the groundwater system (GW; in Pa/m; red, flow upward; blue, flow downward) along with ice and groundwater flow vectors (arrows) of the (a) high and (b) low groundwater parameterizations of the flowline model. The maximum and minimum values are above and below (respectively) the color bars.

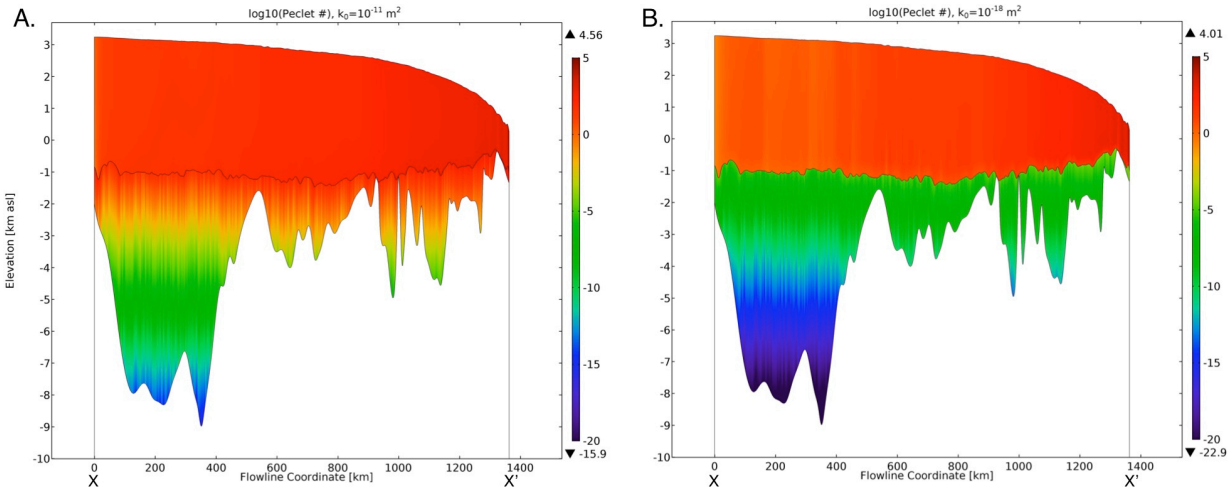

Figure S4.15. Péclet number for heat flux (in powers of ten; >0 (i.e. 10^0), advection dominant; <0, diffusion dominant) along with ice and groundwater flow vectors (arrows) of the (a) high and (b) low groundwater parameterizations of the flowline model with sliding. The maximum and minimum values are above and below (respectively) the color bars.

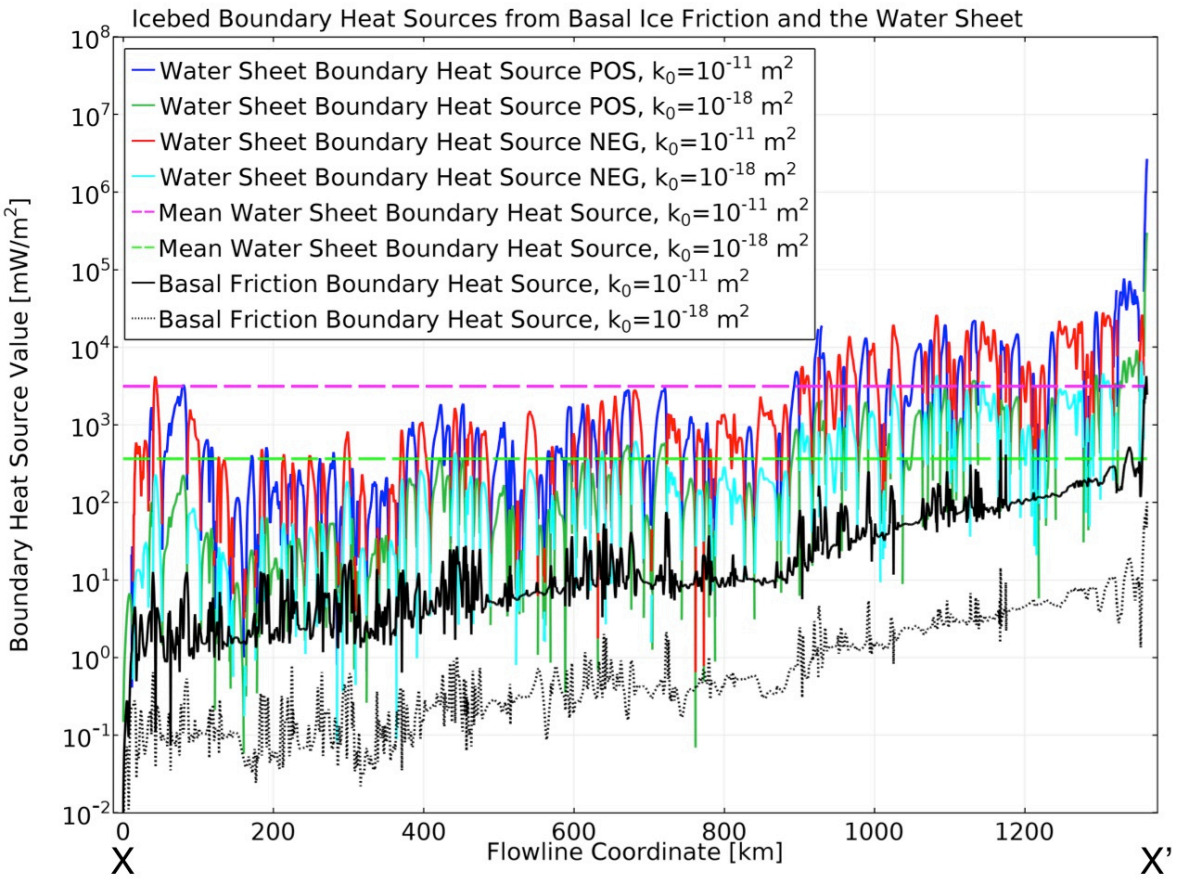

Figure S4.16. Boundary heat sources at the ice/bed interface from basal friction and horizontal water sheet transport. Horizontal heat flux advected through the water sheet for the sliding model. Because the fluxes range many orders of magnitude above and below zero, the positive (POS) and negative (NEG) components are shown separately. Positive (boundary heat source) means that the heat is moving out of the fluid, into the system, whereas, negative (boundary heat sink) implies that the heat leaves the system with the advected water. This sign is dependent on the horizontal temperature gradient at the ice/bed interface. Also, an average is displayed for the fluxes in order to define the overall sign and magnitude of the flux. The means for the high and low groundwater parameterizations with sliding are 3,155.5 and 367.06 mW/m^2, respectively. The means for the high and low groundwater parameterizations with no slip (not shown; similar overall trend but lower) are 1,272.0 and 361.81 mW/m^2, respectively. The heat fluxes from the friction at the base of the ice along the ice/bed interface are only from the simulations including sliding.

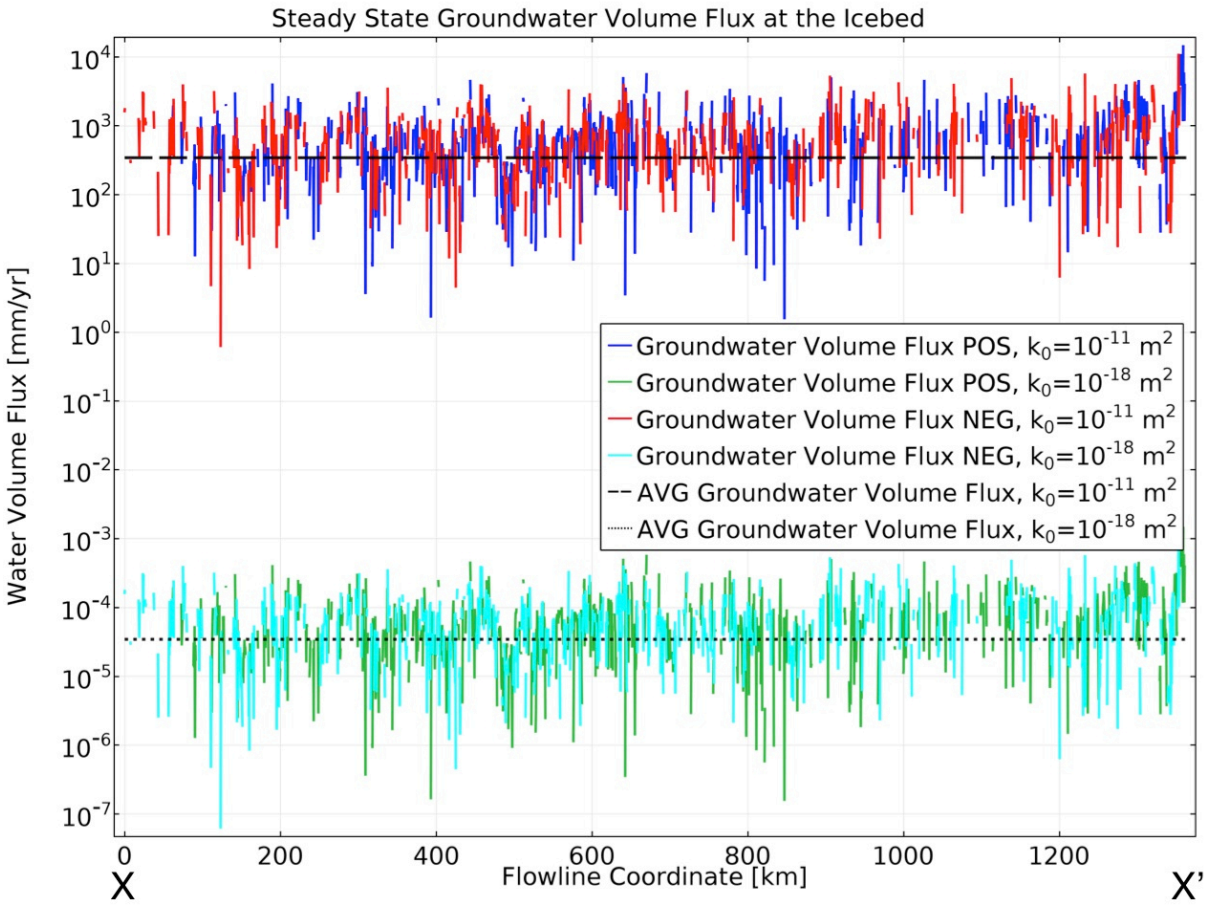

Figure S4.17. Basal water sheet groundwater sources (and sinks, if negative) along the model flowline shown in Figure 4.1 for the simulation including sliding. For fluxes ranging many orders of magnitude above and below zero, the positive (POS) and negative (NEG) components are shown separately. Also, where the values are split into the two components, an average is displayed for all values in order to define the overall sign and magnitude of the flux. The mean for the high groundwater ($k_0 = 10^{-11}$ m^2) and low groundwater ($k_0 = 10^{-18}$ m^2) are 346.83 and 3.46×10^{-5} mm/yr, respectively. As the groundwater properties are the same in the simulation without sliding (not shown), their mean values are the same. Figure 4.9 shows these groundwater volume flux trends along with the other water sheet sources.

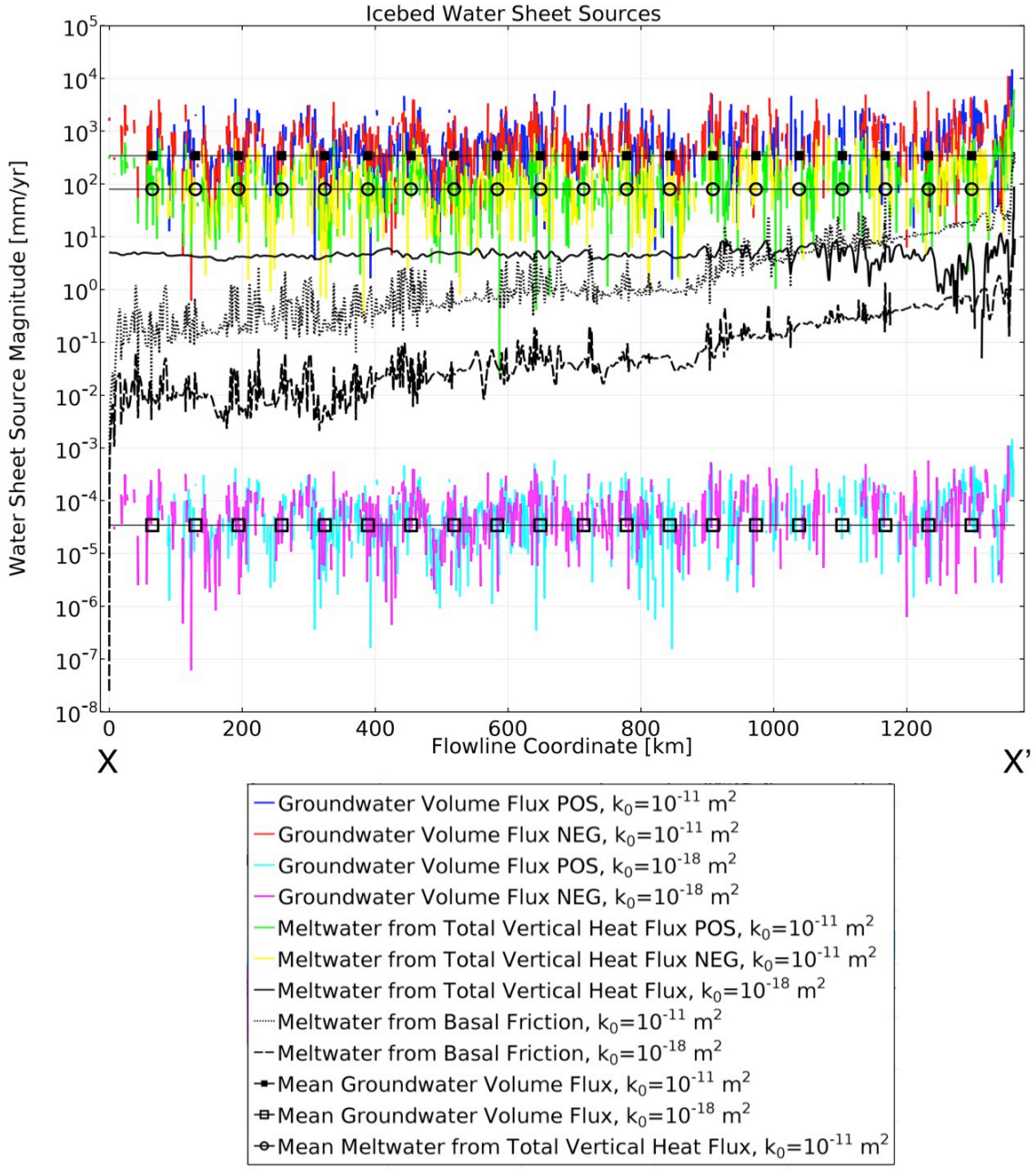
Icebed Water Sheet Sources
Water Sheet Source Magnitude [mm/yr]
Flowline Coordinate [km]
X
X'
Groundwater Volume Flux POS, k0=10-11 m2
Groundwater Volume Flux NEG, k0=10-11 m2
Groundwater Volume Flux POS, k0=10-18 m2
Groundwater Volume Flux NEG, k0=10-18 m2
Meltwater from Total Vertical Heat Flux POS, k0=10-11 m2
Meltwater from Total Vertical Heat Flux NEG, k0=10-11 m2
Meltwater from Total Vertical Heat Flux, k0=10-18 m2
Meltwater from Basal Friction, k0=10-11 m2
Meltwater from Basal Friction, k0=10-18 m2
Mean Groundwater Volume Flux, k0=10-11 m2
Mean Groundwater Volume Flux, k0=10-18 m2
Mean Meltwater from Total Vertical Heat Flux, k0=10-11 m2

Figure S4.18. Basal water sheet sources (and sinks, if negative) along the model flowline shown in Figure 4.1 for the simulation including sliding. For fluxes ranging orders of magnitude above and below zero, the positive (POS) and negative (NEG) components are shown separately. Also, where the values are split into the two components, an average is displayed for all values in order to define the overall sign and magnitude of the flux. The means for the high groundwater ($k_0 = 10^{-11}$ m^2), low groundwater ($k_0 = 10^{-18}$ m^2), and high (groundwater) total vertical heat flux melt are 346.83, 3.46×10^{-5}, and 85.02 mm/yr, respectively. As the groundwater properties are the same in the simulation without slip (not shown), their mean values are the same. The mean for the high total vertical heat flux from the simulation without sliding (not shown) is 72.5 mm/year. For the simulations run without sliding, the input from basal friction would be 0 mm/year. Figure 4.9 shows the groundwater volume flux trends more clearly with the melt components lumped together.

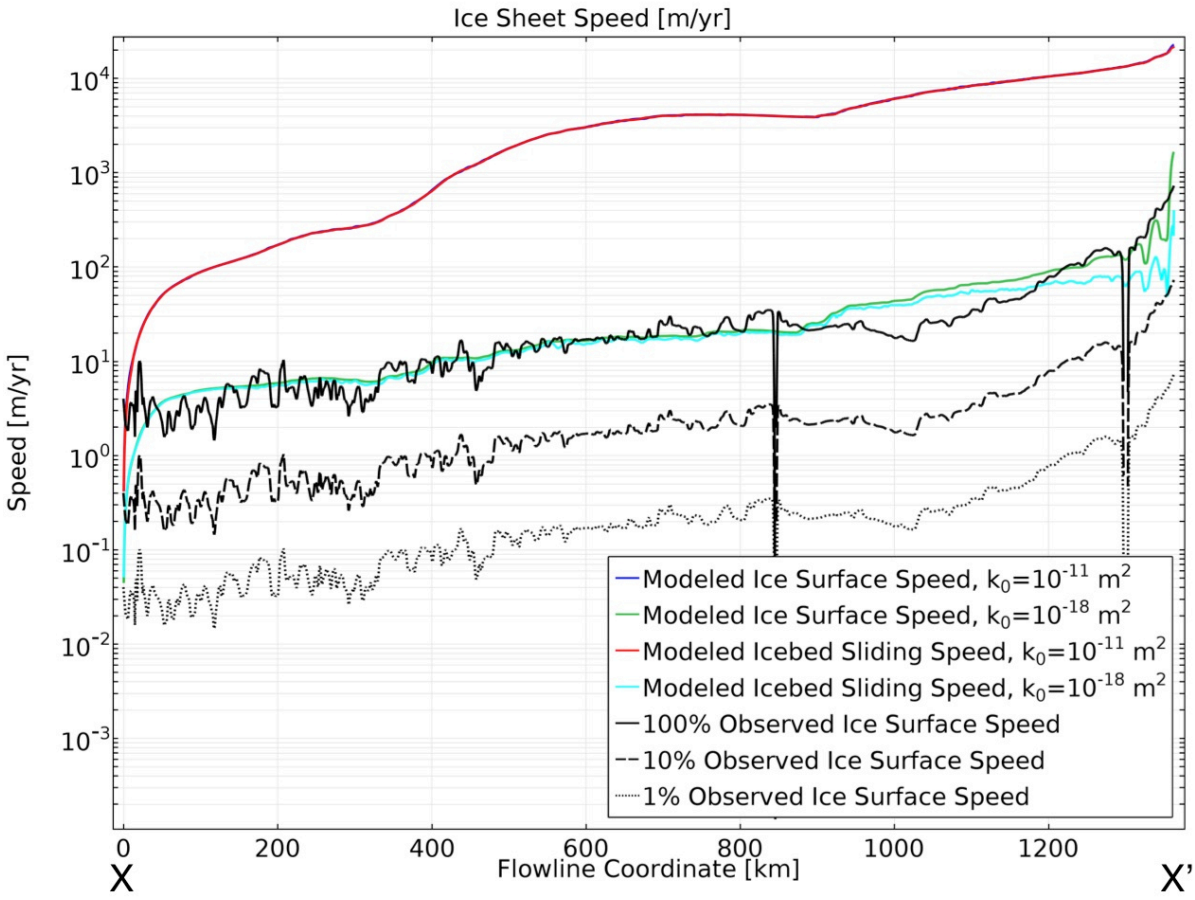

Figure S4.19. Modeled ice surface and bed speeds along the model flowline (see Figure 4.1) for the low groundwater scenario with sliding ($c_f = 2\times10^{12}$ for $k_0 = 10^{-18}$ m^2). Note that the high groundwater scenario is also plotted but is not realistic. The full (100%) and partial (10% and 1%) observed ice surface speeds [*Rignot et al.*, 2011] are included for comparison. The sliding simulations were calibrated by iteratively matching the high groundwater parameterization's results of ice surface speed to the observed values.

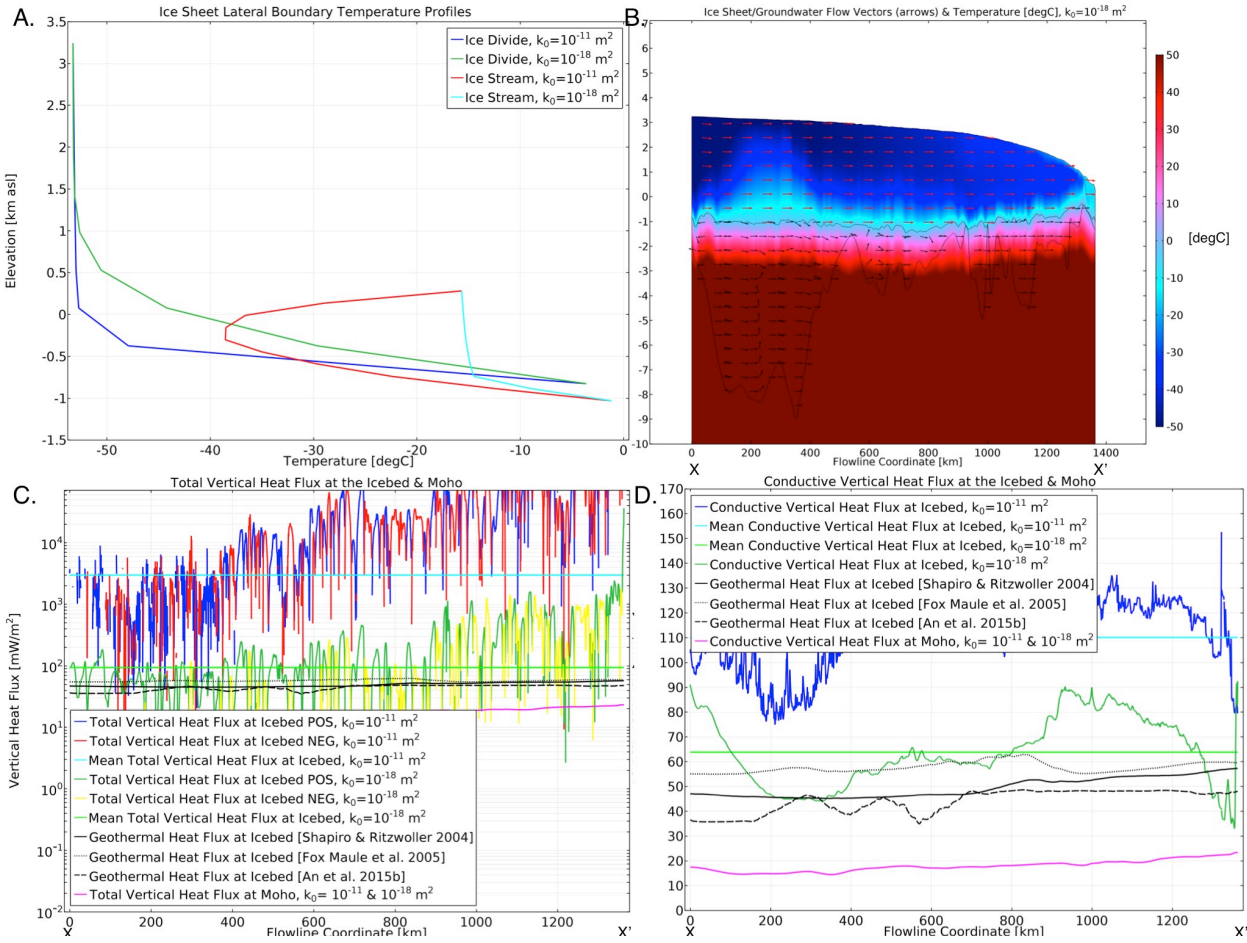
A.
Ice Sheet Lateral Boundary Temperature Profiles
Ice Divide, k0=10-11 m2
Ice Divide, k0=10-18 m2
Ice Stream, k0=10-11 m2
Ice Stream, k0=10-18 m2
Elevation [km asl]
Temperature [degC]
B.
Ice Sheet/Groundwater Flow Vectors (arrows) & Temperature [degC], k0=10-18 m2
[degC]
Flowline Coordinate [km]
X
X'
C.
Total Vertical Heat Flux at the Icebed & Moho
Vertical Heat Flux [mW/m2]
Total Vertical Heat Flux at Icebed POS, k0=10-11 m2
Total Vertical Heat Flux at Icebed NEG, k0=10-11 m2
Mean Total Vertical Heat Flux at Icebed, k0=10-11 m2
Total Vertical Heat Flux at Icebed POS, k0=10-18 m2
Total Vertical Heat Flux at Icebed NEG, k0=10-18 m2
Mean Total Vertical Heat Flux at Icebed, k0=10-18 m2
Geothermal Heat Flux at Icebed [Shapiro & Ritzwoller 2004]
Geothermal Heat Flux at Icebed [Fox Maule et al. 2005]
Geothermal Heat Flux at Icebed [An et al. 2015b]
Total Vertical Heat Flux at Moho, k0= 10-11 & 10-18 m2
Flowline Coordinate [km]
X
X'
D.
Conductive Vertical Heat Flux at the Icebed & Moho
Conductive Vertical Heat Flux at Icebed, k0=10-11 m2
Mean Conductive Vertical Heat Flux at Icebed, k0=10-11 m2
Mean Conductive Vertical Heat Flux at Icebed, k0=10-18 m2
Conductive Vertical Heat Flux at Icebed, k0=10-18 m2
Geothermal Heat Flux at Icebed [Shapiro & Ritzwoller 2004]
Geothermal Heat Flux at Icebed [Fox Maule et al. 2005]
Geothermal Heat Flux at Icebed [An et al. 2015b]
Conductive Vertical Heat Flux at Moho, k0= 10-11 & 10-18 m2
Flowline Coordinate [km]
X
X'

Figure S4.20. Various model results from the low groundwater sliding calibration ($c_f = 2\times10^{12}$ for $k_0 = 10^{-18}$ m^2). (a) Represents the lateral boundary temperatures for both simulations (i.e. high/low groundwater). (b) Computed temperatures for the results from the low groundwater scenario. Note that the pressure melting temperature ranges from 0° to about -4° Celsius (see Figure S4.2). (c) Total vertical heat flux (in mW/m^2) comparisons at the ice/bed interface and Moho along the model flowline shown in Figure 4.1. Both simulations produced the same heat flux at the Moho. Note that both the high and low groundwater results have been split into positive (POS) and negative (NEG) components for proper comparison. A mean of both heat flux results for each of the parameterizations of groundwater is shown as a solid horizontal bar. The means for the high and low groundwater parameterizations with slip are 2,995.1 and 94.381 mW/m^2, respectively. (d) Vertical conductive component of the heat flux (in mW/m^2). The means for the high and low groundwater parameterizations are 110.12 and 63.889 mW/m^2, respectively. Note that the three most commonly used, recent vertical geothermal heat flux datasets for East Antarctica [*Shapiro and Ritzroller*, 2004; *Fox Maule et al*., 2005; and *An et al*., 2015b], sampled along the model flowline, have been plotted for comparison, as in Figure 4.8.

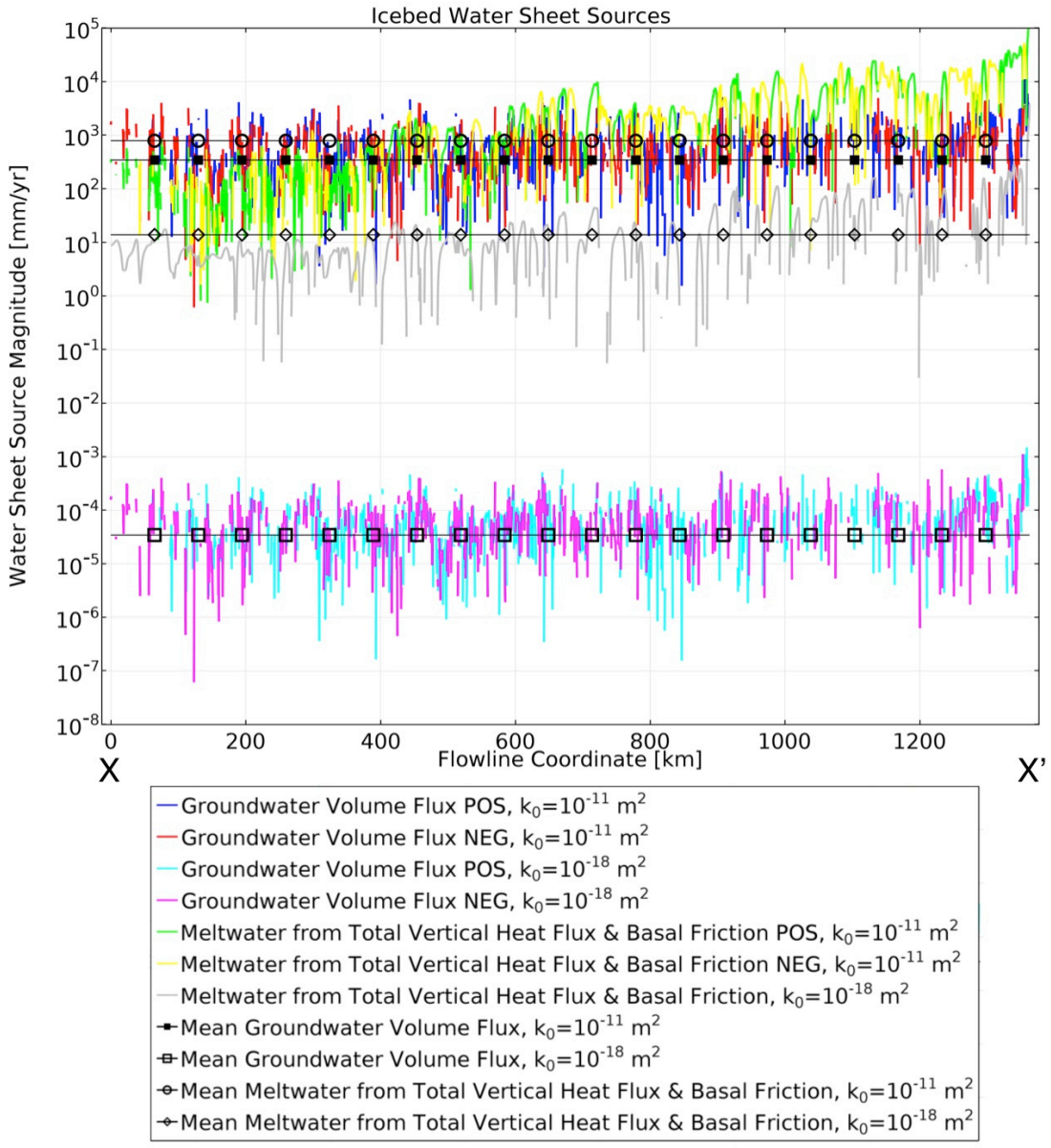
Icebed Water Sheet Sources
Water Sheet Source Magnitude [mm/yr]
Flowline Coordinate [km]
X
X'
Groundwater Volume Flux POS, k0=10-11 m2
Groundwater Volume Flux NEG, k0=10-11 m2
Groundwater Volume Flux POS, k0=10-18 m2
Groundwater Volume Flux NEG, k0=10-18 m2
Meltwater from Total Vertical Heat Flux & Basal Friction POS, k0=10-11 m2
Meltwater from Total Vertical Heat Flux & Basal Friction NEG, k0=10-11 m2
Meltwater from Total Vertical Heat Flux & Basal Friction, k0=10-18 m2
Mean Groundwater Volume Flux, k0=10-11 m2
Mean Groundwater Volume Flux, k0=10-18 m2
Mean Meltwater from Total Vertical Heat Flux & Basal Friction, k0=10-11 m2
Mean Meltwater from Total Vertical Heat Flux & Basal Friction, k0=10-18 m2

Figure S4.21. Basal water sheet sources (and sinks, if negative) along the model flowline shown in Figure 4.1 for the simulation including sliding similar to Figure 4.9 from the main text but calibrated to the low groundwater scenario with sliding ($c_f = 2\times10^{12}$ for $k_0 = 10^{-18}$ m^2). For fluxes ranging many orders of magnitude above and below zero, the positive (POS) and negative (NEG) components are shown separately. Also, where the values are split into the two components, an average is displayed for all values in order to define the overall sign and magnitude of the flux (except for the low meltwater total from heat flux and friction which only shows the positive component). The mean for the high groundwater ($k_0 = 10^{-11}$ m^2), low groundwater ($k_0 = 10^{-18}$ m^2), high (groundwater) total vertical heat flux/basal friction melt, and low (groundwater) total vertical heat/basal friction flux melt are 346.83, 3.46×10^{-5}, 794.4, and 13.973 mm/yr, respectively.

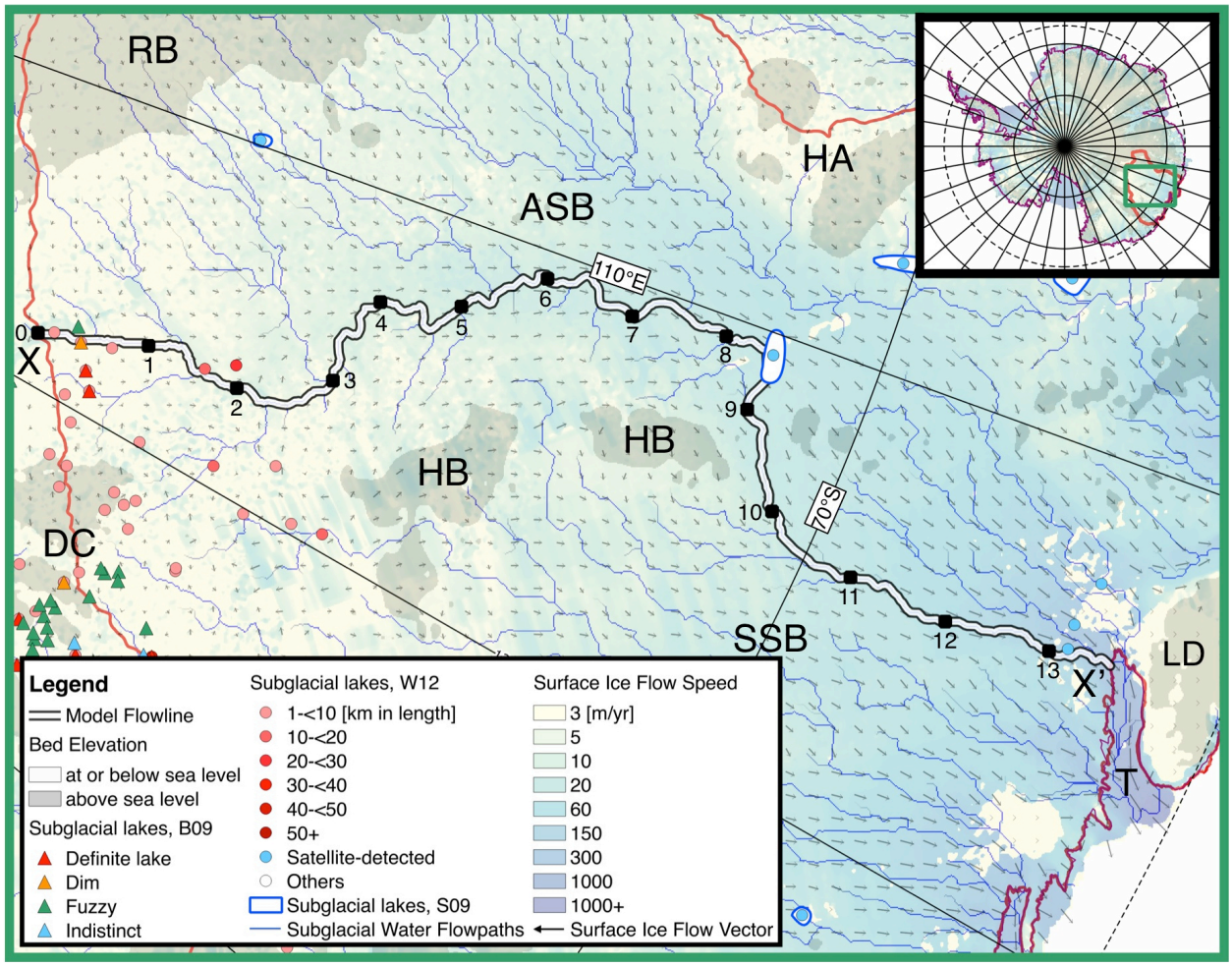
RB
HA
ASB
110°E
70°S
HB
HB
DC
SSB
LD
X
X'
T
0
1
2
3
4
5
6
7
8
9
10
11
12
13
Legend
Model Flowline
Bed Elevation
at or below sea level
above sea level
Subglacial lakes, B09
Definite lake
Dim
Fuzzy
Indistinct
Subglacial lakes, W12
1-<10 [km in length]
10-<20
20-<30
30-<40
40-<50
50+
Satellite-detected
Others
Subglacial lakes, S09
Subglacial Water Flowpaths
Surface Ice Flow Speed
3 [m/yr]
5
10
20
60
150
300
1000
1000+
Surface Ice Flow Vector

Figure S4.22. Map of the Totten Glacier and surrounding ice sheet catchment emptying along the Sabrina Coast in East Antarctica with the model flowline (X to X'; 1,363 km in total length with 100 km segments noted) discussed in this article. Important places or those discussed in this article are highlighted; ASB – Aurora Subglacial Basin, DC – Dome C, HA – Highland A, HB – Highland B, LD – Law Dome, RB – Ridge B, SSB – Sabrina Subglacial Basin, and T – Totten Glacier. The red outline represents the larger ice catchment boundaries [*Zwally et al.,* 2012] and, where at the coast, represents overlap with the grounding line [*Bindschadler et al.,* 2011]; the precise catchment for Totten Glacier was measured and is displayed as a function of flowline coordinate in Figure S4.1. Surface ice flow speeds and direction are from the MEaSUREs dataset [*Rignot et al.,* 2011]. The subglacial water flowpaths and the bed elevation are based on the Bedmap2 dataset [*Fretwell et al.,* 2013]. All latitude and longitude graticules in the inset and main figure are in 10° increments with the Antarctic Circle shown as a dashed line. The subglacial lake inventory references are: B09 – *Blankenship et al*. [2009], S09 – *Smith et al*. [2009], and W12 – *Wright and Siegert* [2012]. A version of this map with the background indicating bed elevation instead of measured ice surface speed is given in Figure 4.1.

4.10 SUPPLEMENTARY REFERENCES

An, M., D. A. Wiens, Y. Zhao, M. Feng, A. Nyblade, M. Kanao, Y. Li, A. Maggi, and J.-J. Lévêque (2015b), Temperature, lithosphere-asthenosphere boundary, and heat flux beneath the Antarctic Plate inferred from seismic velocities, J. Geophys. Res. Solid Earth, 120, 8720–8742, doi:10.1002/2015JB011917.

Comiso, J. C. (2000), Variability and trends in Antarctic surface temperatures from in situ and satellite infrared measurements. Journal of Climate, 13(10), 1674-1696.

Fox Maule, C., M. E. Purucker, N. Olsen, and K. Mosegaard (2005), Heat flux anomalies in Antarctica revealed by satellite magnetic data., Science, 309(5733), 464–467.

Le Brocq, A., A. Payne, M. Siegert, and R. Alley (2009), A subglacial water-flow model for West Antarctica, J. Glaciol., 55(193), 879–888.

Shapiro, N. M., and M. H. Ritzwoller (2004), Inferring surface heat flux distributions guided by a global seismic model: Particular application to Antarctica, Earth Planet. Sci. Lett., 223(1-2), 213–224.

Chapter 5: Conclusion

5.1 SYNTHESIS

From the efforts in testing the general hypothesis shown in the previous chapters, it is apparent that groundwater most likely has measurable effects on the dynamics of ice sheets, specifically the East Antarctic Ice Sheet. Generally, I have shown that probable groundwater systems underneath the interior of the East Antarctic Ice Sheet (especially within the Aurora, Sabrina, and Wilkes Subglacial Basins) can likely carry and transport most, if not all, of the meltwater produced. Additionally, I have shown that groundwater can strongly affect the flux of heat (positively, as well as, negatively) at the ice/bed interface under kilometers of relatively slow and fast moving ice. Also, I have not only shown that groundwater systems under the East Antarctic Ice Sheet are strongly controlled by the ice sheet dynamics but that groundwater systems feedback to the ice dynamics mostly through basal processes but also via changes to the ice rheology.

In Chapter 2, I hypothesized that groundwater systems may be the main water transport mechanism over (distributed, inefficient; see Figure 1.3) water sheets at large scales in the interiors of ice sheets where melt rates are very low. I compared melt rate magnitudes to potential groundwater volume fluxes and also calculated the theoretical transmissivity ranges of subglacial water sheet and groundwater flow systems. I found that theoretical groundwater systems are on par with or more transmissive than water sheets for the upper half of the permeability spectrum. In addition, I developed a two-dimensional flow path model that connected subglacial lakes near Dome C, East Antarctica. This model integrated subglacial water sheet and hypothetical groundwater flow forcing, better bridging two historically disparate modeling frameworks – subglacial hydrology and ice sheet hydrogeology. My model results suggest that the water sheet thickness can be highly dependent on groundwater flux and that the water sheet transmissivity is within the total range of the modeled groundwater system transmissivity. I infer from these results that subglacial lake stability underneath continental ice sheets and, possibly basal radar reflections, may be due to groundwater flow.

In Chapter 3, I presented the results of two numerical models describing contributions of groundwater and heterogeneous heat sources to ice dynamics directly relevant to basal processes in East Antarctica. A two-phase, one-dimensional hydrothermal model demonstrated the importance of groundwater flow in vertical heat flux advection near the ice/bed interface. The results indicated that typical, conservative vertical components of groundwater volume fluxes (from either topographical gradients or vertically channeled flow) on the order of ±1-10 mm/yr can alter vertical heat flux by ±50-500 mW/m^2 given parameters typical for the interior of East Antarctica. This heat flux has the potential to produce considerable volumes of meltwater depending on basin geometry and geothermal heat production. A one-dimensional hydromechanical model demonstrated that groundwater is mainly recharged into saturated, partially poroelastic (i.e. vertical stress only; not coupled to a deformation equation) sedimentary aquifers during ice advance. During ice retreat, groundwater discharged into the ice/bed interface, which may contribute to water budgets on the order of 0.1-1 mm/yr. I also presented an estimated map of potentially heterogeneous heat flow provinces using radiogenic heat production data from East Antarctica and southern Australia, calculated sedimentary basin depths, and radar-derived bed roughness. I overlaid these together to delineate the areas of greatest potential effect from these modeled processes on the ice sheet dynamics of the East Antarctic Ice Sheet.

In Chapter 4, I hypothesized that recent geophysical investigations' discoveries of large sedimentary basins under the potentially unstable Totten Glacier Catchment of East Antarctica may play a crucial role (via groundwater systems) in the subglacial water transport, basal processes, and dynamics of the ice sheet (rheological and sliding behavior). Given recent observations and the hypothesis, I constructed numerical models that linked lithospheric heat generation and transport, subsurface fluid and heat transport, and Stokes-flow ice dynamics to various groundwater-forcing functions. I designed these models for an ice flowline that runs the centerline of the entire ice catchment from the ice

divide in central East Antarctica to the grounding line at Totten Glacier. I found that, given some specific assumptions about the base of the ice sheet, various groundwater forcing applied under the ice sheet showed measurable differences in the ice sheet's dynamics and rheological structure; although, the link between the change in the internal thermal structure of the ice sheet and the heat transfer from the advection of groundwater in the basin was not clear, which requires further work. However, the groundwater did have a direct impact heavily on the subglacial hydrological system that lead to very measurable differences in the sliding speed of the modeled ice flowline. From these results, I asserted that groundwater systems under the Totten Glacier Catchment should be given further consideration in future ice sheet modeling assessments pending further geophysical and geological exploration to better define the basins.

5.2 GOING FORWARD

My numerical model presented in Chapter 2 demonstrates a basic method for coupling water sheet transport to two-dimensional groundwater model output forcing, which represents my initial attempt to connect two segmented communities trying to solve very closely related problems [cf. *Flowers*, 2015; *Person et al.*, 2012]. My approach is especially well suited for ice sheets that are thick enough to support a pressure-melting temperature at their base with minimal basal ice velocities (i.e. low frictional melt component). For ice sheets that do not meet these criteria, other approaches such as groundwater/channel coupling [*Boulton et al.*, 2007] may be more appropriate or the groundwater system may be negated altogether [e.g. *Kyrke-Smith et al.*, 2014] if the flux magnitudes are small enough when compared to a very efficient basal water system. My model, as a two-dimensional model, may suffer due to a lack in accommodation of three-dimensional effects and interpolation biases in the topography. It is also possible that large heterogeneities in the hydrogeologic properties of the subsurface could cause deviations from the model. One example of this is karstic limestone (high, heterogeneous conductivity), which has been proposed for the area

[*Forieri et al.*, 2004], further supporting my hypothesis of a groundwater-dominant hydrologic system. However, my results from Chapter 2 do demonstrate that further advancement of subglacial groundwater transport mechanisms needs to take place (given the availability of greater subglacial geophysical and geologic information, another important task for current Antarctic research) and be incorporated into the subglacial hydrologic components of ice sheet models.

The continental ice sheet modeling community will eventually need to incorporate the effects demonstrated in Chapter 3 when simulating ice dynamics in the interior of the East Antarctic Ice Sheet if higher accuracy estimates of future ice volume are to be calculated. While it is highly likely that the physical effects presented in Chapter 3 are not as crucial to understand in areas of higher ice velocity (i.e. outlet glaciers), a significant fraction of the total ice sheet maybe affected by such processes and, thus, should be considered. For example, the added complexity to the geothermal heat flux parameterization for continental ice sheet models could add significant value to their usage if incorporated. Further efforts to better define the subglacial geology of the region will help resolve the great uncertainties that exist in the thermal and mechanical properties of the East Antarctic subsurface and lead to better estimations of heat flux and groundwater volume flux rates (specifically targeting the areas denoted in Figure 3.8 as questions marks). Future efforts in continuing to test the aforementioned hypothesis in Chapter 3 should focus on coupling these processes together in multidimensional models.

Through my novel methodology linking groundwater forcing to a steady thermomechanical ice sheet flowline model with basal hydrology in Chapter 4, I initially assessed diagnostically whether groundwater flux at the ice/bed interface has a measurable effect on ice dynamics for the Totten Glacier Catchment of East Antarctica. While it is currently unclear whether the hypothetical groundwater forcing on the modeled heat flux and thermal structure of the ice sheet is direct, the potential impact on the subglacial hydrological system may have more direct impact on the actual dynamics

of the Totten Glacier Catchment system. I asserted this as the groundwater forcing has a direct effect on the water system at the ice/bed interface, which does have an effect on the ice sliding velocity for my sliding function and most likely for other sliding functions. I also noted that just the presence of the geophysically estimated sedimentary basins underlying the ice/bed interface along my model flowline alone has an effect on the thermal structure of the ice sheet but this requires further analysis to determine the relationship better.

While the methodology presented in Chapter 4 is not a fully comprehensive way to determine groundwater's potential impact to this study area, I do however believe that this work is a foundation for other studies to build upon and a guide to those interested in better understanding the complexities of the Totten Glacier Catchment portion of the East Antarctic Ice Sheet. Those interested in the glaciology of this system or its significance in large-scale ice sheet modeling may want to consider the impacts that groundwater may have on it or similar systems in East Antarctica. The reality is that the geologic and geophysical work necessary to properly constrain these groundwater systems has not taken place and may not anytime soon in the future. However, I believe that given future geophysical and eventually geologic research in critical submarine basins of East Antarctica, particularly the Aurora and Sabrina subglacial basins, that it will be feasible to incorporate more realistic groundwater systems into the ice sheet models utilized for the area.

Future efforts based on the work of Chapter 4 would likely need to investigate the effect of leaving the ice base temperature as part of the numerical solution (instead of fixing the temperature), finding a way to base groundwater flux from melt at the ice/bed interface rather than assumed overburden pressure, and adding control of permafrost formation for where the modeled temperatures in the sedimentary basins go below the pressure-melting temperature and cause groundwater to slow down or freeze. Extending the model to a fully three dimensional model domain would enable the ability to test

whether groundwater flow systems behaved identically to the water sheet systems or whether they may flow in different directions possibly leading to anomalous water at the bed. Future work should also incorporate transient behavior in the ice sheet thickness development and the pore pressure as some transient effects in the groundwater system could linger as the ice sheet evolves (such as in *Bense and Person* [2008], *Lemieux et al.* [2008], or *Gooch et al.* [2016]). The result of these holistic analyses would yield a better, more realistic ice sheet model of the Totten Glacier Catchment system that better meets the needs of those needing to assess future ice sheet outlet contributions to sea level from East Antarctica.

5.3 REFERENCES

Bense, V. F., and M. A. Person (2008), Transient hydrodynamics within intercratonic sedimentary basins during glacial cycles, J. Geophys. Res., 113, F04005, doi:10.1029/2007JF000969.

Boulton GS, R. Lunn, P. Vidstrand, and S. Zatsepin (2007), Subglacial drainage by groundwater–channel coupling, and the origin of esker systems: Part 2 – theory and simulation of a modern system, Quat. Sci. Rev., 26, 1091–1105.

Flowers, G. E. (2015), Modelling water flow under glaciers and ice sheets, Proc. A, (471).

Forieri, A., L. Zuccoli, A. Bini, A. Zirizzotti, F. Remy, and I. E. Tabacco (2004), New bedrock map of Dome C, Antarctica, and morphostructural interpretation of the area, Ann. Glaciol., 39(1), 321-325.

Gooch, B. T., D. A. Young, and D. D. Blankenship (2016), Potential groundwater and heterogeneous heat source contributions to ice sheet dynamics in critical submarine

basins of East Antarctica, Geochem. Geophys. Geosyst., 17, doi:10.1002/2015GC006117.

Kyrke-Smith, T. M., R. F. Katz, and A. C. Fowler (2014), Subglacial hydrology and the formation of ice streams, Proc. Phys. Soc. London, Sect. A, 470, 20,130,494, doi:10.1098/rspa.2013.0494.

Lemieux, J.-M., E. Sudicky, W. Peltier, and L. Tarasov (2008), Dynamics of groundwater recharge and seepage over the Canadian landscape during the Wisconsinian glaciation, J. Geophys. Res., 113, F01011, doi:10.1029/2007JF000838.

Person, M., V. Bense, D. Cohen, and A. Banerjee (2012), Models of ice-sheet hydrogeologic interactions: A review, Geofluids, 12, 58–78.

References

Aitken, A. R. A., D. A. Young, F. Ferraccioli, P. G. Betts, J. S. Greenbaum, T. G. Richter, J. L. Roberts, D. D. Blankenship, and M. J. Siegert (2014), The subglacial geology of Wilkes Land, East Antarctica, Geophys. Res. Lett., 41, 2390–2400.

Alley, R. B., D. D. Blankenship, C. R. Bentley, and S. T. Rooney (1986), Deformation of Till beneath Ice Stream-B, West-Antarctica, Nature, 322(6074): 57-59.

Alley, R. B. (1989), Water-pressure coupling of sliding and bed deformation: I. Water system, J. Glaciol., 35(119), 108–118.

Bense, V. F., and M. A. Person (2008), Transient hydrodynamics within intercratonic sedimentary basins during glacial cycles, J. Geophys. Res., 113(F4), F04005, doi:10.1029/2007JF000969.

Blankenship, D. D., C. R. Bentley, S. T. Rooney and R. B. Alley (1986), Seismic Measurements Reveal a Saturated Porous Layer beneath an Active Antarctic Ice Stream, Nature 322(6074): 54- 57.

Blankenship, D. D., et al. (1993), Active volcanism beneath the West Antarctic ice sheet and implications for ice-sheet stability. Nature 361, 526–529.

Boger, S. D. (2011), Antarctica—Before and after Gondwana, Precam. Res., 19, 335–371, doi: 10.1016/j.gr.2010.09.003.

Boulton, G. S., T. Slot, K. Blessing, P. Glasbergen, T. Leijnse, and K. van Gijssel (1993), Deep circulation of groundwater in overpressured subglacial aquifers and it's geological consequences, Quat. Sci. Rev., 12, 739–745.

Boulton, G. S., P. B. Caban, and K. van Gijssel (1995), Groundwater flow beneath ice sheets: Part I—Large scale patterns, Quat. Sci. Rev., 14, 545–562.

British Antarctic Survey: Antarctica Overview Map, (2007), http://lima.usgs.gov/documents/LIMA_overview_map.pdf, accessed: 2016-03-19.

Breemer, C. H., P. U. Clark, and R. Haggerty (2002), Modeling the subglacial hydrology of the late Pleistocene Lake Michigan lobe, Laurentide Ice Sheet, Geol. Soc. Am. Bull., 114(6), 665–674.

Carson, C. J., S. McLaren, J. L. Roberts, S. D. Boger, and D. D. Blankenship (2013), Hot rocks in a cold place: high sub-glacial heat flow in East Antarctica, J. Geol. Soc. London., 171(1), 9–12.

Carter, S. P., D. D. Blankenship, D. A. Young, and J. W. Holt (2009), Using radar-sounding data to identify the distribution and sources of subglacial water: Application to Dome C, East Antarctica, J. Glaciol., 55(194), 1025–1040, doi:10.3189/002214309790794931.

Clarke, G. K. C., S. G. Collins, and D. E. Thompson (1984), Flow, thermal structure, and subglacial conditions of a surge-type glacier, Can. J. Earth Sci., 21, 232–240.

Clarke, G. K. C. (1987), Subglacial till: A physical framework for its properties and processes, J. Geophys. Res., 92, 9023–9037.

Creyts, T. T., and C. G. Schoof (2009), Drainage through subglacial water sheets, J. Geophys. Res., 114, F04008, doi:10.1029/2008JF001215.

Dalziel, I. W. D. (1991), Pacific margins of Laurentia and East Antarctica-Australia as a conjugate rift pair: Evidence and implications for an Eocambrian supercontinent, Geology, 19, 598–601.

Echelmeyer, K. (1987), Anomalous heat flow and temperatures associated with subglacial water flow, The Physical Basis of Ice Sheet Modelling (Proceedings of the Vancouver Symposium, August 1987). IAHS Publ. no. 170.

Fahnstock, M., W. Abdalati, I. Joughin, J. Brozena, and P. Gogineni (2001), High geothermal heat flow, basal melt and the origin of rapid ice flow in central Greenland, Science, 294, 2338–2342.

Ferraccioli, F., E. Armadillo, T. Jordan, E. Bozzo, and H. Corr (2009), Aeromagnetic exploration over the East Antarctic Ice Sheet: A new view of the Wilkes Subglacial Basin, Tectonophysics, 478(1-2), 62–77.

Flowers, G. E., S. J. Marshall, H. Björnsson, and G. K. C. Clarke (2005), Sensitivity of Vatnajökull ice cap hydrology and dynamics to climate warming over the next 2 centuries, J. Geophys. Res. Earth Surf., 110(F2), F02011.

Flowers, G. E. (2015), Modelling water flow under glaciers and ice sheets, Proc. A, (471).

Fox, D. (2010), Could East Antarctica be headed for big melt?, Science, 328(June), 1630–1631.

Frederick, B. C. (2015), Submarine Sedimentary Basin Analyses for the Aurora and Wilkes Subglacial Basins and the Sabrina Coast Continental Shelf, East Antarctica, Ph.D. dissertation, Univ. of Texas, Austin, Texas, USA.

Fretwell, P., et al. (2013), Bedmap2: Improved ice bed, surface and thickness datasets for Antarctica, The Cryosphere, 7, 375–393, doi:10.5194/tc-7-375-2013.

Gallagher, S. J., G. Villa, R. N. Drysdale, B. S. Wade, H. Scher, Q. Li, M. W. Wallace, and G. R. Holdgate (2013), A near-field sea level record of East Antarctic Ice Sheet instability from 32 to 27 Myr, Paleoceanography, 28, doi: 10.1029/2012PA002326

Gibson, G.M., J.M. Totterdell, L.T. White, C.M. Mitchell, A.R. Stacey, M.P. Morse, and A. Whitaker (2013), Pre-existing basement structure and its influence on continental rifting and fracture zone development along Australia's southern rifted margin, J. Geol. Soc., 170, 365–377.

Glen, J.W., (1955), The creep of polycrystalline ice, Proc. Roy. Soc. Lond. A228 (1175), 519–538.

Goeller, S., M. Thoma, K. Grosfeld, and H. Miller (2012), A balanced water layer concept for subglacial hydrology in large scale ice sheet models, The Cryosphere, 6(6), 5225–5253, doi:10.5194/tcd-6-5225-2012.

Gooch, B. T., D. A. Young, and D. D. Blankenship (2016), Potential groundwater and heterogeneous heat source contributions to ice sheet dynamics in critical submarine basins of East Antarctica, Geochem. Geophys. Geosyst., 17, doi:10.1002/2015GC006117.

Gooch, B.T., S. P. Carter, O. Ghattas, D. A. Young, and D. D. Blankenship (in review), Groundwater dominance in the subglacial hydrology of ice sheet interiors: example at Dome C, East Antarctica, The Cryosphere Discuss.

Gooch, B.T., M. Rückamp, D. A. Young, and D. D. Blankenship (in preparation), Groundwater impact on the Totten Glacier Catchment basal water system: Results of a thermomechnical ice sheet model, J. Geophy. Res. Earth Surf.

Goodge, J. W., and C. M. Fanning (2010), Composition and age of the East Antarctic Shield in eastern Wilkes Land determined by proxy from Oligocene-Pleistocene glaciomarine sediment and Beacon Supergroup sandstones, Antarctica, Geological Society of America Bulletin, 122(7-8), 1135–1159, doi:10.1130/B30079.1.

Goodge, J. W., C. M. Fanning, D. M. Brecke, K. J. Licht, and E. F. Palmer (2010), Continuation of the Laurentian Grenville Province across the Ross Sea Margin of East Antarctica, The Journal of Geology, 118(6), 601–619, doi:10.1086/656385.

Goodge, J. W., and C. A. Finn (2010), Glimpses of East Antarctica: Aeromagnetic and satellite magnetic view from the central Transantarctic Mountains of East Antarctica, Journal of Geophysical Research, 115(B9), B09103, doi:10.1029/2009JB006890

Hewitt, I. (2011), Modelling distributed and channelized subglacial drainage: The spacing of channels, J. Glaciol., 57(202), 302–314, doi:10.3189/002214311796405951.

Kingslake J, and F. Ng (2013), Modelling the coupling of flood discharge with glacier flow during jökulhlaups, Ann. Glaciol. 54, 25–31, doi:10.3189/2013AoG63A331.

Le Brocq, A., A. Payne, M. Siegert, and R. Alley (2009), A subglacial water-flow model for West Antarctica, J. Glaciol., 55(193), 879–888.

Lemieux, J. M., E. A. Sudicky, W. R. Peltier, and L. Tarasov (2008), Dynamics of groundwater recharge and seepage over the Canadian landscape during the Wisconsinian glaciation, J. Geophys. Res. Earth Surf., 113(F1), F01011.

Li, X., B. Sun, M. J. Siegert, R. G. Bingham, X. Tang, D. Zhang, X. Cui, and X. Zhang (2010), Characterisation of subglacial landscapes by a two-parameter roughness index, J. Glaciol., 56, 831–836, doi:10.3189/ 002214310794457326.

Livingstone, S. J., C. D. Clark, J. Woodward, and J. Kingslake (2013), Potential subglacial lake locations and meltwater drainage pathways beneath the Antarctic and Greenland ice sheets, The Cryosphere, 7(6), 1721–1740, doi:10.5194/tc-7-1721-2013.

Lliboutry, L. (1968), General theory of subglacial cavitation and sliding of temperate glaciers. J. Glaciol., 7(49), 21-58.

Llubes, M., C. Lanseau, and F. Remy (2006), Relations between basal condition, subglacial hydrological networks and geothermal flux in Antarctica, Earth Planet. Sci. Lett., 241(3-4), 655–662, doi:10.1016/j.epsl.2005.10.040.

McLaren, S., M. Sandiford, M. Hand, N. Neumann, L. Wyborn, and I. Bastrakova (2003), The hot southern continent; heat flow and heat production in Australian Proterozoic terranes, Spec. Pap. - Geol. Soc. Am., 372, 157–167.

Mellor, M. and R. Testa (1969). Effect of temperature on the creep of ice. Journal of Glaciology, 8:131–145.

Neuzil, C. E. (2012), Hydromechanical effects of continental glaciation on groundwater systems, Geofluids, 12(1), 22-37.

Nye, J. F. (1976) Water flow in glaciers: Jökulhlaups, tunnels and veins, J. Glaciol., 17, 181–207.

Pattyn, F. (2010), Antarctic subglacial conditions inferred from a hybrid ice sheet/ice stream model, Earth Planet. Sci. Lett., 295(3-4), 451–461, doi:10.1016/j.epsl.2010.04.025.

Pattyn, F., S. Carter, and M. Thoma (2015), Advances in modelling subglacial lakes and their interaction with the Antarctic ice sheet, Phil. Trans. R. Soc.

Person, M., B. Dugan, J. B. Swenson, L. Urbano, C. Stott, J. Taylor, M. Willett (2003) Pleistocene hydrogeology of the Atlantic continental shelf, New England. Geo. Soc. of America Bulletin, 115, 1324–43.

Person, M., J. McIntosh, V. Bense, and V. H. Remenda (2007), Pleistocene hydrology of North America: The role of ice sheets in reorganizing groundwater flow systems, Rev. Geophys., 45(3), RG3007.

Person, M., V. Bense, D. Cohen, and A. Banerjee (2012), Models of ice-sheet hydrogeologic interactions: A review, Geofluids, 12(1), 58–78.

Piotrowski, J. (1997), Subglacial hydrology in north-western Germany during the last glaciations: Groundwater flow, tunnel valleys and hydrological cycles, Quat. Sci. Rev., 16, 169–185.

Rémy, F., T. Laurent, B. Legresy, A. Forieri, C. Bianchi, and I. E. Tabacco (2003), Lakes and subglacial hydrological networks around Dome C, East Antarctica, Ann. Glaciol., 37, 252–256.

Röthlisberger, H. (1972), Water pressure in intra- and subglacial channels, J. Glaciol., 11(62), 177–203.

Schoof, C. (2010), Ice-sheet acceleration driven by melt supply variability, Nature, 468(7325), 803–806, doi:10.1038/nature09618.

Schoof, C., I. J. Hewitt, and M. A. Werder (2012), Flotation and free surface flow in a model for subglacial drainage. Part 1. Distributed drainage, Journal of Fluid Mechanics, 702, 126–156, doi:10.1017/jfm.2012.165.

Shepard, M. K., B. A. Campbell, M. H. Bulmer, T. G. Farr, L. R. Gaddis, and J. J. Plaut (2001), The roughness of natural terrain: A planetary and remote sensing perspective, J. Geophys. Res., 106, 32,777–32,795.

Shreve, R. L. (1972), Movement of water in glaciers, J. Glaciol., 11(62), 205–214.

Siegert, M. J., J. P. Taylor, and J. Antony (2005), Spectral roughness of subglacial topography and implications for former ice-sheet dynamics in East Antarctica, Global Planet. Change, 45, 249–263.

Singhal, B. B. S., and R. P. Gupta (2010), Applied hydrogeology of fractured rocks (Vol. 430). New York: Springer.

Stearns, L., B. Smith, and G. Hamilton (2008), Increased flow speed on a large East Antarctic outlet glacier caused by subglacial floods, Nat. Geosci., 1(12), 827–831, doi:10.1038/ngeo356.

Sykes J, S. Normani, and Y. Yin (2011), OPG's deep geologic repository for low and intermediate level nuclear waste, NWMO DGR-TR- 2011-16, 256 P.

Tulaczyk, S., W. B. Kamb, and H. F. Engelhardt (2000), Basal mechanics of ice stream B, West Antarctica 2. Undrained plastic bed model, J. Geophys. Res, 105, 483–494.

van Weert, F. H. A., K. van Gijssel, A. Leijnse, and G. S. Boulton (1997), The effects of Pleistocene glaciations on the geohydrological system of northwest Europe, J. Hydrol., 195(1–4), 137–159.

Veevers, J. J., and A. Saeed (2011), Age and composition of Antarctic bedrock reflected by detrital zircons, erratics, and recycled microfossils in the Prydz Bay-Wilkes Land-Ross Sea-Marie Byrd Land sector (70°–240°E), Gondwana Res., doi: 10.1016/j.gr.2011.03.007.

Walder, J. (1986), Hydraulics of subglacial cavities, J. Glaciol., 32(112), 439–445.

Walder, J. S., and A. Fowler (1994), Channelized subglacial drainage over a deformable bed, J. Glaciol., 40(134), 3–15.

Weertman, J. (1966), Effect of a basal water layer on the dimensions of ice sheets, J. Glaciol., 6(44), 191–207.

Weertman, J. (1972), General theory of water flow at the base of a glacier or ice sheet, Rev. Geophys., 10(1), 287–333, doi:10.1029/RG010i001p00287.

Werder, M. A., I. J. Hewitt, C. G. Schoof, and G. E. Flowers (2013), Modeling channelized and distributed subglacial drainage in two dimensions, J. Geophys. Res. Earth Surf., 118, 2140–2158, doi:10.1002/jgrf.20146.

Williams, R.S., and D. K. Hall (1993), Glaciers, in Atlas of Satellite Observations Related to Global Change, R. J. Gurney, J.L. Foster and C. L. Parkinson, Cambridge University Press, London, 401-422.

Wingham, D. J., M. J. Siegert, A. Shepherd, and A. S. Muir (2006), Rapid discharge connects Antarctic subglacial lakes, Nature, 440, 1033–1036, doi:10.1038/nature04660.

Wright, A. P., et al. (2012), Evidence of a hydrological connection between the ice divide and ice sheet margin in the Aurora Subglacial Basin, East Antarctica, J. Geophys. Res., 117, F01033, doi:10.1029/2011JF002066.

Wright, A. P., D. A. Young, J. L. Bamber, J. A. Dowdeswell, A. J. Payne, D. D. Blankenship, and M. J. Siegert (2014), Subglacial hydrological connectivity within the Byrd Glacier catchment, East Antarctica, J. Glaciol., 60(220), 345–352, doi:10.3189/2014JoG13J014.

Young, D. A., et al. (2011), A dynamic early East Antarctic Ice Sheet suggested by ice-covered fjord landscapes, Nature, 474(7349), 72–75.

Alley, R. B. (1989), Water-pressure coupling of sliding and bed deformation, I, Water system, J. Glaciol., 35, 108–118.

Athy, L. F. (1930), Density, porosity, and compaction of sedimentary rocks, AAPG Bull., 14, 1– 23.

Boulton, G. S., and A. S. Jones (1979), Stability of temperate ice sheets resting on beds of deformable sediment, J. Glaciol., 24, 29–43.

Boulton, G. S., P. E. Caban, and K. Van Gijssel (1995), Groundwater flow beneath ice sheets: part 1—Large scale patterns, Quat. Sci. Rev., 14, 545–562.

Boulton GS, R. Lunn, P. Vidstrand, and S. Zatsepin (2007), Subglacial drainage by groundwater–channel coupling, and the origin of esker systems: Part 2 – theory and simulation of a modern system, Quat. Sci. Rev., 26, 1091–1105.

Carter, S. P., D. D. Blankenship, M. E. Peters, D. A. Young, J. W. Holt, and D. L. Morse (2007), Radar-based subglacial lake classification in Antarctica, Geochem. Geophys. Geosyst., 8, Q03016, doi:10.1029/2006GC001408.

Carter, S. P., D. D. Blankenship, D. A. Young, M. E. Peters, J. W. Holt, and M. J. Siegert (2009a), Dynamic distributed drainage implied by the flow evolution of the 1996–1998 Adventure Trench subglacial lake discharge, Earth Planet. Sci. Lett., 283(1–4), 24–37, doi:10.1016/j.epsl.2009.03.019.

Carter, S. P., D. D. Blankenship, D. A. Young, and J. W. Holt (2009b), Using radar-sounding data to identify the distribution and sources of subglacial water: Application to Dome C, East Antarctica, J. Glaciol., 55(194), 1025–1040, doi:10.3189/002214309790794931.

Carter, S. P., H. A. Fricker, D. D. Blankenship, J. V. Johnson, W. H. Lipscomb, S. F. Price, and D. A. Young (2011), Modeling 5 years of subglacial lake activity in the MacAyeal Ice Stream (Antarctica) catchment through assimilation of ICESat laser altimetry, J. Glaciol., 57(206), 1098–1112.

Carter, S. P., H. A. Fricker, and M. R. Siegfried (2015), Active lakes in Antarctica survive on a sedimentary substrate – Part 1: Theory, The Cryosphere Discuss., 9, 2053-2099, doi:10.5194/tcd-9-2053-2015.

Christianson, K., R. W. Jacobel, H. J. Horgan, S. Anandakrishnan, and R. B. Alley (2012), Subglacial Lake Whillans—Ice-penetrating radar and GPS observations of a shallow active reservoir beneath a West Antarctic ice stream, Earth Planet. Sci. Lett., 331-332, 237–245, doi:10.1016/j.epsl.2012.03.013.

Creyts, T. T., and C. G. Schoof (2009), Drainage through subglacial water sheets, J. Geophys. Res., 114, F04008, doi:10.1029/2008JF001215.

Dupain-Triel, J. L. (1791), La France considérée dans les différentes hauteurs de ses plaines: ouvrage spécialement destiné al'instruction de la jeunesse, (BN, Cartes et Plans, map No. Ge. D.15126) Hérault, Paris.

Flowers, G. E., and G. K. C. Clarke (2002), A multicomponent coupled model of glacier hydrology: 1. Theory and synthetic examples, J. Geophys. Res., 107(B11), 2287, doi:10.1029/2001JB001122.

Flowers, G. E. (2015), Modelling water flow under glaciers and ice sheets, Proc. A, (471).

Forieri, A., L. Zuccoli, A. Bini, A. Zirizzotti, F. Remy, and I. E. Tabacco (2004), New bedrock map of Dome C, Antarctica, and morphostructural interpretation of the area, Ann. Glaciol., 39(1), 321-325.

Frederick, B. C. (2015), Submarine Sedimentary Basin Analyses for the Aurora and Wilkes Subglacial Basins and the Sabrina Coast Continental Shelf, East Antarctica, Ph.D. dissertation, Univ. of Texas, Austin, Texas, USA.

Fretwell, P., et al. (2013), Bedmap2: Improved ice bed, surface and thickness datasets for Antarctica, The Cryosphere, 7, 375–393, doi:10.5194/tc-7-375-2013.

Fricker, H. A., et al. (2007), An active subglacial water system in West Antarctica mapped from space, Science, 315(5818), 1544–1548, doi:10.1126/science.1136897.

Hauke, G., and T. J. R. Hughes (1994), A unified approach to compressible and incompressible flows, Computer Methods in Applied Mechanics and Engineering, 113(3), 389-395.

Huybrechts, P. (1993), Glaciological modelling of the late cenozoic East Antarctic Ice Sheet: Stability or dynamism?, Geogr. Ann., 75A(4), 221–238.

Jiang, X.-W., L. Wan, X.-S. Wang, S. Ge, and J. Liu (2009), Effect of exponential decay in hydraulic conductivity with depth on regional groundwater flow, Geophys. Res. Lett., 36, L24402, doi:10.1029/2009GL041251.

Kyrke-Smith, T. M., R. F. Katz, and A. C. Fowler (2014), Subglacial hydrology and the formation of ice streams, Proc. Phys. Soc. London, Sect. A, 470, 20,130,494, doi:10.1098/rspa.2013.0494.

Le Brocq, A. M., A. J. Payne, and M. J. Siegert (2006), West Antarctic balance calculations: Impact of flux-routing algorithm, smoothing and topography, Comput. Geosci., 32(10), 1780–1795.

Le Brocq, A., A. Payne, M. Siegert, and R. Alley (2009), A subglacial water-flow model for West Antarctica, J. Glaciol., 55(193), 879–888.

Lemieux, J.-M., E. Sudicky, W. Peltier, and L. Tarasov (2008), Dynamics of groundwater recharge and seepage over the Canadian landscape during the Wisconsinian glaciation, J. Geophys. Res., 113, F01011, doi:10.1029/2007JF000838.

Parrenin, F., et al. (2007), The EDC3 chronology for the EPICA dome C ice core, Clim. Past, 3(3), 485–497.

Pattyn, F. (2010), Antarctic subglacial conditions inferred from a hybrid ice sheet/ice stream model, Earth Planet. Sci. Lett., 295(3-4), 451–461, doi:10.1016/j.epsl.2010.04.025.

Person, M., J. McIntosh, V. Bense, and V. Remenda (2007), Pleistocene hydrology of North America: The role of ice sheets in reorganizing groundwater systems, Rev. Geophys., 45, RG3007, doi:10.1029/2006RG000206.

Person, M., V. Bense, D. Cohen, and A. Banerjee (2012), Models of ice-sheet hydrogeologic interactions: A review, Geofluids, 12, 58–78.

Peters, M. E., D. D. Blankenship, S. P. Carter, S. D. Kempf, D. A. Young, and J. W. Holt (2007), Along-track focusing of airborne radar sounding data from West Antarctica for improving basal reflection analysis and layer detection, IEEE Trans. Geosci. Remote Sens., 45(9), 2725–2736, doi:10.1109/TGRS.2007.897416.

Piotrowski, J. (1997), Subglacial hydrology in north-western Germany during the last glaciations: Groundwater flow, tunnel valleys and hydrological cycles, Quat. Sci. Rev., 16, 169–185.

Schroeder, D. M., D. D. Blankenship, D. A. Young, A. E. Witus, and J. B. Anderson (2014), Airborne radar sounding evidence for deformable sediments and outcropping

bedrock beneath Thwaites Glacier, West Antarctica, Geophys. Res. Lett., 41, 7200–7208, doi:10.1002/2014GL061645.

Sclater, J. G., and P. Christie (1980), Continental stretching: An explanation of the post-mid-cretaceous subsidence of the central North Sea basin, J. Geophys. Res. Solid Earth, 85(B7), 3711-3739.

Shapiro, N. M., and M. H. Ritzwoller (2004), Inferring surface heat flux distributions guided by a global seismic model: Particular application to Antarctica, Earth Planet. Sci. Lett., 223, 213–224.

Shreve, R. L. (1972), Movement of water in glaciers, J. Glaciol., 11(62), 205–214.

Siegert, M. J., J. P. Taylor, and J. Antony (2005), Spectral roughness of subglacial topography and implications for former ice-sheet dynamics in East Antarctica, Global Planet. Change, 45, 249–263.

Siegert, M. J., A. Le Brocq, and A. J. Payne (2007), Hydrological connections between Antarctic subglacial lakes and the flow of water beneath the East Antarctic Ice Sheet, in Glacial Sedimentary Processes and Products, Spec. Publ., vol 39, edited by M. J. Hambrey et al., pp. 3–10, Int. Assoc. of Sedimentol., Malden, Mass.

Siegert, M. J., N. Ross, H. Corr, B. Smith, T. Jordan, R. G. Bingham, F. Ferraccioli, D. M. Rippin, and A. Le Brocq (2014), Boundary conditions of an active West Antarctic subglacial lake: implications for storage of water beneath the ice sheet, The Cryosphere, 8 (1), 15–24, doi:10.5194/tc-8-15-2014.

Singha, K., and S. P. Loheide II (2011), Linking physical and numerical modelling in hydrogeology using sand tank experiments and COMSOL Multiphysics, Int. J. Sci. Educ., 33(4), 547–571.

Singhal, B. B. S., and R. P. Gupta (2010), Applied Hydrogeology of Fractured Rocks, Kluwer Acad., Dordrecht, The Netherlands.

Stauffer, P. H. (2006), Flux flummoxed: A proposal for consistent usage, Ground water, 44(2), 125-128.

Stearns, L., B. Smith, and G. Hamilton (2008), Increased flow speed on a large East Antarctic outlet glacier caused by subglacial floods, Nat. Geosci., 1(12), 827–831, doi:10.1038/ngeo356.

Tikku, A. A., et al. (2005), Influx of meltwater to subglacial Lake Concordia, East Antarctica, J. Glaciol., 51(172), 96–104.

Weertman, J. (1966), Effect of a basal water layer on the dimensions of ice sheets, J. Glaciol., 6(44), 191–207.

Wingham, D. J., M. J. Siegert, A. Shepherd, and A. S. Muir (2006), Rapid discharge connects Antarctic subglacial lakes, Nature, 440, 1033–1036, doi:10.1038/nature04660.

Wright, A., and M. Siegert (2012), A fourth inventory of Antarctic subglacial lakes Antarctic, Science, 24(06), 659–664, doi:10.1017/S095410201200048X.

Wright, A. P., et al. (2012), Evidence of a hydrological connection between the ice divide and ice sheet margin in the Aurora Subglacial Basin, East Antarctica, J. Geophys. Res., 117, F01033, doi:10.1029/2011JF002066.

Wright, A. P., D. A. Young, J. L. Bamber, J. A. Dowdeswell, A. J. Payne, D. D. Blankenship, and M. J. Siegert (2014), Subglacial hydrological connectivity within the Byrd Glacier catchment, East Antarctica, J. Glaciol., 60(220), 345–352, doi:10.3189/2014JoG13J014.

Young, D. A., et al. (2011), A dynamic early East Antarctic Ice Sheet suggested by ice-covered fjord landscapes, Nature, 474(7349), 72–75.

Carter, S. P., D. D. Blankenship, D. A. Young, and J. W. Holt (2009b), Using radar-sounding data to identify the distribution and sources of subglacial water: Application to Dome C, East Antarctica, J. Glaciol., 55(194), 1025–1040, doi:10.3189/002214309790794931.

Fretwell, P., et al. (2013), Bedmap2: Improved ice bed, surface and thickness datasets for Antarctica, The Cryosphere, 7, 375–393, doi:10.5194/tc-7-375-2013.

Aitken, A. R. A., D. A. Young, F. Ferraccioli, P. G. Betts, J. S. Greenbaum, T. G. Richter, J. L. Roberts, D. D. B., and M. J. Siegert (2014), The subglacial geology of Wilkes Land, East Antarctica, Geophys. Res. Lett., 41, 2390–2400.

Alley, R. B. (1989), Water-pressure coupling of sliding and bed deformation: I. Water system, J. Glaciol., 35(119), 108–118.

Athy, L. F. (1930), Density, porosity, and compaction of sedimentary rocks, AAPG Bulletin, 14(1), 1-24.

Bamber, J. L., R. L. Layberry, and S. P. Gogineni (2001), A new ice thickness and bed data set for the Greenland ice sheet: 1. Measurement, data reduction, and errors, J. Geophys. Res., 106(D24), 33773-33780.

Beardsmore, G. R., and J. P. Cull (2001), Crustal heat flow: a guide to measurement and modelling. Cambridge University Press.

Bense, V. F., and M. A. Person (2008), Transient hydrodynamics within intercratonic sedimentary basins during glacial cycles, J. Geophys. Res., 113, F04005, doi:10.1029/2007JF000969.

Bindschadler, R., H. Choi, and ASAID Collaborators (2011), High-resolution Image-derived Grounding and Hydrostatic Lines for the Antarctic Ice Sheet, National Snow and Ice Data Center, Boulder, Colo., doi:10.7265/N56T0JK2.

Blankenship, D. D., C. R. Bentley, S. T. Rooney, and R. B. Alley (1986), Seismic measurements reveal a saturated porous layer beneath an active Antarctic ice stream, Nature, 322, 54–57.

Blankenship, D. D., R. E. Bell, S. M. Hodge, J. M. Brozena, J. C. Behrendt, and C. A. Finn (1993), Active volcanism beneath the West Antarctic ice sheet and implications for ice-sheet stability, Nature, 361, 526–529.

Blankenship, D. D., D. L. Morse, C. A. Finn, R. E. Bell, M. E. Peters, S. D. Kempf, S. M. Hodge, M. Studinger, J. C. Behrendt, and J. M. Brozena (2001), Geologic Controls on the Initiation of Rapid Basal Motion for West Antarctic Ice Streams: A Geophysical Perspective Including New Airborne Radar Sounding and Laser Altimetry Results, in The West Antarctic Ice Sheet: Behavior and Environment (eds R. B. Alley and R. A. Bindschadler), American Geophysical Union, Washington, D. C.

Bohlander, J., and T. Scambos (2007), Antarctic coastlines and grounding line derived from MODIS Mosaic of Antarctica (MOA), Boulder, Colorado USA: National Snow and Ice Data Center, Digital media

Boulton, G. (2010), Drainage pathways beneath ice sheets and their implications for ice sheet form and flow: the example of the British Ice Sheet during the Last Glacial Maximum. J. Quaternary Sci., 25: 483–500.

Carson, C. J., and M. Pittard (2012), A Reconaissance Crustal Heat Production Assessment of the Australian Antarctic Territory (AAT). Geoscience Australia.

Carson, C. J., S. McLaren, J. L. Roberts, S. D. Boger, and D. D. Blankenship (2013), Hot rocks in a cold place: high sub-glacial heat flow in East Antarctica, J. Geol. Soc. London., 171(1), 9–12.

Champion, D. C., A. R. Budd, M. S. Hazell, and A. Sedgmen, (2007), OZCHEM National Whole Rock Geochemistry Dataset, Geoscience Australia.

Christoffersen, P., M. Bougamont, S. P. Carter, H. A. Fricker, and S. Tulaczyk (2014), Significant groundwater contribution to Antarctic ice streams hydrologic budget, Geophys. Res. Lett., 41, 1–8.

Clarke, G. K. C., S. G. Collins, and D. E. Thompson (1984), Flow, thermal structure, and subglacial conditions of a surge-type glacier, Can. J. Earth Sci., 21, 232–240.

Comiso, J. C. (2000), Variability and trends in Antarctic surface temperatures from in situ and satellite infrared measurements. Journal of Climate, 13(10), 1674-1696.

Cutler, P. M., D. R. MacAyeal, D. M. Mickelson, B. R. Parizek, and P. M. Colgan (2000), A numerical investigation of ice-lobe-permafrost interaction around the southern Laurentide ice sheet, J. Glaciol., 46(153), 311–325.

Drewry, D. (1976), Sedimentary basins of the East Antarctic craton from geophysical evidence. Tectonophysics, 36(1), 301-314.

Echelmeyer, K. (1987), Anomalous heat flow and temperatures associated with subglacial water flow, The Physical Basis of Ice Sheet Modelling (Proceedings of the Vancouver Symposium, August 1987). IAHS Publ. no. 170.

Ferraccioli, F., E. Armadillo, T. Jordan, E. Bozzo, and H. Corr (2009), Aeromagnetic exploration over the East Antarctic Ice Sheet: A new view of the Wilkes Subglacial Basin, Tectonophysics, 478(1-2), 62–77.

Flowers, G. E., S. J. Marshall, H. Björnsson, and G. K. C. Clarke (2005), Sensitivity of Vatnajökull ice cap hydrology and dynamics to climate warming over the next 2 centuries, J. Geophys. Res. Earth Surf., 110(F2), F02011.

Fox Maule, C., M. E. Purucker, N. Olsen, and K. Mosegaard (2005), Heat flux anomalies in Antarctica revealed by satellite magnetic data., Science, 309(5733), 464–467.

Frederick, B. C. (2015), Submarine Sedimentary Basin Analyses for the Aurora and Wilkes Subglacial Basins and the Sabrina Coast Continental Shelf, East Antarctica, Ph.D. dissertation, Univ. of Texas, Austin, Texas, USA.

Fretwell, P., et al. (2013), Bedmap2: Improved ice bed, surface and thickness datasets for Antarctica, Cryosphere, 7(1), 375–393.

Gleeson, T., L. Smith, N. Moosdorf, J. Hartmann, H. H. Dürr, A. H. Manning, L. P. H. van Beek, and A. M. Jellinek (2011), Mapping permeability over the surface of the Earth, Geophys. Res. Lett., 38, L02401.

Gleeson, T., N. Moosdorf, J. Hartmann, and L. P. H. van Beek (2014), A glimpse beneath earth's surface: GLobal HYdrogeology MaPS (GLHYMPS) of permeability and porosity, Geophys. Res. Lett., 41, 3891–3898.

Grasby, S., K. Osadetz, R. Betcher, and F. Render (2000), Reversal of the regional-scale flow system of the Williston basin in response to Pleistocene glaciation, Geology, 28(1986), 635–638.

Grasby, S. E., and Z. Chen (2005), Subglacial recharge into the western Canada sedimentary basin—Impact of Pleistocene glaciation on basin hydrodynamics, Geol. Soc. Am. Bull., 117(3/4), 500–514.

Hughes, T., A. Sargent, and J. Fastook (2011), Ice-bed coupling beneath and beyond ice streams: Byrd Glacier, Antarctica, J. Geophys. Res. Earth Surf., 116(F3), 1–17.

Huybrechts, P., and J. Oerlemans (1988), Evolution of the East Antarctic ice sheet: A numerical study of thermo-mechanical response patterns with changing climate, Ann. Glaciol., 11, 52–59.

Ingebritsen, S. E., C. E. Neuzil, and W. E. Sanford (2006), Groundwater in geologic processes, Cambridge University Press.

Jaupart, C. (1986), On the average amount and vertical distribution of radioactivity in the continental crust, in Burrus, J., ed., Thermal Modeling in Sedimentary Basins: ´Editions Technip, Paris, 33–47.

Jiang, X. W., L. Wan, X. S. Wang, S. Ge, and J. Liu (2009), Effect of exponential decay in hydraulic conductivity with depth on regional groundwater flow, Geophys. Res. Lett., 36, L24402.

Jiang, X. W., L. Wan, M. B. Cardenas, S. Ge, and X. S. Wang (2010), Simultaneous rejuvenation and aging of groundwater in basins due to depth-decaying hydraulic conductivity and porosity, Geophys. Res. Lett., 37, L05403.

Jordan, T. A., F. Ferraccioli, E. Armadillo, and E. Bozzo (2013), Crustal architecture of the Wilkes Subglacial Basin in East Antarctica, As revealed from airborne gravity data, Tectonophysics, 585, 196–206.

Lachenbruch, A. H. (1970), Crustal temperature and heat production: Implications of the linear heat-flow relation, J. Geophys. Res., 75(17), 3291-3300.

Lemieux, J. M., E. A. Sudicky, W. R. Peltier, and L. Tarasov (2008a), Dynamics of groundwater recharge and seepage over the Canadian landscape during the Wisconsinian glaciation, J. Geophys. Res. Earth Surf., 113(F1), F01011.

Lemieux, J. M., E. A. Sudicky, W. R. Peltier, and L. Tarasov (2008b), Simulating the impact of glaciations on continental groundwater flow systems: 1. Relevant processes and model formulation, J. Geophys. Res. Earth Surf., 113, F03017.

Lowe, A. L., and J. B. Anderson (2003), Evidence for abundant subglacial meltwater beneath the paleo-ice sheet in Pine Island Bay, Antarctica, J. Glaciol., 49(164), 125–138.

Mackintosh, A., et al. (2011), Retreat of the East Antarctic ice sheet during the last glacial termination, Nat. Geosci., 4(3), 195–202.

McIntosh, J. C., G. Garven, and J. S. Hanor (2011), Impacts of Pleistocene glaciation on large-scale groundwater flow and salinity in the Michigan Basin, Geofluids, 11(1), 18–33.

McKenna, T. E., and J. M. Sharp Jr. (1998), Radiogenic heat production in sedimentary rocks of the gulf of Mexico basin, south Texas, AAPG Bull., 82, 484–496.

McLaren, S., M. Sandiford, M. Hand, N. Neumann, L. Wyborn, and I. Bastrakova (2003), The hot southern continent; heat flow and heat production in Australian Proterozoic terranes, Spec. Pap. - Geol. Soc. Am., 372, 157–167.

Mellor, G. L., and L. Kantha (1989), An ice-ocean coupled model, J. Geophys. Res., 94(89), 10937–10954.

Mengel, M., and A. Levermann (2014), Ice plug prevents irreversible discharge from East Antarctica, Nat. Clim. Chang., 4(May), 451–455.

Mosley-Thompson, E., J. F. Paskievitch, A. J. Gow, and L. G. Thompson (1999), Late 20th Century increase in South Pole snow accumulation, J. Geophys. Res., 104, 3877-3886.

Neuzil, C. E. (2012), Hydromechanical effects of continental glaciation on groundwater systems, Geofluids, 12(1), 22-37.

Neuzil, C. E. (2015), Interpreting fluid pressure anomalies in shallow intraplate argillaceous formations. Geophys. Res. Lett., 42, 4801–4808. doi: 10.1002/2015GL064140.

Pattyn, F. (2008), Investigating the stability of subglacial lakes with a full Stokes ice-sheet model, J. Glaciol., 54(185), 353–361.

Pattyn, F. (2010), Antarctic subglacial conditions inferred from a hybrid ice sheet/ice stream model, Earth Planet. Sci. Lett., 295(3-4), 451–461.

Person, M., J. McIntosh, V. Bense, and V. H. Remenda (2007), Pleistocene hydrology of North America: The role of ice sheets in reorganizing groundwater flow systems, Rev. Geophys., 45(3), RG3007.

Person, M., V. Bense, D. Cohen, and A. Banerjee (2012), Models of ice-sheet hydrogeologic interactions: A review, Geofluids, 12(1), 58–78.

Petrunin, A. G., I. Rogozhina, A. P. M. Vaughan, I. T. Kukkonen, M. K. Kaban, I. Koulakov, and M. Thomas (2013), Heat flux variations beneath central Greenland's ice due to anomalously thin lithosphere, Nat. Geosci., 6, 746–750, doi:10.1038/ngeo1898.

Piotrowski, J. (2006), Groundwater under ice sheets and glaciers, Glacier Sci. Environ. Chang., 50–60.

Piotrowski, J. A., P. Hermanowski, and A. M. Piechota (2009), Meltwater discharge through the subglacial bed and its land-forming consequences from numerical experiments in the Polish lowland during the last glaciation, Earth Surf. Process. Landforms, 34, 481–492.

Pollard, D., R. M. DeConto, and A. A. Nyblade (2005), Sensitivity of Cenozoic Antarctic ice sheet variations to geothermal heat flux, Glob. Planet. Change, 49(1-2), 63–74.

Pollard, D., R. M. Deconto, and R. B. Alley (2015), Potential Antarctic Ice Sheet retreat driven by hydrofracturing and ice cliff failure, Earth Planet. Sci. Lett., 412, 112–121.

Price, P. B., O. V Nagornov, R. Bay, D. Chirkin, Y. He, P. Miocinovic, A. Richards, K. Woschnagg, B. Koci, and V. Zagorodnov (2002), Temperature profile for glacial ice at the South Pole: implications for life in a nearby subglacial lake., Proc. Natl. Acad. Sci. U. S. A., 99(12), 7844–7847.

Rajaram, M., S. P. Anand, K. Hemant, and M. E. Purucker (2009), Curie isotherm map of Indian subcontinent from satellite and aeromagnetic data, Earth Planet. Sci. Lett., 281(3-4), 147–158.

Rignot, E., J. Mouginot, and B. Scheuchl (2011), Ice flow of the Antarctic Ice Sheet, Science, 333, 1427–1430.

Sandiford, M., and S. McLaren (2002), Tectonic feedback and the ordering of heat producing elements within the continental lithosphere, Earth Planet. Sci. Lett., 204, 133–150.

Schroeder, D. M., D. D. Blankenship, D. A. Young, and E. Quartini (2014), Evidence for elevated and spatially variable geothermal flux beneath the West Antarctic Ice Sheet, Proc. Natl. Acad. Sci., 111(25), 9070-9072.

Sclater, J. G., and P. Christie (1980), Continental stretching: An explanation of the post-mid-cretaceous subsidence of the central North Sea basin, J. Geophys. Res. Solid Earth, 85(B7), 3711-3739.

Shapiro, N. M., and M. H. Ritzwoller (2004), Inferring surface heat flux distributions guided by a global seismic model: Particular application to Antarctica, Earth Planet. Sci. Lett., 223(1-2), 213–224.

Shepard, M. K., B. A. Campbell, M. H. Bulmer, T. G. Farr, L. R. Gaddis, and J. J. Plaut (2001), The roughness of natural terrain: A planetary and remote sensing perspective, J. Geophys. Res., 106, 32777-32795.

Siegel, J., D. Lizarralde, B. Dugan, and M. Person (2014), Glacially generated overpressure on the New England continental shelf: Integration of full-waveform inversion and overpressure modeling, J. Geophys. Res, 119, 3393–3409.

Siegert, M. J., and J. A. Dowdeswell (1996), Spatial variations in heat at the base of the Antarctic ice sheet from analysis of the thermal regime above subglacial lakes, J. Glaciol., 42(142), 501–509.

Singhal, B. B. S., and R. P. Gupta (2010), Applied hydrogeology of fractured rocks (Vol. 430). New York: Springer.

Stauffer, P. H. (2006), Flux flummoxed: A proposal for consistent usage, Ground Water, 44(2), 125–128.

Studinger, M., R. E. Bell, W. R. Buck, G. D. Karner, and D. D. Blankenship (2004), Sub-ice geology inland of the Transantarctic Mountains in light of new aerogeophysical data, Earth Planet. Sci. Lett., 220(3-4), 391–408.

Sun, B., J. C. Moore, T. Zwinger, L. Zhao, D. Steinhage, X. Tang, D. Zhang, X. Cui, and C. Martín (2014), How old is the ice beneath Dome A, Antarctica?, The Cryosphere, 8, 1121–1128.

Thoma, M., K. Grosfeld, C. Mayer, and F. Pattyn (2012), Ice-flow sensitivity to boundary processes: A coupled model study in the Vostok Subglacial Lake area, Antarctica, Ann. Glaciol., 53(60), 173-180.

Turcotte, D. L., and G. Schubert (2002), Geodynamics, Cambridge University Press.

Van Liefferinge, B., and F. Pattyn (2013), Using ice-flow models to evaluate potential sites of million year-old ice in Antarctica, Clim. Past, 9(5), 2335–2345.

Waddington, E. (1987), Geothermal heat flux beneath ice sheets, The Physical Basis of Ice Sheet Modelling (Proceedings of the Vancouver Symposium, August 1987), IAHS Publ. no. 170.

Waples, D. W. (2001), A New Model for Heat Flow in Extensional Basins: Radiogenic Heat, Asthenospheric Heat, and the McKenzie Model, Nat. Resour. Res., 10(2), 227–238.

Wessel, P., and W. H. F. Smith (1996), A global, self-consistent, hierarchical, high-resolution shoreline database, J. Geophys. Res., 101(B4), 8741–8743.

Wilch, E., and T. J. Hughes (2000), Calculating basal thermal zones beneath the antarctic ice sheet, J. Glaciol., 46(153), 297-310.

Winkelmann, R., M. A. Martin, M. Haseloff, T. Albrecht, E. Bueler, C. Khroulev, and A. Levermann (2011), The Potsdam Parallel Ice Sheet Model (PISM-PIK) - Part 1: Model description, Cryosphere, 5(3), 715-726.

Wright, A., and M. Siegert (2012), A fourth inventory of Antarctic subglacial lakes, Antarct. Sci., 24(6), 659-664.

Young, D. A., et al. (2011), A dynamic early East Antarctic Ice Sheet suggested by ice-covered fjord landscapes, Nature, 474(7349), 72–75.

Zwally, H. J., M. B. Giovinetto, M. A. Beckley, and J. L. Saba (2012), Antarctic and Greenland drainage systems, GSFC Cryospheric Sciences Laboratory.

Bohlander, J., and T. Scambos (2007), Antarctic coastlines and grounding line derived from MODIS Mosaic of Antarctica (MOA), Boulder, Colorado USA: National Snow and Ice Data Center, Digital media.

Carson, C. J., S. McLaren, J. L. Roberts, S. D. Boger, and D. D. Blankenship (2013), Hot rocks in a cold place: high sub-glacial heat flow in East Antarctica, J. Geol. Soc. London., 171(1), 9–12.

Fretwell, P., et al. (2013), Bedmap2: Improved ice bed, surface and thickness datasets for Antarctica, Cryosphere, 7(1), 375–393.

McLaren, S., M. Sandiford, M. Hand, N. Neumann, L. Wyborn, and I. Bastrakova (2003), The hot southern continent; heat flow and heat production in Australian Proterozoic terranes, Spec. Pap. - Geol. Soc. Am., 372, 157–167.

Sandiford, M., and S. McLaren (2002), Tectonic feedback and the ordering of heat producing elements within the continental lithosphere, Earth Planet. Sci. Lett., 204, 133–150.

Waples, D. W. (2001), A New Model for Heat Flow in Extensional Basins: Radiogenic Heat, Asthenospheric Heat, and the McKenzie Model, Nat. Resour. Res., 10(2), 227–238.

Aitken, A. R. A., D. A. Young, F. Ferraccioli, P. G. Betts, J. S. Greenbaum, T. G. Richter, J. L. Roberts, D. D. B., and M. J. Siegert (2014), The subglacial geology of Wilkes Land, East Antarctica, Geophys. Res. Lett., 41, 2390–2400.

Aitken, A. R. A., et al. (in rev.) East Antarctic Ice Sheet bed erosion indicates repeated large-scale retreat and advance events, Nature.

Alley, R. B. (1996), Toward a hydrologic model for computerized ice-sheet simulations, Hydrol. Proc., 10, 649–660.

An, M., D. A. Wiens, Y. Zhao, M. Feng, A. A. Nyblade, M. Kanao, Y. Li, A. Maggi, and J. Lévêque (2015a), S-velocity model and inferred Moho topography beneath the Antarctic Plate from Rayleigh waves, J. Geophys. Res. Solid Earth, 120, 359–383, doi:10.1002/2014JB011332.

An, M., D. A. Wiens, Y. Zhao, M. Feng, A. Nyblade, M. Kanao, Y. Li, A. Maggi, and J.-J. Lévêque (2015b), Temperature, lithosphere-asthenosphere boundary, and heat flux beneath the Antarctic Plate inferred from seismic velocities, J. Geophys. Res. Solid Earth, 120, 8720–8742, doi:10.1002/2015JB011917.

Athy, L. F. (1930), Density, porosity, and compaction of sedimentary rocks, AAPG Bulletin, 14(1), 1-24.

Bamber, J. L., F. Ferraccioli, I. Joughin, T. Shepherd, D. M. Rippin, M. J. Siegert, and D. G. Vaughan (2006), East Antarctic ice stream tributary underlain by major sedimentary basin, Geology, 34, 33–36.

Beardsmore, G. R., and J. P. Cull (2001), Crustal heat flow: a guide to measurement and modelling. Cambridge University Press.

Bense, V. F., and M. A. Person (2008), Transient hydrodynamics within intercratonic sedimentary basins during glacial cycles, J. Geophys. Res., 113, F04005, doi:10.1029/2007JF000969.

Bindschadler, R., H. Choi, and ASAID Collaborators (2011), High-resolution Image-derived Grounding and Hydrostatic Lines for the Antarctic Ice Sheet, National Snow and Ice Data Center, Boulder, Colo., doi:10.7265/N56T0JK2.

Blankenship, D.D., S. P. Carter, J. W. Holt, D. L. Morse, M. E. Peters, and D. A. Young (2009), Antarctic Subglacial Lake Classification Inventory, Boulder, Colorado USA, National Snow and Ice Data Center, http://dx.doi.org/10.7265/N5CN71VX.

Boulton, G., & J. Hartikainen (2004), Thermo-hydro-mechanical impacts of coupling between glaciers and permafrost, Elsevier Geo-Engineering Book Series, 2, 293-298.

Boulton, G.S., R. Lunn, P. Vidstrand, and S. Zatsepin (2007), Subglacial drainage by groundwater–channel coupling, and the origin of esker systems: Part 2 – theory and simulation of a modern system, Quat. Sci. Rev., 26, 1091–1105.

Budd, W. F., and D. Jenssen (1987), Numerical modelling of the large-scale basal water flux under the West Antarctic Ice Sheet, in Dynamics of the West Antarctic Ice Sheet, edited by C. J. van der Veen, and J. Oerlemans, pp. 293–320, D. Reidel, Norwell, Mass.

Carson, C. J., S. McLaren, J. L. Roberts, S. D. Boger, and D. D. Blankenship (2013), Hot rocks in a cold place: high sub-glacial heat flow in East Antarctica, J. Geol. Soc. London., 171(1), 9–12.

Chen, J. L., C. R. Wilson, D. D. Blankenship, and B. D. Tapley (2009), Accelerated Antarctic ice loss from satellite gravity measurements, Nat. Geosci., 2(12), 859–862.

Clarke, G. K. C., S. G. Collins, and D. E. Thompson (1984), Flow, thermal structure, and subglacial conditions of a surge-type glacier, Can. J. Earth Sci., 21, 232–240.

Comiso, J. C. (2000), Variability and trends in Antarctic surface temperatures from in situ and satellite infrared measurements. Journal of Climate, 13(10), 1674-1696.

Cuffey, K., and W. S. B. Paterson (2010), The Physics of Glaciers, 4th ed., Elsevier, Burlington, Mass.

Cutler, P. M., D. R. MacAyeal, D. M. Mickelson, B. R. Parizek, and P. M. Colgan (2000), A numerical investigation of ice-lobe-permafrost interaction around the southern Laurentide ice sheet, J. Glaciol., 46(153), 311–325.

Drewry, D. (1976), Sedimentary basins of the East Antarctic craton from geophysical evidence. Tectonophysics, 36(1), 301-314.

Echelmeyer, K. (1987), Anomalous heat flow and temperatures associated with subglacial water flow, The Physical Basis of Ice Sheet Modelling (Proceedings of the Vancouver Symposium, August 1987). IAHS Publ. no. 170.

Flowers, G. E., S. J. Marshall, H. Björnsson, and G. K. C. Clarke (2005), Sensitivity of Vatnajökull ice cap hydrology and dynamics to climate warming over the next 2 centuries, J. Geophys. Res. Earth Surf., 110(F2), F02011.

Flowers, G. E. (2008), Subglacial modulation of the hydrograph from glacierized basins, Hydrol. Processes, 22, 3903–3918, doi:10.1002/hyp.7095.

Flowers, G. E. (2015), Modelling water flow under glaciers and ice sheets, Proc. A, (471).

Fox Maule, C., M. E. Purucker, N. Olsen, and K. Mosegaard (2005), Heat flux anomalies in Antarctica revealed by satellite magnetic data., Science, 309(5733), 464–467.

Frederick, B. C., (2015), Submarine Sedimentary Basin Analyses for the Aurora and Wilkes Subglacial Basins and the Sabrina Coast Continental Shelf, East Antarctica, Ph.D. dissertation, Univ. of Texas, Austin, Texas, USA.

Fretwell, P., et al. (2013), Bedmap2: Improved ice bed, surface and thickness datasets for Antarctica, Cryosphere, 7(1), 375–393.

Furlong, K.P., and D. S. Chapman (2013) Heat Flow, Heat Generation, and the Thermal State of the Lithoshpere. Annu. Rev. Earth Planet. Sci., 05/2012. 41, 345–410.

Gleeson, T., L. Smith, N. Moosdorf, J. Hartmann, H. H. Dürr, A. H. Manning, L. P. H. van Beek, and A. M. Jellinek (2011), Mapping permeability over the surface of the Earth, Geophys. Res. Lett., 38, L02401.

Gleeson, T., N. Moosdorf, J. Hartmann, and L. P. H. van Beek (2014), A glimpse beneath earth's surface: GLobal HYdrogeology MaPS (GLHYMPS) of permeability and porosity, Geophys. Res. Lett., 41, 3891–3898.

Glen, J. W. (1955), The creep of polycrystalline ice, Proc. Roy. Soc., Ser. A, 228, 519–538.

Gooch, B. T., D. A. Young, and D. D. Blankenship (2016), Potential groundwater and heterogeneous heat source contributions to ice sheet dynamics in critical submarine basins of East Antarctica, Geochem. Geophys. Geosyst., 17, doi:10.1002/2015GC006117.

Gooch, B. T., S. P. Carter, O. Ghattas, D. A. Young, and D. D. Blankenship (in review), Groundwater dominance in the subglacial hydrology of ice sheet interiors: example at Dome C, East Antarctica, The Cryosphere Discuss.

Greenbaum, J. S., et al. (2015), Ocean access to a cavity beneath Totten Glacier in East Antarctica, Nat. Geosci., 8, 294–298.

Greve, R., and H. Blatter (2009), Dynamics of Ice Sheets and Glaciers, Springer, Dordrecht, Netherlands.

Hooke, R. L. (2005), Principles of Glacier Mechanics, 2nd ed., Cambridge Univ. Press, New York.

Huybrechts, P. (1993), Glaciological modelling of the late cenozoic East Antarctic Ice Sheet: Stability or dynamism?, Geogr. Ann., 75A(4), 221–238.

Jaupart, C. (1986), On the average amount and vertical distribution of radioactivity in the continental crust, in Burrus, J., ed., Thermal Modeling in Sedimentary Basins: ´Editions Technip, Paris, 33–47.

Jiang, X. W., L. Wan, X. S. Wang, S. Ge, and J. Liu (2009), Effect of exponential decay in hydraulic conductivity with depth on regional groundwater flow, Geophys. Res. Lett., 36, L24402.

Kyrke-Smith, T. M., and A. C. Fowler (2014), Subglacial swamps, Proc. R. Soc. A, 470, 20140340, doi:10.1098/rspa.2014.0340.

Lachenbruch, A. H. (1970), Crustal temperature and heat production: Implications of the linear heat-flow relation, J. Geophys. Res., 75(17), 3291-3300.

Le Brocq, A., A. Payne, M. Siegert, and R. Alley (2009), A subglacial water-flow model for West Antarctica, J. Glaciol., 55(193), 879–888.

Lemieux, J.-M., E. Sudicky, W. Peltier, and L. Tarasov (2008), Dynamics of groundwater recharge and seepage over the Canadian landscape during the Wisconsinian glaciation, J. Geophys. Res., 113, F01011, doi:10.1029/2007JF000838.

Li, X., E. Rignot, M. Morlighem, J. Mouginot, and B. Scheuchl (2015), Grounding line retreat of Totten Glacier, East Antarctica, 1996 to 2013, Geophys. Res. Lett., 42, 8049–8056, doi:10.1002/2015GL065701.

McKenna, T. E., and J. M. Sharp Jr. (1998), Radiogenic heat production in sedimentary rocks of the gulf of Mexico basin, south Texas, AAPG Bull., 82, 484–496.

McLaren, S., M. Sandiford, M. Hand, N. Neumann, L. Wyborn, and I. Bastrakova (2003), The hot southern continent; heat flow and heat production in Australian Proterozoic terranes, Spec. Pap. - Geol. Soc. Am., 372, 157–167.

Mellor, G. L., and L. Kantha (1989), An ice-ocean coupled model, J. Geophys. Res., 94(89), 10937–10954.

Nye, J. F. (1957), The distribution of stress and velocity in glaciers and ice sheets, Proc. R. Soc. London, Ser. A, 239, 113–133.

Pattyn, F. (2002), Transient glacier response with a higher-order numerical ice-flow model, J. Glaciol., 48, 467–477.

Pattyn, F. (2010), Antarctic subglacial conditions inferred from a hybrid ice sheet/ice stream model, Earth Planet. Sci. Lett., 295(3-4), 451–461.

Pattyn, F., et al. (2012), Results of the Marine Ice Sheet Model Intercomparison Project, MISMIP, Cryosphere Discuss., 6, 267–308, doi:10.5194/tcd-6-267-2012.

Petrunin, A. G., I. Rogozhina, A. P. M. Vaughan, I. T. Kukkonen, M. K. Kaban, I. Koulakov, and M. Thomas (2013), Heat flux variations beneath central Greenland's ice due to anomalously thin lithosphere, Nat. Geosci., 6, 746–750, doi:10.1038/ngeo1898.

Pollard, D., R. M. DeConto, and A. A. Nyblade (2005), Sensitivity of Cenozoic Antarctic ice sheet variations to geothermal heat flux, Glob. Planet. Change, 49(1-2), 63–74.

Pollard, D., R. M. Deconto, and R. B. Alley (2015), Potential Antarctic Ice Sheet retreat driven by hydrofracturing and ice cliff failure, Earth Planet. Sci. Lett., 412, 112–121.

Pritchard, H. D., S. R. M. Ligtenberg, H. A. Fricker, D. G. Vaughan, M. R. van den Broeke, and L. Padman (2012), Antarctic ice-sheet loss driven by basal melting of ice shelves, Nature, 484(7395), 502–505.

Rignot, E., J. Mouginot, and B. Scheuchl (2011), Ice flow of the Antarctic Ice Sheet, Science, 333, 1427–1430.

Sandiford, M., and S. McLaren (2002), Tectonic feedback and the ordering of heat producing elements within the continental lithosphere, Earth Planet. Sci. Lett., 204, 133–150.

Sclater, J. G., and P. Christie (1980), Continental stretching: An explanation of the post-mid-cretaceous subsidence of the central North Sea basin, J. Geophys. Res. Solid Earth, 85(B7), 3711-3739.

Shapiro, N. M., and M. H. Ritzwoller (2004), Inferring surface heat flux distributions guided by a global seismic model: Particular application to Antarctica, Earth Planet. Sci. Lett., 223(1-2), 213–224.

Shreve, R. L. (1972), Movement of water in glaciers, J. Glaciol., 11(62), 205–214.

Siegert, M. J., J. P. Taylor, and J. Antony (2005), Spectral roughness of subglacial topography and implications for former ice-sheet dynamics in East Antarctica, Global Planet. Change, 45, 249–263.

Siegert, M. J., A. Le Brocq, and A. J. Payne (2007), Hydrological connections between Antarctic subglacial lakes and the flow of water beneath the East Antarctic Ice Sheet, in Glacial Sedimentary Processes and Products, Spec. Publ., vol 39, edited by M. J. Hambrey et al., pp. 3–10, Int. Assoc. of Sedimentol., Malden, Mass.

Singhal, B. B. S., and R. P. Gupta (2010), Applied hydrogeology of fractured rocks (Vol. 430). New York: Springer.

Smith, B. E., H. A. Fricker, I. R. Joughin, and S. Tulaczyk (2009), An inventory of active subglacial lakes in Antarctica detected by ICESat (2003–2008), J. Glaciol., 55, 573–595, doi:10.3189/002214309789470879.

Stauffer, P. H. (2006), Flux flummoxed: A proposal for consistent usage, Ground Water, 44(2), 125–128.

Taylor, J., M. J. Siegert, A. J. Payne, M. J. Hambrey, P. E. O'Brien, A. K. Cooper, and G. Leitchenkov (2004), Topographic controls on post-Oligocene changes in ice-sheet dynamics, Prydz Bay region, East Antarctica, Geology, 32, 197–200, doi:10.1130/G20275.1.

Waples, D. W. (2001), A New Model for Heat Flow in Extensional Basins: Radiogenic Heat, Asthenospheric Heat, and the McKenzie Model, Nat. Resour. Res., 10(2), 227–238.

Weertman, J. (1966), Effect of a basal water layer on the dimensions of ice sheets, J. Glaciol., 6(44), 191–207.

White, D. A. (2013), Cenozoic landscape and ice drainage evolution in the Lambert Glacier–Amery Ice Shelf system, Geological Society, London, Special Publications, 381(1), 151-165.

Wilkens, N. (2014), Pine Island Glacier-a 3D full-Stokes model study, Ph.D. dissertation, University of Hamburg, Hamburg, Germany.

Wilkens, N., J. Behrens,T. Kleiner, D. Rippin, M. Rückamp, and A. Humbert (2015), Thermal structure and basal sliding parametrisation at Pine Island Glacier–a 3-D full-Stokes model study, The Cryosphere, 9(2), 675-690.

Wright, A. P., M. J. Siegert, A. M. Le Brocq, and D. B. Gore (2008), High sensitivity of subglacial hydrological pathways in Antarctica to small ice sheet changes, Geophys. Res. Lett., 35, L17504, doi:10.1029/2008GL034937.

Wright, A., and M. Siegert (2012), A fourth inventory of Antarctic subglacial lakes, Antarct. Sci., 24(6), 659-664.

Wright, A. P., et al. (2012), Evidence of a hydrological connection between the ice divide and ice sheet margin in the Aurora Subglacial Basin, East Antarctica, J. Geophys. Res., 117, F01033, doi:10.1029/2011JF002066.

Young, D. A., et al. (2011), A dynamic early East Antarctic Ice Sheet suggested by ice-covered fjord landscapes, Nature, 474(7349), 72–75.

Zwally, H. J., M. B. Giovinetto, M. A. Beckley, and J. L. Saba (2012), Antarctic and Greenland drainage systems, GSFC Cryospheric Sciences Laboratory.

An, M., D. A. Wiens, Y. Zhao, M. Feng, A. Nyblade, M. Kanao, Y. Li, A. Maggi, and J.-J. Lévêque (2015b), Temperature, lithosphere-asthenosphere boundary, and heat flux beneath the Antarctic Plate inferred from seismic velocities, J. Geophys. Res. Solid Earth, 120, 8720–8742, doi:10.1002/2015JB011917.

Comiso, J. C. (2000), Variability and trends in Antarctic surface temperatures from in situ and satellite infrared measurements. Journal of Climate, 13(10), 1674-1696.

Fox Maule, C., M. E. Purucker, N. Olsen, and K. Mosegaard (2005), Heat flux anomalies in Antarctica revealed by satellite magnetic data., Science, 309(5733), 464–467.

Le Brocq, A., A. Payne, M. Siegert, and R. Alley (2009), A subglacial water-flow model for West Antarctica, J. Glaciol., 55(193), 879–888.

Shapiro, N. M., and M. H. Ritzwoller (2004), Inferring surface heat flux distributions guided by a global seismic model: Particular application to Antarctica, Earth Planet. Sci. Lett., 223(1-2), 213–224.

Bense, V. F., and M. A. Person (2008), Transient hydrodynamics within intercratonic sedimentary basins during glacial cycles, J. Geophys. Res., 113, F04005, doi:10.1029/2007JF000969.

Boulton GS, R. Lunn, P. Vidstrand, and S. Zatsepin (2007), Subglacial drainage by groundwater–channel coupling, and the origin of esker systems: Part 2 – theory and simulation of a modern system, Quat. Sci. Rev., 26, 1091–1105.

Flowers, G. E. (2015), Modelling water flow under glaciers and ice sheets, Proc. A, (471).

Forieri, A., L. Zuccoli, A. Bini, A. Zirizzotti, F. Remy, and I. E. Tabacco (2004), New bedrock map of Dome C, Antarctica, and morphostructural interpretation of the area, Ann. Glaciol., 39(1), 321-325.

Gooch, B. T., D. A. Young, and D. D. Blankenship (2016), Potential groundwater and heterogeneous heat source contributions to ice sheet dynamics in critical submarine basins of East Antarctica, Geochem. Geophys. Geosyst., 17, doi:10.1002/2015GC006117.

Kyrke-Smith, T. M., R. F. Katz, and A. C. Fowler (2014), Subglacial hydrology and the formation of ice streams, Proc. Phys. Soc. London, Sect. A, 470, 20,130,494, doi:10.1098/rspa.2013.0494.

Lemieux, J.-M., E. Sudicky, W. Peltier, and L. Tarasov (2008), Dynamics of groundwater recharge and seepage over the Canadian landscape during the Wisconsinian glaciation, J. Geophys. Res., 113, F01011, doi:10.1029/2007JF000838.

Person, M., V. Bense, D. Cohen, and A. Banerjee (2012), Models of ice-sheet hydrogeologic interactions: A review, Geofluids, 12, 58–78.